PROCEEDINGS OF THE CEReS INTERNATIONAL SYMPOSIUM ON REMOTE SENSING

"Maximization of the Use of Satellite Data for Understanding the Earth Environment"

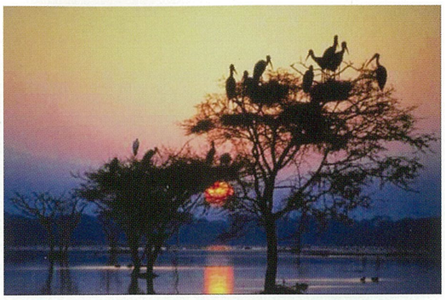

Chiba University, Japan
December 13 - 14, 2005

Published by Center for Environmental Remote Sensing (CEReS),
Chiba University,
1-33 Yayoi-cho, Inage, Chiba, 263-8522 Japan

CEReS: http://www.cr.chiba-u.jp/
Symposium: http://www2.cr.chiba-u.jp/symp2005/

Cover Designed by T. Ishiyama

Proceedings of The 11th CEReS International Symposium on Remote Sensing

"Maximization of the Use of Satellite Data for Understanding the Earth Environment"

December 13-14, 2005

Organized by
Center for Environmental Remote Sensing (CEReS),
Chiba University, Japan

Supported by the Remote Sensing Society of Japan (RSSJ)

(Editors)
J. Tetuko S. S., T. Ishiyama and R. Tateishi

Preface

On behalf of Center for Environmental Remote Sensing, Chiba University and the Organizing Committee, I am most delighted to thank all participants of the 11th CEReS International Symposium on Remote Sensing with special theme on "Maximization of the use of satellite data for understanding the earth environment". The Symposium was held on 13 to 14 December 2005 at University Convention Hall (Keyaki Kaikan), Chiba University under the auspices of Center for Environmental Remote Sensing, Chiba University with the support of the Remote Sensing Society of Japan (RSSJ).

This Symposium focused on a series of important subjects from satellite data processing to environmental analysis; i) global or large area satellite data processing including synthetic aperture radar (SAR), ii) global land cover / land use mapping, iii) human impact on environment and sea ice, iv) land cover and climate change, v) regional environmental characteristics and global changes. The Symposium was highlighted by the invited presentations by experts on these subjects in two days. The poster presentations were held to encourage wider discussions by active researchers of these fields.

This Symposium was an event focused upon the most important fields related to science and technology in remote sensing and environment. Many researchers and students from all over the world discussed in detail how to maximize the use of satellite data to understand the earth environment.

Finally, the Organizing Committee hopes this symposium could enrich the knowledge of the participants to promote the remote sensing field, especially in the environmental monitoring.

Prof. Ryutaro Tateishi
General Chairman.

Contents

(Papers)

CEOP centralized data system and integrated analysis tools

Kenji Taniguchi[1], Toshihiro Nemoto[2], Eiji Ikoma[3], Masaki Yasukawa[4], Toshio Koike[5] and Masaru Kitsuregawa[6]

[1,5] Dept of Civil Eng, Univ. of Tokyo
[2,4,6] Institute of Industrial Science, Univ. of Tokyo
[3]Center for Spatial Information Science, Univ. of Tokyo
E-mail: taniguti@hydra.t.u-tokyo.ac.jp

Abstract

The amount of earth environmental data has increased explosively because of recent advances in observational techniques. On the CEOP (Coordinated Enhanced Observing Period) project, in order to improve our understanding of water and energy cycle, large amount of data is collected and archived. In this paper, we introduce the CEOP centralized data system and integrated analysis tool. The centralized system enables us to retrieve, browse, analyze and download CEOP data set, and it improves accessibility and usability of the CEOP data. Three dimensional data visualization system is developed with the fusion of various products and the cutting out of demanded arbitrary surface. Developing an easy-to-use interface for non-computational researchers. The CEOP data system is developed at Institute of Industrial Science, University of Tokyo. This paper also explains the design of the system.

1. Introduction

Water and energy cycle is important for peoples' life and the climate system. At the same time, there has been drastic progress in techniques for observing the earth environment, and as a result, the volume of earth observation data has increased. On the CEOP (Coordinated Enhanced Observing Period) project, large amount of data are being collected and archived in order to improve our understanding of water and energy cycle. CEOP data consist of three kinds of data, those are in-situ data, satellite data and model output data. The in-situ data are a temporal series of air temperature, pressure, humidity, precipitation and so on at 35 reference sites around the world. The satellite data are remotely sensed data from the operational satellites, such as TERRA, AQUA, TRMM, NOAA and so on. The model output data are generated by numerical weather prediction centers. These data have various dimensions, spatial and temporal resolutions, precision, formats, coordinate systems. The total amount of the data is almost 100TB per year. This paper explains the design and implementation of data server in addition to the browse and analysis interface which enable researchers to use our system easily.

It uses tape library system and disk arrays to store the data, however, the location of data is hidden from users. The users can retrieve data without considering data location. The browse and analysis interface is the client of the data server and it provides the users with menu based integrated access tools to the data server. The connection between the clients and the server is based on HTTP. The users can access all kinds of data through the same interface without taking account of data type. The users can view the retrieved data as graphic charts or bitmap images depend on their dimension directly from the server. Some analysis operations such as average, difference, correlation, and so on can be applied into one or more retrieved data on the server through the interface.

2. Data

2.1. CEOP data

Three kinds of data are planned to be archive on the CEOP project. They are in-situ data, model output data and satellite data.

The in-situ data are a temporal series of the values observed at 35 reference sites around the world. Each reference site has one or more stations. The in-situ data are divided into three categories, namely surface observation, subsurface observation and upper air observation. The surface observation consists of air temperature, pressure, humidity, precipitation, heat flux, radiation and so on at the ground level. The subsurface observation is composed of soil temperature, soil water content and soil heat flux for 2cm to 175cm depth. The upper air observation consists of air temperature, humidity, pressure and so on measured by radiosonde. The all values are not always observed at a reference site. The sorts of the observed values and observation frequency depend on the reference site. The total amount of in-situ data for two year and three months is almost 600MB.

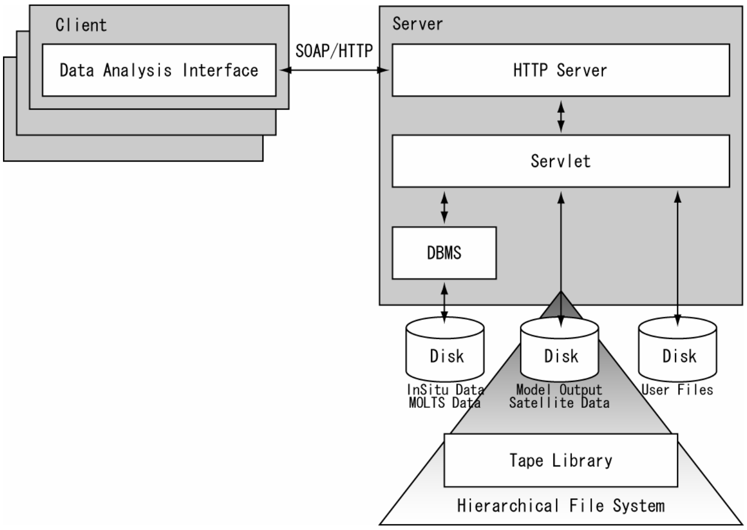

Figure 1

The model output data is the gridded values from global forecast model or assimilation system generated by 10 num erical weather forecast centers. Two types of model output, namely gridded data and site-specific time series at each of the reference site are planned to archive. The latter time series are designated as MOLTS (Model Output Location Time Series). The gridded data are three dimensional data and each cell has several prognostic variables such as air temperature, humidity, pressure and so on. The forecast length, assimilation intervals, the grid systems of the models and also the variables in models are different each other. The MOLTS data are one dimensional time series of variables at the reference site extracted from gridded data. The total amount of model output data is almost 20TB.

The satellite data are remotely sensed data from the sensors on the operational satellites such as DMSP SSM/I, TRMM TMI, TRMM PR, GMS S-VISSR, NOAA AVHRR, TERRA/AQUA MODIS, AQUA AMSR-E and so on. The satellite data are two dimensional data and each sensor has one or more channels. Though these data are geometrically corrected by the data supplier, their resolutions depend on the sensor and the channel. The observation time may vary day by day even if the same satellite. The total amount of satellite data is almost 200TB.

2.2. Data for integrated analysis tools

In addition to CEOP centralized data system, we have developed a prototype system of analysis tools for large volume data set.

For the analysis system, monthly average data for global precipitation from 1979 to 2000 and daily average data from 1997 to 2000, which are in the GPCP(Global Precipitation Climatology Project) data set. The resolution is 1 degree per pixel on every side. And, because OLR (Outgoing Long-wave Radiation) is useful to describe summer monsoons as an indication of convective activity in a tropical area, we use OLR data from 1975 to 2000 provided by NOAA (National Oceanic and Atmospheric Administrator). The resolution is 2.5 degrees on every side. Reanalysis data of NCEP/NCAR (National Center for Environmental Prediction / National Center for Atmospheric Research) for atmospheric data is archived and used. The resolution is also 2.5 degrees on every side and frequency is daily. We use sea surface temperature data provided by TMI (TRMM Microwave Imager) on TRMM (Tropical Rainfall Measuring Mission). This data has a 0.25 degree spatial resolution, and three day average temporal resolution from December 1997. Atmospheric Infrared Sounder (AIRS) onboard Aqua, NASA's satellite, is designed by NASA Jet Propulsion Laboratory. With other satellite sensors onboard Aqua, cloud effects can be reduced and vertical distribution of atmospheric temperature and water vapor and other atmospheric elements can be detected by AIRS. In this study, data of atmospheric temperature and water vapor are used. Spatial resolution is 0.25deg*0.25deg in horizontal direction, and 28 layers in vertical direction. Details are described in the web site of "AIRS data support".

3. System

3. 1. CEOP centralized data archiving system

- System architecture

The CEOP centralized data system is based on a client-server model. The architecture of the system is shown in Figure 1. The communication protocol between server and client is HTTP. The requests from clients are at first received at the HTTP server and then they are sent to the data manager. The data manager is a servlet program. It receives the requests from clients through the HTTP server and then it generates SQL commands for data search or executes analysis operations according to the user requests. One dimensional data such as in-situ data and MOLTS data are stored in DBMS, however, two and three dimensional data such as gridded model output data and satellite data are stored as files on the hierarchical file system and only their metadata are stored in DBMS. There are several reasons why we do not manage two or three dimensional data as Large Objects (LOB) in DBMS. First, the accessing a LOB in DBMS is slower than accessing a file. Second, existing implementations of LOBs tend to lack support for the hierarchical storage management system. Although the gridded model output data and the satellite data are stored on the hierarchical file system, small images around the reference sites clipped from the global data are stored on disks. Generally the values around the reference sites are necessary to compare the values from ground observations and that of model output or that of remotely sensed data. To store the small portions on the disks instead of hierarchical file system we can reduce the response time. The location of the data is hidden from the users. The users do not have to consider where the data are stored. The data server automatically migrates and retrieves the appropriate data from DBMS, disks or hierarchical file system as the user requests and sends them to the clients. The DBMS manages the one dimensional data and the metadata for all data. We use a commercial DBMS and JDBC for the connection between DBMS and the data manager.

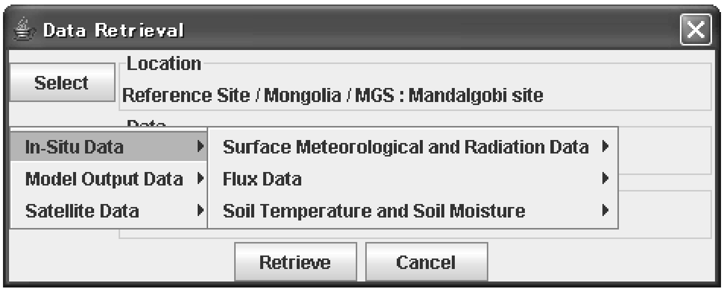

Figure 2

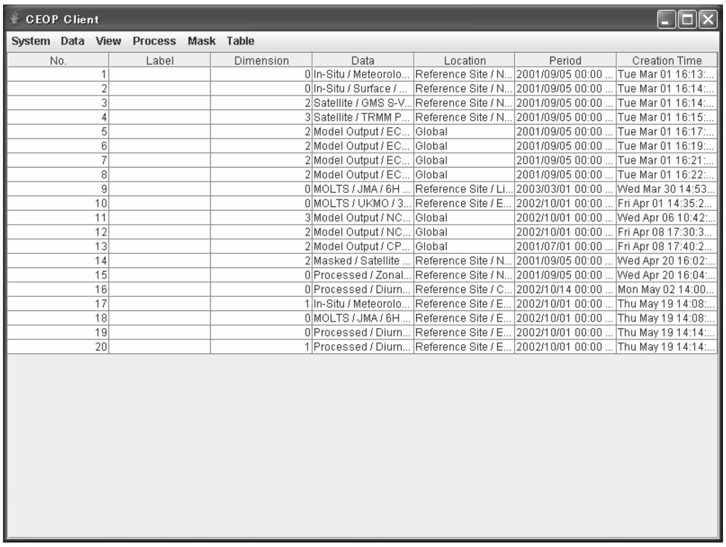

Figure 3

The graphical user interface (GUI) in the client system roughly consists of two parts, HTTP browser and data analysis interface. The communication between clients and servers are based on HTTP and the data analysis interface is written in JAVA. Accordingly, the client does not need any special hardware or software. Only HTTP browser and JAVA runtime environment are required. Since many kinds of current computers and operating systems support HTTP browser and JAVA runtime environment, the GUI for the data server works on many kinds of computers. The usage of the data analysis interface is described in the next section.

- Browse and analysis interface

The user accesses to the data server page through the HTTP browser at first and then authentication page is shown. After the user passes the password check, the user can access to the data listed in his/her work space. The requested data is specified by three items, location (reference site name), data name and temporal period. The available location and data name are listed in the menus. The user can select year and month in the menu as the temporal period or input the start date and time and the end of those (Figure 2). Clicking the button to retrieve, the request is transferred to the server. The server parses the requests, generates the SQL command, sends it to the DBMS and stores the result portion into the user’s area. The items in the data management window correspond to the result portions in the data server. The retrieved data can be displayed as a line chart (Figure 4) and a bitmap image (Figure 5). Users can specify any of the time, height, latitude and longitude as x and y axis of the graph or the image. When the result portion has more than three dimensions, the values in the axis except x or y axis can be changed by the slider bar on the bottom of the line graph window or the

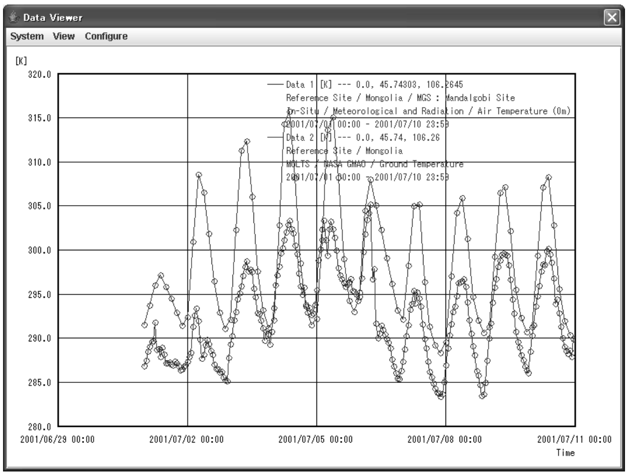

Figure 4

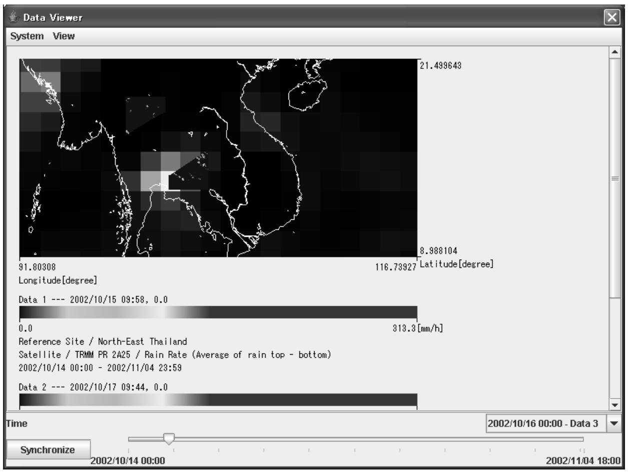

Figure 5

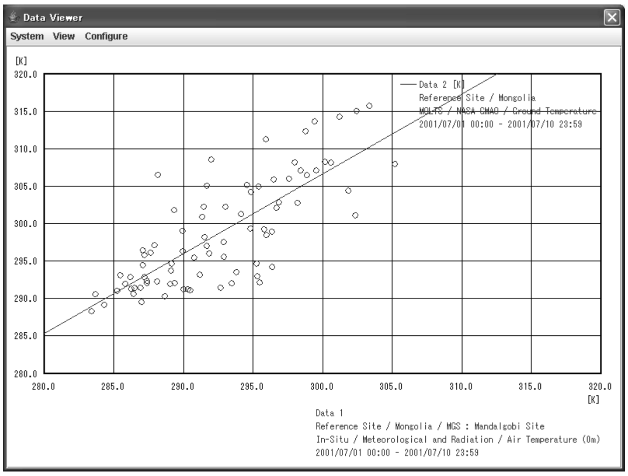

Figure 6

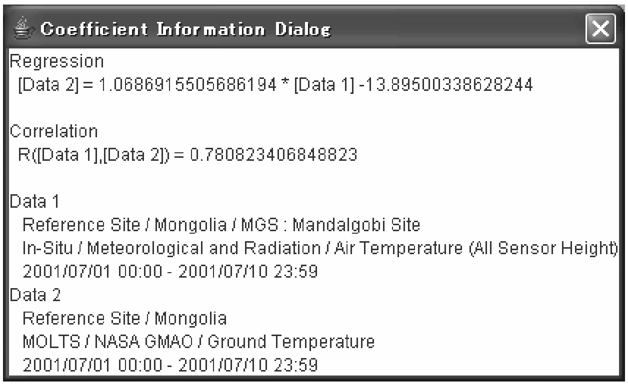

Figure 7

bitmap image window. For example, when the user specify longitude as x axis and latitude as y axis to generate the bitmap images of the temporal series of global sea surface temperature, he can change the time by the slider bar on the bottom of the window. A scatter diagram can also be drawn (Figure 6). In the diagram, the regression lines are also drawn. The regression coefficients and the correlation coefficients are shown in the coefficient information window (Figure 7).

The analysis operation is executed to the retrieved data. The user selects one or more retrieved data and then pushes the appropriate analysis command button. The analysis request is sent to the data server and the data manager executes the operation to the selected data in the user's area. In the current preliminary version, only simple analysis commands such as calculating average, maximum, minimum and so on are available (Figure 8). The data processed by the analysis operation are also stored into the user's area and they are listed in the data management window. They can be targets of analysis operations again. The user can apply the analysis operations onto the processed data again and again.

3.2. Integrated data integration tools

3.2.1. Correlation Coefficient Analysis Tools

Statistical analysis is used for extracting correlations between phenomena in meteorology. However, in the very large data sets that we targeted for this study, statistical analysis is quite difficult using general software. Moreover, the data we are targeting has not only simple correlations between two data, but also various other kinds of correlation such as spatial differences, temporal differences, and the difference of values; thus it requires tools which enable flexible handling and analysis and the ability to specify conditions. In this study, we introduce a tool which can compute correlation coefficient while specifying conditions such as time (term), space (area), value, temporal resolution and spatial resolution. With this tool, assuming that some natural phenomena may happen not at the same time but with some delay (time lag), a user can analyze the correlation between phenomena with different times (time lag correlation)

Using this method, users can find not only relationship between spatially separate points but also temporally separate points (such as a phenomenon happening a few days after the base phenomenon). We developed a GUI which can operate these tools via the Web. With this GUI, users can specify various conditions and visualize the results. It also allows multiple users to use it from remote locations.

When users log on our system, Top Page (Figure 8) will appear.

In the right frame, user can specify as follows:

- Choose 1 base data for correlation analysis
- Choose some (multiple) target data for correlation analysis
- Year, Month, Date
- Term
- Specify base area for base data
- Choose the window for displaying results (Same window of this page or other)

Then, the user's specified area on a world map will be displayed in the upper left frame for checking the area, and user will be asked the value of the threshold for visualization and the mode for processing. User can select whether results are immediately displayed or the system will notify user by e-mail after processing.

In this window, the results of different days of lag are lined up at horizontal direction, and the results of different value are lined up at vertical direction. In other words, one result shows correlation coefficients between spatial averaged time sequential and all points of the whole globe for a time lag period, year, month, date. Positive correlation points are shown as red points, and negative ones are shown as blue points, the darkness of color means it is strong and weak.

Such a display method enables users to understand change of correlation as time goes on and which data has a strong correlation with the base data by comparing the result at vertical direction.

If a user clicks interesting data on this window (Figure 9), a new window will appear and a higher resolution image is displayed, and the graph of area averaged time sequential data is displayed in the lower window. Clicking a point such as one with very high correlation on the global map of this window, more detailed information on each point and each time will be shown in new window.

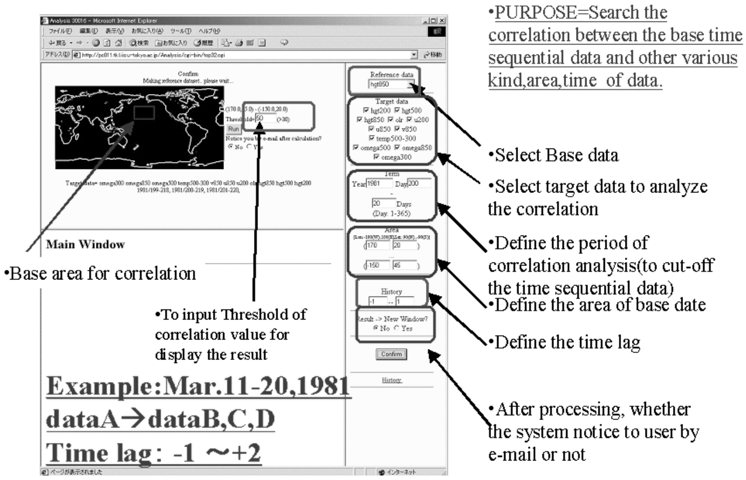

Figure 8

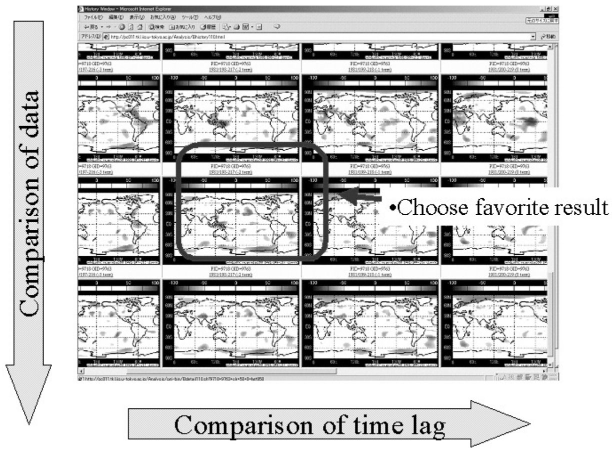

Figure 9

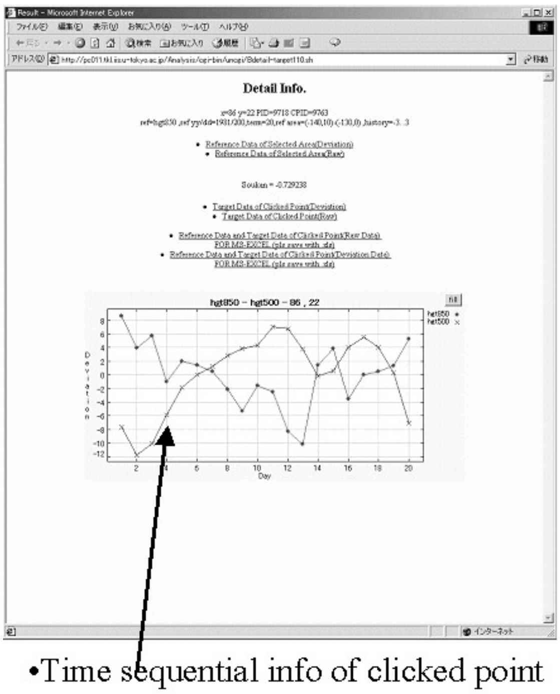

Figure 10

3.2.2 AIRS 3D Visualization system

-Basic design of AIRS visualization system

In this study, following two functions are required for the system;

-3D visualization

-Data subset and visualization for arbitrary curved surface

Two dimensional horizontal or vertical cross section is not sufficient method to utilize three dimensional data. For fully utilization of three dimensional data, virtual reality markup language (VRML) is used in this system. VRML does not require any commercial software and works on web browser, and it enables to see three dimensional data from arbitral view points.

At the same time, cross section is helpful to understand phenomena. However, software which have been used in meteorological research community has not allowed to make cross section in arbitral cross section. Sometimes, this limitation possibly leads misunderstandings of reality. Then, the second function is developed in this study.

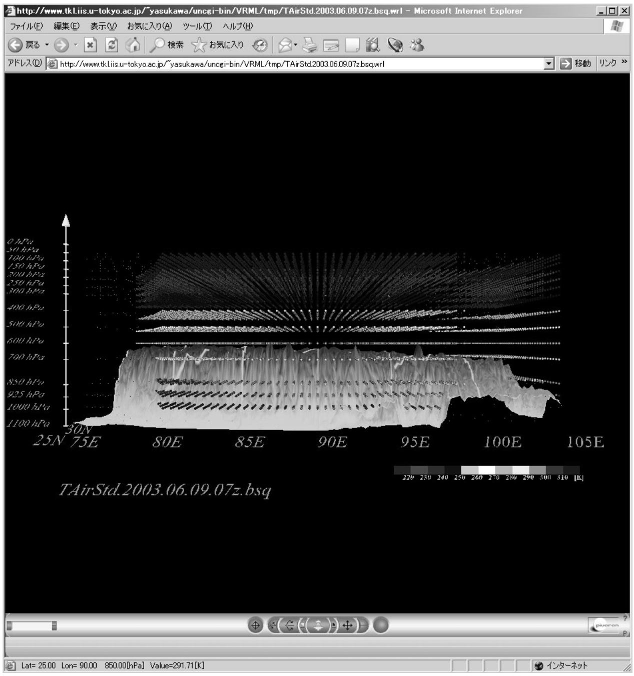

Figure 11

-VRML

In this system, three dimensional visualization of AIRS data is realized with web browser using VRML 2.0. By using VRML, users can view data from any direction and distance in virtual reality space. Overlaying geographical data, morphological feature and its effect on phenomena can be recognized at the same time (Figure 11). VRML also enables to plot multiple variables in the same space (Figure 12). Relationship among several elements can be recognized and it is useful for analysis.

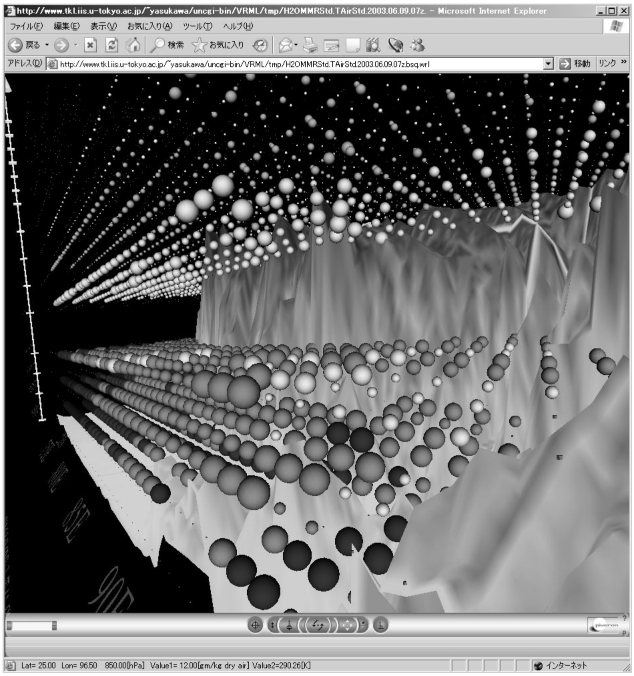

Figure 12

-Subset and plot on arbitral curved surface

In this system, users can select arbitral vertical section by inputting longitude and latitude on the user interface (Figure 13). First, data is retrieved from data server. Retrieved data is re-sampled by using selected curved cross section and visualized by GrADS. Images are made for selected period (Figure 14). These images are viewed as animation by choosing appropriate option. Plotted images can be overlay on VRML and viewed with geographical features. This system can also make horizontal 2D plot and overlay it in virtual reality space. These functions enable us to understand vertical distribution of a variable and horizontal 2D atmospheric condition in the same moment.

4. Summary

Progress in observation and monitoring technology in meteorology has enabled researchers to find new knowledge because of an increase in data volume. However, it has also brought some problems regarding methods and environments to use those huge volume data effectively and practically.

In this paper, centralized data system and integrated data using system for huge amount data developed by Institute of Industrial Science, University of Tokyo in CEOP activity were introduced.

CEOP centralized data system has managing functions for huge and various formatted data set. Users can retrieve, list and visualize data in their work space. At the same time, the data can be downloaded through the interface.

Moreover, the system enables us to process retrieved data with basic mathematics functions. The data server has been opened to the CEOP community tentatively.

At the same time, collaborating closely with the researchers who are using earth environmental data, analyzing tools for large volume data set are developed. Tools are based on web technologies for easy access and usage.

Though our current preliminary data server supports only simple operations, it may be helpful for studies related on water and energy cycle. We are now implementing more analysis functions and improving the system and also develop more flexible and effective tools with the feed back opinion from active users.

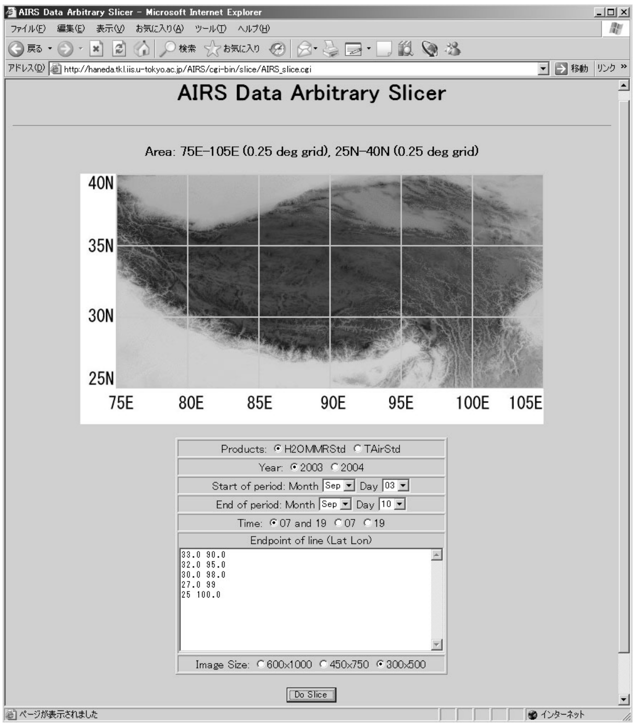

Figure 13

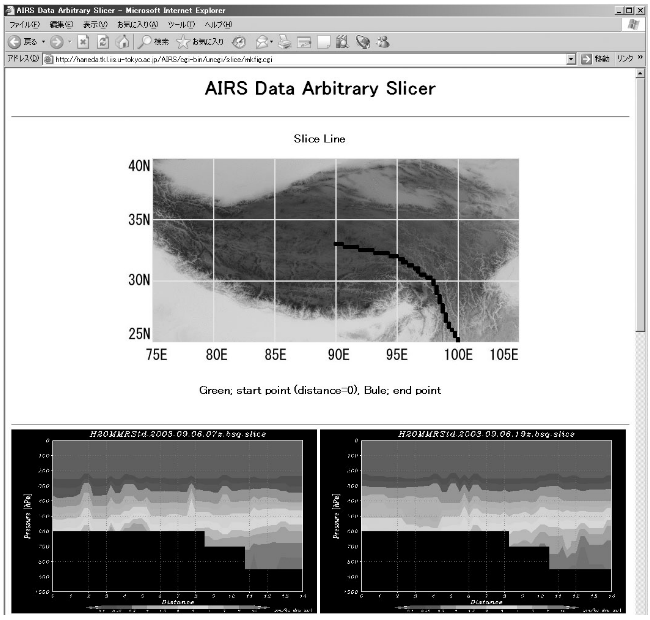

Figure 14

References

[1] Stolte E., Praun C., Alonso G. and Gross T.: Scientific Data Repositories – Designing for a Moving Target, *ACM SIGMOD 2003*.

[2] CEOP Home Page: http://monsoon.t.u-tokyo.ac.jp/ceop/.

[3] Nemoto T., Ikoma E. and Kitsuregawa M.: Design of data server for CEOP data, *Proceedings of the 2nd Asia Pacific Association of Hydrology and Water Resources Conference*, Vol.2, pp.558-565, 2004.

[4] Jet Propulsion Laboratory (NASA), "AIRS - Atmospheric Infrared Sounder -, "http://www-airs. jpl.nasa.gov/

[5] Jeanne Behnke, Alla Lake, "EOSDIS: Archive and Distribution Systems in the Year 2000, " Proceeding of 8th NASA Goddard Conference, pp.313-324, Mar. 2000.

[6] NASA Goddard Earth Sciences Data and Information Services Center (GES DISC) / Distributed Active Archive Center (DAAC), "AIRS data support, " http://daac.gsfc.nasa.gov/atmodyn/airs/

[7] Kitsuregawa Lab., "Satellite Image Archive at Institute of Industrial Science, University of Tokyo", http://www.tkl.iis.u-tokyo.ac.jp/SIAIIS/

[8] Kitsuregawa Lab., "Data Visualization System for Earth Environmental Researchers, " http://www.tkl. iis.u-tokyo.ac.jp:8080/DV/

[9] U.S. Geological Survey (USGS), "GTOPO30 - Global Topographic Data -, " http://edcdaac.usgs. gov/gtopo30/gtopo30.asp

[10] Center for Ocean-Land-Atmosphere Studies (COLA), "GrADS Data Server (GDS), " http://grads.iges. org/grads/gds/gds.html

[11] Nemoto, T. and M. Kitsuregawa, CEOP Data Server and Browse/Analysis Interface, Proceedings of CEOP/IGWCO Joint Meeting, 2005

[12] Ikoma, E., K. Taniguchi, T. Koike and M. Kitsuregawa, Development of a Visual Data Mining Application for Earth Environmental Data, Proceedings of CEOP/IGWCO Joint Meeting, 2005

[13] Yasukawa. M., T. Nomoto, T. Koike and M. Kitsuregawa, Development of a Visualization System in Earth Observation Satellite Data with Three-dimensional Information such as AIRS Data, DBSJ Letters, vol.4 (1), 2005 (in Japanese)

[14] T. Koike, "The Coordinated Enhanced Observing Period – an initial step for integrated global water cycle observation", WMO Bulletin, vol.53, no.2, pp.115-121, April 2004.

TRMM PR, its possibility and limitation for the global mapping of precipitation

Masafumi HIROSE
Earth Observation Research and Application Center, JAXA
E-mail: hirose@eorc.jaxa.jp

Abstract

Data potential of eight-year data observed by the spaceborne radar, TRMM PR, was examined in view of the sufficiency of the sampling and the precipitation property. The degree of a biased climatology of monthly rainfall and the detection ratio of the significant diurnal signature were investigated. The eight-year data clarified a wide-range of the increasing possibilities and enhanced issues. Uncertainty of the precipitation structure adjacent to the surface was addressed as one of the cross-cutting issues.

1. Introduction

The Precipitation Radar (PR) on the Tropical Rainfall Measuring Mission (TRMM) satellite is the first and only spaceborne radar since the end of 1997. More than 12 TB of data had been stored. Given the growing number of data samples without any deterioration, we can apply the data to the climate research where long-term observations are essential to fundamental research needs. In this presentation, the increasing possibility and the performance limitations are introduced.

2. Unique strengths and the sampling issue of TRMM PR data

The primal uniqueness is the global 3-D observation of precipitation echo. It first observed accurate stratiform and convective rainfall over land and ocean. The regional diversity of precipitation profiles is recognized to be of great importance for any other conventional retrieval of precipitation. Main keywords of other unique points would be the attenuation correction by using the path-integrated attenuation, observation from the non-sun-synchronous orbit, and the combination with other sensors on the same platform. On the other hand, the biggest issue for most of possible users is the insufficient sampling. The bias of sampling for each local hour is a critical problem for one-month data analyses. The seasonal data also contain this problem since it consists of the insufficient intraseasonal dataset.

In order to mitigate this issue for the analyses of the seasonal and intraseasonal variation, the usefulness of the multiple-year data was examined. Figure 1 shows the variation of the sampling for each local time, and the change by the data accumulation. The minimum number of the sampling was significantly increased for 8 years. It is 1.4 times more than that of 7 years, and 8 times more than that of 3 years. The accumulated number of samples for the minimum-sampling hour, 3-4 LT, was about 875 samples over 0.5 degree box in August over Tibet. TRMM PR data are becoming climatologically significant and reliable dataset and enabled us to examine the precipitation variability in less time and in fine scale.

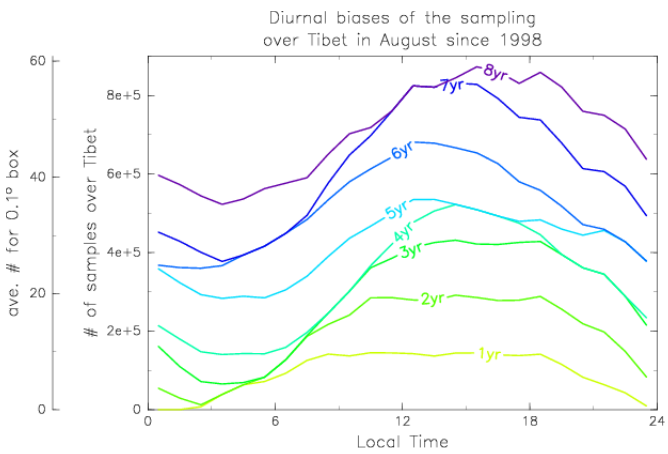

Fig. 1. The accumulated number of hourly samples over Tibet in August since 1998.

3. The temporal variation of rainfall depicted from the long-term data

The detection of the diurnal signature would be a good barometer for assessment of the impact of the long-term data accumulation since it needs sufficient hourly samples in fine spatial scale. We considered the significant diurnal peak based on sufficient samples as the time of maximum rainfall with consecutive positive anomalies for more than three hours. For one summer season, the diurnal signature was ambiguous in most places. The occurrence frequency of the diurnal signal has been increasing according to the increase of the sampling as shown in Fig. 2. For eight summer seasons, 20 % of regions could be detected as the region with the significant diurnal signature. For all season during 8 years, the number became doubled. Looking into Tibet, 80 % of the region was detected, implying the uniform mechanism therein. The TRMM satellite will be on orbit at least until 2009. There should be further examined the increasing possibilities in utilizing the dataset. Each regional characteristics of the diurnal signature prompt our speculation of possible research topics (not shown).

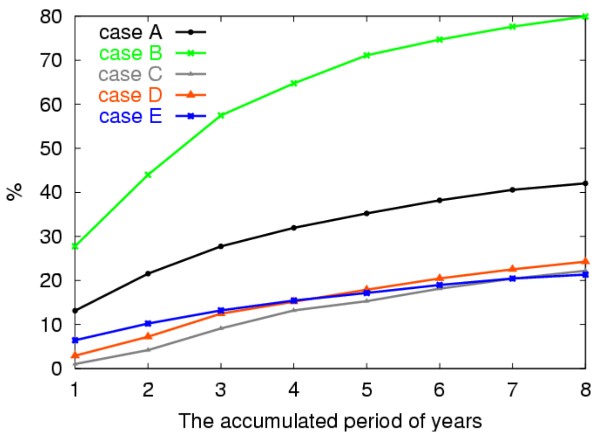

Figure 2. Year to year change of the percentage of significant features of time of maximum rainfall. Case A-E corresponds to the detection rate of the diurnal feature with temporal continuity (case A), over Tibet (case B), over the eastern part of the south Atlantic (case C), and over the globe but for JJA (case D), and that with spatial continuity in addition to the temporal continuity (case E).

Recently, a precipitation system climatology has it going on [e.g., Nesbitt and Zipser, 2003]. Its concept is that climatic variability consists of individual factors and should be understood as conglomerates of precipitation systems. The total rainfall amount is the sum of the individual pixel rain intensities that are grouped into the precipitation systems. The eight-year observation captured millions of precipitation systems over the global tropics. For example, we can understand what kind of precipitation systems makes the regional characteristics of the diurnal variation [e.g., Hirose and Nakamura, 2005]. The global and regional understandings of precipitation properties will deepen from the further data accumulation and a diversity of researches.

4. Remaining issues of the precipitation retrieval

A number of the ground validation of TRMM PR showed that adequate "truth" of global map of rainfall is still in absence. Instead, the reduction of differences in rainfall estimates, about 5 % in average, between TRMM PR and TMI has been discussed by evaluating each data properties. Major possible error sources are listed: Regional variation of the drop size distribution, radar calibration, uncertainty of attenuation correction for water vapor/cloud/precipitation, non-uniform-beam-filling effect, rain profiles in the surface clutter, the temporal variation of the freezing level, the variation of the ice particles, and so on. Most of them are considered in the latest algorithm. However, they are still in controversy.

As an example of current activities, uncertainty in the surface rainfall estimates is focused on. Any radar cannot observe rainfall rate at the surface due to the surface clutter. Around nadir and at the edge of the swath, the most frequent near-surface level was 500 and 1750 m, and the ninety-fifth percentile was 750 and 2000 m, respectively (Fig. 3). Hence, in the latest algorithm, it has been estimated by assuming several constant slope of dBZe in the clutter region. The slope was obtained from the wind profiler and TRMM PR observation. It is generally decreasing considering on the slower terminal velocity near the surface. The height smearing effect of the near-surface levels on rainfall rate and the regional variation of the slope near the surface have not been clear yet.

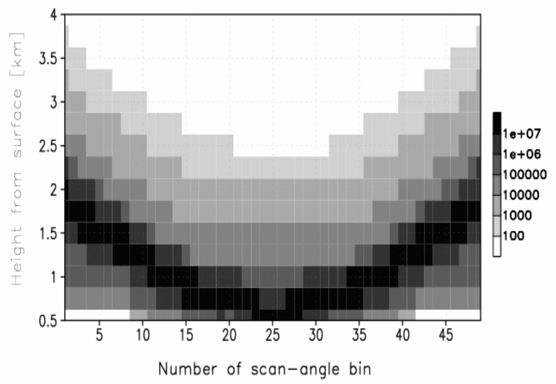

Fig. 3. The number of the lowest levels by altitude diagram for each angle bin in case of no-rain over ocean during 1998-2000.

As a comparative example, another surface rainfall was estimated by using the vertical gradient of rainfall rate near the surface at nadir. Compared with our estimates utilizing the profiling capability of TRMM PR, the difference between estimated surface rainfall and near-surface rainfall was almost same on the global average but becomes large over the tropical land and over the mid-latitudes in winter (Fig. 4). Rain at 2 km was 6.6 % smaller than that at 1 km. There is few statistics of the vertical gradient below the level of 1 km. With the collaboration of other ground-based observations, some kind of physical model is needed, considering on the regional variation of the precipitation type and the environment.

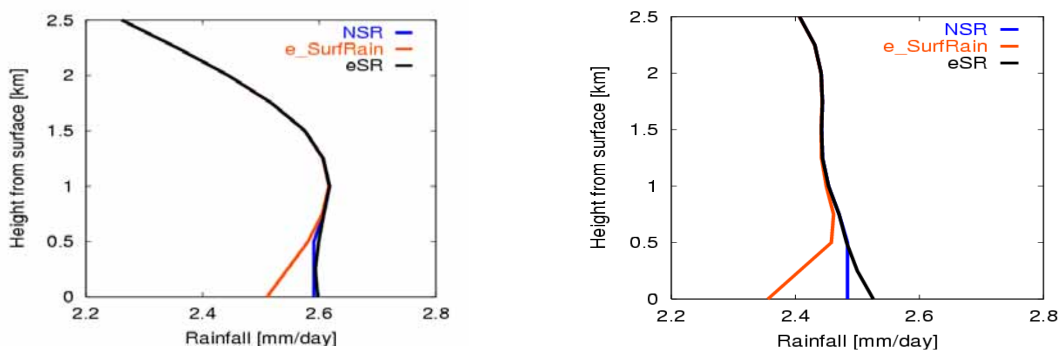

Fig. 4. Altitudinal differences of averaged rainfall over the global tropics (left) and over land (right). Dark colored lines indicate the observed and extrapolated vertical rain profiles. The other is estimated in the latest algorithm.

5. Conclusion

The long-term data accumulation enabled us to investigate more accurate rainfall at various temporal and spatial scales such as the intraseasonal and diurnal scales. Furthermore, it gives an opportunity to resolve the constituents of a particular climate regime as being congregations of various precipitation systems. The comprehensive and interdisciplinary discussions are needed for further scientific and algorithm benefits.

References

Boccippio, D. J., W. A. Petersen, and D. J. Cecil (2005), The tropical convective spectrum. PartI: Archetypal vertical structures, *J. Clim.*, *18*, 2744-2769.

Hirose, M., and K. Nakamura (2005), Spatial and diurnal variation of precipitation systems over Asia observed by the TRMM Precipitation Radar, *J. Geophys. Res.*, *110*, D05106, doi:10.1029/2004JD004815.

Nesbitt, S. W., and E. J. Zipser (2003), The diurnal cycle of rainfall and convective intensity according to three years of TRMM measurements, *J. Clim.*, *16*, 1456-1475.

Necessary paths for developing harmonized global land use classification systems

Christophe DUHAMEL

Landsis g.e.i.e. 49, boulevard de la Pétrusse L-2320 Luxembourg

Tel.: +352 26.84.78.18, E-mail: christophe.duhamel@landsis.lu

Abstract

Existing land use classification systems suffer from the proximity of a cumbersome neighbour - land cover- and from a lack of theoretical background in terms of structuring information. This paper aims at describing the possible steps which could constitute the necessary basis for a better individualisation of land use and therefore a better availability of land use data sets in the future.

1. Introduction

Land use information is of significant value for a wide range of regional and global studies (George & Nachtergaele 2002). However there is a paucity of global data sets that contain land use information and the quality of available information is variable, often presenting a confused mixture of land use and land cover categories. The existing defined land use categories are often inadequate for studies that focus on the collection of aspects of land use and on context related socio-economic data.

Development of information systems on land use has considerably increased these last years under various initiatives at international level (UN, EU), research community level and national levels. Among the various possible sets of information on land, land use is occupying a specific place but intertwined with land cover Although many initiatives have been launched in order to improve the availability and the quality of land use information the result is extremely scarce and discouraging: many announced land use datasets are just adaptations or direct copies of land cover sets. This is partly resulting from a lack of consciousness on the importance to build a sound theoretical framework together with a careful analysis of user's requirement; or partly resulting from evidence: land use data is difficult to collect into global data sets or lastly partly resulting from a lack of conceptualization of the land use domain.

In terms of harmonization of data sets, one element is fundamental in order to structure the information: the question of classification. Since classifications are not built in order to create an aesthetic effect, there is a close development between the development of scientific concepts and classifications. Classification systems are always the mirrors of the conceptualization of the domain to be investigated.

Objective of this paper will be therefore to discuss the main paths or the necessary prerequisites to propose classifications for land use answering user's requirements and taking into account capabilities of available data collection tools through an appropriate theoretical background. The presentation of the necessary elements to be taken into account for structuring land use information will follow the general concepts of classification systems embracing (adapted from Sutcliffe 1993 and Hull 1998):

- (Chapter 2) the demarcation of a universe of discourse (what is land use)
- (Chapter 3) the establishment of a classification of all land use objects in this universe
- (Chapter 4) a system for naming the groups[1] linked to the structure of the classification so-established
- (Chapter 5) the procedures for allocating any land use object to one and only one established group.

[1] Words like family, kind, membership, category, cluster, set, collection, class, group have in common that they are all members of the "genus" of class-of-objects words while at the same time they differ one from another according to their species within that genus. (Sutcliffe). They may be utilized indifferently without any impact on the system itself

2 The demarcation of a universe of discourse (what is land use)

The demarcation of the universe of discourse (in our case the domain of investigation) implies a clear identification of theoretical commitments (what is land use) and what are the subsequent land use objects.

Any given portion (Duhamel 1995) of Earth's surface can be observed and described in various ways, which may interact according to the distance separating the observer from the observation; the instruments utilized (human eye, aerial photography, satellite sensors); the way the observation is stored into information systems (lists, nomenclatures, attributes); the observation units chosen (catchment's areas, parcels, raster cells, specific objects) and the period of observation. When observing a portion of Earth's surface, several questions may arise: **what is this**, **what is it for**, why and how is it like this, was it like this before, will it stay like this in the future etc…? The two first questions (what is this, what is this for) are of interest since they are corresponding to two "easy ways" for observing Earth: land cover and 'functional" land use.

2.1 Land

Land is a term widely used throughout the world but definitions are not frequently given. The interdepartmental working group on land use planning (IDWG-LUP) at FAO proposed in 1994 the following definition*: "A delineable area of the earth's terrestrial surface, embracing all attributes of the biosphere immediately above or below this surface, including those of the near surface climate, the soil and terrain forms, the surface hydrology including shallow lakes, rivers, marshes and swamps, the near-surface sedimentary layers and associated groundwater and geohydrological reserves, the plant and animal populations, the human settlement pattern and physical results of past and present human activity (terracing, water storage or drainage structures, roads, buildings, etc.)".*

This definition has immediate practical consequences on land use: from a pragmatic point of view and considering the importance and the significance in terms of economic value of multiple-use aspects for "urban" areas, the understanding of land should also embrace uses above and below the ground level. Particular problems may be found with mine deposits, subways beneath urban areas, water resources, mushroom beds, areas used for oil extraction. In order to limit potential problems it has been recommended (Duhamel 1998) to restrict its application to reasonable cases. It is suggested to allow "urban" uses above and below the ground level (case of buildings with shops at ground level, flats and offices above, car parks below). For specific cases such as extraction activities of natural resources, it has been suggested to restrict the extension of such uses to their physical impact at ground level (oil well, entrance of mushroom beds etc.). This principle may be generalized for any kind of uses. Given the context of global information systems and the difficulty to establish clear thresholds between land and water (particularly for wetlands), it is also recommended to extend the concept of land to inland water areas and tidal flats.

Distinguishing the concepts of land cover and land use is not at all a complex task: however many information systems are confusing the two dimensions as if the same patient (land) would have two simultaneous disturbances which could not be separated. A simple solution -already described- (Duhamel 1995) is to look at **the material the objects are made of (land cover)** and **the function they serve (land use)**. In order to base the discussion on agreed concepts, a short reminder on the concepts of land cover and land use is given.

2.2 Land cover

Land cover, as previously mentioned, corresponds to a physical description of land. The definition proposed, adapted from (Di Gregorio & Jansen 1997) is: *the observed physical cover of the earth's surface* This description enables various biophysical categories to be distinguished - basically, areas of vegetation (trees, bushes, fields, lawns), bare soil and hard surfaces (rocks, buildings) and wet areas/bodies of water (sheets of water and watercourses, wetlands). In most cases, land cover is directly detectable by human observation or less directly from remote sensing. A very useful comparison can be made with approaches characterizing commodities where objects are just described according to the material they are made of, corresponding to the physical aspect of land Cover,

2.3 Land use

For land use, various approaches are proposed into the literature. Two main "schools" may be distinguished (Duhamel 1998). The first one, termed functional corresponds to *the description of land in terms of its socio-economic purpose* (agricultural, residential, forestry etc...): this will be the approach referred as land use in this paper. This approach is extremely easy to handle since it has direct correspondences into widely utilized statistical nomenclatures such as ISIC. The second one, termed sequential (Stomph & Fresco 1991) has been particularly developed for agricultural purposes: *a series of operations on land, carried out by humans, with the intention to obtain products and/or benefits through using* *land resources.* Without entering into the details of this approach, the sequential approach should be only treated if necessary (and possible) as a modular approach below the agricultural function

2.4 Land cover vs Land use

Distinguishing between land cover and land use is in principle quite easy but not often reflected into the existing systems. One major issue to be dealt with is that land cover and land use are often intertwined. It is sometimes possible (Duhamel 1998) to determine the functional aspect (land use) from the physical aspect (land cover). A parcel of land covered by a field of wheat can reasonably be associated with agricultural use. Similarly, it is possible to infer physical aspects from functional aspects. An area used for forestry purpose could reasonably be assumed to correspond to a "tree"-type class. However one physical class may correspond to a large number of functional classes. For example, grassland may correspond to a lawn in a town, an airport runway, a sown meadow, rough pasture, a golf course—or even a church roof in Iceland. Conversely, one and the same functional class may correspond to several physical classes: for example, a residential area consists of lawns, buildings, tarmac roads, trees, and bare soil.

Contrary to land cover, land use is difficult to "observe". For example, it is often difficult to decide if grasslands are used or not for agricultural purposes. The information coming from the source of observation may not be sufficient and may require additional information or existing maps/statistics or characteristics on the ground indicating the use (in the example of grasslands mentioned above: the presence or absence of animals, the presence or absence of elements indicating that animals were grazing). Inference from land cover is therefore a possible (but not sufficient) solution when- global data sets on land cover may be populated easily and regularly. Conversely land use data sets require enormous investments when complete coverage is desired.

Even if it is difficult to justify it when analyzing both user needs and the possible costs of simultaneously acquiring, using, and managing data obtained through separate approaches, there are strong methodological and technical arguments in favor of systematic separation of land cover and land use. The importance of the knowledge for the two aspects may be illustrated with one example (Table 1) adapted from Lund 1998.

Table 1: Observation of a portion of land at 4 different dates

Table 1	Date1	Date2	Date3	Date4
LAND COVER	TREES (Chestnut trees)	TREES (Chestnut trees)	TREES (Chestnut trees)	TREES (Chestnut trees)
LAND USE	Forestry use (Timber)	Agricultural use (Chestnut production)	Agricultural use (Grazing area)	Forestry use (Timber)

The observation of the land cover dimension could lead to a unique interpretation of no visible change throughout the whole period considered. Conversely, the observation of land use sequences could be rapidly interpreted as a deforestation sequence between Date 1 and Date 2 and afforestation between Date 3 and Date 4. It is now easy to understand the difficulties to infer land use from land cover in some cases. With a combined system registering separately the two dimensions, the simultaneous recording of both land cover and land use hampers any false interpretation. It also brings a high richness in terms of information content.

2.5 Land use objects and observation units

As geographical information, land use data has also to deal with basic theoretical issues such as the question of land use objects, land use observation units and the influence of scale on observation and data collection.

The meaning of land use object is a complex problem: the description (categorical classification) of a part of the earth's surface pre-supposes that the area is clearly defined in space. Objects are easily identifiable if the spaces are plots of farmland or built-up areas, as they have physical boundaries (enclosures, hedges, fences, clear division between crops).

One of the typical problems encountered is the problem of mixed objects. Three types of mixtures exist on land:

- Mixtures "by juxtaposition" where many objects may be observed simultaneously within a portion of land: for example mixed crops on a same parcel or orchards utilized for grazing. In general, a partition into basic objects is recommended or, if not appropriate, the application of a pro-rata rule as applied in agricultural statistics for intercropping. Unfortunately the general tendency is to create mixed classes, leading in general to a profusion of categories.
- Mixtures "by superposition" are to be found for example in buildings, where floors could have a different socio-economic purpose: a dominant use approach is recommended.

- Temporal mixtures when for a specific period of observation (agricultural campaign) there is a succession of crops or succession of bare soils and crops on the same parcel: changes are to e observed in terms of land cover, less frequently in terms of land use.

It is also important to address the issue of observation units. One observation unit may be an aggregate of objects. Conversely, an object could be divided into various observation units. For example, an observation unit can be a parcel composed of two different crops (mixture by juxtaposition). A big parcel of wheat may be observed through several units of observation (points in a grid system, cells in a raster system). The choice of observation units is important since it has impacts on the way the information systems will be built: impacts on the reproducibility (and therefore the reliability) of the observation over time.

2.6 Collecting data on land use

Two main approaches are considered for land use: geographic approaches (mapping) and statistical approaches (sample surveys)

Through **mapping** approaches, the coverage of the territory is exhaustive. Main source of information is generally photo-interpretation or processing of aerial photographs and earth observation data together with ground truth. Choice of observation units is driven by technical constraints: the scale of observation (you observe what you can) and the scale of restitution of information (you map what you can) leading to the concept of minimum mapable area. According to scale, identification of objects will not be the same: what you observe and map at 1:10.000, is different from what you observe and map at 1:250,000. There is no doubt (Eiden 2001) that remote sensing data represent a data source which contributes to a deeper understanding of processes on the earth's surface and enables map production up to scales of 1:5.000.. It is still important to remind that remote sensing images capture only land cover, i.e. the physical features. Although one can interfere from some land cover categories to land use, remote sensing images are not really suitable for this aim.

Suitable alternative approaches to acquire land use data are **area frame surveys**. Statistical surveys provide information on samples from a population. Sampling theory is applied so that inference about the whole area can be made. The sample is made of a set of area units: the statistical units may be of different size (points, areas) or different shape (squares, circles). One significant advantage of sampling approaches is the possibility of being independent of the difficult problem of observation units: the population (whole territory) may be divided up into a grid on a systematic basis; each area unit thus obtained being a statistical unit (observation unit) of the same size and same shape. These approaches are commonly used in agricultural statistics and also widely applied in ecological monitoring surveys (e.g. Countryside Survey in United Kingdom).

A good illustration of the capabilities of area frame sampling surveys is given by the LUCAS project launched in 2000 by the Directorate General of Agriculture of the European Commission and Eurostat (the Statistical Office of the European Communities). Objectives of the system are to carry out an area-frame survey based on points in order to collect information on land cover and land use, to establish a common sampling base among Member States and to extend the scope of the survey from the normal agricultural domain to aspects relating to the environment, multi-use, landscape and sustainable development. A first survey was conducted in the 15 EU member States in 2001-2002, followed by a new survey in 2003, including three new EU Accessing Countries. In 2006, the exercise will be repeated in 23 countries with a revised methodology (initially an unstratified two phase design, now a two-phase sampling of unclustered points with stratification):

- The survey will be based on a systematic sample (base sample) of around 4.000.000 points defined through a 1-km grid which is covering the entire European Union, the regular grid being intersected with boundaries in order to extract points on the EU territory and allocate them by country.

- The LUCAS master sample is a subset of the base sample. It corresponds to a 2-km grid and consists of around 1,000,000 points.

- Each point of the master sample is photo-interpreted (recent ortho-photos or, when ortho-photos were not available, on satellite imagery) in order to obtain a stratification of land cover

- From the stratified master sample, a sub-sample of points is extracted to be classified by field visit according to a full land cover and land use classification system (around 250.000 points – field sample).

- Surveyors will be collecting the land cover and land use information on the field sample. In addition, on a 250 m straight line (= transect) in an easterly direction from the point, land cover changes will be registered and landscape pictures taken from each point.

- In addition to the field work, a separate survey ("double-blind survey") on 5% of points will be carried out by independent surveyors.

Due to the fact that only parts of the territory are observed (in that specific case, just points), data can be gathered at a very detailed level and results can be extrapolated to larger reference zones (EU level or national level for big countries). Moreover, the implementation of such area frame sampling is relatively simple and results may be made available rapidly after the survey.

Compared to exhaustive mapping where, in principle, only land cover may be directly collected, sample surveys may provide rapid results with accuracy estimates on both land cover and land Use, thus enabling periodic (annual or seasonal) surveys. Another advantage is the possibility to utilize the sample base for conducting specific surveys or incorporating specific issues such as noise, erosion, landscape. .

2.7 Additional prerequisites before classifying land use

Independently of the general rules that should govern the construction of classification systems (see chapter 3), specific constraints due to the intrinsic nature of geographic data are to be taken into account. Two principles of consistency have been identified (Duhamel 1995): spatial consistency (classification systems should be designed in a way to allow compatibility of results between various geographical locations), temporal consistency (observation should be recorded at time of observation[2] in order to be able to measure changes between two stocks, the classification system should avoid classes taking into account previous or future land uses). It is also important to ensure the independence of the system from the data collection tools (a lot of systems have been built on the basis of the technical capacities of the tools, e.g. remote sensing)

3. The establishment of a classification of all the land use objects

Since there is generally no natural or best classification of a set of objects as such (Spärck Jones 1970), the elaboration of a classification requires either formal criteria of goodness of fit, or, if a classification is required for a purpose, a precise statement of that purpose. There is no easy way to decide whether an attribute is the most important criteria to utilize when classifying objects: it simply depends of the purpose of the classification. It is also important to accept (Hjörland 2002) working at the level of preciseness that we have access to, i.e. this is the condition under which we have to work and we cannot change this by requiring something that is not available to us. This does not however change the fundamental insight (Spärck Jones 1970): we have to base the classifications on knowledge about their purposes, to satisfy both the internal criteria of classification and the external requirements of the users.

The establishment of a classification of all the land use objects has to result into the organisation of sub-classes of the domain through a (hierarchical) series of nested categories that have been arranged to show relationships to one another. Significant attributes of land use objects should be chosen taking into account that any set of land use objects may be unfortunately classified in an unlimited number of ways according to our language and mental conceptual structures. Any proposed land use classification system is conceptual, describing selected aspects of the real world: the same reality might well be described according to several classifications (Duprat 1972). Groups of land use objects have therefore to be described through the selection of shared characteristics that make the members of each group similar to one another and unlike members of other groups. Each of the successive partitions means that "objective" characteristics have been taken into consideration, and implies a conscious choice. Criteria of land use classification are therefore deeply related to relevance: it is not the inherent qualities of the land use objects that determine the criteria of classification.

It is also important to remind that classification is both an information-losing process and an information gaining process (Spärck Jones, 1970). Information is lost because the particular relationships among the objects are ignored in detail but gains may be found in the sense that it is made explicit that some objects are alike. Any member of a class can be treated as if it possessed some or all properties of the group. The fact that an object is a member of a class enables to make an inference about it. The purpose for which the classification is designed necessarily shapes its structure and content, this is why each user, in general, builds an individual classification adapted to specific needs: spontaneous development of classifications therefore leads inevitably to incompatibility: this is frequent for land use

[2] This is a strong argument against sequential approaches of land use requiring a window of observation difficult to implement and to harmonize

classifications. Two main schools of classification may be described: the classical theory, based on properties (dating back to Aristotle) and the prototype theory (Kühn 1970)

3.1 Classifications based on properties

The classical theory assumes that land use objects would be allocated according to a set of individually necessary and jointly sufficient properties. An important consequence is that although a class is agreed upon, the identification of class and non-class members need not always to be based on the same characteristics or set of characteristics.

Another important point is also to consider that links and relations between objects and/or groups are linked through a complex net of relationships, likenesses, affinities or neighborhoods. In general, this net is transformed into a tree, some links considered as important or significant have to be chosen according to a particular point of view. These links or relations are of different types in land cover and land use (Wüster 1971): logical links (industrial: chemical, iron transformation, car industry …); ontological links = whole and part (residential area - house); co-ordination links (maize-wheat); time links (bare soil - crop). These links and relations may be combined and presented from broader to narrower concepts. To a certain extent links between land cover are mainly ontological (whole-and-part: forest > stand > tree) while land use links are mainly logical (industrial: chemical, iron transformation etc...). Two main approaches may be highlighted as part of the classical approach: top-down tree approaches and classifier approaches.

The most known solution is a **top-down tree**. Many nomenclatures are built following this a-priori approach: the domain of study is divided into categories and sub-categories, according to certain objectives and purposes. The method has strong disadvantages: the tree is a rigid structure leading to difficulties if modifications are to be made without alteration to the former structure of information. The only possibility for modifying is creating more detailed levels on the basis of the categories already existing (in this case when the existing tree is no more adapted to the needs, additional levels do not solve the problem). Other disadvantages are the unequalled development of the sectors and the exaggerated importance of aggregated concepts created from the first partition

Another approach is to develop a tool consisting of a **combinatory system** applied on a common basis. This basis is just a set of necessary characteristics to describe the objects. These characteristics, once identified and defined uniformly (Ekholm 1996) allow, through combinations, the definition of the objects and the grouping of the objects for all possible systems. Characters may have different "expressions": character states and may be used in the decision rule of classifying objects into a given classification system In order to avoid the problem of hierarchy of classifiers, it is recommended to develop, instead of hierarchical and rigid schemes, a "flat" combinatory system (or faceted system) applied on a common basis of classifiers of equal weight, this basis just being a set of necessary characteristics to the description of the objects (Duhamel 1995).

3.2 Classifications based on prototypes

The prototype theory proposes that land use objects in a similarity class need bear no more than a family resemblance to their fellows (Kühn 1970), and hence that the concepts corresponding to these similarity classes are family resemblance concepts. This method aims at bringing out empirically from different existing classification systems some prototypes/kernels which will set up the beginning of main categories. It implies in general the gathering of existing classification systems on the domains to be considered and their confrontation and analysis in order to answer the different user requirements. This method has the objective to compare existing systems assuming that major aggregates could be common for many users or approaches. General aggregates, commonly accepted through various nomenclatures, may constitute the core (kernels/prototypes) and items which may be allocated to different aggregates according to the different classification systems constitute the margins. The number of nomenclatures to consider is however to be limited since the more classifications are taken into account, the fewer kernels will be identified, since the probability of discovering objects not belonging to the core increases as different points of view are encountered.

4. The system for naming and describing land use groups

A system for naming and describing land use groups linked to the structure of the classification so-established has also to be clearly established. Six main basic components have been described (Duhamel 2001):

- principle of completeness, a class must be found for any object to be classified: the union of all classes in the first grouping must equal the original collection)
- absence of overlap: anything can be classified in only one class, all classes of the same rank must be pair-wise disjoint and an object may not belong to more than one class of the same rank
- general rules of interpretation (cases of overlap, ontological or logical relations between objects, problems of mixtures)
- rules concerning the elaboration of headings and labels (kernel method of description, definitions by extension and intension, boundaries problems, cross-references of exclusions and inclusions)

- elaboration of index of objects
- principles of coding

An example of a system for naming and describing groups may be found into the LUCAS system proposed by the European Commission. An example of the textual description of a land cover class and its links with land use is given herewith. Principles of completeness and absence of overlap are easily met through definitions by intension (the textual definition of the class) and by extension (list of possible objects being part of the class), including boundaries rules (inclusions and exclusions), coding and relationships between that land cover class and land uses. Pictures of prototypes of the class are also provided to the surveyor in order to facilitate the identification and the allocation to the class.

Extract from LUCAS land cover – land use nomenclature

D SHRUBLAND

Areas dominated (more than 20% of the surface) by shrubs and low woody plants generally below 5 meters of height. It may include sparsely occurring trees within a limit of a tree-crown area density of 10%

D01 Shrubland with sparse tree cover

Areas dominated (more than 20% of the surface) by shrubs and low woody plants generally below 5 meters of height, including sparsely occurring trees within a limit of a tree-crown area density between 5 and 10 %

this class includes:

Scrub land (pines, rhododendrons, maquis, matorral and deciduous thickets)

Heathland with gorse, heather or broom

this class excludes:

Shrubland where tree cover is more than 10% (C)
Shrub-like crops: orchards, vineyards in production (B7-B8))

Principles of observation

Extended window of observation

Links with Land Use (U)

D01 ➢ U11	Agricultural use: grazing
D01 ➢ U12	Forestry (Wood production)
D01 ➢ U36x	Leisure areas
D01 ➢ U40 Wooded areas not utilized	
D01 ➢ U50 Wetland	

5. The procedures for allocating any land use object to a class

This corresponds to the procedures for allocating any land use object to one and only one previously classified and named class. The approaches for allocating any land use object to a group are directly linked with the types of classification system built. In the case of classifier approaches, objects will be systematically matched with candidate classes through a predefined set of inherent traits utilizing for example a decision tree. In other cases (top-down trees or prototypes) the process is theoretically more empirical since the link between the object and the class has to deal with an intermediate level: the concept. This process, described theoretically through the so-called meaning triangle of Richards-Ogden (Duhamel 1996), aims at establishing a link between the object and the class: this is why it is fundamental to have made available a textual part of the classification following the principles described into the previous chapter (in particular the definitions by intension and extension). Fortunately, in many cases, an object may be immediately identified and the allocation to a class may be done directly or through the utilization of an index of objects (a good example of index may be found into the UK Land use database).

6. Conclusions

Developing a land use classification system needs therefore (it was the objective of this paper) to be **systematic**:

- the strict application of a series of precise procedures should ensure -through an **appropriate framework**- that any land use objects may be classified into an appropriate class and should allow a reduction of the initial population of objects into a set of nested categories.

However two **pragmatic** issues remain to be dealt with:

- **the purpose of the classification**
  it is a strong guideline for the construction of a classification system: user's needs have to be strongly reflected (sometimes a real challenge when policy and decision makers have to express their needs in terms of data at various geographic levels (Croi 2001) and existing classification and information systems should be taken into account.

- **the scarce opportunities to collect exhaustive data on land use on large areas**
  the increasing availability of remote sensing data has unfortunately low concrete impact on land use data availability: if inference from land cover is sometimes possible, a direct observation on the ground remains invaluable. This is one of the most interesting aspects (and paradox) of land use information: making available detailed and accurate information on land use is only possible when limited portions of earth can be observed (statistical approaches); conversely detailed and exhaustive information on land cover is easily available at global level (mapping approaches).

References

CROI W. (2001) Information requirements – Data specification. Manual of concepts on land cover and land use information systems p.p. 53-59, Eurostat, Luxembourg
DI GREGORIO A. & JANSEN L.J.M (1997), A New Concept for a Land Cover Classification System. Earth Observation and Environmental Classification, 1997, Conference Proceedings, 13-16 October 1997, Alexandria, Egypt, 10p.p.
DI GREGORIO A. & JANSEN L.J.M (1998), FAO Land Cover Classification System: Classification Concepts and User Manual, Nairobi, Rome, 1998, FAO.
DUHAMEL C. (1995), Statistical framework for land cover and land use information systems (CLUSTERS), Eurostat Remote sensing and statistics programme, Luxembourg 28 p.p
DUHAMEL C. (1997), Towards a generative system of land cover and land use nomenclatures. Development of a Harmonized Framework for Multi-Purpose Land Cover/Land Use Information Systems derived from Earth Observation Data. European Commission, CESD-Communautaire, Luxembourg 52 p.p..
DUHAMEL C. (1998), First approximation of a reference land use classification, FAO, Rome, 31 p.p.
DUHAMEL C. **& VIDAL C**. (1999), Objectives, tools and nomenclatures. Proceedings of the Eurostat seminar on Land cover and Land use information systems for European policy needs, Luxembourg
DUHAMEL C (2000), System for classifying Land cover and land Use of LUCAS project in the E.U., Eurostat-Landsis g.e.i.e., Luxembourg 50p.p.
DUHAMEL C. (2001), Definition of general terms on land cover and land use, Classification Systems. Manual of concepts on land cover and land use information systems p.p. 11-28, Eurostat, Luxembourg
DUHAMEL C. (2003), Land use and land cover including their classification. EOLSS (Encyclopaedia of Life Support Systems), UNESCO, Paris
DUPRAT H. (1972) Les conditions linguistiques du transfert technologique
EIDEN G. (2001) Data collection tools. Manual of concepts on land cover and land use information systems p.p. 30-52, Eurostat, Luxembourg
FAO (1994), Interdepartmental Working Group on Land Use Planning.
FEGER, H. (2001), Classification: Conceptions in the social sciences. International Encyclopaedia of the Social and Behavioural Sciences Vol 3, pp. 1966-1973.
GEORGE. H. & NACHTERGAELE F.O. (2002), Land use data, Review paper on status of land use data, FAO, Rome, 12 p.p.
HJORLAND B (2002), Epistemology and the socio-cognitive perspective in information science. Journal of the American Society for Information Science and technology Vol 53 Nº4 pp. 257-270
HJORLAND B. & PEDERSEN K.N. (2005), A substantive theory of classification for information retrieval. Journal of documentation Vol 61 Nº5 pp. 582-597, Emerald Group
HULL, D.L. (1998), Taxonomy. Routledge Encyclopaedia of Philosophy, Version 1.0, London: Routledge
ISIC. Rev 3 (1996), International Standard Industrial Classification for all Economic Activities, UN Statistics Division, 1996.

KÜHN, T.S. (1962, 1970, 1996), The structure of Scientific Revolutions, University of Chicago Press, Chicago
SIMPSON G.G (1961), Principles of Animal Taxonomy, New York, Columbia University Press.
SOKAL R.R. & SNEATH P.H.A (1974), Numerical Taxonomy: the Principles and practice of numerical Classification, W.H. Freeman and Company, San Francisco.
SPÄRCK JONES K. (1970), Some thoughts on classification for retrieval. Journal of documentation Vol 26 Nº2 pp. 89-101, Emerald Group
STOMPH T.J. & FRESCO L.O. (1991), Procedure and database for the Description and Analysis of Agriculture Land Use, FAO, Rome, Draft 76 p.p.
SUTCLIFFE J.P. (1993) Concept, class and category in the tradition of Aristotle. Categories and concepts: theoretical views and inductive data analysis Van Mecheler et al. (eds) Academic press, London

Harmonisation of land-use class sets to facilitate compatibility and comparability of data across space and time

Louisa J.M. Jansen
Land/natural resources consultant, Via Girolamo Dandini 21, 00154 Rome, Italy
Tel.: +39-065757719, E-mail: Louisa.Jansen@tin.it

Abstract

Harmonisation of land-use class sets should consider both space and time, as the objective should include harmonisation of land-use change in order to analyse environmental processes and problems. Existing systems make only a limited contribution to data harmonisation and data standardisation as they contain many inconsistencies in the adherence to the fundamental principles of classification and use a variety of basic units of measurement, in addition to the lack of agreement on the definition of land use. Though the meaning of land use varies among sectors, the set of key parameters used is limited. Analysis of major existing class sets reveals that two parameters suffice: function that describes land use in an economic context and activity that is defined as the combination of actions resulting in a certain type of product.
An example of land-use harmonisation in Albania illustrates how the creation of a reference system based upon the principles of classification, using the synergy between classification and information technology concepts and based upon the function and activity parameters can facilitate harmonisation between land-use class sets in parallel to achieving land-use change harmonisation. Comparison with remotely sensed based land-cover related land-use data illustrates that land use contains many aspects that go beyond land cover. Land-use change operates over a range of scales in space and time and analysis at different levels of data is necessary in order to detect the patterns at the different data levels.
The way forward to harmonisation of land-use class sets is adoption of a parametric approach. Further research is necessary to define quantitative measures for the harmonisation result at class level and between two class sets.

Keywords: Land use; Land-use change; Classification; Data harmonisation; Data standardisation.

1. Introduction

Land-use change knowledge has become increasingly important in order to analyse environmental processes and problems, such as uncontrolled urban development, deteriorating environmental quality, loss of prime agricultural lands, expansion of agriculture into areas that comprise either fragile ecosystems (e.g., wetlands and steep lands) or a high value with respect to biodiversity (e.g., humid tropical forests) or areas with a high incidence of diseases (e.g., malaria, river blindness). These processes and problems must be understood if living conditions and standards are to be improved or maintained at current levels (Anderson et al., 1976; Dumanski and Pieri, 2000). Land-use change, as one of the main driving forces of (global) environmental change, is central to sustainable development (Meyer and Turner, 1994; Walker et al., 1997; Walker, 1998; Lambin et al., 2000). It is, therefore, essential to have detailed and in-depth knowledge of not only land-use processes and problems but also of land uses. Such information is required at multiple scales as support at the local, regional, state and cross-border co-operation levels.

Nowadays emphasis is shifting from static land-use data collection towards more dynamic environmental modelling in order to understand the past, monitor the present situation and to predict future trajectories (Lambin et al., 2000; McConnell and Moran, 2001; Dolman et al., 2003). This implies the importance to re-examine existing land-use data sets and attempt to harmonise them to make comparisons within and between countries and to compile time series with which to analyse the change dynamics and detect trends. Data harmonisation will be required as it is unrealistic to work only with new standardised class sets, with major financial and intellectual investments having been made in existing class sets and survey programmes that use established methods of classification (Wyatt et al., 1997; Wyatt and Gerard, 2001).

The Land Use Cover Change (LUCC) programme element of the International Geosphere-Biosphere Programme (IGBP) and International Human Dimensions Programme on Global Change (IHDP) mentioned in their science/research plan (Turner et al., 1995) that classification and data are a cross-cutting integrating activity for which data availability and data quality need to be analysed and a classification structure suitable for various requirements need to be devised. In addition, McConnell and Moran (2001) highlight two key issues:

- Both space and time considerations are essential for making land-use data compatible and hence comparable.
- Harmonisation of land-use classifications includes harmonisation of land-use *change,* as we need to understand land-use change processes for decision making as explained above.

Therefore, any discussion on harmonisation of land-use class sets should address not only existing or proposed classifications but also data quality, space and time dimensions and land-use change.

In this paper the harmonisation of land-use class sets, or correspondence between land-use class sets, will emphasize the semantic aspect of class sets consisting of the class definitions as these imply the parameters used in the formation of classes. Class descriptions contribute to the definition of boundary conditions that should be applied unequivocally and consistently when establishing correspondence between classes belonging to different class sets in order to avoid errors in data interpretation. The level of confidence with which such class correspondence is established is highest when the same parameters have been applied; differences in the applied parameters, and thus in boundary conditions, produce lower confidence levels. Complete correspondence is not always obtainable when harmonising data, thus there is a need to establish rules in order to reach the highest level of confidence possible.

2. Definition of the domain of interest

2.1 Land use

An international agreement on the definition and classification of land use does not exist though many attempts have been made (Guttenberg, 1965; IGU, 1976; Kostrowicki, 1977 and 1980; UNEP/FAO, 1994; Baulies and Szejwach, 1998; Duhamel, 1998; McConnell and Moran, 2001; Jansen and Di Gregorio, 2002). Consequently, a common terminology is lacking. The term “land use” has different meanings across disciplines and, as a result, implies a set of mostly unidentified parameters. These different perspectives on land use are, however, all valid. In the context of this paper land use is defined as “*the type of human activity taking place at or near the surface*” (Cihlar and Jansen, 2001).

Land use is determined by natural, economic, institutional, cultural and legal factors. In general, possible land uses are limited by biophysical constraints. These include climate, topography, soils and the geological substrate, presence or availability of water and the type of vegetation. Agricultural practices differ from one region to another and different types of land uses are practised on the same type of land in different areas, depending on the history, local traditions and way of life, apart from the biophysical constraints (Cihlar and Jansen, 2001). The location of an area with respect to other types of land uses, such as residential and industrial areas, is also an important factor (e.g., the location of a commune close to main urban centres and its proximity to, for example, an airport) (Jansen, 2003). Economic incentives as part of policy (e.g., the EU Common Agricultural Policy) can affect land-use patterns.

2.2 Classification

Classification is defined as "*the ordering or arrangement of objects into groups or sets on the basis of relationships. These relationships can be based upon observable or inferred properties*" (Sokal, 1974). Thus, classification denotes a process. The term "classification" embodies two meanings (Duhamel, 1998): (1) establishment of groupings of all objects in a given field (according to Sokal's definition); and (2) using the established groupings in order to decide the membership status of other objects (e.g., in remote sensing the imagery is used for the identification process of objects). The term "classification system" includes not only the definition of the domain investigated and the classification process of the objects, but also a considered set of principles, or methodology, to assign individual land uses to land-use classes and these are arranged according to a set of adopted rules. Furthermore, it includes information for evaluating the reliability of assignment of objects to the various classes. Not only the quality of the data should be documented, but also the quality of the harmonisation.

Classifying all the objects in the domain of interest requires some basic principles, which have been described in detail elsewhere (e.g., EUROSTAT, 1991; UNEP/FAO, 1994; FAO, 1997; LANES, 1998; Duhamel, 1998; Jansen and Di Gregorio, 1998; Di Gregorio and Jansen, 2000). The key principles are:

- Completeness and absence of overlap of classes;
- Existence of definitions and explanatory notes;
- Existence of an index of objects;
- Spatial and temporal consistency; and
- Independence from scale and data collection tools.

Since many existing classifications and map legends do adhere only in part to these principles, as will be demonstrated later on, the use of the term "class sets" has been preferred in this paper.

2.3 Data standardisation and data harmonisation

Data standardisation is defined as "*the use of a single standard basis for classification of a specific subject*", whereas data harmonisation is defined as "*the intercomparison of data collected or organised using different classifications dealing with the same subject matter*" (McConnell and Moran, 2001). The understanding between data standardisation and data harmonisation is fundamental:

- Data standardisation will allow direct comparison of class sets but would disregard the financial and intellectual investments made in established methods and data sets; and
- Data harmonisation will allow countries and institutions to continue to use existing data systems and classifications but when definitions are imprecise, ambiguous or absent problems arise. Moreover, if many class sets are involved the number of pair-wise class combinations becomes excessive because comparison of n data sets requires $n(n-1)/2$ comparisons to be made.

The problem of excessive pair-wise class combinations can be resolved by developing a common reference system. Correspondence between classes may then be inferred from the explicit record of how each class relates to the reference system. The advantage is that translation of class sets into the reference system would be required just once. In addition, such a reference system would be well suited to form the basis for a generally accepted classification that could be promoted as future standard. At the same time a reference system could form the sound basis for a data model for use in geo-databases needed to manage information on land (Wyatt et al., 1993; McConnell and Moran, 2001; Jansen et al., 2005b).

3. Previous attempts at land-use harmonisation and standardisation

An important effort for establishment of an international recognised statistical system was made by the United Nations Statistical Division with the publication of the International Standard Classification of all Economic Activities (ISIC) in 1948 with three major revisions in 1958, 1968 and 1989 (UN, 1989).

The International Geographic Union established the Commission on World Land-Use Survey in 1949 (IGU, 1976). A legend for a world map at a scale of 1:1,000,000 was developed combining land-cover characteristics with function. This scale was quickly abandoned in favour of national land-use surveys at much larger scales in Great Britain, Italy, Japan, Malaysia, Poland and Sri Lanka. Furthermore, the IGU established the Commission on Agricultural Typology that tried in the period 1964-1976 to produce a system dedicated to agriculture. The work of this Commission was discontinued after 1976 though some of its members continued and completed the Types of Agriculture Map of Europe in 1983 (Kostrowicki, 1977, 1982 and 1984). Contacts with FAO were made in the early 1970s when the interest in a world agricultural classification increased due to the growing food crisis. In 1983, Kostrowicki proposed a land-use classification system, including non-agricultural land uses, which was a prime mover behind a proposal to UNESCO in 1987 for a world land-use map (Kostrowicki, 1980, 1983a and 1983b). However, nothing came of it.

The American Society of Planning Officials identified different dimensions of land use at an early stage (Guttenberg, 1959 and 1965). Guttenberg (1965) also identified different "modes" for classification: referential, appraisive and prescriptive (Figure 1). However, most of the existing classifications remain in the referential mode, as it is the most neutral one, and frequently deal with observable characteristics, such as land cover and actual activity, and derived characteristics, such as function and legal aspects. The appraisive mode casts land use in the light of social interests and values that differ according to local prevailing customs.

Insert Figure 1.

In the period 1969-1971, a study was made by the Commission on Geographic Applications of Remote Sensing of the Association of American Geographers. The results were published in 1971 by Anderson and further elaborated in 1976 (Anderson et al., 1976). This remote sensing driven classification was based upon the World Land-Use Survey system (Paludan, 1976) and evolved in the period of the first LANDSAT launch. The system represents the traditional subdivision in land-use terminology for built-up and agricultural lands, and land-cover terminology for natural vegetation, water, snow and ice.

The Economic Commission for Europe of the United Nations proposed a Standard International Classification of Land Use that would allow comparison of national land-use statistics (ECE-UN, 1989). However, this is a mixture of land-cover and land-use terminology and the classes are not exhaustive.

The interest in reviewing and updating the U.S. Standard Land-Use Coding Manual (Urban Renewal Administration, 1965) led to the initiative of the Land-Based Classification Standards (LBCS) project, co-ordinated by the Research Department of the American Planning Association in corporation with several U.S. departments and agencies (APA, 1999). This effort is based upon recognition of various categories in which land use is traditionally classified: activity, function, structure-type, site development character and ownership. These categories have each there own set of characteristics and classification takes place across these multiple categories. The effort addresses many of the problems that previous systems had but remains at the level of a system divided into several descriptive classes. The choice of categories may be disputed.

The Land Utilization Type (LUT), as developed by FAO in the Framework for Land Evaluation (FAO, 1976) and in the Guidelines for Land-Use Planning (FAO, 1984), has been widely used as a generalised description of agricultural land use in terms of inputs, two levels only, and outputs for which suitability could only be defined imprecisely. This concept was based upon a shortened list of the land-use variables identified by the IGU, the difference being the application of a qualitative land-use description in the Framework. The concept was too imprecise to be applied at farm level or for production planning, it contained only one (plot) level and reflected more a potential than an actual land-use class, while being qualitative in nature. One should note, though, that this concept was adapted to the requirements of a land evaluation system and as such, it has been used in numerous regional or district crop suitability, capability and pre-feasibility studies (pers. comm. F.O. Nachtergaele, FAO). The matching of potential agricultural land uses with the land through a series of decisions and ratings yielded into a quite complicated expert system, thus the methodology became the reverse of being transparent. In the late 1980s, at FAO attempts were undertaken to improve the LUT concept. The matching of precisely defined qualities and characteristics of the land unit with broadly, usually qualitative LUTs resulted in the limited use of the quantitative land resource data. A series of FAO commissioned studies was initiated as well as collaboration with UNEP (Remmelzwaal, 1989; Adamec, 1992; Mücher et al., 1993; UNEP/FAO, 1994; ITC/FAO/WAU, 1996; Wyatt et al., 1998). Adamec (1992) was the first to define the land-use type as "*a series (or sequence) of operations (or activities) carried out (or undertaken) to produce (or harvest) products or benefits for consumption or sale*" but he recognised at the same time the difficulty to apply individual operations or their sequence and dates of execution as parameters plus the inputs already employed. Nonetheless, this definition was adopted by the ITC/FAO/WAU effort resulting in the Land-Use Database (1996). In this database, the primarily agricultural land-use class is independent from scale, the basic unit being the plot. The database permits user-defined hierarchical structures, comparison, and a number of standardised parameters are included. However, the database allows users to add or change parameters and definitions along with the order of parameters to fit a specific aim. If the objective of classification is a contribution to data harmonisation and data standardisation, another approach should be selected. The study by Wyatt et al. (1998) was an effort at outlining the parameters to be used for globally applicable definition of land uses. The idea of analysis of existing systems in order to extract the set of parameters to be used for building a reference system would have been valid if existing classifications were used. However, the analysis was based upon a number of legends, hence indicating gaps in the completeness of land-use classes and parameters used. Duhamel (1998) clearly identified that the above-mentioned studies and some selected national class sets suffer from the lack of systematic analysis of what defines land use, in addition to the insufficient adherence to the fundamental principles of classification mentioned earlier (Table 1).

Insert Table 1.

The current view of the way forward is to promote a *parametric approach* to classification. The explicit use of quantitative parameters will facilitate harmonisation between class sets if the same set of parameters is used. In many existing class sets one will find (Jansen and Di Gregorio, 2002):

- Inconsistent application of land-cover or land-use parameters, i.e. land-cover parameters are being used to distinguish land uses and vice versa;
- Inconsistent use of parameters at same level of classification, i.e. in one category a certain parameter is used and in a related category a completely different one is used;
- Use of different parameters between classes, i.e. for subdivision of a class into three subclasses more than one parameter is used; and
- Use of non-inherent characteristics, i.e. using characteristics that are not related to the subject but describe, for instance, its environment (e.g., climate, physiography, altitude from a DEM, etc.).

Although the underlying reasons for making subdivisions based upon different parameters may be valid, they show that parameters do not always have the same weight in making distinctions. Such decisions are usually not well-documented in the accompanying reports of the class sets. This hampers harmonisation of class sets, as re-interpretations of not well-documented decisions are likely to differ between persons within one country and between countries. The actual class sets make an insufficient contribution to data harmonisation and standardisation. Efforts to increase harmonisation and standardisation do not necessarily lead to loss of pragmatic decisions on the choice of parameters as the focus should be on the logical and functional consistent application of a set of inherent land-use parameters that are clearly separated from non-inherent parameters (Jansen and Di Gregorio, 2002; Jansen, 2003).

However, if an international agreement on the definition of land uses will not be reached and a common terminology found, data harmonisation will remain an impossible task, let alone attempting data standardisation. It is therefore important to underline commonalities in the existing approaches and identify a set of commonly used parameters in the class sets.

4. Major parameters for harmonisation of class sets

An analysis of several existing class sets shows that statistical data are often collected on the basis of economic purpose and/or activities (ECE-UN, 1989; UN, 1989; UN, 1998), natural resources related disciplines tend to amalgamate land-cover characteristics with activity or function (Anderson, 1976; IGU, 1976; CEC, 1995; FAO, 1998), while legal aspects are described by land rights or patents and other related legal conditions (FAO, 1998; UN, 1998). Table 2 provides an overview of the most commonly used major parameters applied by various international systems. "Function" refers to economic purpose, "activity" refers to a process resulting in a similar type of products, "biophysical" refers to the material and immaterial environment (e.g., vegetation, land cover, geology, etc.) and "legal" refers to the context of existing laws and regulations.

Insert Table 2.

Table 2 shows that the major land-use parameters utilised by sectoral class sets are limited. Though the meaning of land use varies widely among sectors, the set of major parameters is apparently not so broad. Just two parameters suffice to describe any land use: *function* and *activity*. The function approach describes land uses in an economic context. This type of approach answers the aim of land uses and is commonly used in sectoral land-use descriptions (e.g., agriculture, forestry, fisheries, etc.). The approach is able to group land uses together that do not possess the same set of observable characteristics but serve the same purpose, the so-called polythetic view (Sokal, 1977). An example of such land uses is "agriculture" that may come in many forms, dealing with plants or animals, related to extraction, production or service characteristics. These "agricultural" land uses share a large proportion of characteristics but do not necessarily agree in any one characteristic (e.g., bee-keeping versus annual rainfed maize cropping). The activity approach describes what actually takes place on the land in physical or observable terms. Activity is defined as "*the combinations of actions that result in a certain type of product*" (UN, 1989) and refers to a process. The term "activity" does not mean that one needs to witness the activity as observer at the moment that it is being carried out, but one may observe the results and infer the activity. It is important to note that the function approach is independent of the activity approach: a variety of activities may serve a single function (e.g., both farm housing and farming activities serve agriculture).

Widely known and used systems for economic activities are: (1) the 3rd revision of the International Standard Classification of all Economic Activities (ISIC) of the United Nations Statistical Commission (UN, 1989) (Table 3), which ensures harmonisation with other main economic classifications, such as the Central Product Classification (UN, 1998) (the CPC was developed for the purpose to measure outputs, i.e. products and services. Each category is accompanied by a reference to the ISIC class where the output is mainly produced (industrial origin parameter), classification of products is based on the physical characteristics of the goods or the nature of services rendered); and (2) the Nomenclature des Activités de la Communauté Européenne (NACE rev. 1) of the Commission of the European Communities, which first two levels are compatible with ISIC (CEC, 1993).

Insert Table 3.

The usefulness of the function and activity parameters is apparent. Function groups all land used for the same economic purpose independent of the type of activities taking place, whereas activity groups all land undergoing a certain process resulting in a certain type of product that may serve different functions. The result of a combined approach will be a flexible data set where re-grouping of parameters can take place for a wide variety of queries.

The level of data collection increases notably from the function to the activity concept. The use of the function parameter as first level parameter is also a pragmatic choice as most major functional groupings can be detected with limited investment of human and financial resources, whereas the activity parameter would require substantial investments in data acquisition.

5. Basic units of measurement

Land use lacks a common unit of analysis, the so-called basic unit of measurement. The definition of the this unit differs according to the purpose of data collection and/or analysis. Sometimes a statistical sample area is used, sometimes the unit is based upon mapping units at a particular scale (e.g., minimum mapping unit in the case of thematic mapping) and sometimes the cadastral parcel unit is used. These three basic units of measurement are discussed in more detail below.

5.1 Cadastral land parcel

In many countries, the smallest land unit that one can define coincides with the cadastral land parcel unit, which is the lowest-level unit of the cadastre and thus has a legal status. In the cadastral system not only the spatial extent of these land parcels is recorded and their ownership but often also the occurring land-use or land-cover related information (e.g. arable land with building). In order to have a flexible approach in which different units of measurement can be aggregated, the cadastral land parcel can be selected as the basic unit of measurement for land use. These cadastral land parcel units can be regrouped according to ownership, by cadastral zone and by the various levels of administrative units (e.g., village, commune or district level). Furthermore, the land parcel units may be regrouped according to similar type of uses and socio-economic properties in order to identify land-use systems (e.g., if the different cadastral parcels are grouped at the level of ownership and/or leasing, the level of a socio-economic unit can be reached in which also the availability and use of technology can be incorporated).Thus, there is flexibility in the use and regrouping of the data that will serve different levels of decision making in land-use planning and policy. Another advantage is that land-use change analyses will be possible at a level that corresponds with decisions made by the individual landowner or landholder.

Land registration and the cadastre need to be seen as part of the process of natural resources planning and management. They deal with two of the world's major resources, i.e. land and information. Land information is necessary in many government activities. The registers may be used for land taxation, the rights over public utilities over private land or along public roads for facilities such as electricity and water may need to be protected, infrastructures need to be maintained and/or improved, restrictions may be necessary where misuses occur, etc. The cadastre should therefore be seen as an integral part of the land management system (Dale, 1995).

The use of the land is closely related to land rights, which may be associated with certain limitations or constraints. In addition, the period over which certain land rights are held is important. An owner that has land rights for a long period may be more inclined to make investments than one who has land rights for a very restricted period. Access to land and ownership may thus impede or restrict the use of the land. Land rights constitute a condition under which land use develops. Land rights may restrict the choice of the various options of land use and it is, therefore, an important determinant of what type of actual uses may be found in a particular place and time. The type of land rights and who is holding these land rights (e.g., individual, family or private company) are recorded in the cadastral system.

5.2 Land-cover polygon

Land use describes the use of the object "land" and thus needs to be tied to a methodology in which the object is defined. This has led to the common practice to combine land use with land cover in the same class set, thereby attaching use to what you see because of what people do on the surface of the Earth.

However, land use has many aspects that go beyond land cover (e.g., socio-economics, legal aspects). Therefore, too much emphasis on land cover embodies the risk not to capture several aspects of land use.

The advantages of using land-cover polygons as basic unit of measurement are that cover can be observed and that tools like remote sensing and geographic information systems can help in a first stratification of the land-cover-related uses. Consequently, a spatial relationship is established between land use and land cover. A problem arises where land-use delineations do not concur with land-cover polygons. Several uses may take place within one land cover (e.g., in a building), as well as one land use may be applied to various land-cover types (e.g., certain types of free grazing). In the cases where the boundaries concur, one can aggregate either the land uses or the land covers. However, a land use may be confined to part of a land cover or parts of several land-cover polygons. In such cases, a further analysis and delineation would be required in order to define the basic unit of measurement. In practice, most of the land has been designated a certain function that applies to the whole unit under consideration. The cases that a land cover with a specific function does not concur with the land use are rare (e.g., certain types of recreation or tourism) (Jansen and Di Gregorio, 2003 and 2004). A methodology for mapping land use based upon available land-cover polygons is described by Cihlar and Jansen (2001). One should note that the land-cover/land-use relationship may change with time, thus establishment of the relationship alone is not enough.

5.3 Statistical sample unit

Statistics are often based upon a selection of areas that are representative for a much larger area, the so-called statistical sample unit. In Table 1 for instance the TER-UTI class set uses an area of $9m^2$ distributed in a systematic manner over the country territory to do annual systematic observations. This methodology has also been applied in Bulgaria besides France. This provided, among other projects, the experience integrated into the Land Use/Cover Area Frame Statistical Survey (LUCAS) launched by EUROSTAT and the Directorate General of Agriculture. LUCAS is making observations using a systematic grid: on a regular grid of 18 by 18km, each grid element contains 12x30 rectangular primary sampling units covering 90ha. In addition, there are 10 secondary sampling units per primary sampling unit. The secondary sampling unit area is considered as being equal to $7m^2$ (a circle with a diameter of 3m). These sampling units are revisited on a regular basis in order to describe them anew and analyse any changes. In 2005, this methodology has been revised in a regular grid of 1 by 1km covering the entire EU providing the base sample. From this base sample, the LUCAS master sample is extracted corresponding to a regular grid of 2 by 2km (e.g., 1 million points) where each point is photo-interpreted in order to stratify the sample in seven generic strata. From the stratified master sample, a sub-sample will be extracted for classification by field visit according to the full LUCAS class set (pers. comm. C. Duhamel, Landsis g.e.i.e).

6. Data quality

Harmonisation of class sets requires the analysis of data quality because correspondence between two class sets having two very different qualities may not be meaningful. In the metadata of each class set, parameters should be described related to the *positional and thematic accuracy*. The positional accuracy when using remote sensing can be divided into:

- Geo-referencing, i.e. the technical solutions for projecting the imagery onto the selected projection and spheroid aiming at providing for each pixel on the image its position on the ground by the means of a tern of coordinates.
- Location control, i.e. the correspondence between the coordinates of any arbitrary chosen point on the image and its position on the ground by the confrontation with better accuracy source data.
- Registration, i.e. the precision of the drawing/digitising system adopted defined as the difference between the same lines when interpretation is repeated of the same feature.

A statistically valid design for estimating accuracy parameters has three parts: (1) the response design specifies which data are to be collected at each sample location; (2) the sampling design specifies the locations at which the response data are to be acquired; and (3) the analysis lays out the formulas and tests to be applied to the observations (Boschetti et al., 2005).

One of the most common means of expressing thematic accuracy in remote sensing is the preparation of a classification *confusion matrix*, sometimes called *error matrix* or *contingency table*. The confusion matrix compares on a class-by-class basis, the relationship between known reference data, i.e. the ground truth, and the corresponding results of classification either in the form of pixels, cluster of pixels, polygons or groups of polygons (Lillesand and Kiefer, 2000).

Semantic harmonisation of class sets should consider the data quality aspect in a comprehensive manner and would need to address also the following two aspects that are still at the level of research (Jansen et al., 2005b):

- A quantitative measure should be provided of the harmonisation result of a class. In existing examples, the impression is often given that class correspondence is 100%, whereas more often than not the result will be much lower.
- A quantitative measure should be provided for the overall correspondence between two class sets similar to the overall accuracy calculated from the confusion matrix.

7. Example: land-use harmonisation in Albania

7.1 Use of a reference system and a data model

The land-use data harmonisation process is illustrated with an example form the EU Phare Land-Use Policy II (LUP II) project in Albania based upon the cadastral parcel as basic unit of measurement (Jansen, 2003; Jansen et al., 2006). The LUP II results are compared to the World Bank Albanian National Forest Inventory (ANFI) project based upon the land-cover polygon as basic unit of measurement and a class set defined with the FAO/UNEP Land Cover Classification System (Jansen et al., 2005a). The Albanian government needed an analysis of land-use change dynamics to better understand the past, monitor the current situation and to predict future trajectories in order to plan land uses and develop and implement appropriate policies. In the example data quality aspects have not been quantified as the basis for the harmonisation effort is the cadastre, where in the past land use has been systematically recorded, implying high data accuracy.

A standard hierarchical methodology for description of land use has been developed for Albania, as there is no such methodology available or an international land-use reference system. The developed Land-Use Information System of Albania (LUISA) adopts the function and activity parameters for systematic description and has been developed in complete synergy by the subject-matter specialist and information technology specialist.

Harmonisation between class sets can be achieved on the condition that the data structure of existing data sets is integrated in the newly developed class set. Here, problems may arise and if so they should be overcome. It may mean having to compromise and accommodate certain classes in a specific position in the class set that is neither the most suitable when considering the concepts adopted nor enhancing the class set’s internal consistency. Adoption of a hierarchical system will allow the applicability at various scales, from national, regional, to local. In addition, the class set structure is linked to a data structure, so one should not only be familiar with the subject matter of land use and the principles of classification, but also with information technology concepts (e.g., relational databases or object oriented approaches). In the above discussion, it is assumed that a common set of attributes distinguishes the classes to be compared and that class differences are primarily due to differences in boundary conditions. In the case of land use, this is a reasonable assumption (Wyatt et al., 1997).

In the context of the LUP II project, four data sets covering the period 1991-2003 (e.g., under socialist government, before and after privatisation) are important:

1. Statistical data from the Institute of Statistics (INSTAT) comprising seven classes;
2. Cadastral data from the Immovable Property Registration System (IPRS Kartela) comprising 41 classes (spatially explicit data);
3. Commune data comprising 14 classes (spatially explicit data); and
4. LUISA data comprising 48 classes where the most detailed levels of the hierarchy were used for land-use data collection (spatially explicit data).

Correspondence between classes of the available class sets has been inferred from the explicit record of how each class relates to LUISA using the available definitions. Three class sets would lead to three comparisons to be made for each class, whereas four class sets would request six comparisons per class. It was therefore more efficient to use LUISA as reference system. During its development, LUISA has been systematically and thoroughly tested. For the purpose of the LUP II project the land-use categories have been limited to four that each are linked to a set of laws. Each of these categories branches out into different levels, each level having its own set of classes and use of parameters, definitions and guidelines (Figure 2).

Insert Figure 2.

A link that is often ignored at an early stage of classification comprises the structure of data resulting from classification in a geo-database. The *data model* developed for the LUP II project distinguishes *spatial features* (e.g., land-use and soils) from *linear features* (e.g., roads and channels). The latter two classes are however also related to land-use because roads form the transport network, whereas channels form the drainage and irrigation network. This division has important implications for the way in which roads and channels appear in LUISA. In the data model linear features have been split into several segments; for each road or channel segment data is collected that deal with their actual state and maintenance. The advantage of having such segment information is that the user of the data can identify, for example, if anywhere on a road used for transporting agricultural products to the nearby market there is a segment that is in such a bad state that a vehicle cannot pass. If the road would be a single feature in the database, such an analysis would be impossible. Another example can be given using channels. In many class sets, one will find the class "irrigated agriculture" where the parameter irrigation is applicable to the whole polygon. In practice, irrigation channels may function only in part due to their maintenance state but such a polygon would still carry the parameter irrigated. A much more flexible approach is to separate irrigation channels from the agricultural fields and to split the channels in segments. Such a distinction permits the user to identify those fields that are actually irrigated from those that cannot be irrigated due to segment information on the state of the irrigation channels. One will thus not find every single possibility of a class in LUISA because of the data model adopted. It is sufficient to record roads and channels as land *cover* because the segment information can be combined with these features at a later stage of the data integration process in order to define land use.

Once correspondence with LUISA was established for each class of the class sets, land-use change could be analysed using just LUISA. Using different class sets with several classes results in numerous land-use changes making a meaningful analysis difficult. LUISA does not only act as a reference system for harmonisation of land-use class sets, it also acts as a reference system for harmonisation of land-use change. The LUISA class structure, i.e. the data structure, is tailored in an efficient and logical manner in order to identify land-use change processes. In principle, *land-use modifications* occur within a land-use category and the degree of modification depends on the level of the class (e.g., at Level IV modification is small, at Level III medium and at Level II high) and *land-use conversion* occurs between land-use categories. The exceptions are the Non-agricultural land-use classes, where modifications occur within one group (e.g., within Urban uses, within Transport, within Utilities, etc.) and conversions between groups (e.g., from Unproductive to Urban uses, or from Water bodies & waterways to Extraction & mining). In the Agricultural, Forests and Pasture & Meadows land-use categories conversions occur between categories, whereas modifications occur within a single category within and between groups (e.g., within the Agricultural Land-uses modifications exist within Permanent Crop Cultivation or between Temporary Crop Cultivation and Permanent Crop Cultivation, etc.). For the interpretation of land-use change a piece of software was written, the Land-Use Change Analyses (LUCA), that groups the changes according to the land-use change processes modification and conversion as shown in Table 4.

Insert Table 4 and Figure 3.

The harmonisation process between the different class sets and for harmonisation of land-use change using LUISA as reference system is shown in Figure 3.

7.2 Results of correspondence between the class sets

Correspondence between the classes of the four systems is important when using existing data sets coming from different sources at different levels of detail and trying to integrate and harmonise them in a geo-database. A table of correspondence has been prepared (Table 5) that shows that correspondence is often of the type one-to-many or many-to-many, especially when classes used at national level (e.g., INSTAT) are correlated with classes used at more detailed levels (e.g., IPRS Kartela, Commune and LUISA). However, if one looks at the more detailed level of the cadastral parcel unit of the IPRS Kartela and LUISA class sets, the many-to-many relationships occur less frequently and one gets a better idea about the correlation of single classes (Table 6 and 7).

Insert Tables 5, 6 and 7.

Some classes of IPRS Kartela do not correspond with a class of LUISA because they either occur below ground (e.g., 130, 332) and have not been included, or do not address a land-use (e.g., 344). Other classes are of a more generic nature than the detail of the classes used in LUISA resulting in a one-to-many relationship (e.g., 108, 110 and 118) or vice versa (e.g., LUISA classes 91, 92 and 93 with various IPRS Kartela classes). Other classes are more closely related to a land *cover* than a land-*use* (e.g., 118, 119, 135 and 336) and the relation with land use is not always apparent.

LUISA classes 95, 113, 114, 122, 124 and 133 do not correspond with any IPRS Kartela class. More detail has been introduced in the description of Agricultural and Non-agricultural land-uses. Suitable agricultural lands are limited in Albania and it is regarded as important to know why they might not be utilised for production of agricultural goods and/or services in the current agricultural year or for longer periods. The LUISA classes distinguished in the Forests and Pastures and Meadows categories have been introduced to better distinguish their range of uses instead of focussing mainly on their different land-cover type.

7.3 Comparison with the ANFI remotely sensed land-cover/use data set

The World Bank financed Albanian National Forest Inventory (ANFI) project provided an analysis of spatially explicit land-cover/use change dynamics in the period 1991-2001 using the FAO/UNEP Land Cover Classification System for codification of classes, satellite remote sensing and field survey for data collection and elements of the object-oriented geo-database approach to handle changes as an evolution of land-cover/use objects, i.e. polygons, over time to facilitate change dynamics analysis (Jansen et al., 2005a). Land-cover/use changes are the results of many interacting processes and each of these operates over a range of scales in space and time (Verburg et al., 2003). The detailed LUISA land-use data can be compared to the coarser ANFI data (scale 1:2,500 and 1:100,000 respectively), as far as space and time considerations both data sets represent more or less the same period (1991-2003 and 1991-2001 respectively), but the analysis of each data set gives a somewhat different view on the change dynamics at detailed versus aggregated data levels. At aggregated data levels the local variability of spatially explicit land-cover/use changes may be obscured, whereas patterns can be shown that at more detailed data levels may remain invisible and vice versa (Veldkamp et al., 2001).

The LUISA data set permits analysis of changes at the level of the individual cadastral parcel unit, thereby highlighting changes at the level of the landowner and/or land user. The ANFI data set provides a national overview of the major change processes, such as deforestation, urbanisation and increased pasture, but cannot provide conclusive evidence on especially the use of agricultural land (Jansen et al., 2005a). The LUISA data set provides an insight into the non-use of low productivity areas in hilly terrain and the extensive forms of agriculture practised on prime agricultural land because of the lack of fertilizer use and the breakdown of irrigation systems (Jansen et al., 2006). These two spatially explicit data sets are therefore complementary when analysing change dynamics.

It is important to note that the use of remote sensing for land cover is a common approach. Interpretation of satellite images can provide a quick overview of the type and location of different land-cover types. Often land-use elements are inferred from land cover (e.g., detection of a field pattern results in the class “agriculture”). However, the above example clearly demonstrates that land use requires a different approach because it contains many aspects that go beyond land cover. Even with the use of the most detailed satellite images, such aspects will not be covered.

7.4 Correspondence with an international class set

Reference should also be made to internationally established class sets used to describe national level land-use/cover data. These systems are not immediately related to the work of the LUP II project, but the value of the project outputs will be enhanced if correspondence to especially EU wide operational systems is assured. This will facilitate accession of Albania into the EU and continuity in data collection routines.

Land use is of high importance in the definition and evaluation of common sectoral policies in the EU, e.g. on environment, agriculture, transport and the integration of those policies in a comprehensive assessment and planning of the territory. EUROSTAT, the Statistical Office of the European Communities, has the mission to provide the EU with high quality statistical information service. To support policy formulation EUROSTAT launched in co-operation with the Directorate General responsible for Agriculture in 2000 the Land-Use/Cover Area Frame Statistical Survey (LUCAS) project that has been applied in the period 2001-2005 and it will be applied in a revised form in 2006 in 23 EU Member States.

Overall objectives of this survey are (EUROSTAT, 2001):

1. Collection of harmonised data (i.e. unbiased estimates) at EU level of the main land-use and land-cover areas and changes.
2. Inclusion not only of the usual agricultural domain but also the aspects linked with environment, multi-functionality, landscape and sustainable development.
3. A common sampling base (e.g., sampling frame, class set and data management) that interested Member States can use to obtain representative data at national, but also regional, level by increase of the sampling rate while respecting the general LUCAS approach.
4. Evaluation of the strengths and weaknesses of a point area frame survey as one of the pillars of the future Agriculture Statistical System (area frame means that the observation units are territorial subdivisions instead of agricultural holdings as used in the Farm Structure Survey).

Insert Table 8 and 9.

The main LUCAS land-use categories (version 1.0) are shown in Table 8. Correspondence with LUISA is shown, although based upon a different basic unit of measurement, in Table 9 at the individual class level. Only the LUISA classes related to land tenure (e.g., 11, 12 and 13) do not correspond with a LUCAS category, which is logical as they are distinguished using a non-inherent land-use parameter (Jansen, 2003).

8. Discussion and conclusions

Land use has been defined and interpreted in many different ways depending on the sector. The multi-disciplinary nature of the subject has hampered the development of a standardised methodology for classification as well as harmonisation of land uses worldwide. Existing class sets have been reviewed in order to distil the key elements but there is a genuine lack of consistency in applied methodology and adherence to the principles of classification, and a variety of basic units of measurement are used. Evaluation of the main parameters used in the existing class sets leads to the conclusion that the combination of just two parameters may suffice: function together with activity. Function is centred on the purpose of land uses, whereas activity groups all land undergoing a certain process resulting in a certain type of product.

The example in Albania shows how the use of a reference system, based upon the function and activity parameters and using the cadastral parcel as basic unit of measurement, may facilitate harmonisation of class sets in parallel with the achievement of harmonisation of land-use change. This reference system can form the basis for future standardisation of land-use class sets in Albania. In addition, the use of synergies between classification and information technology concepts (e.g., data model and resulting geo-database structure) should be enhanced.

Comparison of the cadastral-parcel-based class set of Albania with a polygon-based class set at coarser resolution shows that different levels of detail are needed when analysing land-use change. Remote sensing is a useful tool for gaining a quick overview of land-cover related land uses but the potential for a detailed and in-depth knowledge of land use is limited as other aspects, such as socio-economics, institutional, cultural and legal factors, are not captured by remotely sensed based land cover. Therefore, remote sensing can make a valuable contribution but its limits should be clear and complementary approaches should be used. Understanding land-use change dynamics does not only help to identify vulnerable places, but also vulnerable (groups of) land users that on their own are incapable to respond in the face of environmental processes and problems.

The way forward for harmonisation of land-use class sets is to promote and fully develop a parametric approach to classification. Commonalities in existing approaches should be emphasized and a set of commonly used parameters should be identified. Lessons can be learnt from harmonisation attempts at local, regional and national levels that are equally valid for a globally applicable land-use classification. Furthermore, a quantitative measure should be defined to express the harmonisation result of a class and between class sets.

Acknowledgements

This paper was prepared for the 12th Center for Environmental Remote Sensing (CEReS) International Symposium on Remote Sensing entitled “Maximizing the use of satellite data for understanding the Earth environment”, held 13-14 December 2005, Chiba, Japan. The author would like to sincerely thank the organising committee.
In addition, Christophe Duhamel (Landsis g.e.i.e., Luxembourg) is thanked for his suggestions concerning LUCAS and Giancarlo Carrai (SVALTEC S.r.l., Florence) for his comments on an earlier draft.

References

Adamec, J., 1992. Land-use classification study. First draft. Internal working paper. FAO, Rome.

Anderson, J.R., Hardy, E.E., Roach, J.T., Witmer, R.E., 1976. A land-use and land-cover classification system for use with remote sensor data. Geological Survey Professional Paper No. 964. U.S. Government printing office, Washington, D.C.

APA, 1999. Land-based classification standard. Second draft. American Planning Association, Research Department. Chicago, US.

Baulies, X., Szejwach, G., 1998. LUCC Data requirements workshop – survey of needs, gaps and priorities on data for land-use/land-cover change research. Organised by IGBP/IHDP-LUCC and IGBP Data and Information Systems (DIS), 11-14 November 1997. LUCC Report Series No. 3, LUCC International Project Office, Barcelona.

Boschetti, L., Foody, G.M., Friedl, M.A., Hansen, M.C., Herold, M., Mayaux, P., Morisette, J.T., Stehman, S.V., Strahler, A.H., Woodcock, C.E., 2005. Global land-cover validation: recommendations for evaluation and accuracy assessment of global land-cover maps. EC Joint Research Centre, Ispra, Italy.

CEC, 1993. Nomenclature des activités de la communauté européenne (NACE). Première révision. Règlement 761/93 du Conseil. Commission of the European Communities, Brussels.

Cihlar, J., Jansen, L.J.M., 2001. From land cover to land use: a methodology for efficient land-use mapping over large areas. *The Professional Geographer* 53(2): 275-289.

Dale, P.F., 1995. Land reform, land registration and the cadastre – a comparative analysis between Bulgaria, Hungary and Rumania.

Di Gregorio, A., Jansen, L.J.M., 2000. Land-cover classification system (LCCS): classification concepts and user manual. FAO/UNEP/Cooperazione italiana, Rome. (with CDROM)

Dolman, A.J., Verhagen, A., Rovers, C.A. (Eds.), 2003. Global environmental change and land use. Kluwer Academic Publishers, Dordrecht.

Duhamel, C., 1998. First approximation for a land-use classification. CESD-Communautaire, Luxembourg. FAO commissioned study.

Dumanski, J., Pieri, C., 2000. Land quality indicators: research plan. *Agriculture, Ecosystems and Environment*, 81:93-102.

ECE-UN, 1989. Proposed ECE standard international classification of land use. Economic Commission for Europe of the United Nations, Geneva.

EUROSTAT, 1991. EUROSTAT spatial statistics. Task force internal report on land-use statistics, EUROSTAT, Luxembourg.

EUROSTAT, 2001. Land-use/cover area frame statistical survey (LUCAS). Version 1.0. Eurostat, Luxembourg.

FAO, 1976. A framework for land evaluation. Soils Bulletin 32. FAO, Rome.

FAO, 1984. Guidelines: land evaluation for rainfed agriculture. Soils Bulletin 52. FAO, Rome.

FAO, 1998. FAO Statistical databases (FAOSTAT). FAO, Rome.

Guttenberg, A.Z., 1959. A multiple land-use classification system. *Journal of the American Institute of Planners*, 25: 143-50.

Guttenberg, A.Z., 1965. New directions in land-use classification. American Society of Planning Officials. Chicago.

IGU, 1976. World land-use survey. Report of the Commission to the General Assembly of the International Geographic Union. *Geographica Helvetica* No. 1. Pp. 28.

ITC/FAO/WAU, 1996. The land-use database. A knowledge-based software program for structured storage and retrieval of user-defined land-use data sets. Draft version, January 1996.

Jansen, L.J.M., 2003. A standard methodology for land-use description and harmonisation of data sets. Technical report 2. EU Phare Land-Use Policy II project. AGROTEC S.p.A. Consortium, Rome. 81p.

Jansen, L.J.M., Carrai, G., Morandini, L., Cerutti, P.O., Spisni, A., 2005a. Analysis of the spatio-temporal and semantic aspects of land-cover/use change dynamics 1991-2001 in Albania at national and district levels. *Environmental Monitoring & Assessment*, in print.

Jansen, L.J.M., Carrai, G., Petri, M., 2006, Land-use change dynamics 1991-2003 at cadastral parcel level in Albania: an object-oriented geo-database approach. In: Koomen, E., Bakema, A., Stillwell, J., Scholten, H. (Eds.), 2006. Simulating land-use change. Springer Publishers. 300pp. (with CDROM)

Jansen, L.J.M., Di Gregorio, A., 1998. The problems with current land-cover classifications: development of a new approach. Land-cover and land-use information systems for European policy needs, Luxembourg, 21-23 January 1998. E.C. EUROSTAT Studies and Research, Edition 1999, Theme 5: 93-102.

Jansen, L.J.M., Di Gregorio, A., 2002. Parametric land-cover and land-use classifications as tools for environmental change detection. *Agriculture, Ecosystems & Environment* 91(1-3): 89-100.

Jansen, L.J.M., Di Gregorio, A., 2003. Land-use data collection using the "Land-cover Classification System" (LCCS): results from a case study in Kenya. *Land Use Policy* 20(2): 131-148.

Jansen, L.J.M., Di Gregorio, A., 2004. Obtaining land-use information from a remotely sensed land-cover map: results from a case study in Lebanon. *Int. Journal of Applied Earth Observation and Geoinformation* 5: 141-157.

Jansen, L.J.M., Groom, G.B., Carrai, G., 2005b. Semantic data harmonisation of land-cover class sets using the FAO/UNEP Land-cover Classification System - Translator Module (LCCS-TM). Submitted to *Int. Journal of Applied Earth Observation and Geoinformation*.

Kostrowicki, J., 1977. Agricultural typology concept and method. Agricultural Systems No. 2:33-45.

Kostrowicki, J., 1980. A hierarchy of world types of agriculture. In: N. Mohammed (Ed.), 1992. New dimensions in agricultural geography. Vol. I - Historical dimensions of agriculture. Pp. 163-203.

Kostrowicki, J., 1982. Types of agriculture map of Europe: concept, method, techniques. In: N. Mohammed (Ed.), 1992. New dimensions in agricultural geography. Vol. I - Historical dimensions of agriculture. Pp. 227-249.

Kostrowicki, J., 1983a. Land-use survey, agricultural typology and land-use systems: introductory remarks. Rural Systems, Vol. 1 No. 1.

Kostrowicki, J., 1983b. Land-use systems and their impact on environment. An attempt at a classification. Adv. Space Res. Vol. 2, No. 8:209-215.

Kostrowicki, J., 1984. Types of agriculture in Europe: a preliminary outline. Geographia Polonica 50:131-149.

Lambin, E.F., Rounsevell, M.D.A., Geist, H.J., 2000. Are agricultural land-use models able to predict changes in land-use intensity? *Agriculture, Ecosystems and Environment*, Vol. 82: 321-331.

Lambin, E.F., Turner, B.L., Geist, H.J., Agbola, S.B., Angelsen, A., Bruce, J.W., Coomes, O.T., Dirzo, R., Fischer, G., Folke, C., George, P.S., Homewood, K., Imbernon, J., Leemans, R., Li, X., Moran, E.F., Mortimore, M., Ramakrishnan, P.S., Richards, J.F., Skånes, H., Steffen, W., Stone, G.D., Svedin, U., Veldkamp. T.A., Vogel, C., Xu, J., 2001. The causes of land-use and land-cover change: moving beyond the myths. *Global environmental change*, Vol. 11: 261-269.

LANES, 1998. Development of a harmonized framework for multi-purpose land-cover/land-use information systems derived from earth observation data. Final report. Concerted Action of the European Commission, Research Programme on the Environment and Climate. CESD-Communautaire, Luxembourg.

Lillesand, T.M., Kiefer, R.W., 2000. Remote sensing and image interpretation. Fourth edition. John Wiley & Sons, New York.

Meyer, W.B., Turner, B.L. (Eds.), 1994. Changes in land use and land cover: a global perspective. Cambridge University Press, Cambridge, UK.

McConnell, W.J., Moran, E.F. (Eds.), 2001. Meeting in the middle: the challenge of meso-level integration. An international workshop on the harmonization of land-use and land-cover classification. LUCC Report Series No. 5. Anthropological Center for Training and Research on Global Environmental Change - Indiana University and LUCC International Project Office, Louvain-la-Neuve.

Mücher, C.A., Stomph, T.-J., Fresco, L.O., 1993. Proposal for a global land-use classification. Internal final report, February 1993. FAO/ITC/WAU, Wageningen.

Paludan, C.T., 1976. Land-use surveys based on remote sensing from high altitudes. In: IGU, 1976. World land-use survey. Report of the Commission to the General Assembly of the International Geographic Union. *Geographica Helvetica*, 1: 117-24.

Remmelzwaal, A., 1989. Classification of land and land use. First approach. Internal working paper. FAO, Rome.

Sokal, R., 1974. Classification: purposes, principles, progress, prospects. *Science*, Vol. 85 (4157): 1115-1123.

Turner, B.L., Skole, D., Sanderson, S., Fischer, G., Fresco, L.O., Leemans, R., 1995. Land-use and land-cover change science research plan. IGBP Global Change Report No.35/ Human Dimensions Programme Report No. 7. International Geosphere-Biosphere Programme/Human Dimensions of Environmental Change Programme, Stockholm/Geneva.

UNEP/FAO, 1994. Report on the UNEP/FAO expert meeting on harmonizing land-cover and land-use classifications. Geneva, 23-24 November 1993. GEMS report series No.25. Nairobi.

UN, 1989. International standard classification of all economic activities (ISIC). Third revision. United Nations Statistics Division, Statistical Classifications Section, New York.

UN, 1998. Central product classification (CPC). Version 1.0. United Nations Statistics Division, Statistical Classifications Section, New York.

Urban Renewal Administration, 1965. Standard land-use coding manual: a standard system for identifying and coding land-use activities (SLUCM). Urban Renewal Administration, Housing and Home Financing Agency, and Bureau of Public Roads, Department of Commerce. Washington D.C.

Veldkamp, A, Kok, K., De Koning, G.H.J., Verburg, P.H., Bergsma, A.R., 2001. The need for multi-scale approaches in spatial specific land-use change modelling. *Environmental Modelling and Assessment*, Vol. 6: 111-121.

Verburg, P.H., De Groot, W.T., Veldkamp, A., 2003. Methodology for multi-scale land-use change modelling - concepts and challenges. In: Dolman, A.J., Verhagen, A. and Rovers, C.A.(Eds.), 2003. Global environmental change and land use. Kluwer Academic Publishers, Dordrecht. pp. 17-51.

Walker, B., 1998. GCTE and LUCC – a natural and timely partnership. *LUCC Newsletter* 3. pp 3-4.

Walker, B., Steffen, W., Canadell, J., Ingram, J. (Eds.), 1997. The terrestrial biosphere and global change: implications for natural and managed ecosystems. Synthesis volume. IGBP Book Series 4. Cambridge University Press, Cambridge, UK.

Wyatt, B.K., Greatorex-Davies, J.N., Hill, M.O., Parr, T.W., Bunce, R.G.H., Fuller, R.M., 1993. Comparison of land-cover definitions. Countryside 1990 series, Vol. 3. Report prepared for the Department of the Environment by the Institute for Terrestrial Ecology (ITE). Natural Environment Research Council, UK. Pp. 131 (with diskette).

Wyatt, B.K., Billington, C., De Bie, K., De Leeuw, J., Greatorex-Davies, N., Luxmoore, R., 1997. Guidelines for land-use and land-cover description and classification. ITE/WCMC/ITC/UNEP/FAO Internal unpublished working document. ITE, Monkshood, UK.

Wyatt, B.K., Gerard, F.F., 2001. What's in a name? Approaches to the inter-comparison of land-use and land-cover classifications. In: Groom, G., Reed, T. (Eds.), 2001. Strategic landscape monitoring for the Nordic countries, TemaNord 2001:523. Nordic Council of Ministers, Copenhagen.

Figure 1. Analysis of land-use planning (adapted from Guttenberg, 1965)

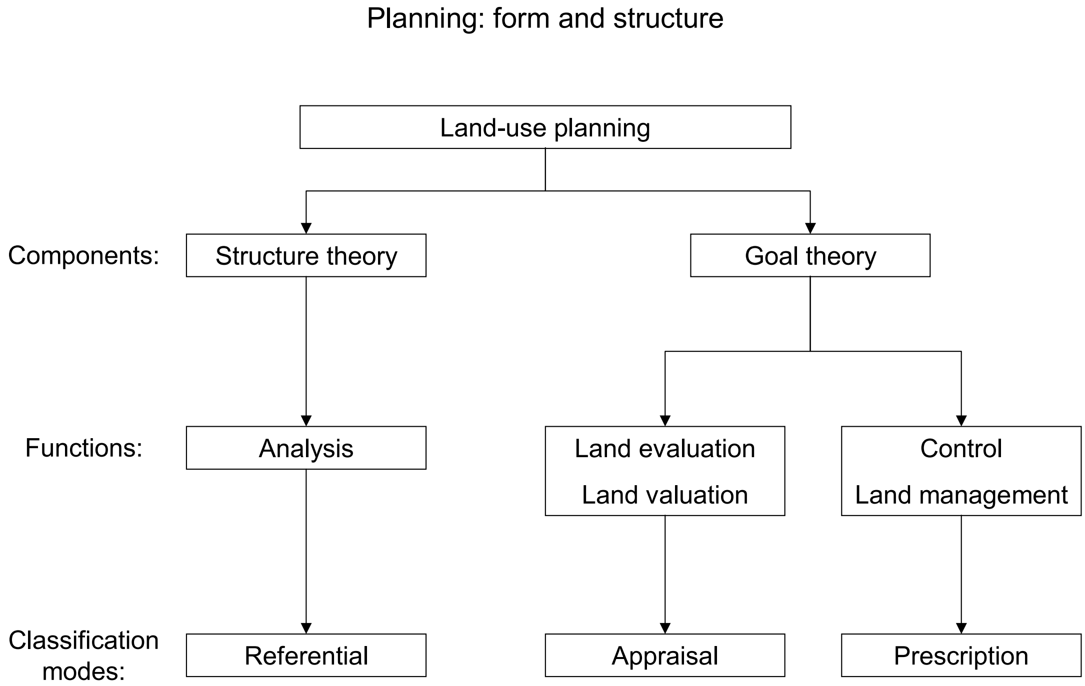

Figure 2. Overview of the LUISA class set with the four main categories Agricultural, Forests, Pasture & Meadows and Non-agricultural land uses (Jansen, 2003; Jansen et al., 2006)

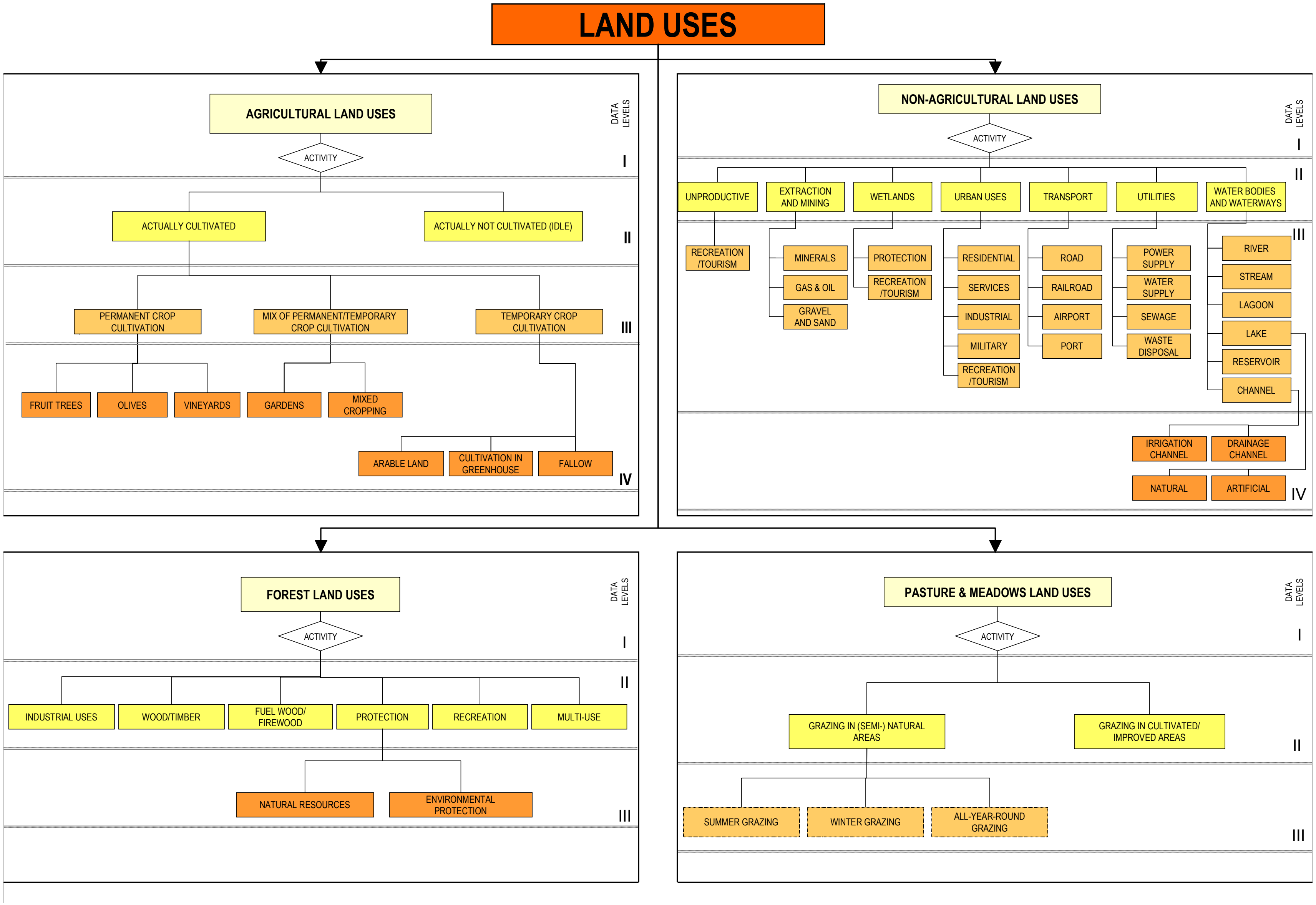

Figure 3. Harmonisation of class sets in Albania using a reference system (LUISA) and harmonising land-use change (LUCA)

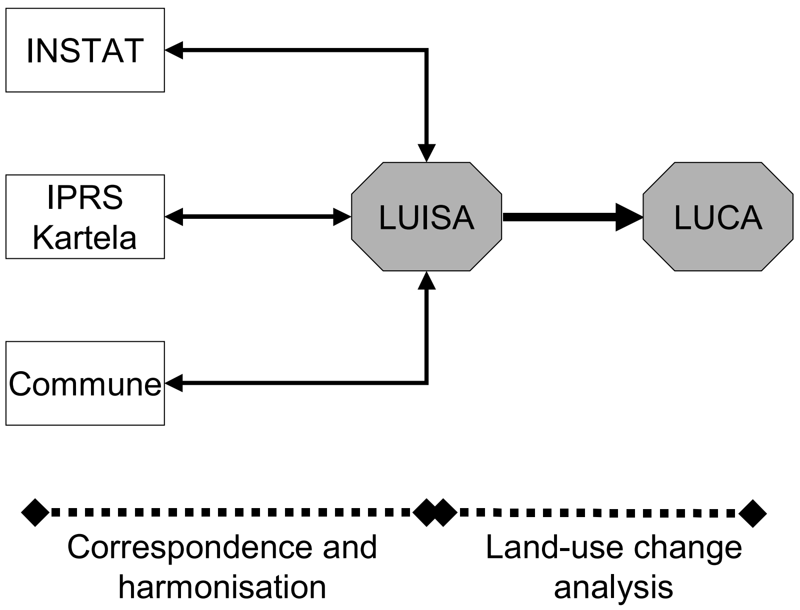

6 Table 1. Overview of adherence of selected systems to the general principles of classification (based upon Duhamel, 1998).

Land-use system / Principles	Anderson (1976)	ECE-UN (1989)	UK Land use (1972)	TER-UTI (1994)	Remmelzwaal (1989)	Adamec (1992)	Young (1993)	Mücher *et al.* (1993)
Completeness	only applicable to USA (as intended)	more applicable to northern European countries than Mediterranean	fulfilled	fulfilled	not fulfilled, too much geared towards agriculture	fulfilled	not fulfilled, some land uses are missing	fulfilled
Absence of overlap	absent	absent	fulfilled	fulfilled	potential confusion between mixed classes	absent	potential confusion between certain classes	fulfilled
Observation unit	not addressed	not addressed	spatial unit, hereditary and zone	a circle of $9 m^2$	not addressed	not addressed	unit of management; population census unit	unit of biophysical management (e.g., plot)
Tool independent	remote sensing dependent	not addressed	independent	independent	not addressed	not addressed	not addressed	independent
Definitions and explanatory notes	no systematic reporting, definitions read like comments	definitions exist; unsystematic explanatory notes	non-existent	no definitions; explanations are given	no systematic definitions; no explanatory notes	non-existent	non-existent	non-existent
Interpretation rules	LC and LU are mixed	general usage of mixed classes; dominance is not defined	all uses are recorded, no weighing in mixed classes	hierarchy of uses requested but no rules exist to define	multiple uses are not discussed	non-existent	multiple uses are recognised: primary use refers to the value added to the holding	multiples uses exist; multiple sequences of operations are not dealt with
Inclusion of new objects	not mentioned, there is often an *Other* category	no systematic approach followed	possible	possible	not addressed	not addressed	not addressed	not addressed
Index of objects	non-existent	non-existent	existing	existing	non-existent	non-existent	non-existent	non-existent
Correspondence with other systems	non-existent	tentative correspondence with socio-economic systems	national Standard Industrial Classification (SIC)	table of correspondence with earlier versions	non-existent	non-existent	non-existent	non-existent

7

Table 2. Analysis of land-use characteristics used by several main class sets [1]

Main sector	Land-use characteristics			
	Function	Activity	Biophysical	Legal
Agriculture	x	x	x	
Fisheries	x	x	x	
Forestry	x	x	x	x
Economics	x	x		
Sociology	x	x		
Statistics	x	x	x	
Industry		x		x
Housing	x	x	x	x
Services		x		x

[1] Based upon: World Land-Use Survey (IGU, 1976), Anderson (Anderson *et al*., 1976), ISIC 3rd revision (UN, 1989), Standard International Classification of Land Use (ECE-UN, 1989), NACE 1st revision (CEC, 1993), Central Product Classification (UN, 1998), FAOSTAT (FAO, 1998), Land-Based Classification Standard (APA, 1999). For “forestry”, use was also made of http://home/att.net/~gklund/DEFpaper.htm.

Table 3. The main categories of ISIC, 3rd revision (UN, 1998).

International Standard Industrial Classification of All Economic Activities		
Codes		Description of category
A	01	Agriculture, Hunting and Related Service Activities
	02	Forestry, Logging and Related Service Activities
B		Fisheries
C		Mining and Quarrying
D		Manufacturing
E		Electricity, Gas and Water Supply
F		Construction
G		Wholesale and Retail Trade
H		Hotels and Restaurants
I		Transport, Storage and Communication
J		Financial Intermediation
K		Real Estate, Renting and Business Activities
L		Public Administration and Defence
M		Education
N		Health and Social Work
O		Other Community, Social and Personal Service Activities
P		Private Households with Employed Persons
Q		Extra-Territorial Organizations and Bodies

Table 4. Grouping of the land-use changes according to LUCA (Jansen, 2003; Jansen et al., 2006)

Type of land-use change			Code
No change		Correspondence	1
Modifications	Low level	Low level modification in Agriculture	201
		Low level modification in Forests	202
		Low level modification in Pastures	203
		Low level modification in Non-Agriculture	204
	Medium level	Medium level modification in Agriculture	301
		Medium level modification in Forests	302
		Medium level modification in Pastures	303
		Medium level modification in Non-Agriculture	304
	High level	High level modification in Agriculture	401
		High level modification in Forests	402
		High level modification in Pastures	403
		High level modification in Non-Agriculture	404
Conversions		Agriculture-to-Forest	5
		Agriculture-to-Pasture	6
		Agriculture-to-Non Agriculture	7
		Forest-to-Pasture	8
		Forest-to- Agriculture	9
		Forest-to-Non Agriculture	10
		Pasture-to-Agriculture	11
		Pasture-to-Forest	12
		Pasture-to-Non Agriculture	13
		Non Agriculture-to-Agriculture	14
		Non Agriculture-to-Forest	15
		Non Agriculture-to-Pasture	16
Unknown		No correspondence [2]	99

[2] “No correspondence” means that the land-use change is unlikely to occur.

14 Table 5. Correspondence between land-use classes from different class sets at a generic level (Jansen, 2003)

Legal categories	Land-use classes		Class sets: INSTAT [3]	IPRS Kartela [4]	Commune [5]	LUISA [6]
Agriculture	Used agricultural area		b	-	1	1, 2, 3, 4, 5, 6, 7
		Area with arable land crops	c, d	101, 102	1a	6, 7
		Area with permanent crops	f	116, 125, 128, 131, 148	1b, 1c, 1d	1, 2, 3, 4, 5
	Non-utilised agricultural area		e	-	-	8, 9
Pastures and meadows		Grassland and pastures	g	108, 110, 153	2, 3a	51, 52, 53, 54, 55
Forests		Forests	h	118	3	31, 32, 33, 34, 35, 36, 37
Non-agricultural lands		Water bodies	-	107, 109, 111, 120, 138, 153	4a	131, 132, 133, 134, 135, 136, 137, 138
		Wetlands	-	336	-	81, 82
		Built-up areas	-	100, 103, 106, 114, 121, 129, 130, 136, 144, 152, 213, 261, 332, 337, 338, 339, 340, 341, 342	4b, 4c, 4d, 4e	91, 92, 93, 94, 95, 111, 112, 113, 114, 121, 122, 123, 124
		Barren	-	119, 135	4f	61
		Mining/extraction	-	117, 343	-	71, 72, 73

15

[3] a=Total Area (not represented in the table), b=Used agricultural area (UAA), c=Cultivated area with arable land crops, d=Main crops (the first ones), e=Non-utilised agricultural area, f=Area with permanent crops, g=Grassland and pasture, h=Forests.

[4] For explanation of the codes see Table 6. Classes 130, 332 and 344 not included.

[5] 1=Agriculture, 1a=Arable, 1b=Vineyards, 1c=Fruit trees, 1d=Olives, 2=Pastures, 3=Forest, 3a=Brush land, 4=Non-agricultural, 4a=Water body, 4b=Built-up, 4c=Cemetery, 4d=Roads, 4e=Railway, 4f=Barren.

[6] For explanation of the codes, see Table 7.

16 Table 6. Correspondence between land-use classes at the level of the cadastral parcel unit (Jansen, 2003)

IPRS Kartela land-use classes [7]		LUISA
Code	Class names	Class codes [8]
100	Apartment	91
101	Arable	6, 7, 8, 9
102	Arable + garden	6, 7, 8, 9
103	Water treatment facility	123
106	Building non-residential	92, 93, 94
107	Channel	137, 138
108	Pasture	51, 52, 53, 54, 55
109	Lake	134, 135
110	Meadows	51, 52, 53, 54, 55
111	River	131
114	Block of flats	91
116	Fruit trees	1
117	Oil well	72
118	Forest	31, 32, 33, 34, 35, 36, 37
119	Barren	61
120	Reservoir	136
121	Road	111
125	Garden (of private building)	4
128	Olives	2
129	Cemetery	92
130	Tunnel, underground	-
131	Vineyards	3
135	Rocky	61
136	Public area	92
138	Stream	132
144	Transformer building (step-up or step-down)	121
148	Fruit trees + garden	5
152	Railroad	112
153	Barrier (natural or artificial)	51, 52, 53, 54, 137, 138
213	Building for residential purpose	91
261	Sport field	92
332	Underground	-
336	Marsh	81, 82
337	Sidewalk	111
338	Unit (consisting of small shop or bar)	92
339	Garage	91
340	Studio	91
341	Power plant	121
342	Area associated to power plant	121
343	Mine area	71, 73
344	Transport equipment	-

17

[7] The IPRS Kartela classes do not have a hierarchical data structure, their structure is flat.
[8] For the explanation of the codes see Table 7.

18 Table 7. Correspondence between the land-use classes of LUISA and IPRS Kartela [9] (Jansen, 2003)

Category	LUISA Code	Description	IPRS Kartela Code
Agricultural land-uses	1	Fruit trees	116
	2	Olives	128
	3	Vineyards	131
	4	Gardens	125
	5	Mixed cropping	148
	6	Arable lands	101, 102
	7	Cultivation in greenhouse	101, 102
	8	Fallow lands	101, 102
	9	Actually not cultivated (idle and abandoned) lands	101, 102
Forests	31	Industrial forests uses	118
	32	Forests for wood/timber production	118
	33	Forests for fuel wood/firewood	118
	34	Protection of natural resources	118
	35	Forests for environmental protection	118
	36	Forests for recreation	118
	37	Multi-use forests	118
Pastures and Meadows	51	Grazing in (semi-) natural areas	108, 110, 153
	52	Summer grazing in (semi-) natural areas	108, 110, 153
	53	Winter grazing in (semi-) natural areas	108, 110, 153
	54	All-year-round grazing in (semi-) natural areas	108, 110, 153
	55	Grazing in cultivated/improved areas	108, 110
Non-agricultural land-uses	61	Recreation/tourism in unproductive areas	119, 135
	71	Mineral extraction and mining	343
	72	Gas and oil extraction	117
	73	Gravel and sand extraction/mining	343
	81	Protection of wetlands	336
	82	Recreation/tourism in wetlands	336
	91	Residential area	100, 114, 213, 339, 340
	92	Services	106, 129, 136, 261, 338
	93	Industrial area	106
	94	Military area	106
	95	Recreation/tourism in urban areas	-
	111	Road	121, 337
	112	Railroad	152
	113	Airport	-
	114	Port	-
	121	Power supply	144, 341, 342
	122	Water supply	-
	123	Sewage	103
	124	Waste disposal	-
	131	River	111
	132	Stream	138
	133	Lagoon	-
	134	Natural lake	109
	135	Artificial lake	109
	136	Water reservoir	120
	137	Irrigation channel	107, 153
	138	Drainage channel	107, 153

[9] For the hierarchical data structure of LUISA see Figure 2; for explanation of the IPRS Kartela codes see Table 6.

19 Table 8. LUCAS version 1.0 (EUROSTAT, 2001)

Land-Use/Cover Area Frame Statistical Survey	
Code	Land-use Category name
U11	Agriculture
U12	Forestry
U13	Fishing
U14	Mining – Quarrying
U21	Energy Production
U22	Industry – Manufacturing
U31	Transport, Communication, Storage, Protective Works
U32	Water, Waste Treatment
U33	Construction
U34	Commerce, Finance, Business
U35	Community services
U36	Recreation, Leisure, Sport
U37	Residential
U40	Unused

20

Table 9. Correspondence between the land-use classes of LUISA and LUCAS 1.0 (Jansen, 2003)

Category	LUISA [10] Code	Land-use category code	LUCAS 1.0 Code
Agricultural land-uses	1	Fruit trees	U11
	2	Olives	U11
	3	Vineyards	U11
	4	Gardens	U11
	5	Mixed cropping	U11
	6	Arable lands	U11
	7	Cultivation in greenhouse	U11
	8	Fallow lands	U11
	9	Actually not cultivated (idle and abandoned) lands	U11
Forests	31	Industrial forests uses	U12
	32	Forests for wood/timber production	U12
	33	Forests for fuel wood/firewood	U12
	34	Protection of natural resources	U12
	35	Forests for environmental protection	U12
	36	Forests for recreation	U12
	37	Multi-use forests	U12
Pastures and Meadows	51	Grazing in (semi-) natural areas	U11
	52	Summer grazing in (semi-) natural areas	U11
	53	Winter grazing in (semi-) natural areas	U11
	54	All-year-round grazing in (semi-) natural areas	U11
	55	Grazing in cultivated/improved areas	U11
Non-agricultural land-uses	61	Recreation/tourism in unproductive areas	U36
	71	Mineral extraction and mining	U14
	72	Gas and oil extraction	U14
	73	Gravel and sand extraction/mining	U14
	81	Protection of wetlands	?
	82	Recreation/tourism in wetlands	U36
	91	Residential area	U37
	92	Services	U34, U35, U36
	93	Industrial area	U22
	94	Military area	U35?
	95	Recreation/tourism in urban areas	U36
	111	Road	U31
	112	Railroad	U31
	113	Airport	U31
	114	Port	U31
	121	Power supply	U21
	122	Water supply	U32
	123	Sewage	U32
	124	Waste disposal	U32
	131	River	U13, U32
	132	Stream	U13, U32
	133	Lagoon	U13, U32
	134	Natural lake	U13, U32
	135	Artificial lake	U13, U32
	136	Water reservoir	U13, U32
	137	Irrigation channel	U32
	138	Drainage channel	U32

[10] For the hierarchical data structure of LUISA see Figure 2.

Forest fire analysis for several years in Russia by using NOAA satellite

Jun-ichi KUDOH
Center for Northeast Asian Studies, Tohoku University, Japan
E-mail:kudoh@cneas.tohoku.ac.jp

Abstract

The main purpose of this work was to construct an efficient algorithm for forest fire detection method using NOAA satellite images. The forest fire analysis using this NOAA satellite has been done by various researchers. However, most of the method can detect the fire but a lot of false fire also appeared in the results and missing of actual fire also happened in some cases. Here we analyzed four satellite based fire detection methods to compare the fundamental differences, problems and effectiveness. To do so we used the data from AVHRR of NOAA-16 of a period of three to six months for Sakhalin and Japan region. Considering their problems and drawbacks an improved fire detection method with statistical analysis has been constructed here. Our method has reduced the false fire detection very significantly as well as detected the actual fire with high accuracy. This method can be applied to a real time forest fire monitoring system for Russia and Southeast Asian region, which is very important for early warning and early detection of fire for reducing the damages of forest fire. And also this study applied Siberian forest fire analysis for several years.

1. Introduction

A large-scale forest fire happens frequently in all parts of the world. Forest fire has serious economic implications: destruction of habitats, forests damage, costs of fire fighting and so on. Nowadays it is very important and sensitive issue in Russia and Southeast Asian region since a large scale fire occurs frequently. A huge amount of exhaustion of carbon dioxide by the forest fires is thought to be a cause of global warming. The earth environment is changing because of this global warm and air pollution [1]. At present specialist examines the damage situation after an occurrence of large-scale forest fire and it is thought that wide-ranging monitor by the satellite remote sensing may have lots of advantages in fire fighting.

A wide range real time monitoring by remote sensing satellite is essential for the grasp of the fire occurrence situation. The AVHRR (Advanced Very High Resolution Radiometer) observed on the NOAA satellite series is one of the most widely used satellite sensor for fire detection. Figure 1 shows an outline of NOAA weather satellite observation system operated by National Oceanic and Atmospheric Administration. The AVHRR provides daily data (two scenes for each operational platform) approximately at 1.1km spatial resolution, in five channels (Ch1= 0.58–0.68μm, Ch2=0.723–1.10μm, Ch3=3.55–3.93μm, Ch4=10.5–11.3μm, Ch5= 11.5–12.5μm). Moreover, the long-term availability of AVHRR data provides a good information source for obtaining an indicator of seasonal fire activity on a global scale [2]. In this work we used the NOAA-16 AVHRR data that received in Sendai (Japan) and Novosibirsk (Russia), and transferred to Tohoku University.

Here the problems of the early methods are enumerated so far and an improved fire detection algorithm is developed by using NOAA AVHRR images. Then the proposed method is applied to detect actual fire and compared with the results of fire detection by other methods. This work was performed in two regions, Sakhalin and Japan.

First, NOAA-16 AVHRR data is processed geometric correction and radiometric correction by a program which is provided by NEC [3]. This program processes geometric correction by using TBUS data. But this program cannot process high accuracy geometric correction. Therefore, further geometry correction with higher accuracy is performed by using the method proposed by M. Nakano [4] In this method GCP is created automatically and perspective transformation is used as the geometric correction algorithm.

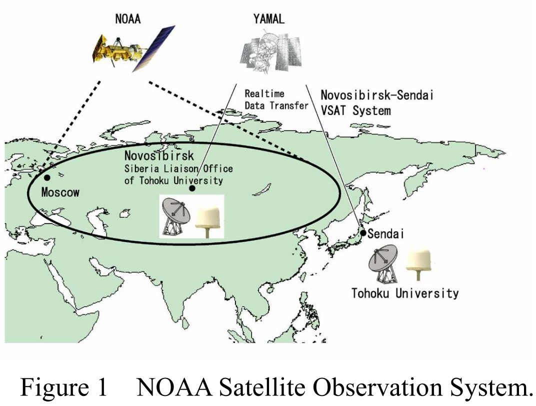

Figure 1 NOAA Satellite Observation System.

2. Fire Detection methods with AVHRR Data

AVHRR data has been widely used for fire detection for more than a decade [5] and the accuracy of detection criteria for both large and small fires has rarely been assessed using actual fire data [6] [7] [8]. In general the thermal value of Ch3 is used in most fire detection methods. It is known that the brightness temperature of Ch3 rises due to the fire point [9] [10]. Moreover, the rise like in Ch3 is not seen in Ch4 though the rise of the brightness temperature also happens to Ch4. Most of the classical AVHRR fire detection procedures are based on fixed threshold values deduced by empirical analyses [9] [10] [11] [12] [7]. Limits in the adoptability of threshold methods have been suggested by several authors (see for example Pozo et al. [13], Boles and Verbyla [6], Cuomo et al. [8]).

A contextual approach was devised to take into account the different observational and environmental conditions mainly based on spatial statistics computed from pixels within variable sized windows around candidate fire pixels. The spatial statistics are applied to pixels previously selected as potential fires from multi-spectral threshold tests [14] [15] [6].

Four fire detection methods (proposed by Flasse et. al., [4] Nakayama et al. [15], Boles and Verbyla [6], J. Kudoh[17]) have been studied using NOAA AVHRR images for Sakhalin and Japan region. Sakhalin region is chosen as large scale forest fire frequently happens. Japan region is compared to verify the false detection of fire where the cause of false detection can be made for the rising brightness value of Ch3 by the other factor rather than forest fire. It is thought that the tendency of rising brightness temperature of Ch3 as well as the possibility of false detection was high in this region.

2.1 Method of Flasse

Flasse et. al.[14] proposed a contextual algorithm which principles approach were first reviewed by Justice and Dowty [18]. The choice of thresholds used in these contextual approaches was first driven by Kaufman et. al. [9]. Further references were looked for Kennedy et. al. [10]. Flasse algorithm consists of two stages: first the selection of candidate pixels which could be potential fires (PFs) and second the confirmation of PF by comparing with their immediate neighbors as a fire point [14]. A pixel is selected as a PF by considering the following conditions:

$$T_3 \geqq 316K \quad (1)$$

$$T_3 - T_4 \geqq 10K \quad (2)$$

$$T_4 \geqq 250K \quad (3)$$

where T_3 and T_4 (in deg K) are AVHRR brightness temperatures of Ch3 and Ch4 respectively.

A PF is classified and retained as a fire when it appears to be different enough from its background. For each PF statistical information is calculated for a variable size context window (from 3 x 3 to 15 x 15 pixels) around the PF and at least 25% of neighboring pixels are considered as fire background. PF is confirmed as fire when

$$T_3 > \mu_{3bg} + 2\sigma_{3bg} + 3K \quad (4)$$

$$T_3 - T_4 \geqq \mu_{3\text{-}4bg} + 2\sigma_{3\text{-}4bg} \quad (5)$$

Here, μ is the average value and σ is the standard deviation of the background.

2.2 Method of Boles

Usually a forest fire happens in the region, where NDVI (Normalized Deference Vegetation Index) is high e.g. forest. Therefore, Boles first specify the forest by observing NDVI and added Fuel Mask algorithm to the fire condition to reduce the false detection of the places like deserts or sea. Since the NDVI before a fire point indicates a high value, NDVI for past one month is measured and the highest NDVI is assumed as MVC which is used as threshold to the fire condition.

Boles detect a fire by using the expressions mentioned below.

Fuel Mask Algorithm:

$$MVC > 0.3 \quad (6)$$

Detection of PF

$$T_3 \geqq 308K \quad (7)$$

$$T_4 > 284K \quad (8)$$

$$T_3 - T_4 > 10K \quad (9)$$

Fire detection

$$T_3 > \mu_{3bg} + 1.5\sigma_{3bg} \quad (10)$$

$$T_3 - T_4 > \mu_{3\text{-}4bg} + 1.5\sigma_{3\text{-}4bg} \quad (11)$$

$$R_2 > \mu_{2bg} + \sigma_{2bg} \quad (12)$$

where R_2 is reflectivity of Ch2.

Here the false detection may reduced because the place with the possibility of fire occurrence is specified from the situation of past vegetation and a more certain fire may be detected.

2.3 Method of Nakayama

Nakayama et. al. improved the part where the standard deviation is used in Contextual algorithm by using the mean deviation. Moreover, it tests the part that will be used as a background. The fire detection is done as follows:

Detection of PF

$T_3 > 320K$ (13)
$T_3 - T_4 > 6K$ (14)
$R_2 < 25\%$ (15)
Background test
$T_3 < 318K$ (16)
$T_3 - T_4 < 12K$ (17)
Fire detection
$T_3 - T_4 > \mu_{3-4bg} + \max(\delta_{3-4bg}, 4K)$ (18)
$T_4 > \mu_{4bg} + \delta_{4bg} - 3K$ (19)
Here δ is the mean deviation of background.

2.4 Method of Kudoh

Kudoh et. al. proposed the fire detection method that uses the feature of the fire point obtained from Three Dimensional Histogram of Ch1, Ch3 and Ch5 which is made from past fire information. First of al, 14 years forest fires information from NOAA AVHRR images were accumulated in a Three Dimensional Histogram. Accumulated area was in Far East Russia about 1100 km square region with 681 scenes, 55983 points. Actually the fire is detected from these past AVHRR images by using the method of Flasse. Next, it looks for actual fire point as a result of confirmation by watching the deterioration of NDVI, the presence of smoke and the changes of the temperature in time series. Obtained fire point is collected as fire information and plotted in Three Dimensional Histogram (Kudoh et. al., 2003). To detect a fire the threshold is assumed as the saturation value of 1023 for Ch3 (Ch3 ≧ 1023). So, Two Dimensional Histogram composed on Ch1 and Ch5 is obtained, which makes some looped area of the accumulated fire corresponding to occurrence number as shown in figure 2. These circles provide reliable fire detection category. Those pixels enter into this category are considered as actual fire. In this category the accuracy of the fire detection goes up by using the number of frequency four or more.

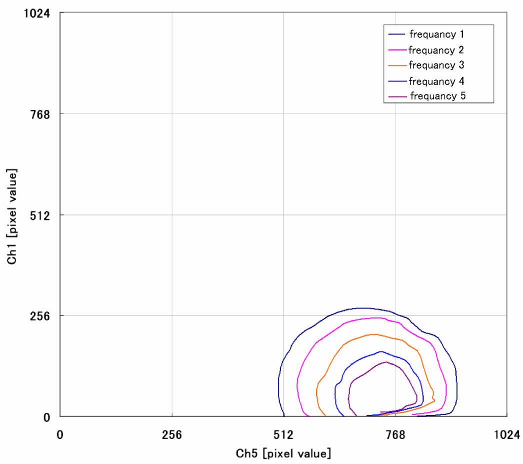

Figure 2 The fire category in Two Dimensional Histogram.

3. Comparisons and Problems Finding

To compare the results of fire detection, above four methods were applied in two regions, Sakhalin and Japan. In Sakhalin, the applied period was from June to August, 2003 as a large number of forest fire happened frequently. It is from May to September, 2004 in Japan when a marvelous heat was intense and high temperature was recorded in various places. It is thought that the tendency of rising brightness temperature of Ch3 as well as the possibility of false detection was high in this region especially during those periods. Therefore, the false fire detection by each method will be verified.

3.1 Comparison in Sakhalin region

An image of NOAA 16 on June 17, 2003 where a fire broke out in the Sakhalin region has been applied for each method. The obtained result of each method for Sakhalin region is shown in figure 3. Detected fire points indicated by red dots in each image of the figures. It is clear that all method adequately detected the actual fire where a fire breaks out in the center of the image and smoke is generated.

Flasse et al. Nakayama et al. Boles et al. Kudoh et al.

Figure 3 Comparison among the results of early methods in Sakhalin region (NOAA-16 on June 17, 2003).

Moreover, the false detection also happened more or less for each method. False detection is appeared in the sea, here and there for the method of Flasse. Since the fire occurrence place is specified by using MVC in the Boles method, the false detection in the sea is not appeared. However, the false detection in the cloud region stands out probably for the setting of low threshold. The false detection tendency for Nakayama method also looks like Flasse method. In Kudoh method, comparing with others, the false detection is found very few though the actual fire has been detected adequately. It is very clear to understand that in case of Flasse et. al. and Kudoh et. al. the false fire detection is comparatively a little. Next these two methods have been applied for Japan region.

3.2 Comparison in Japan region

The results of fire detection for an image of NOAA-16 on 7 July 2004 is shown in figure 4 and figure 5 for Flasse and Kudoh method respectively. Either methods detected huge red fire points which were actually false fire points. As in reality there were happened no forest fire on that time. In case of Flasse method in figure 4, false detection happened in the coastline and the cloud area. In figure 5, Kudoh method showed the false detection mainly in the central area of Tokyo and other area where the value of brightness temperature of Ch3 were very high.

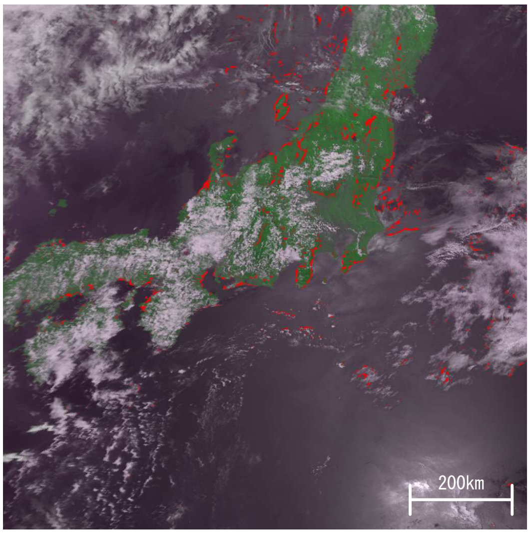

Figure 4 Result of Flasse method in Japan region.

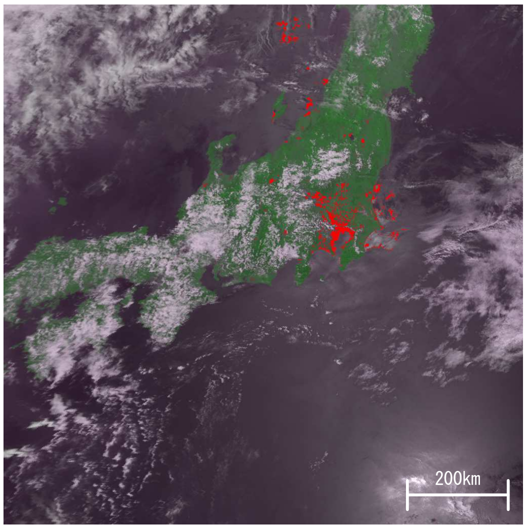

Figure 5 Result of Kudoh method in Japan region.

In the graph of figure 6 shows the comparison of detected fire points for each method applied in Japan region for the image of NOAA-16 on July 7, 2004. In vertical positioned values are the fire points that actually are the false fire points, because the fire that observed with NOAA in the graph has hardly happened in Japan.

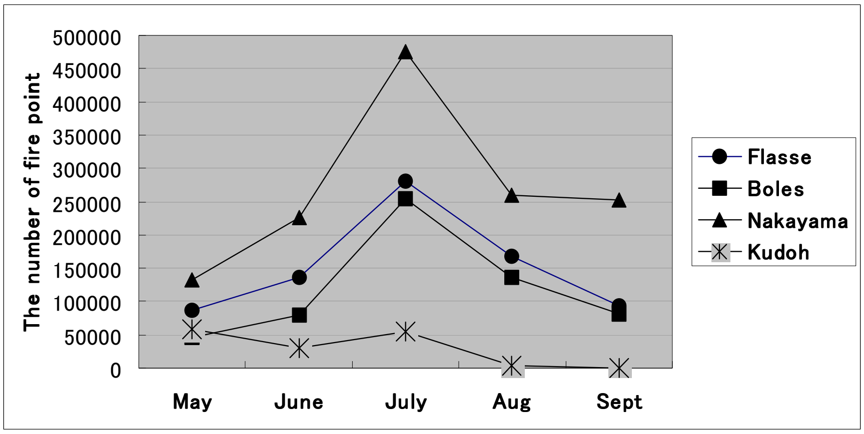

Figure 6 Comparison of detected fire points in Japan region, 2004.

Since fire has been detected based on the brightness temperature of Ch3 in cases of Flasse, Boles and Nakayama, the maximum number of false fire has been detected on the period of July when a high temperature was recorded in Tokyo and other places of Japan. The least false fire has been detected by Kudoh et. al. among the other methods since this method has detected a fire by the threshold processing for Ch3.

To find the reasons of this false detection gray scale images for Ch3 on July 7, 2004 of NOAA-16 in Japan region has been plotted and analyzed as shown in figure 7 and figure 8. Since the method of Flasse have detected a fire by the comparison with the surrounding background, a lot of false detection went out at the part where the brightness temperature of Ch3 is turned such as the coastline and the cloud region as in figure 7. In case of Kudoh et. al. method a fire has been detected by the threshold processing of Ch3. Therefore, a lot false detection is appeared in the part where the value of brightness temperature of Ch3 is very high (figure 8).

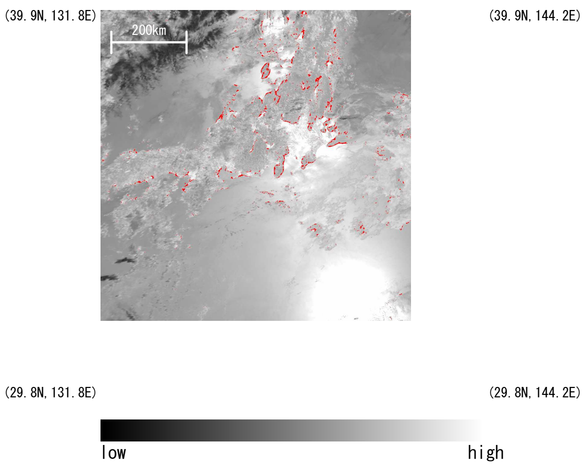

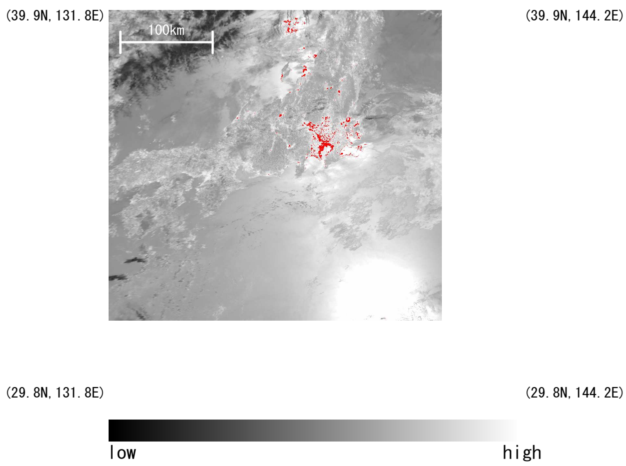

Figure 7 Case of Ch 3 method of Flasse.

Figure 8 Case of Ch 3 method of Kudoh.

From the above comparisons it is very clear that the accuracy of fire detection is highly dependent on the rising brightness value of Ch3. The brightness value of Ch3 fluctuates largely with the change of temperature with latitude and season. It can goes up by the reasons other than the fire such as 1) the rise of temperature by season in urban area or in desert, 2) the highly developed sun rise which makes reflection of the sun light on the sea. It can be confirmed here in figure 8 that a very high value was produced by the reflection of the sun light on the sea and false fires were detected on those spots.

Moreover, the rise of the brightness temperature of Ch3 is radiated by the rise of the temperature in summer in Tokyo and its surrounding area which is thought to be a cause of the false detection in Japan region in July 2004 by Kudoh method, figure 8. We presumed that the accuracy of fire detection may goes up if these problems can be considered in fire condition.

4. Proposed Method

From all the above comparisons and discussion it is clear that in case of Kudoh method, the difficulties of fire detection were comparatively low among the other methods. The main difficulties in fire detection were false detection. That means the fire has been detected in places where fires did not appear in real. First of all, it is thought that the false fire detection can be decreased by specifying the region where the possibility of fire occurrence is present (such as forest), using NDVI (used in Boles et. al. method). So, the possibility of the false detection in the sea might be removed. Moreover, the rise of brightness temperature of Ch3 goes up gradually due to seasonal factor (such as in summer) whereas the rise goes up sharply for a forest fire. So it is thought that the fire can be detected more accurately if we consider these natures in fire condition.

4.1 Algorithm

Here we proposed a new fire detection method by improving the Kudoh et. al. technique and by reducing the false fire detection using statistical analysis. Figure 9 shows the flowchart of proposed algorithm. First of all, the image where it wants to detect a fire is called a target image. From the target image, NDVI is observed for past one month and MVC is calculated from the highest value of these NDVI.

It is thought that the false detection of the places such as sea, to which it comparatively rises the temperature of Ch3, can be decreased by considering this MVC to the fire condition. Actually in this step the places with the possibility of fire occurrence (such as forest) are specified from the situation of past one month vegetation.

Then we applied Kudoh method to detect the fire points from those specified places. It was assumed that some false detection might be appeared due to the rise of brightness temperature of Ch3 by the seasonal factor rather than a fire. To remove this false detection a statistical analysis is done over those fire points.

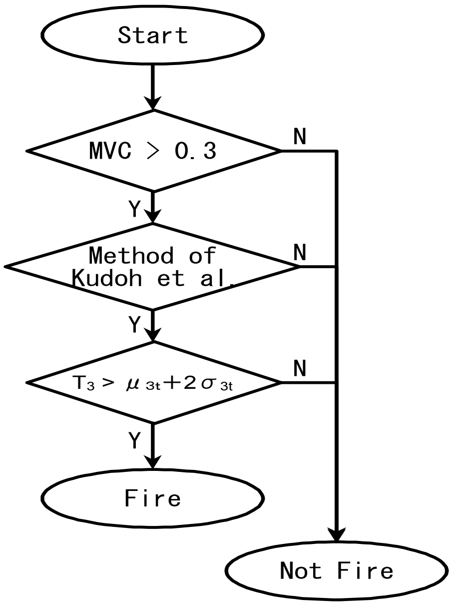

Figure 9 Flowchart of Proposed method.

In statistical analysis a threshold value has been fixed to remove this false detection and added in the fire condition. First of all, from the target image the value of mean and standard deviation of each pixel for past 20 days from the target day has been calculated for Ch3. At this time the part of cloud region in the target image has not been used. Since the brightness temperature of Ch3 for cloud region is lower than the actual ground level, the average value might be lower in calculation. For this purpose it has been avoided the influence of cloud region. Finally a threshold value is obtained from these mean and standard deviation values of Ch3 by considering the equation (20).

$$T_3(x, y) \geqq \mu_t(x, y) + 2\sigma_t(x, y) \qquad (20)$$

Here, $T_3(x, y)$ is the value of Ch3 of target image on (x, y) coordinates, $\mu_t(x, y)$ is the mean value of Ch3 for past 20 days from target day and $\sigma_t(x, y)$ is the standard deviation on (x, y) coordinates. When the value of Ch3 of a pixel was higher than this threshold, it was considered as a fire point.

4.2 Results and evaluation

Our new method is applied in Sakhalin and Japan region by using the same images of NOAA-16 for same period which were used previously in the comparisons on early methods. Then the evaluation has been done by comparing the results of our method with the results of Kudoh method. This verification has been done for both Sakhalin and Japan region as mentioned below.

4.3 Sakhalin region

Figure 10 shows the image of NOAA-16 for the fire detection results of our method in Sakhalin region on June 17, 2003. It is seen in the image of Sakhalin that fire points have detected adequately at the center with smoke as fires mentioned by the red points. Moreover, it is understood that very few false detection appeared in the image of Sakhalin region. No false detection appeared in the sea or cloud region as it was appeared for Flasse or Boles method. The main difficulties of fire detection have been overcome in this method.

Figure 11 shows the graph of comparison between Kudoh et. al. and our proposed method for fire detection points in Sakhalin on 2003. From this graph it is clear that our method detected the fire for Sakhalin region almost in the same degree as it is detected by Kudoh method. It is confirmed that proposed method can detect the actual fire in the same degree of accuracy as it can by the Kudoh method.

Figure 10 Result of proposed method in Sakhalin on June 17, 2003.

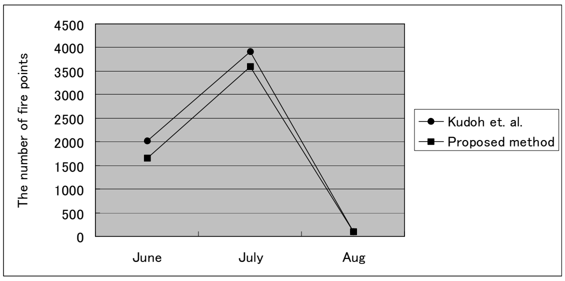

Figure 11 Comparison of the fire points in Sakhalin region, 2003.

4.4 Japan region

The results of fire detection by proposed method for an image of NOAA-16 on 7 July 2004 in Japan region is shown in figure 12. It shows that very few false fire points have been detected here in Japan region by our method. It is clear that the number of false fire points decreased greatly if we compare this result with the result of Kudoh as shown in figure 5.

A high temperature continued by the intense heat in Japan region from May to September 2004. Therefore, a lot of false fire detection was found in Kudoh technique. Figure 13 shows the graphical comparison of fire points found in our method and Kudoh method for Japan region in 2004. The fire points as shown in graph were actually false fire points. Very little false detection appeared in our method. It is clear that in our method the number of false fire points has decreased greatly in the comparison to Kudoh method. Our method is improved by decreasing the number of false fire detection and makes fire detection much more efficiently than early methods. However a few number of false fires appeared as it was not possible to remove all false fire to maintain the high accuracy of actual fire detection.

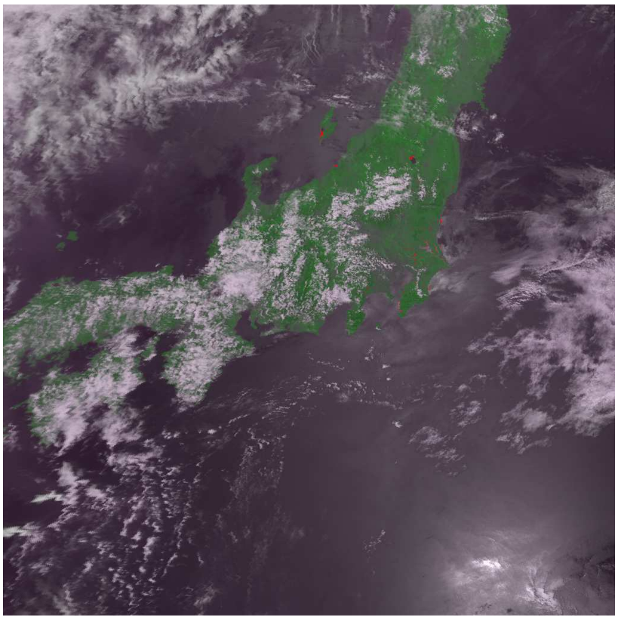

Figure 12 Result of proposed method in Japan on July 7, 2004.

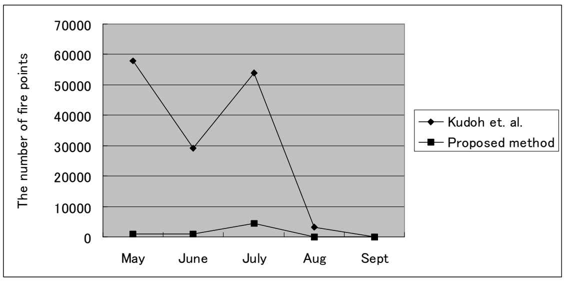

Figure 13 Comparison of false detection points in Japanese region, 2004.

5. Applied for Siberian Region

This study applied Siberian forest fire analysis from 2002 to 2004 for every April to September. The analysis area is divided 15 regions including Siberia, Mongolia and north China shown in figure 14. Each region is 1024x1024 size for AVHRR image.

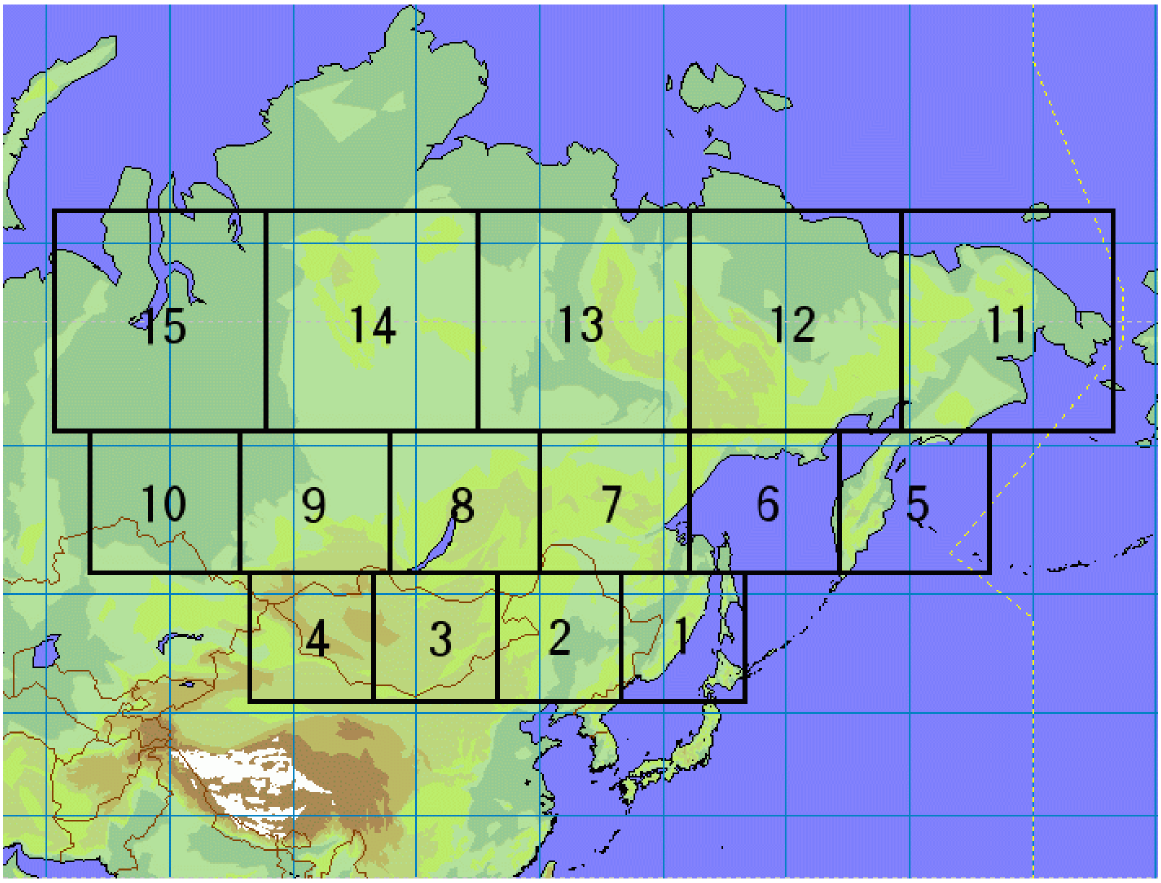

Figure 14 Divided regions map for Siberia forest fire analysis.

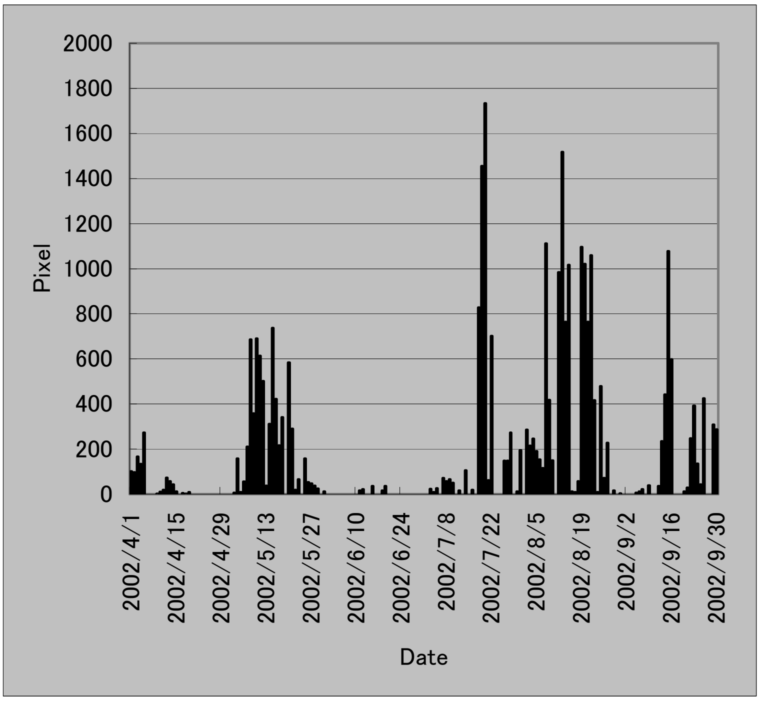

Figure 15 Detected hot spot pixel in Siberia 2002.

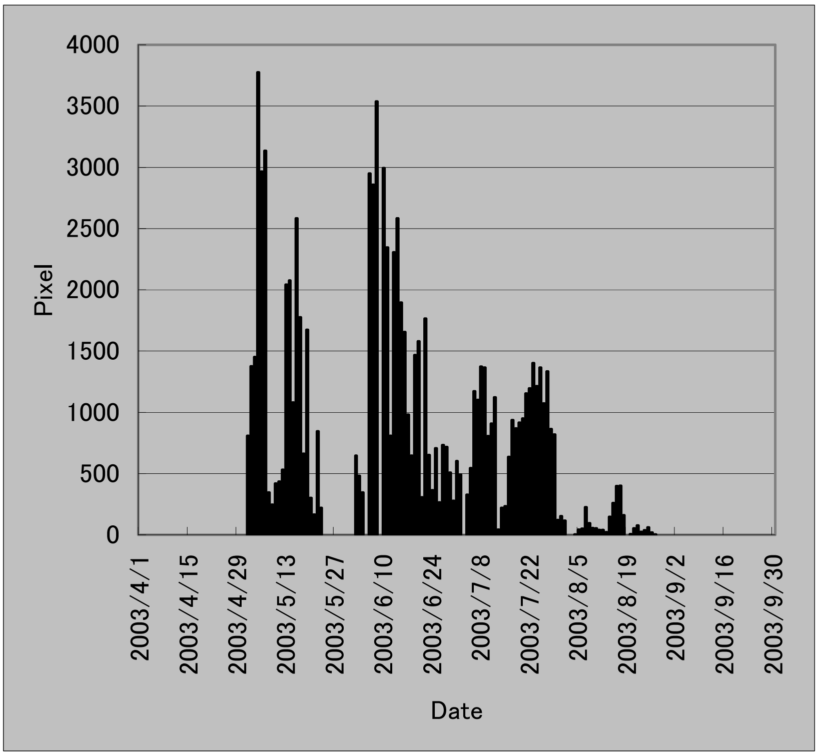

Figure 16　Detected hot spot pixel in Siberia 2003.

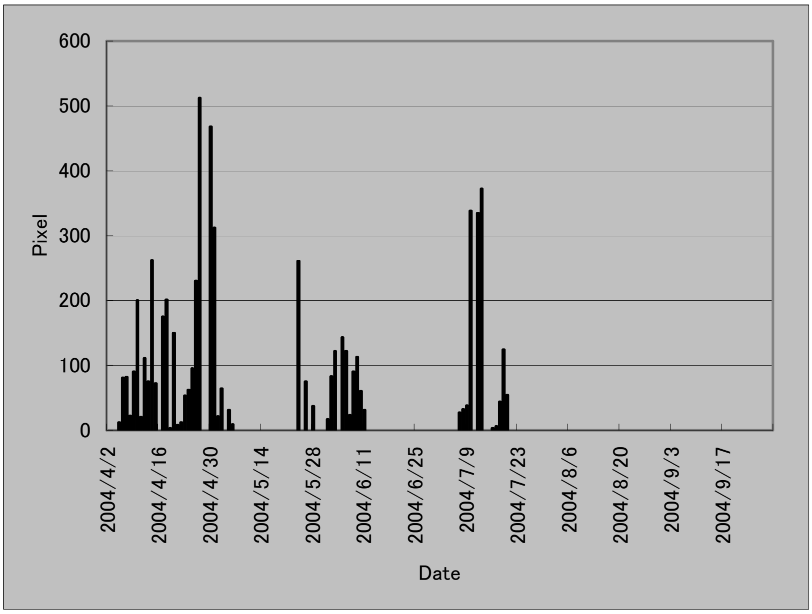

Figure 17　Detected hot spot pixel in Siberia 2004.

The detected hot spot pixel is shown in figure15 – figure 17. This study is continued to more yearly analysis to find the fire pattern, feature, and affecting Japan.

6. Conclusions

In this work a new fire detection method using NOAA AVHRR images have been constructed. Our method detected the actual fire with the degree of high accuracy by overcoming the difficulties of actual fire detection. Moreover it reduced the number of false fire detection very significantly. In this work to maintain the high accuracy of actual fire detection it could not be possible to remove 100% false detection. Our method can be used to provide a real time fire monitoring system and can be calculated the burned area more accurately. A future subject is to find out the cause of these few false fire points that appeared in our results.

7. References

[1]FRA 2000 (Global Forest Resources Assessment 2000 - Main report), FAO forestry paper 140.
[2]EVA, H., and LAMBIN, E. F.,Remote Sensing of biomass burning in tropical regions: sampling issue and multisensor approach. Remote Sensing of Environment, 64, 292–315(1998).
[3]NEC CORPORATION, NOAA receiving and processing manual (in Japanese)(1996).
[4]M. NAKANO, Y.HARAMOTO, J.KUDOH, An automatic GCP creation method for geometric correction for Multi-time NOAA/AVHRR images, Journal of the remote sensing society of Japan, Vol.25, No.2, pp. 191-197(2005).
[5]LEVINE, J. S. (editor), Global Biomass Burning, Cambridge, MA: MIT Press (1991).
[6]BOLES S. H., and DAVID L. VERBYLA, Comparison of Three AVHRR-Based Fire Detection Algorithms for Interior Alaska, Remote Sensing of Environment, 72, 1-16(2000).
[7]LI, Z., NADON, S., and CIHLAR, J., Satellite-based detection of Canadian boreal forest fire: development and application of the algorithm. International Journal of Remote Sensing, 21, 3057–3069 (2000).
[8]CUOMO, V., LASAPONARA, R., and TRAMUTOLI, V., Evaluation of a new satellite based method for forest fire detection. International Journal of Remote Sensing, 22, 1799–1826 (2001).
[9]KAUFMAN, Y., TUCKER, C. J. and FUNG, I., Remote sensing of biomass burning in the tropics. Journal of Geophysical Research, 95, 9927-9939 (1990).
[10]KENNEDY, P. J. BELWARD, A. S., AND GREGOIRE, J. M., An improved approach to fire monitoring in West Africa using AVHRR data. International Journal of Remote Sensing, 15, 2235-2255 (1994).
[11]RAUSTE, Y., HERLAND, E., FRELANDER, H., SOINI, K., KUOREMAKI, T., and RUOKARI, A., Satellite-based forest fire detection for fire control in boreal forests. International Journal of Remote Sensing, 18, 2641–2656 (1997).
[12]ARINO, O., and MELINOTTE, J. M., The 1993Africa fire map. International Journal of Remote Sensing, 19, 2019–2023 (1998).
[13]POZO, D., OLMO, F. J., and ALADOS-ARBOLEDAS, L., Fire detection and growth monitoring using a multitemporal technique on AVHRR mid-infrared and thermal channels. Remote Sensing of Environment, 60, 111–120 (1997).
[14]FLASSE S.P., CECCATO P., A contextual algorithm for AVHRR.re detection, Int.J.Remote Sensing, Vol.17, No.2, 419-424 (1996).
[15]NAKAYAMA, M.MAKI, C.D.ELIVIDGE, S.C.LIEW, Contextual Algorithm adapted for NOAA-AVHRR.re detection in Indonesia, Int. J. Remote Sensing,Vol.20, No.17, 3415-3421 (1999).
[16]BARBOSA, P. M., GREGORIRE, J., and PEREIRA, J. M. C., An Algorithm for Extracting Burned Areas from Time Series of AVHRR GAC Data Applied at a Continental Scale. Remote Sensing of Environment, 69, 253-263 (1999).
[17]J. KUDOH, and K. HOSOI, Two Dimensional Forest Fire Detection Method by Using NOAA AVHRR Images IEEE 2003 International Geoscience and Remote Sensing Symposium 2003, 2494-2495 (2003).
[18]JUSTICE, C. O., and DOWTY, P. (editor), IGBP-DIS satellite fire detection algorithm workshop technical report. IGBP-DIS working paper, 9, 88pp., February 1993, NASA/GSFC, Greenbelt, Maryland, USA

Agricultural Land-Use Change in Northeastern Asia and Climate Change

Katsuo OKAMOTO[1], Junko SHINDO[1] and Hiroyuki KAWASHIMA[2]
[1] National Institute for Agro-Environmental Sciences
[2] Graduate School of Agricultural and Life Sciences, University of Tokyo
E-mail: kokamoto@affrc.go.jp

Abstract
The self-sufficiency of rice in China, which has the largest population in the world, is 100% and Chinese people tend to prefer quality over quantity. The total area of paddy field in the northeastern part of China has increased because the climate conditions in this region are suitable for cultivating *Japonica* rice (short-grain rice). Large quantities of irrigation water are consumed for cultivating rice. Rainfed rice cropping is possible in places with sufficient precipitation, whereas rice cropping in regions with low precipitation is limited in places with easy access to water for irrigation. Flatlands are advantageous for rice cropping because of their geographical and social conditions. The eastern Heilongjiang province of China was selected as the test area for satellite image analysis. Land use/land cover was classified using the Landsat Thematic Mapper (TM) data of 1988 and the Enhanced Thematic Mapper Plus (ETM+) data of 2002. According to the statistics of Heilongjiang Province, the total area of paddy field has increased rapidly since 1995. On the basis of the 1988 land-use/land-cover classification map, areas suitable for rice cropping were determined and compared with the distribution of paddy fields in 2002. Most of the paddy fields in 2002 were changed from dry arable lands in 1988. The areas suitable for rice cropping are those with easy access to water for irrigation. Moreover, as a result of climate changes, air temperature and precipitation may become unsuitable for the cultivation of major cereals in Asia. Conversely, agriculture would affect the environment unfavorably. The major river basins with rice-cropping zones from East to Southeast Asia were studied. The possible changes in water quality in the future were evaluated. The data used included the river course, land-use/land-cover classification, population, climate, nitrous oxide (NOx) emission, and country boundary. Statistical data on rice yield, harvested area, fertilizer usage, food production, food consumption and food trade were also used to construct nitrogen load maps. The nitrogen load changes seasonally depending on the cropping systems used and the amount of precipitation. In the future, nitrogen discharge from humans and fertilizer use will increase along with the increase in population and cultivation intensity. Fertilizer use and NOx deposition will also increase along with economic growth. Therefore, the nitrogen concentration in river water will also increase. Excessive irrigation and fertilizer use during the dry season will result in the further deterioration of water quality, creating nonsustainable ecosystems in river basins.

1. Introduction
The total area of arable cropland has steadily increased throughout the world over the past 300 years (Ramankutty and Foley 1999). This is the reason why food production has increased to sustain the population increase. Consequently, the total area of arable land has increased not only in highly productive areas but also in unfavorable areas.

Asians now represent 55 percent of the world population, and this figure has continued to increase in recent years (Figure 1). Farmers in Asia are increasing rice production to sustain the population increase (Figure 2). Large quantities of irrigation water are consumed for cultivating rice. Hydrological conditions change according to changes in water use in agriculture. Moreover, a paddy field is a source of methane which is one of the greenhouse effect gases (IPCC 1995). Moreover, an abrupt change in land use/land cover and a rapid increase in the total area of paddy field have negative effects on the ecosystem and environment.

In this study, the eastern Heilongjiang province of China was selected as the test area and satellite data acquired on different dates were analyzed. The changes in the total area of paddy field were examined, and the geographical and social conditions of an area to be changed from dry cropland to paddy field were studied. Thereafter, the possible impacts of agriculture to the ecosystem and environment were assessed.

2. Rapid land-use/land-cover change in Northeastern China using Landsat TM/ETM+ data
The self-sufficiency of rice in Asian countries has reached nearly 100%. The self-sufficiency of rice in China, which has the largest population in the world, is 100% and Chinese people tend to prefer quality (eating delicious rice) over quantity (eating heartily). Therefore, the production of good-tasting *Japonica* rice (short-grain rice) has increased compared with that of *Indica* rice (long-grain rice). The total area of paddy field in the northeastern part of China, where the climate conditions fall within the marginal zone for cultivating *Japonica* rice originating from the subtropical zone, has increased. Heilongjiang is now a major rice bowl in China. This province produces about 560 million metric tons of *Japonica* rice per year, according to the estimates from the statistics of FAO (2004) and USDA (1999). The total area of paddy field in Heilongjiang has increased from 2.2×10^3 km^2 to 16.5×10^3 km^2 (7.5-fold) over the past 20 years (Heilongjiang Provincial Bureau of Statistics 2004) (Figure 3).

2.1 Test area of satellite image analysis
The land-use/land-cover change in the northeastern part of China was analyzed using multitemporal Landsat data. The

agricultural region (131˚ 35’-134˚ 33’ E, 46˚ 29’-48˚ 24’ N) that extends to the eastern Sanjiang Plain of Heilongjiang province in China, which includes Fujin City, Tongjiang City, Fuyuan Prefecture and Raohe Prefecture, was selected as the test area (Figure 4). The Heilong Jiang (the River Amur) flows north of this area, the Songhua Jiang flows west of this area into the Heilong Jiang, and the Wusuli Jiang flows east of this area. This area has an annual precipitation of 550-600 mm and is located in a continental monsoon climatic zone. The highest temperature during summer reaches 22-27 ˚C.

2.2 Data used for satellite image analysis

The Landsat Thematic Mapper (TM) data acquired on 25th June 1988 and the Landsat Enhanced Thematic Mapper Plus (ETM+) data acquired on 24th June 2002 (Path-Row=114-27) were used for the land-use/land-cover classification. In the test area, rice seedlings are transplanted simultaneously within a short period from the end of May to the beginning of June. At the end of June, the rice plants are still small and the paddy fields are still submerged. At this time, the crops planted on dry croplands are also small and the soil surfaces are exposed.

The 0.5-degree grid cell data of monthly mean air temperature from 1901 to 2000 (Mitchell *et al*. 2003), were used to examine the changes in cumulative temperature for the rice-cropping season from June to September. The 1978-2000 statistics of the total areas of paddy field and dry cropland derived from the Heilongjiang Statistical Yearbook 2004 (Heilongjiang Provincial Bureau of Statistics 2004) were used to examine the changes in the wheat area. The 1991-2001 statistics of the producer prices of rice, wheat and maize in China (FAO 2004), were used to analyze the impact of the change in the cultivated crop.

2.3 Method for satellite image analysis

The Landsat TM data acquired on 25th June 1988 and ETM+ data acquired on 24th June 2002 were assigned geographical coordinates using the Lambert Azimuthal Equal area projection (origin=110˚ E, 45˚ N), the spheroid WGS84 and the pixel size 30 m x 30 m. The TM/ETM+ data with bands 3 (red), 4 (near infrared), and 5 (middle infrared), in which the middle-infrared band was used in distinguishing submerged paddy fields (Okamoto and Fukuhara 1996), were prepared for the land-use/land-cover classification. These data were classified by the ISODATA method, in which 30 initial classes, 2σ class radius, and 98% convergence limit were used as parameters. The portions of misclassification in the land-cover maps for 1988 and 2002 were corrected by viewing interpretations of composite images, in which bands 5, 4 and 3 of TM/ETM+ data are shown as blue, green and red, respectively. Land-cover classes were reclassified into the following 12 classes: paddy field submerged, paddy field overgrown, bare dry cropland, dry cropland overgrown, bare ground, grassland, woodland, wetland, water, built-up, shade and shadow, and clouds.

The land-use/land-cover changes between 1988 and 2002 were examined by overlapping the1988 and 2002 land-cover maps. Five-hundred- and 1,000-meter buffers around a water source were defined as the water availabile for irrigation. The areas within 500 and 500-1,000 meters from a water source, which included paddy field, wetland and water, were extracted. The land-use/land-cover changes between 1988 and 2002 were examined in terms of the distance to a water source.

2.4 Land-use/land-cover change

According to the Heilongjiang Statistical Yearbook 2004 (Heilongjiang Provincial Bureau of Statistics 2004), the total area of paddy field increased rapidly during both the mid-1980s and mid-1990s (Figure 3). The land-use/land-cover maps are shown in Figure 5. According to the results from a comparison of the land-use/land-cover map of 2002 with that of 1988, the total area of paddy field in the test area increased from 166 km^2 in 1988 to 3,925 km^2 in 2002, that is, it increased 23.6-fold (Table 1(a), Figure 6). The total area of dry cropland in the test area decreased from 11,065 km^2 in 1988 to 8,988 km^2 in 2002, that is, it decreased by 19%. However, the total area of arable land, which included paddy field and dry cropland, increased from 11,231 km^2 in 1988 to 12,913 km^2 in 2002. On the other hand, the total area of wetland decreased from 3,260 km^2 in 1988 to 21 km^2 in 2002. The total areas of woodland and grassland decreased from 15,274 km^2 in 1988 to 13,447 km^2 in 2002. Of the 3,925 km^2 of paddy field in 2002, 96.5 km^2 was also classified as paddy field in 1988; however, 2,523 km^2 was classified as dry cropland in 1988, 509 km^2 grassland, 485 km^2 woodland, and 281 km^2 wetland. It was assumed that wetland had been easily changed to paddy field because of its proximity to rivers. However, only 9% of wetland in 1988 had been changed to paddy field in 2002, whereas 40% of wetland in 1988 had been changed to dry cropland in 2002. That is, the total area changed from wetland to paddy field was smaller than that from wetland to dry cropland.

The total area of dry cropland, grassland and bare ground within 500 meters from a water source was 10,539 km^2 and that within 500-1,000 meters from a water source was 5,164 km^2 (Table 1(b), Figure 7). In 2002, 2,650 km^2 of paddy field was located within 500 meters from a water source, whereas 690 km^2 of paddy field was located within 500-1,000 meters from a water source.

These results suggest that most wetlands in 1988 were reclaimed and changed to dry cropland in 2002, whereas a part of the reclaimed wetland was changed to paddy field. It is possible that the abrupt increase in the total area of paddy field between 1988 and 2002 resulted from the conversion of dry cropland, which was favorably situated near a water source, to paddy field.

The Landsat TM/ETM+ data, which were used in this study, for 1988 and 2002 were acquired on 25th June and 24th June, respectively. As Heilongjiang is a granary of spring wheat and maize, it was concluded that the land-cover class “dry cropland overgrown” was cultivated with spring wheat and “bare dry cropland” was cultivated with maize, referring to a cropping calendar. According to the land-use/land-cover maps, the total area of bare dry cropland was 6,063 km^2 and that of dry cropland overgrown was 5,002 km^2 in 1988, whereas the area of bare dry cropland was 8,988 km^2 and that of dry cropland overgrown was 0 km^2 in 2002 (Table 1(a)). These results suggest that farmers, who cultivated spring wheat in those croplands, stopped wheat cropping and changed their dry cropland to paddy field.

2.5 Climate impact and probable socioeconomic impact on land-use change

Temperature and precipitation are natural factors that have an impact on cereal cropping. The cumulative temperatures of the rice-cropping season (June through September) in 1901-2000 are shown in Figure 8. All the cumulative temperatures at Harbin City, Jiamusi City and Qianjin Prefecture were just above the lower limit for cultivating *Japonica* rice and were nearly constant through the 21st century. On the other hand, the test area has geographically low and flat features. The level of groundwater is high and the cropland in the test area is favorably situated near a water source. Consequently, it is surmised that climate conditions, such as temperature and water, did not cause an abrupt increase in the total area of paddy field.

The producer price and consumer price related to cereal demand are socioeconomic factors that have an impact on cereal cropping and land-use change. According to the Heilongjiang Statistical Yearbook 2004 (Heilongjiang Provincial Bureau of Statistics 2004), the total area of paddy field increased rapidly in both the mid-1980s and mid-1990s (Figure 9). In particular, the total area of paddy field in the mid-1990s increased markedly. The producer prices of rice, wheat and maize in China from 1991 to 2001 are also shown in Figure 9. These three producer prices are not corrected according to inflation. An abrupt increase in the total area of paddy field from 1996 to 1998 followed a sudden increase in producer price. In 1994, the Chinese Government increased the purchase price of cereals by 40% (Chien, X., personal communication, 22 November 2004). The prices shown in Figure 9 are the mean producer prices in China. The producer price of wheat produced in Heilongjiang is lower than that of wheat produced in other provinces because the quality of wheat produced in Heilongjiang is lower than that of wheat produced in other provinces. The producer price of rice produced in Heilongjiang is higher than that of rice produced in other provinces because the price of *Japonica* rice produced in Heilongjiang is higher than that of *Indica* rice produced in the southern provinces. Therefore, the difference between the producer prices of rice and wheat produced in Heilongjiang is larger than those shown in Figure 9. Consequently, it is probable that the high producer price of rice in comparison with the producer prices of other cereals, is one of the strong motivations for converting dry cropland to paddy field.

3. Impacts of agriculture on environment

The population in Asia has steadily increased, as mentioned earlier, and both irrigated cropland total area and agricultural production have also increased to sustain the population increase (Figures 1 and 2). The effects of these changes on the environment are considerable.

The use of nitrogen (N) fertilizer, for example, has increased more than eightfold since 1961 (Figure 10), posing considerable problems for water quality. Japan now uses an average of 100 kg of N equivalent per hectare (ha) of farmland, whereas farms in China and Western Europe use more than 100 kg ha^{-1}. The average yield per unit area in Western Europe is 10 t ha^{-1}, whereas that in China is only about 5 t ha^{-1}. This means that the N fertilizer used in China is released into the environment at a faster rate than that in Western Europe (Kawashima and Okamoto 1999).

In Southeast Asia, the average usage is 70 kg of N ha^{-1} (Kaewthip *et al*. 2003). In some areas in China 500 to 1,900 kg of N ha^{-1} is consumed (Zhang *et al*. 1996). In Japan, 400-1,560 kg of N fertilizer is consumed per hectare (Tokuda and Hayatsu 2001).

The nitrogen load from fertilizer has a considerable impact on water quality (Okamoto *et al*. 2003). The rapidly increasing nitrogen load from fertilizer may even have impacts on the environment and climate through changes in vegetative biomass (NPP: Net Primary Production) and nitrous oxide (N_2O) emission. We constructed a nitrogen load map on the basis of measurements of nitrogen concentrations in major river basins in the eastern part of Asia.

3.1 Test sites for impact analysis of agriculture on environment

Major river basins from East to Southeast Asia were selected as test sites. The major crop in these test sites is rice. Rice production in these regions represent 90% of that in the world. The test sites are located 30-150° E longitude and 90° N-12° S latitude. The test sites included the river basins of Amur, Huanghe (Hwang Ho, Yellow), Chang Jiang (Yangtze), Xi (Hsi, Pearl), Red (Hong Ha, Hungho), Mekong, Chao Phraya (Mae Nam) and Irrawaddy in the eastern part of Asia (Figure 11).

3.2 Data for impact analysis of agriculture

The 0.5° version of the Total Runoff Integrating Pathways (TRIP) data (Oki and Sud 1998) was used to determine river courses in test areas. The global 1-km land-cover data set DISCover (Belward *et al*. 1999) was used for the land-use/land-cover classification of test sites.

The population data of Asia and the Russian Federation (Dao and Eckert 1998, Deichmann 1996) and the statistical data on food consumption and food trade (FAO 2004, National Bureau of Statistics 2000) were used to calculate the nitrogen load from humans. The statistical data on fertilizer use and food production (FAO 2004, National Bureau of Statistics 2000) were used to calculate the nitrogen load from the agricultural sector. The amounts data of NOx emission from the Center for Global and Regional Environmental Research (CGRER) and University of Iowa (Bouwman *et al*. 1995) were adopted for estimating the nitrogen load from the industrial and economic sectors. The monthly mean air temperature and monthly mean precipitation from the mean 1961-1990 climatology values (New *et al*. 1999) were used for calculating the amounts of available water and discharged water in each river basin. The results from a simulation study (Shindo *et al*. 2003) were summarized for each river basin. They were also summarized for countries or provinces in China, using the country boundary data from the World Boundary Databank (CGER 1994) and the provincial boundary data of China (LREIS 1996).

3.3 Method of impact analysis of agriculture

The land-use/land-cover areas from the DISCover (Belward *et al*. 1999) were reclassified into eight categories: irrigated paddy field, rain-fed paddy field, irrigated cropland, rain-fed cropland, woodland, grassland, other land-use/land-cover and water. The typical cropping season of rice in the test sites for each country was determined by referring to Country Rice Facts (Crop and Grassland Service 2000) and Major World Crop Areas and Climatic Profiles (World Agricultural Outlook Board 1994) (Table 2).

Using the results from a simulation study (Shindo *et al*. 2003), the changes in the amount of nitrogen discharged artificially were discussed. The model is based on some assumptions on N discharge. The rate of nitrogen discharge from cropland depends on the cropping systems used. For a single rice cropping, nitrogen is discharged from a paddy field at the rate of 2:1:1 from May to July. For the rice cropping in rotation with wheat, one-half of the annual amount of nitrogen consumption is discharged for rice cropping at the rate of 2:1:1 from May to July, and the rest is discharged equally from October to April. For double rice cropping, nitrogen is discharged at the rate of 2:1:1 from April to June and from August to October. For triple rice cropping, nitrogen is discharged equally every month. From upland cropland, nitrogen is discharged equally every month. Nitrogen from livestock and humans is discharged equally every month. NOx is emitted and deposited equally in the same grid cell every month.

The model mainly consists of two sectors, that is, humans and agricultural land. Humans take in nitrogen from agricultural and marine products such as meat, fowl, eggs and fish, and discharge nitrogen into agricultural land and the environment. Nitrogen is deposited into agricultural land by biological fixation and fertilizer use, depending on the cropping systems used, and is discharged from agricultural products. Agricultural products, particularly cereals, are eaten in by humans and livestock. Livestock takes in nitrogen from cereals and discharges nitrogen into agricultural land and the environment. Livestock meat is eaten by humans. Agricultural and marine products such as meat, fowl, eggs and fish are traded between countries. The above basic figures were distributed equally into countries or provinces. The amounts of nitrogen discharged from arable land and humans in major river basins from 1970 to 2050 were summarized.

3.4 Changes in nitrogen load from fields and humans from 1970 to 2050

The nitrogen load using the results from a simulation study (Shindo *et al*. 2003) was evaluated. The amount of nitrogen discharged from arable land and that from humans were summarized for major river basins (Table 3). In East Asia, that is, the basins of the Amur River and Huanghe River, the nitrogen concentration of river water increased with an increase in the amount of nitrogen load. These river basins have low precipitation and denitrification rates due to a low temperature (Okamoto *et al*. 2003). The efficient use of these water resources is important for sustainable agriculture in these river basins. In Southeast Asia, that is, the basins of the Chao Phraya River and Mekong River, the present nitrogen concentration of river water is low due to a high denitrification rate (Okamoto *et al*. 2003). However, the nitrogen concentration of river water in these river basins will increase as nitrogen load was predicted to increase further. It is feared that the nitrogen concentration will increase during the dry season. The use of these water resources must be efficient for sustainable agriculture.

In 1970, the amount of nitrogen discharged from humans in each river basin was larger than that from arable land (Table 3). The amount of nitrogen discharged from humans increases with population growth. The amount of nitrogen discharged from arable land increases rapidly with an increase in fertilizer use due to economic growth. The rate of increase in the amount of nitrogen discharged from arable land is incomparably larger than that from humans. In 2000, the amount of nitrogen discharged from arable land increased, which is larger than that from humans, except that from the Irrawaddy River basin. In 2050, the amount of nitrogen discharged from arable land in most river basins is predicted to increase markedly, compared with that from humans. Rivers flowing in Southeast Asia are generally abundant in water due to a high precipitation. Nitrogen discharged from humans and arable land is diluted by abundant water. However, it is feared that nitrogen concentration will increase in the basins of the Amur River and Huanghe River due to a low temperature or a low precipitation. It is also feared that the water quality in these river basins will deteriorate due to the overuse of irrigation water.

Humans and farmlands occupy very important positions within the nitrogen flow, both discharging nitrogen directly to the environment. Humans take in nitrogen from crops and discharge it back to agricultural land and the environment. Nitrogen is deposited in farmlands by biofixation and fertilizer use, and is discharged in crops. From this model of nitrogen flow and environmental load in food production, our group simulated the nitrogen load and nitrogen concentration of water at test sites from 1970 to 2050 (Figure 12). The nitrogen load increased rapidly in the northern part of China from 1970 to 2000. Over the next half century, the nitrogen load will continue to increase in China, Vietnam, and the Philippines. The nitrogen concentration in river water has also increased in Northern China, and will continue to increase. The nitrogen load increases in other parts of the world will probably be minimal. The increases in Northern China are the expected result of changes in climactic conditions, namely, poor precipitation and a low rate of denitrification due to the low temperature in this river basin.

4. Conclusions

The Landsat TM/ETM+ data collected over the northeastern part of Heilongjiang, acquired in 1988 and 2002, were classified and the changes in the total area of paddy field were examined. The total area of paddy field increased from 166 km^2 in 1988 to 3,925 km^2 in 2002. The total area of arable land, which included paddy field and dry cropland, increased from 11,231 km^2 in 1988 to 12,913 km^2 in 2002. On the other hand, the total area of wetland decreased from 3,260 km^2 in 1988 to 21 km^2 in 2002. Of the 3,925 km^2 of paddy field in 2002, 2,523 km^2 was dry cropland in 1988. It was assumed that wetland had been easily changed to paddy field because of its proximity to rivers. However, most wetlands in 1988 were reclaimed and changed to dry cropland in 2002. It is possible that an abrupt increase in the total area of paddy field between 1988 and 2002 resulted from the conversion of dry cropland, which was favorably situated near a water source, to paddy field.

The cumulative temperatures of the rice-cropping season in 1901-2000 were just above the lower limit for cultivating *Japonica* rice and were nearly constant through the 21st century. Therefore, temperature did not probably cause the abrupt increase in the total area of paddy field.

An abrupt increase in the total area of paddy field from 1996 to 1998 followed a sudden increase in producer prices. In 1994, the Chinese government increased the purchase price of cereals by 40%. It is probable that the high producer price of rice, compared with those of other cereals, is one of the strongest motivations for converting dry cropland to paddy field.

Hydrological conditions change according to changes in water use in agriculture. It is also considered that a sudden change in hydrological conditions and land-use/land-cover negatively affects the ecosystem and environment.

Nitrogen load is predicted to increase from 1970 through 2050. This trend is clear in the eastern part of China, Vietnam and the Philippines. The reason is that N fertilizer usage is increasing. The concentrations of nitrogen (NO_3-N) are also predicted to increase from 1970 through 2050. This trend is clear in the northern part of China. The reason is that N fertilizer usage is increasing and this region has a low precipitation. The nitrogen load from farmlands will be far higher than that from humans (settlements), with increasing N fertilizer usage and economic growth.

Thus, agriculture has a negative impact on the ecosystem, from the viewpoint of nitrogen cycle. It is feared that the ecosystem will be affected more severely. Therefore, we suggest that the use of water resources and fertilizer must be efficient for sustainable agriculture.

References

Belward, A. S., Estes, J. E., and Kline, K. D., 1999, The IGBP-DIS global 1-km land-cover data set DISCover: a project overview. *Photogrammetric Engineering & Remote Sensing*, **65**(9), 1013-1020.

Bouwman, A. F., Van der Hoek, K. W., and Olivier, J. G. J., 1995, Uncertainties in the global source distribution of nitrous oxide. *Journal of Geophysical Research*, **100**, 2785-2800.

CGER (Center for Global Environmental Research), 1994, World Boundary Databank; PC ARC/INFO 'EXPORT' Version. In *GRID Global Data Sets: Documentation Summaries, edited by H. Harasawa*, National Institute for Environmental Studies: Tsukuba.

Chien, X., Personal communication, 22 November 2004, Researcher, Japan International Research Center for Agricultural Sciences, Tsukuba, Japan.

Crop and Grassland Service, 2000, Country Rice Facts. In *http://www.fao.org/WAICENT/FAOINFO/GRICULT/AGPC/doc/riceinfo/Corifa.htm*, International Rice Commission, The Food and Agriculture Organization (FAO): Rome.

Dao, H., and Eckert, D., 1998, GNV198 - Human Population and Administrative Boundaries Database for the Russian Fed. In *http://www.grid.unip.ch/data/ grid/gnv198.html*, (Geneva: GRID-Geneva, United Nations Environment Programme (UNEP)).

Deichmann, U., 1996, GNV197 - Human Population and Administrative Boundaries Database for Asia. In *http://www.grid.unip.ch/data/grid/gnv197. html*, (Geneva: GRID-Geneva, UNEP).

FAO (The Food and Agriculture Organization), 2004, FAOSTAT Home Page. In *http://apps.fao.org/*, (Rome: FAO of the United Nations).

Heilongjiang Provincial Bureau of Statistics (ed), 2004, *Heilongjiang Statistical Yearbook 2004*, Heilongjiang Provincial Bureau of Statistics, (Beijing: China Statistics Press).

IPCC (Intergovernmental Panel on Climate Change), 1996, *Climate Change 1995: The Science of Climate Change, edited by J. T. Houghton, L. G. Meira Filho, B. A. Callander, N. Harris, A. Kattenberg, and K. Maskell*, (Cambridge: Cambridge University Press).

Kaewthip, J., Kawashima, H., and Ohga, K., 2003, Projection of nitrogen load from food consumption and production in Thailand. *Journal of the Japanese Agricultural Systems Society*, **19**, 151-159.

Kawashima, H., and Okamoto, K., 1999, Global distribution of arable land, cereal yield and nitrogenous fertilizer use. *Journal of the Japanese Agricultural Systems Society*, **15**(1), 73-76.

LREIS (State Key Laboratory of Resources and Environmental Information System), 1996, *Earth Science Database Series: Resources and Environment Database of China (LREIS Data 1:4,000,000)*, Institute of Geography of the Chinese Academy of Sciences: Beijing (CD-ROM), (with manual in Chinese and English).

Mitchell, T. D., et al., 2003, A comprehensive set of climate scenarios for Europe and the globe (in preparation).

National Bureau of Statistics, 2000, *China Statistical Yearbook-2000*. (Beijing: China Statistics Press), CD-ROM.

New, M., Hulme, M., and Jones, P., 1999, Representing Twentieth-Century space-time climate variability. Part I:

Development of a 1961-90 mean monthly terrestrial climatology. *Journal of Climate*, **12(3)**, 829-856.

Okamoto, K., and Fukuhara, M., 1996, Estimation of paddy field area using the area ratio of categories in each mixel of Landsat TM. *International Journal of Remote Sensing*, **17**(9), 1735-1750.

Okamoto, K., Shindo, J., and Kawashima, H., 2003, Land-use, water resources and nitrogen load in major river basins in Asia. In *River Basin Management II, edited by C. A. Brebbia,* (Southampton: WIT Press, U.K., ISBN: 1-85312-966-6), 423-429.

Oki, T., and Sud, Y. C., 1998, Design of Total Runoff Integrating Pathways (TRIP) - a global river channel network. *Earth Interactions*, **2** (http://earthinteractions.org/).

Ramankutty, N., and Foley, J. A., 1999, Estimating historical changes in global land cover: Croplands from 1700 to 1992. *Global Biogeochemical Cycles*, **13**(4), 997-1027.

Shindo, J., Okamoto, K., and Kawashima, H., 2003, A model based estimation of nitrogen flow in the food production-supply system and its environmental effects in East Asia. *Ecological Modelling*, **169**, 197-212.

Tokuda and Hayatsu, 2001, Nitrous oxide emission potential of 21 acidic tea field soils in Japan. *Soil Science and Plant Nutrition*, **47**, 637-642.

USDA (United States Department of Agriculture), 1999, Chinese Rice Production. In *http://www.usda.gov/oce/waob/jawf/profiles/html/chi/chiric.html*, (Washington: USDA).

UT (University of Texas) Library Online, 2001, Perry-Castañeda Library Map Collection. In *http://www.lib.utexas.edu/maps/*, (Austin: University of Texas).

World Agricultural Outlook Board, 1994, *Major World Crop Areas and Climatic Profiles. Agricultural Handbook No. 664*, (Washington: U.S. Department of Agriculture (USDA)).

Zhang et al., 1996, Nitrate pollution of groundwater in northern China. *Agriculture Ecosystems and Environment*, **59**, 223-231.

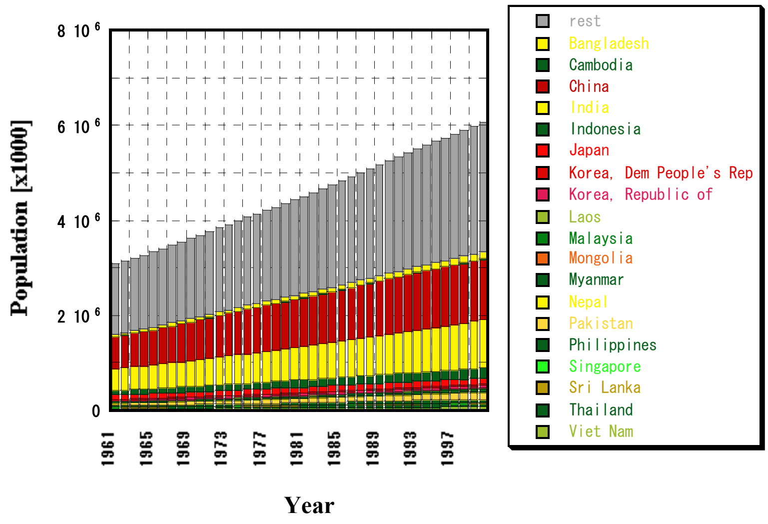

Figure 1 Population in Asia and the world.
Source: FAOSTAT Home Page (FAO 2004)

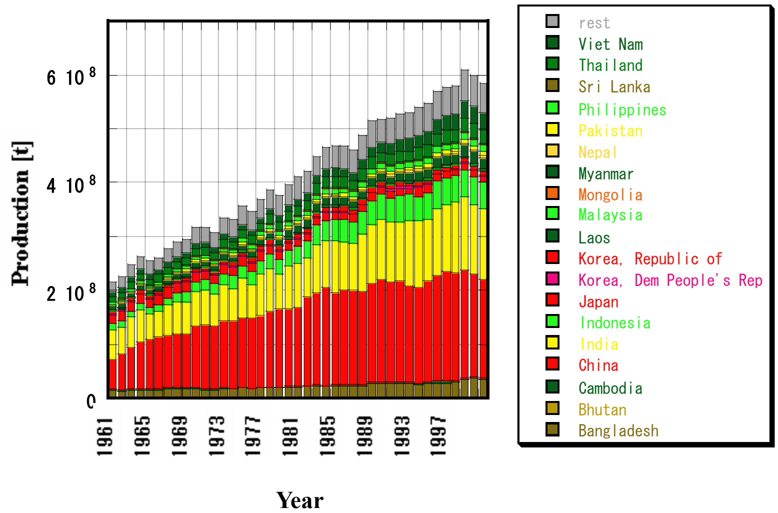

Figure 2 Rice production in Asia and the world
Source: FAOSTAT Home Page (FAO 2004)

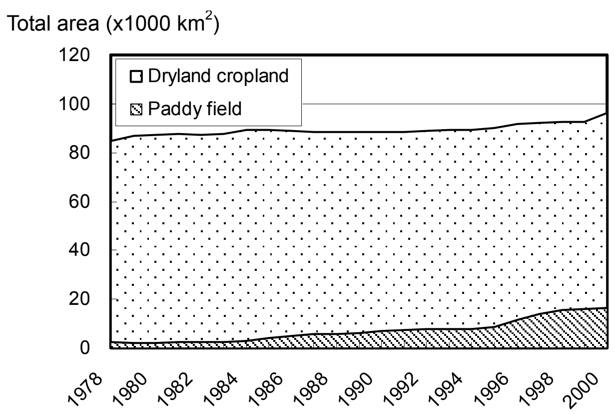

Figure 3 Changes in total areas of paddy field and dry cropland in Heilongjiang, China
Source: Heilongjiang Statistical Yearbook 2004 (Heilongjiang Provincial Bureau of Statistics 2004)

Figure 4 Test area: Eastern Sanjiang Plain, Heilongjiang Province, China (Map is cited from UT Library Online (2001) and is modified)

(a) 25 June 1988

(b) 24 June 2002

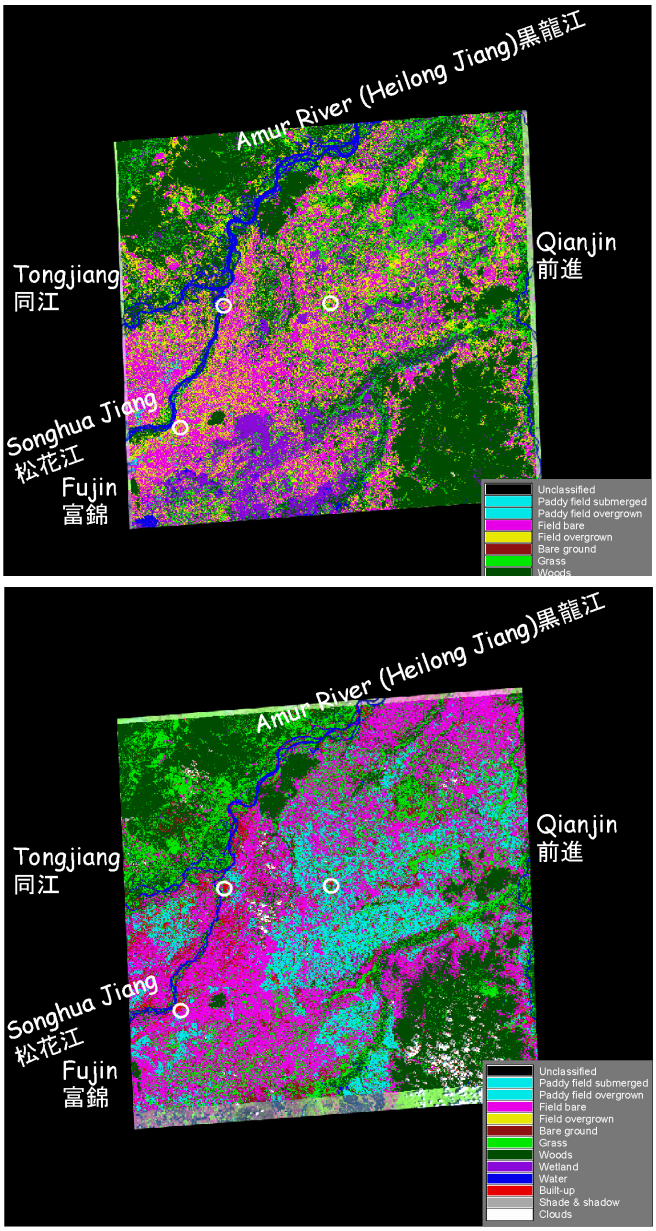

Figure 5 Land-use/land-cover maps; (a) 25 June 1988 and (b) 24 June 2002.

Table 1 Total areas of land-use/land-cover in 1988 and 2002

(a) Changes in total areas of land use/land cover between 1988 and 2002

2002 ＼ 1988	C 1	C 3	C 4	C 6	C 7	C 8	C 9	Total
C 1: Paddy Field Submerged	97	1,740	783	509	485	281	30	3,925
C 3: Bare Dry Cropland	26	2,565	1,812	1,480	1,702	1,304	98	8,988
C 4: Dry Cropland Overgrown	0	0	0	0	0	0	0	0
C 5: Bare Ground	17	588	547	372	365	492	104	2,485
C 6: Grassland	17	902	1,540	2,079	51	1,097	155	5,847
C 7: Woodland	0	0	0	0	7,600	0	0	7,600
C 8: Wetland	0	0	0	1	2	9	8	21
C 9: Water	4	0	0	0	41	0	580	626
C 10: Built-up	2	219	273	58	96	32	22	701
Total	166	6,063	5,002	4,556	10,718	3,260	1,014	81,316

(b) Changes in total areas of land use/land cover between 1988 and 2002 in terms of distance from water source

2002 ＼ 1988	C 1	C 3	C 4	C 6	C 7	C 8	C 9	C13	C14	C15	C16	Total
C 1	97	48	18	16	84	279	30	11	2	2,650	690	3,925
C 3	26	631	436	421	538	1,293	98	285	91	2,871	2,298	8,988
C 4	0	0	0	0	0	0	0	0	0	0	0	0
C 5	17	71	66	60	132	481	104	28	22	1,057	448	2,485
C 6	17	285	315	380	50	1,014	155	0	269	2,288	1,066	5,847
C 7	0	0	0	0	5,436	0	0	454	112	1,152	446	7,600
C 8	0	0	0	0	1	8	8	0	1	3	0	21
C 9	4	0	0	0	14	0	580	0	0	27	1	626
C10	2	34	39	8	22	31	22	9	4	359	170	701
Total	166	1,075	881	891	6,601	3,149	1,014	793	509	10,539	5,164	81,316

The changes in the total areas of classes “C2: paddy field overgrown” in 1988 and 2002, and “C5: bare ground” and “C10: built-up” in 1988 are 0 km^2 and are thus omitted. The class “C13” denotes isolated woodland, “C14” isolated dry cropland, grassland, bare ground and wetland, “C15” regions within 500 meters from a water source, and “C16” regions within 500-1000 meters from a water source.

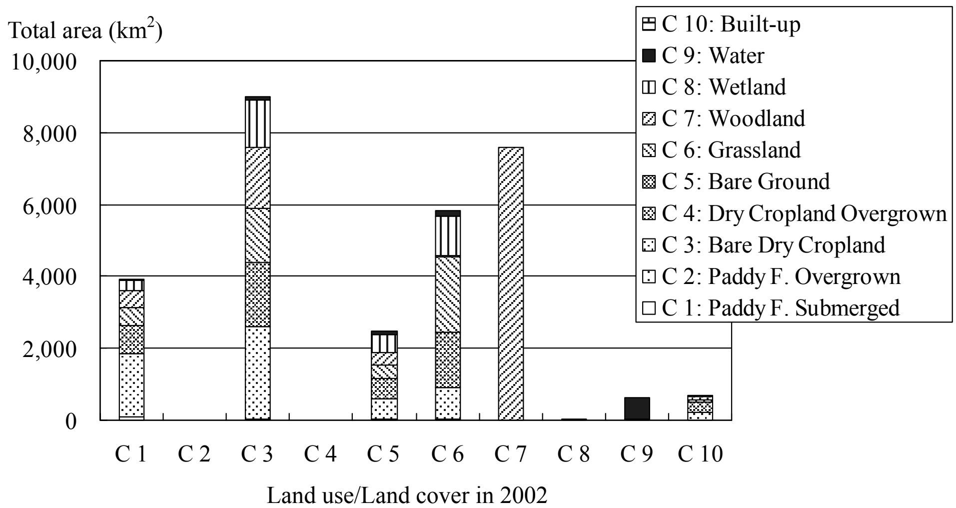

Figure 6 Changes in total areas of land-use/land-cover from 1988 to 2002

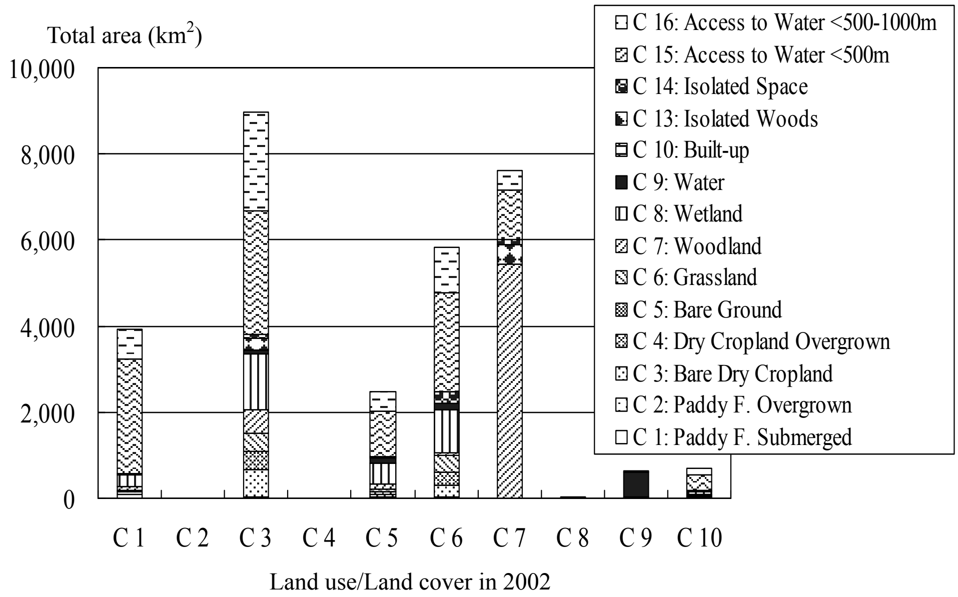

Figure 7 Changes in total areas of land-use/land-cover from 1988 to 2002 in terms of distance from water source: Class "C14: isolated space" is a class of isolated dry cropland, grassland, bare ground and wetland.

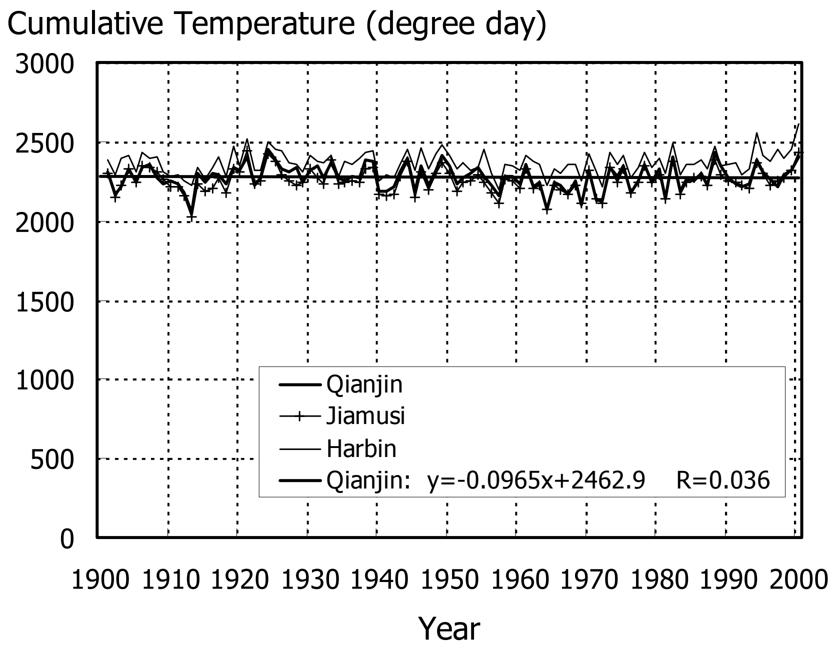

Figure 8 Cumulative temperature changes in Heilongjiang from 1901 to 2000

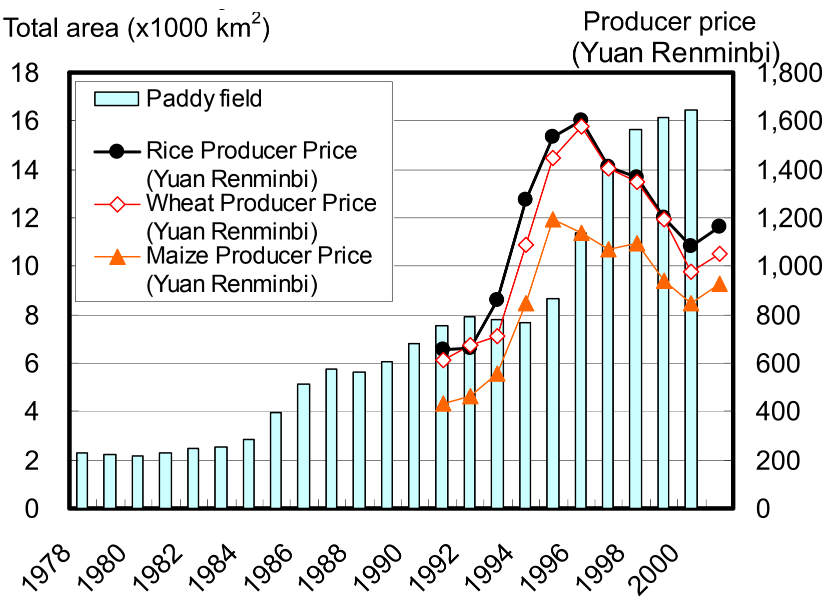

Figure 9 Changes in total area of paddy field in Heilongjiang and producer prices of rice, wheat and maize in China
Source: Heilongjiang Statistical Yearbook 2004 (Heilongjiang Provincial Bureau of Statistics 2004)

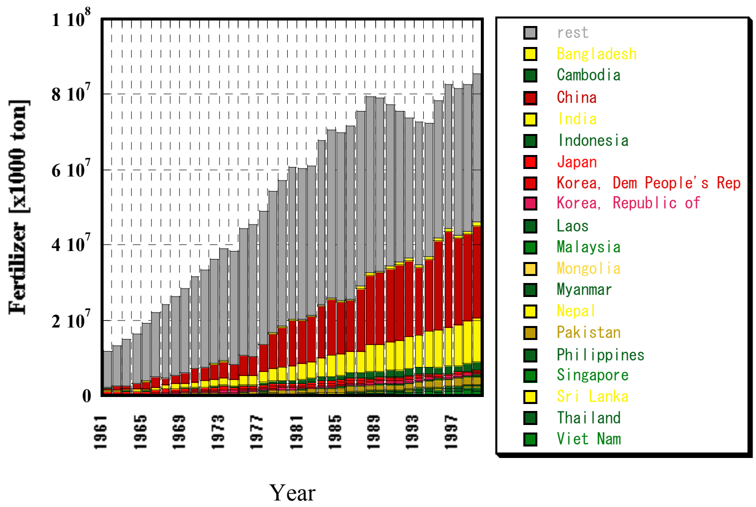

Figure 10 Nitrogen fertilizer usage in Asia and the world.
Source: FAOSTAT Home Page (FAO 2004)

Figure 11 Major river basins in continental Asia (River basin data is cited from the TRIP data (Oki and Sud 1998) and is modified)

Table 2 Typical rice-cropping seasons. Information was obtained from Crop and Grassland Service (2000) and World Agricultural Outlook Board (World Agricultural Outlook Board 1994) with modification.

Country or Region	First Rice-Cropping Season	Second Rice-Cropping Season
Bangladesh	May - October	January - April
Cambodia	July - October	December - April
Northern Part of China	May - August	-
Southern Part of China	March - June	July - October
India	May - October	January - April
Laos	July - October	-
Malaysia	October - December	-
Myanmar	July - October	December - April
Nepal	July - September	-
Pakistan	June - September	-
Thailand	June - September	November - March
Vietnam	June - September	January - April

* The northern part of China is defined as the region north of the Chang Jiang River, and the southern part of China as the region south of the Chang Jiang River.

Table 3 Changes in nitrogen load from arable land and humans from 1970 to 2050. The amount of nitrogen discharged from arable land and (/) that from humans are listed in each column. The amount of nitrogen is expressed in units of 1,000 ton N.

River Name/ Country	1970	2000	2030	2050
Amur/ China and Russian Fed.	103/ 137	1,386/ 304	3,227/ 450	3,277/ 466
Huanghe/ China	157/ 233	2,125/ 516	4,951/ 765	5,028/ 790
Chang Jiang/ China	563/ 908	7,633/ 2,014	17,778/ 2,982	18,054/ 3,082
Xi/ China	113/ 184	1,527/ 408	3,562/ 604	3,630/ 625
Red/ China and Vietnam	29/ 58	368/ 137	938/ 207	1,167/ 237
Mekong/ China, Laos, Cambodia and Vietnam	22/ 159	790/ 306	2,214/ 481	2,831/ 559
Chao Phraya/ Thailand	0/ 66	336/ 136	776/ 181	892/ 196
Irrawaddy/ Myanmar	2/ 75	34/ 229	124/ 299	172/ 342

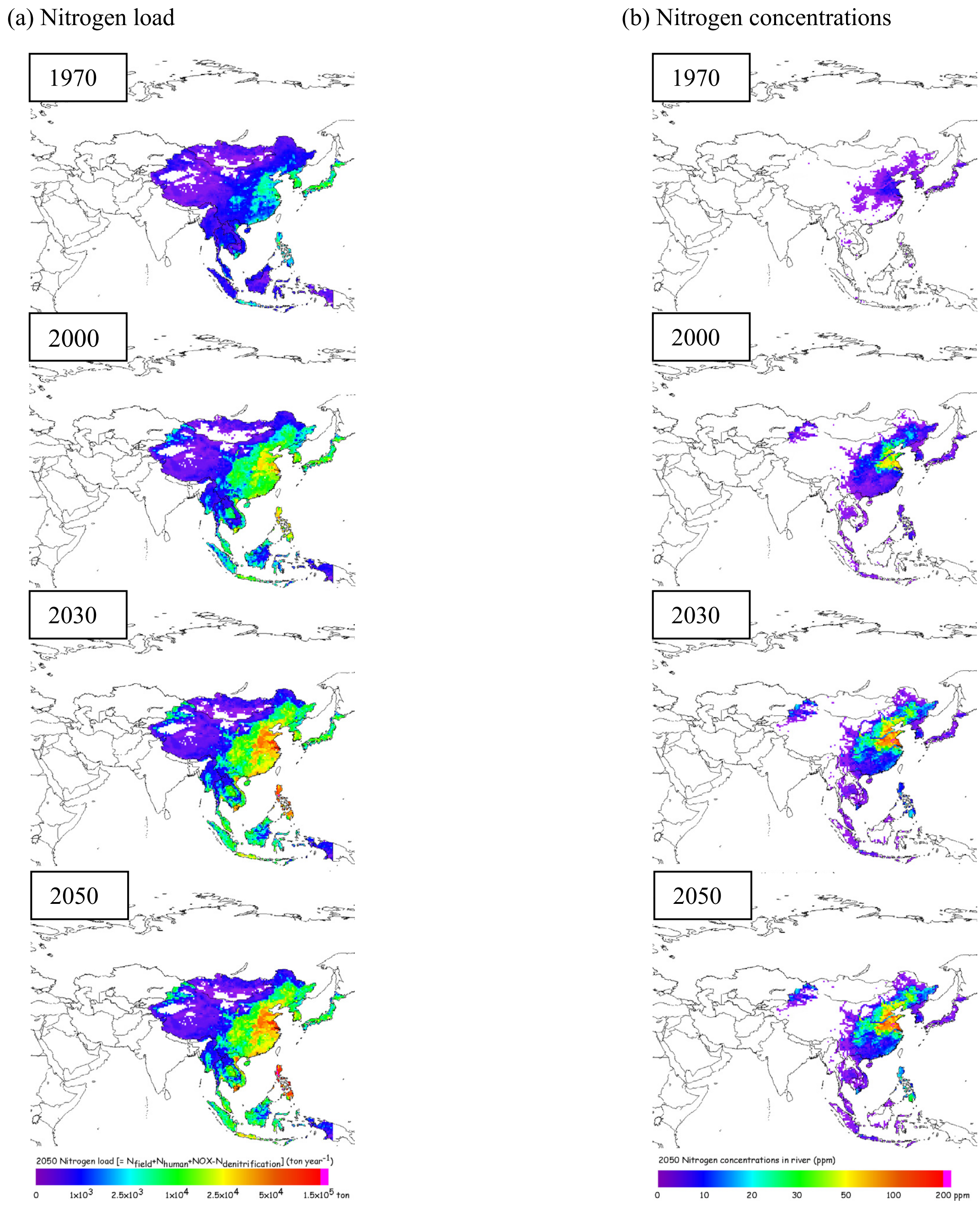

Figure 12 Impacts of food production to water quality in Asia; (a) Nitrogen load (t year^{-1}), and (b) nitrogen concentrations (NO_3-N ppm).

Utilization of Satellite Imagery for Vegetation Drought Monitoring in Indonesia

Eleonora RUNTUNUWU

Indonesian Agroclimate and Hydrology Research Institute
Email: runtunuwu2001@yahoo.com

Abstract:

Drought is a natural hazard that has significant impact on environmental, economic and socio economic aspects. The Indonesian Agroclimate and Hydrology Research Institute (IAHRI) is currently developing a vegetation drought monitoring system by using either the meteorological or satellite imagery as part of its effort to combat the effects of drought in Indonesia. The project methodology is depended on six main steps: (1) Development of meteorological database system, (2) Analysis of vegetation drought using Water and Agroclimate Research Management model (WARM ver. 1.0), (3) Determination the drought index based on meteorological data, (4) Building the ground station High Resolution Picture Transmission (HRPT) AVHRR receiver, (5) Application the remote sensing for vegetation drought monitoring, and (6) On-line spatial drought information delivery. The primary goal of this project is to develop an efficient system in Indonesia to analyze and deliver drought related information to the stakeholders and agricultural industries on the ground for drought preparedness and management.

1. Introduction

There are increasing pressures on water resources as a result of global population growth, economic development and the adverse effects of land use and climate change. Any deficit or limitation in water supply will be most critical in drought periods, and competing water needs maybe the cause of conflicts. Therefore, in order to design and manage water resources schemes, it is essential to monitor the spatial and temporal variability of droughts.

The essential for quantification of drought impacts and monitoring is of critical importance in politically, economically, environmentally of Indonesia. Several users such as top level policy makers at the national level, the governments in province, researchers, farmers, trades and water managers and national/international relief agencies are interested in reliable and accurate drought information in order to mitigate impact on surface and groundwater resources.

Traditional methods of drought monitoring rely on rainfall data, which are limited in the network of stations and incomplete climate data, often inaccurate caused human error or crash equipment and most importantly, difficult to obtain data in near real time either spatially or temporally. In this sense, remote sensing technology has greatly enhanced our ability to monitor and manage the natural resources, especially in the areas of water resources.

2. What is drought?

Tallaksen and Lanen (2004) noted that in general drought is a sustained and regionally extensive occurrence of below average natural water availability, and can thus be characterized as a deviation from normal conditions of variable such as precipitation, soil moisture, groundwater and streamflow. It is a reoccurring and worldwide phenomenon, with spatial and temporal characteristics that differ significantly from one region to another. Jeyaseelan (2003) and Tallaksen and Lanen (2004) illustrated in Figure 1 the different types of droughts, there are: meteorological droughts, agricultural droughts, and hydrological droughts. The impacts can be classified as economic, social, and environmental and it depends on the complex interaction between the physical environment and the socio-economic system.

The primary cause of a drought is the lack of precipitation over a large area and for an extensive period of time, called a *meteorological drought*. The meteorological drought identification is usually carried out on the basis of historic data analysis of rainfall or combined rainfall and evaporation as recorded at meteorological stations. For example is the Standardized Precipitation Index, SPI (McKee *et al.* 1995, Agnew, C.T, 1999). The SPI is a statistical indicator evaluating the lack or surplus of precipitation during a given period of time as a function of the long-term "normal" precipitation to be expected during the period.

The *agricultural drought* is occurred when soil moisture is insufficient to support crops which the water deficit propagates through the hydrological cycle and combined with the high evaporation rates. This drought could be monitored direct to the vegetation since the vegetation condition reflects the overall effect of rainfall, soil moisture, weather and agricultural practices. Therefore, satellite based monitoring of vegetation plays an important role in drought monitoring and early warning. Many studies have shown the relationships of vegetation index and agricultural drought. Thenkabail *et al.* (2004) developed methods that allow two generations of sensors (AVHRR and MODIS) to be combined beneficially for drought assessment and monitoring on a regional and a near-real-time. Park *et al.* (2004) determined the influences of hydrologic soil characteristics on early detection of drought with MODIS thermal emission data and response time of vegetation index to the thermal signals.

Within the hydrological cycle, groundwater is normally the last to react to a drought situation, unless surface water is mainly fed by groundwater. In deep aquifers the slow reaction of groundwater implies that only major meteorological droughts will finally show up as *groundwater droughts*. The lag between a meteorolical and a groundwater drought may amount to months or even years, whereas the lag between a meteorological and streamflow drought varies from days in a flashy catchments to months in a groundwater-fed catchments.

3. Recent Drought Event

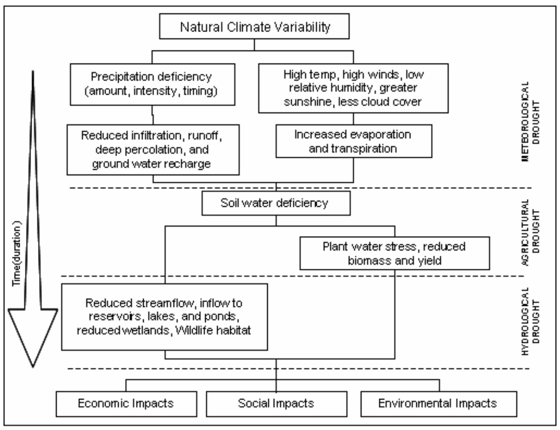

Figure 1. Propagation of drought through the hydrological cycle (Source: Jeyaseelan, 2003)

The area of Indonesia is 2 million sq. km (736,000 sq. mi.), included the maritime area 7,900,000 sq. km. It consists of more than 17,000 tropical islands in an archipelago across the Pacific Ocean, south of Malaysia and the Philippines and north of Australia. Only 1,000 of Indonesia's islands are permanently settled. It has the world's fourth biggest population, with more than 224 million (2004). Its climate is equatorial, but is cooler in the highlands. The climate of Indonesia is generally characterized by two seasons: dry (April to September) and wet (October to March). Based on the number of dry and wet months, the country is divided into 14 agroclimatic zones, of which 11 are considered as sensitive to extreme climate variability since rain fluctuations can upset established cropping patterns.

From 1877 to 1997, 93 percent of the drought years in Indonesia have been linked to El Niño events (http://www.isse.ucar.edu/un/indonesia.html). Several studies show a clear positive correlation between normalized Indonesian rainfall anomalies and the Southern Oscillation Index (SOI). While in El Niño years the onset of the monsoon is later than normal, during La Niña years the onset is earlier in most areas. Therefore, an El Niño event causes delayed planting and consequently a delayed and reduced harvest. A La Niña year offers the possibility of advancing the planting season with an early increased harvest, as well as the possibility of planting an additional crop.

4. Development of Vegetation Drought Monitoring System in Indonesia

Drought monitoring mechanism exists in most of the countries based on ground based information on drought related parameters such as rainfall, weather, crop condition and water availability, etc. Earth observations from satellite are highly complementary to those collected by in-situ systems. Satellites are often necessary for provision of synoptic, wide area coverage and frequent information required for spatial monitoring of drought conditions. The present state of remotely sensed data for drought monitoring and early warning is based on rainfall, surface wetness, temperature and vegetation monitoring.

Since 2003, Indonesian Agroclimate and Hydrology Research Institute (IAHRI) has been developing the vegetation drought monitoring system which could be divided into six main steps: (a) Development of meteorological database system, (b) Analysis of vegetation drought using WARM ver 1.0, (c) Determination the drought index based on meteorological data: Standardized Precipitation Index, (d) Building the ground station High Resolution Picture Transmission (HRPT) AVHRR receiver, (e) Application the remote sensing for drought monitoring, and (f) On-line spatial drought information delivery.

a. Development of meteorological database system in 2003

In the process of implementing vegetation drought monitoring, the acquisition of state-of-the-art equipment for strengthening the national meteorological network of observing stations became necessary. Presently IAHRI has

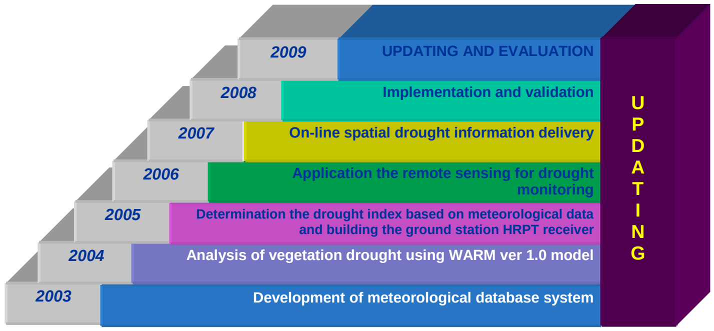

Figure 3. The roadmap of drought monitoring system development 2003-2009

only 75 automatic weather stations (AWS), 4 automatic rainfall stations (ARS), and 26 automatic water level recorders (AWLR), therefore, collecting meteorological data from other institutions (approximately 5000 manual rainfall gauges but 1200 stations collected yet) became important in order to get climate information whole Indonesia (Figure 4). The meteorological data are air temperature minimum (°C), air temperature maximum (°C), mean air temperature (°C), minimum humidity (%), maximum humidity (%), mean humidity (%), rainfall (mm), wind speed (m/s), and global radiation (MJ/m^2).

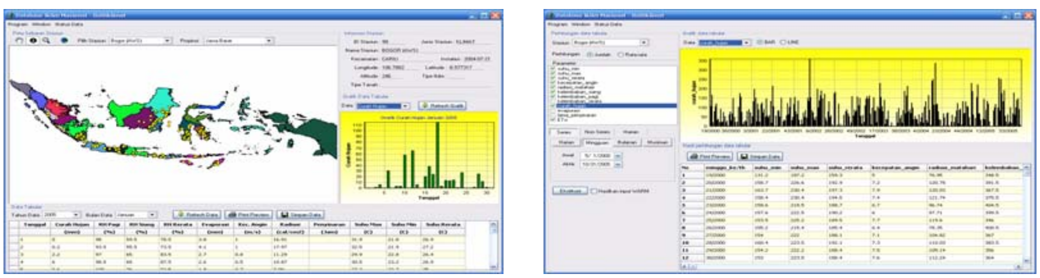

Figure 4. The Indonesian meteorological database system

b. Analysis of vegetation drought using WARM ver 1.0 model (2004).

In 2004, IAHRI has developed a water balance model to analyze the crop water management which connected to the meteorological database. In soil moisture drought condition the model is able to recommend the volume and time for supplemented irrigation information.

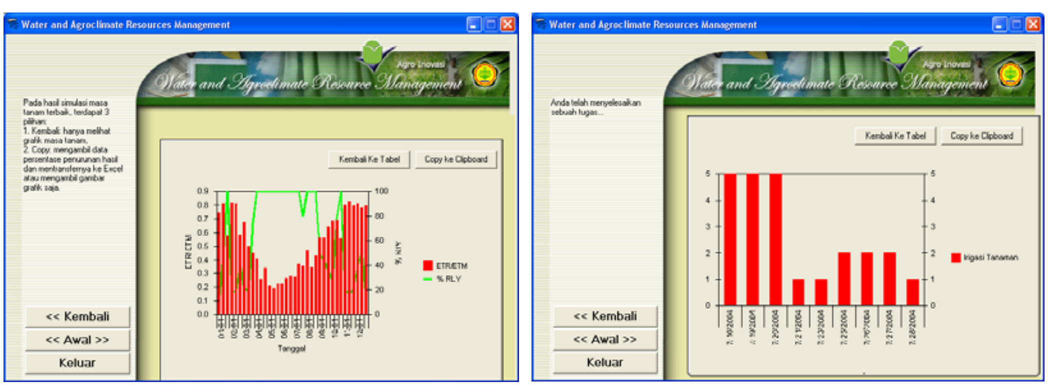

Figure 5. The water balance analysis to (a) estimate the water stress condition and (b) volume and time of supplemented irrigation

c. Determination the drought index based on meteorological data

The SPI is used to study the relationships between drought duration, frequency, and time scale, as described by Agnew (1999). The SPI for each station was determined using this equation: $SPI = \left(X_{ik} - X_i\right)/\sigma_i$, where σ_i is standardized deviation for the ith station, X_{ik} is rainfall for the ith station and kth observation, and X_i is mean rainfall for the ith station. All negative SPI values are taken to indicate the occurrence of drought, while all positive values show no drought. To determine drought intensity, SPI values of equal to or less than -0.50 were used. The frequency of occurrence of drought years within each decade was determined on a station-by station basis by simple statistical means, and the result was then summed over the 40-year period.

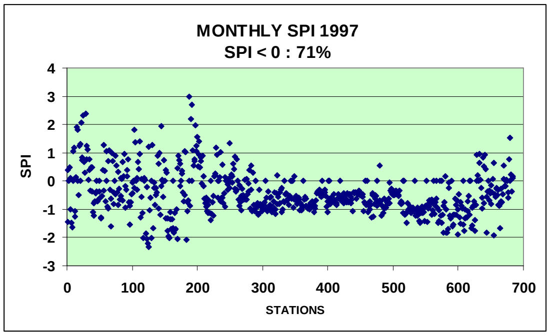

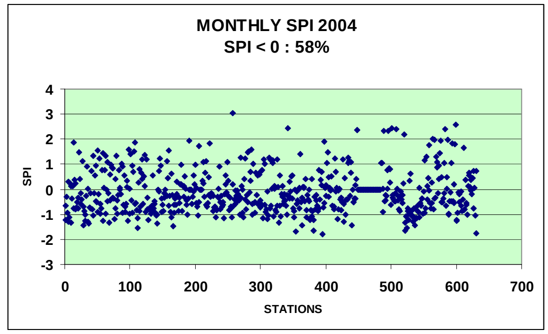

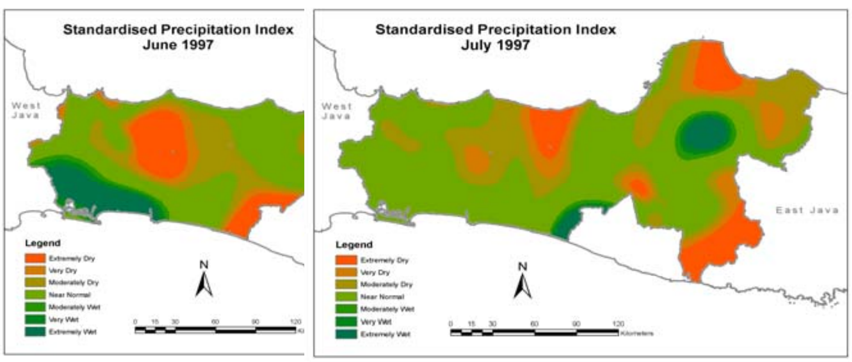

Figure 6. (a) The monthly SPI and (b) The Spiline SPI for 630 stations of Center of Java Province

d. Building the ground station High Resolution Picture Transmission (HRPT) receiver (2005/2006)

In 2005/2006 IAHRI is conducting to build the HRPT ground station. The HRPT service installed on the NOAA satellites which is the main source of high quality data from polar orbiting meteorological satellites. The data stream not only contains full resolution images in digital format from the Advanced Very High Resolution Radiometer (AVHRR) instrument but also the atmospheric information from the suite of sounding instruments. Through HRPT reception the user site can acquire data from three or more consecutive overpasses twice each day from each satellite, giving high resolution data coverage of a region extending to about 1500 km radius from the user station. Compare to other satellites, the HRPT is more coarse spatial resolution, but very high temporal resolution that useful in drought monitoring activities. The imagery gives a snapshot of the meteorological conditions and can also be used for many land applications, while the sounding data gives detailed atmospheric data that may be processed and used in regional weather prediction models.

e. Application the remote sensing for drought monitoring

Kogan (2002) described the world drought condition using Vegetation Condition Index (VCI, Kogan, 2002). Marshall (2003) applied the Apparent Thermal Inertia (ATI) and vegetation indices to determine drought in Cordoba, Argentina. In other case, Bhuiyan (2004) applied various drought indices for monitoring the drought, i.e. Standardized Precipitation Index (SPI), Standardized Water–Level Index (SWI), Normalized Difference Vegetation Index (NDVI), Temperature Condition Index (TCI), and Vegetation Health Index (VHI) over Aravalli Terrain of India. Table 1 showed the drought index for monitoring three types of drought using meteorological and satellite data.

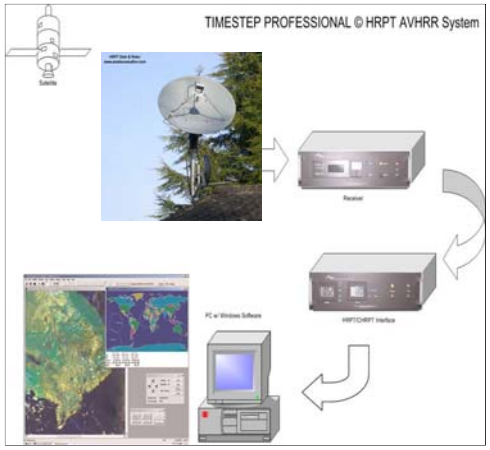

Figure 7. The HRPT function diagram

Many different satellites are used to analyze and monitor drought. For example, Park *et al.* (2004) used Moderate Resolution Imaging Spectroradiometer (MODIS) combined with a climatic water budget model and the STATSGO database within a GIS technology to determine hydrologic soil properties for detecting drought in western – central Kansas.

Table 1. Various drought index for monitoring drought using meteorological data and satellite imagery

No	Drought index	Formula	Range	Normal condition	Severe drought	Healthy vegetation	Types of drought
1.	SPI	$SPI = (X_{ij} - X_{im})/\sigma$	-1 to +1	0	-1	+1	Meteorological
2.	NDVI	$NDVI = (\lambda_{NIR} - \lambda_{RED})/(\lambda_{NIR} + \lambda_{RED})$	-1 to +1	Depends on the location	-1	+1	Agricultural
3.	*DEV_{NDVI}	$DEV_{NDVI} = NDVI_i - NDVI_{mean}$	-1 to +1	0	-1	+1	Agricultural
4.	VCI	$VCI = 100(NDVI - NDVI_{\min})/(NDVI_{\max} - NDVI_{\min})$	0 to 100%	50%	0%	100%	Agricultural
5.	TCI	$TCI = 100(T_{\max} - T_{cur})/(T_{\max} - T_{\min})$	0 to 100%	50%	0%	100%	Agricultural
6.	VHI	$VHI = 0.5(VCI) + 0.5(TCI)$	<10 to > 40	< 30	< 10	> 40	Agricultural
7.	SWI	** $SWI = (W_{ij} - W_{im})/\sigma$	<0 to >4	>1	> 4	< 0	Hydrological

*Drought severity index; ** W_{ij} is the seasonal water level for the ith well and jth observation, W_m is seasonal mean, and σ is its standardization.

Figure 8 (left) shows the August (the driest month) spatial distribution of DEV_{NDVI} over Indonesia on 1996 (wet year), 1997 (driest year) and 1998 (pasca El Nino) where areas in green is healthy vegetation and areas in red is drought affected. In 1997, most of the pixels in the study area have red colour, indicative of the negative deviation from NDVI mean. This result match well with the actual condition in Indonesia since at the time a large part of the country suffered from severe drought, resulting in a huge shortfall in rice production that necessitated the import of over five million metric tons of rice to ensure food availability to the economically weaker sections of the society. In the forestry sector, the effects of large-scale forest fires during 1997-98 were unprecedented, damaging more than 9.7 million ha of forest area. The smoke and trans boundary haze from these fires affected not only Indonesia but also other Southeast Asian countries, in particular Brunei Darussalam, Malaysia and Singapore.

Figure 8 (right) shows the VCI that describes the moisture condition. The high value of VCI (green area) corresponded to unstressed vegetation or undrought condition and the VCI value close to zero percent reflects an extremely dry month. The duration of the successive months period below normal conditions and magnitude of the deviation are two powerful indicators of drought severity. In this case, the VCI and DEV_{NDVI} have similar pattern, therefore we expected they have strong correlation that could be used to monitor the drought.

f. On-line spatial drought information delivery (2007)

The last step of this project is delivering the drought information using internet technology to stakeholders or agricultural industries, since at present, there is no efficient system in Indonesia to analyze and deliver a near-real-time drought-related information. An information system should also allow drought development in the region to be monitored at different scales, such as provinces level and smaller administrative subdivisions.

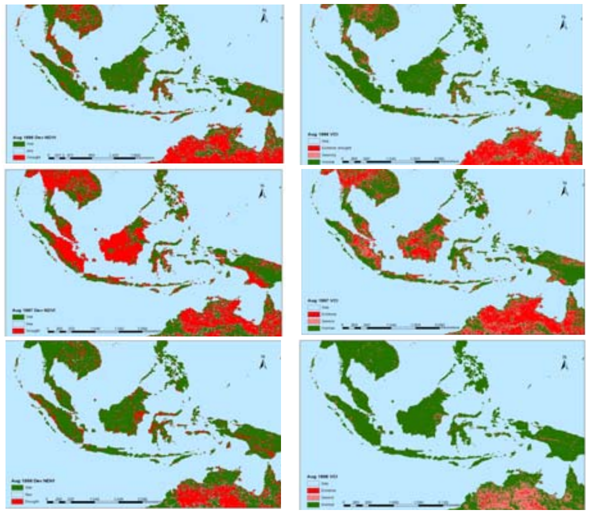

Figure 8. Indonesia drought severity index (left) and vegetation condition index (right) for August 1996, 1997, 1998 based on NOAA image during 1982-1998.

5. Conclusions:

Droughts is one of the most devastating natural hazards in the world, and causing extensive damage to agriculture as well human and wild live and local economies. Therefore, IAHRI is currently developing a vegetation drought monitoring system by using either the meteorological or satellite imagery as part of its effort to combat the effects of drought in Indonesia. The ground meteorological data and remote sensing as well GIS technologies significantly contributes in the vegetation drought analysis. In this paper, brief review of the drought vegetation monitoring system development in Indonesia by IAHRI for drought preparedness and prevention.

References:

Agnew, C.T. 1999. Using the SPI to Identify Drought. Drought Network News, 12(1), pp. 6-12.

Bhuiyan, C. (2004). Various drought Indices for monitoring Drought Condition in Aravalli Terrain of India. http:// www.isprs.org/istanbul2004/comm7/papers/243.pdf.

Marshall, G. (2003). Drought Monitoring using remote Sensing. http://www.ees.nmt.edu/zhou/Geoffrey% 20Marshall.ppt

http://www.isse.ucar.edu/un/indonesia.html

IPCC (2001). Climate Change 2001. The scientific Basis. IPCC Third Assessment Report, Intergovernmental Panel of Climate Change (IPCC), UNEP, WMO, Cambridge University Press, Cambridge, UK.

Jeyaseelan A.T. (2003). Droughts and Floods Assessment and Monitoring using remote Sensing and GIS. Satellite Remote Sensing and GIS Applications in Agricultural Meteorology pp.291-313.

Kogan, F. N. 1997. Global Drought watch From Space.- Bull. Am. Met. Soc., 78, 621-636.

Kogan, F. N. 2000. Contribution of Remote Sensing to Drought Early Warning. In Early Warning Systems for Drought Preparedness and Drought management. Ed. D.A. Wilhite and D.A. Wood. 75-87. Geneva: world Meteorological Organization.

Kogan, F. N. 2002. World Droughts in the New Millenium from AVHRR-based Vegetation Health Indices. Eos, Transaction, Amer. Geophy. Union, 8(48), pp. 562-563.

McKee, T. B., Doesken, N. J., Kleist, J. 1993. The Relationship of Drought Frequency and Duration to Time Scales. Proc. 8th Conf. on Appl. Clim., 17-22 Jan. 1993, Anaheim, CA, 179-184.

McKee, T.B., Doesken, N. J., Kleist, J. 1995. Drought Monitoring with Multiple Times Scales. Proc. 9th Conf. on Appl. Clim., 15-20 Jan. 1995, Dalas, TX, 233-236.

Tallaksen, L. M., and Lanen, H. A. J. (2004). Hydrological Drought. Processes and estimation methods for streamflow and groundwater. Development in Water Science 48. 579 pages.

Thenkabail, P. S., Gamage, M.S. D. N., and Smakhin, V.U. (2004). The Use of Remote Sensing Data for Drought Assessment and Monitoring in Southeast Asia. Research Report 85. IWMI. Colombo, Sri Lanka; International Water management Institute. 27 pages.

Zhang P., Anderson, B., tan B., Huang D., Myneni R. (2005). Potential monitoring of crop production using a satellite-based Climate-Variability Impact Index. Agricultural and Forest Meteorology. Article Press. http://www.elsevier.com/locate/agrformet-3440. 15 pages.

Characteristics of dust event in East Asia: Focus on the Gobi Desert, and Mongolia regions

Yasunori KUROSAKI
Center for Environmental Remote Sensing (CEReS), Chiba University
E-mail: ykurosak@faculty.chiba-u.jp, ykurosaki2004@yahoo.co.jp

Abstract

This study investigated the effect of snow and vegetation covers on dust emission by the correlation analysis of strong wind frequency and dust emission frequency, where the strong wind is defined with a constant threshold 6.5 m/sec. This correlation should be high (low) where the variance of land surface environment is low (large). In addition to this idea, referring to the parameterizations of threshold wind speed by NDVI and snow cover fraction, we built four hypotheses as shown in section 3.1. However, our obtained results disagreed with these in many points, and this indicates problems in the current parameterizations. We will discuss the reasons of these disagreements and some methods will be proposed to clarify these problems.

1. Introduction

Dust gives impacts on our lives from many aspects, which are climate change via radiation process, changes in ice cap albedo, respiratory disease, cropland losses, damages on transportation, ocean fertilization, neutralization of acid rain, disease transmission, etc. Many researchers have developed numerical models of dust cycle (i.e., emission, born, and deposition processes), which have played an important role in assessing such impacts of dust. However the current models have insufficient accuracy especially in the treatment of emission process. One of the reasons of such problem is the immature skill of the treatment of geographic information system (GIS) data concerning land surface environment (e.g., soil particle distribution, soil wetness, vegetation cover, snow cover, land cover type) in dust emission model. In some models, the threshold wind speed of dust emission is parameterized by leaf area index (LAI) derived from Normalized Difference Vegetation Index (NDVI) and snow cover fraction from satellite data (Kurosaki and Mikami, 2004). When we use these parameterizations, the threshold wind speed is high in summer and winter because NDVI and snow cover fraction are large, respectively. Moreover, the interannual variance of threshold wind speed is large as well because of the large variance of NDVI and snow cover fraction.

Kurosaki and Mikami (2005) discussed the variation of land surface environment with the correlation of strong wind frequency and dust emission frequency where the strong wind is defined by a constant threshold wind speed 6.5 m/sec. This correlation should be high (low) where the variance of land surface environment is low (large). Although their analysis period is limited to spring (March, April and May), they obtained following results: (1) the correlation is high in March and April but low in May in the Gobi Desert; (2) they are high in March but low in April and May in the Northern and the Western Mongolia, whose major land cover type is grassland. These results suggest that the vegetation cover begins to suppress dust emission from April in Mongolia and from May in the Gobi Desert.

This study discusses the effect of snow and vegetation covers on dust emission with the correlation of strong wind frequency and dust emission frequency. Although the analysis period is limited to spring in Kurosaki and Mikami (2005), we calculated the correlation coefficient of each month from January to December. From this analysis, we discuss the interannual variance of land surface environment in each month in each region.

2. Data and method

In the discussion of dust emission and surface wind, we used the present weather and the wind speed at a 10 m height included in SYNOP, which is a routine report of 3-hourly surface meteorological data. The period is March 1988 to June 2005. The regions are the Gobi Desert, the Northern Mongolia, and the Western Mongolia, which are given in Kurosaki and Mikami (2005). According to the data from U.S. Geological Survey, the major land cover types are semi desert shrubs in the Gobi Desert, grassland in the Northern Mongolia, and the semi desert shrubs and grassland in the Western Mongolia.

The frequency of dust emission is defined as the percentage of the number of dust emissions to the total number of observations in the given period and the given region. Similarly, the frequency of strong wind is defined, where a strong wind is defined with a constant threshold 6.5 m/sec, which is the threshold wind speed for a dust emission in some numerical models.

Our used snow cover and vegetation cover data are derived from satellite images. The snow cover data is derived from the Special Sensor Microwave/Imager (SSM/I). This product, whose title is Near Real-Time SSM/I EASE-Grid Daily Global Ice Concentration and Snow Extent, is distributed by the National Snow and Ice Data Center (NSIDC). We define the snow cover fraction as the ratio of the number of snow cover days to the total days during the given period. In the discussion of vegetation cover, we used the NDVI of the NOAA/NASA Pathfinder AVHRR Land (PAL) program.

3. Results and discussion

3.1 Seasonal variation

In spring, dust emissions are frequent in the Gobi Desert, and they are frequent as well in the Northern and Western Mongolia, though the dust emission frequencies are lower than those of the Gobi Desert. From summer to winter, dust emissions are observed in the Gobi Desert, though the frequency is low. On the other hand, they are seldom or never observed in the Northern and Western Mongolia. The NDVI are almost the same and very low in these three regions during spring, while they are much larger in the Northern and Western Mongolia than that in the Gobi Desert during summer. In winter, snow cover entirely extends over the Northern and the Western Mongolia. In March, the major dust source regions are not covered by snow. These results suggest that snow and vegetation covers suppress the dust emission in Mongolia during winter and summer. In comparison with these grassland regions (i.e., Mongolia), as the NDVI is not so large and snow cover is seldom observed throughout the year in the Gobi Desert, we can guess that the frequency of strong wind might control the dust emission frequency.

From these results, we can built four hypotheses; (1) the correlations are low in the Northern and the Western Mongolia during winter because of high snow cover fraction; (2) the correlations are low in the same regions during summer because of vegetation cover; (3) the correlations are high in the same regions during spring and autumn because of less snow and vegetation covers; (4) the correlation is high throughout the year in the Gobi Desert because of less snow and vegetation covers throughout the year.

3.2 Correlation of strong wind frequency and dust emission frequency

In the Northern and the Western Mongolia, the correlation of strong wind frequency and dust emission frequency is high in spring and low in summer. This result agrees with the hypotheses given in the previous section. However, the following all results disagree with the hypotheses. The correlation coefficient reaches the highest in winter, although the snow cover fraction is high. Moreover, the correlation is not so high in autumn, although NDVI and the snow cover fraction are not so high. In the Gobi Desert, the correlation coefficient clearly varies with the seasonal march as well as in Mongolia.

These results suggest that the current parameterization of threshold wind speed should not be applied in the dust emission model. Some potential reasons of the above disagreements occur to us. For example, the land surface environment frequently differs in the place and in the season, even if NDVI is the same. Although NDVI is low in Mongolia in both spring and autumn, we can guess possible land surface environment, which are rare vegetation cover in spring and broadly distributing dry grass in autumn. Similarly, although the snow cover fraction is high in winter, if the quality of snow is dry and powdery, the threshold wind speed is not so high. On the contrary, although the snow cover fraction is not so high just like in spring, the threshold wind speed might be very high, if snow is wet. By parameterizing the threshold wind speed by such factors, we can newly define the strong wind by a variable threshold in accordance with snow quality and LAI including dry grass. The correlation coefficient using such variable threshold wind speed can be a good index to validate this parameterization. To achieve this goal, we need GIS data concerning land surface environment obtained from field surveys and satellite observations.

4. Summary

This study investigated the effect of land surface environment on dust emission by the correlation analysis of strong wind frequency and dust emission frequency, where we define the strong wind with a constant threshold. This correlation should be high (low) where the variance of land surface environment is low (large). In addition to this idea, referring to the parameterizations of threshold wind speed by NDVI and snow cover fraction data, we built four hypotheses indicated in section 3.1. However, our obtained results disagreed with these hypotheses, and this pointed out the problems in the current parameterizations. This study presented some potential reasons of these disagreements, which are snow quality and dry grass. One of the methods to validate the effect of these factors on dust emission is to build a new parameterization using such factors. The correlation coefficient using such new parameterization can be a good index to validate this parameterization. To make a parameterization, we need GIS data concerning land surface environment obtained from field surveys and satellite observations.

References

Kurosaki, Y. and M. Mikami (2004), Effect of snow cover on threshold wind velocity of dust outbreak, *Geophys. Res. Lett.*, **31**, L03106, doi:10.1029/2003GL018632.

Kurosaki, Y. and M. Mikami (2005), Regional difference in the characteristics of dust event in East Asia: relationship among dust outbreak, surface wind, and land surface condition, *J. Meteor. Soc. Japan*, **83A**, 1–18.

Land Cover Monitoring over Yellow River Basin in China using Remote Sensing

Masayuki MATSUOKA[1], Tadahiro HAYASAKA[1], Yoshihiro FUKUSHIMA[1], Yoshiaki HONDA[2] and Taikan OKI[3]
[1] Research Institute for Humanity and Nature
[2] Center for Environmental Remote Sensing, Chiba University
[3] Institute of Industrial Science, University of Tokyo
E-mail: matsuoka@chikyu.ac.jp

Abstract

The current status of the study on the land cover monitoring over the Yellow River in China is outlined in this paper. Three kind of optical sensors, MODIS, AVHRR and Landsat have been used in order to understand the recent status and the change for 20 years since 1980 of the land cover. Land cover map is generated from time series of MODIS in 2000. Time series of AVHRR is in production for the change detection. Landsat data will be applied to drastically changed area such as irrigation districts.

1. Introduction

Yellow River in China (figure 1) has been dried up for many days in a year and long distance since 1970s. It is mainly due to the decrease of precipitation in the upstream of the basin and excess water use for the irrigation. Therefore the hydrological model which can deal with the human activity such as dam operation and irrigation has been being developed in Research Revolution 2002 project [1] for the optimal management of river water. Land cover is one of the most important parameter in the model since it reflects human activity as agriculture and it also provides the hydrological characteristics of land surface. The objective of this study is to analyze the land cover and its change for 20 years from 1980 over the Yellow River basin using remote sensing data.

2. Method of the study

The method of this study is shown in figure 2. Three kinds of optical sensor are used depend on its temporal and spatial characteristics. Because the MODIS onboard Terra is new sensor which has been operated since 1999, it is used to understand recent status of the land cover. Land cover classification map has been generated using time series of MODIS product in 2000 combined with DMSP/OLS product. AVHRR has been operated continuously over 20 years and historical data is available since early 80s, hence it is used to detect the change of land cover. The time series of AVHRR data is generated with the spatial resolution of 1 kilometer from the HRPT, LAC and GAC data. Landsat series of sensor i.e. MSS, TM, and ETM+ have quite higher spatial resolution relative to previous two sensors, even though temporal resolution is low in contrast. These data are used for the validation of land cover classification and change detection, and local analysis over the drastically changed area.

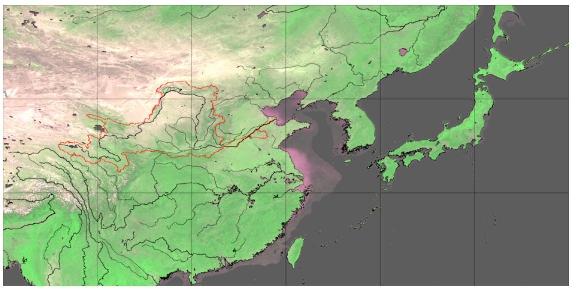

Fig. 1. Yellow River basin.

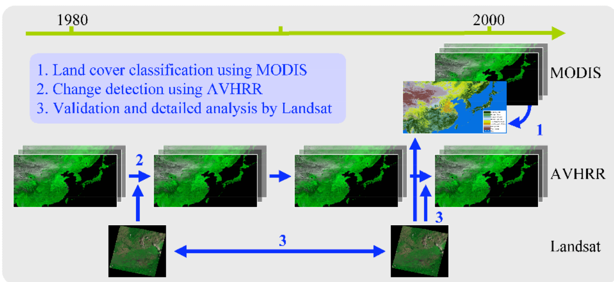

Fig. 2. Method of the study.

3. Land cover classification using MODIS

Land cover map was generated by the classification using time series of MODIS 250 meter resolution reflectance product (MOD09Q1), 500 meter resolution snow product (MOD10A2) and DMSP/OLS nighttime light product in 2000. Eleven kinds of land surface features i.e. annual maximum and minimum NDVI, annual maximum and minimum reflectance in band 1 and 2, annual average reflectance in band 1, monthly average NDVI in April and June, number of snow days in summer season, and human settlements, are derived from MODIS and OLS products (figure 3), and these were input to the simple decision tree classification method shown in figure 4. The threshold values used in decision tree were adjusted manually by comparison of classification result to the other land cover maps. Sixteen types of land cover which include five kinds of agricultural categories were adopted from the hydrological point of view. Classification result is shown in figure 5. This map was compared to two reference data, existing classification map [2] and Chinese census [3][4]. Land cover map categories were aggregated and compared in province base. The result is shown in figure 6. Forest shows good agreement with land cover map, but overestimation relative to the census. Total agricultural field, grassland and barren show the good agreements in both comparison, but individual agricultural categories i.e. paddy field, dry field, and irrigated field resulted in poor agreements. This classification map is used as the base map in the hydrological model.

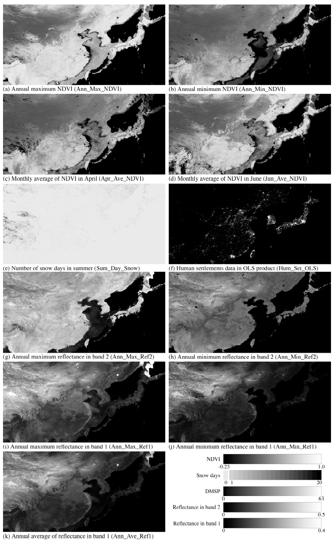

Fig. 3. Land surface features.

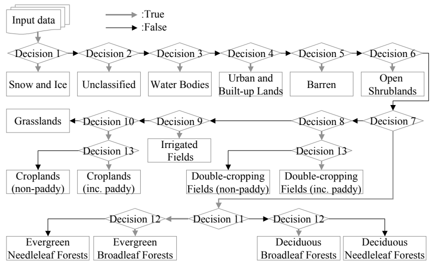

Decision	Criteria	Thresholds
1	Sum_Day_Snow > Threshold	15 days
2	All features but Apr_Ave_NDVI and Jun_Ave_NDVI include error	None
3	Ann_Min_Ref2 < Threshold OR Ann_Min_NDVI < Threshold	5.00 % -0.05
4	Ann_Max_NDVI < Threshold AND Hum_Set_OLS > Threshold	0.45 55
5	Ann_Max_NDVI <= Threshold	0.15
6	Ann_Max_NDVI <= Threshold	0.25
7	Ann_Ave_Refl <= Threshold	5.50 %
8	Apr_Ave_NDVI and Jun_Ave_NDVI have no error AND (Apr_Ave_NDVI - Jun_Ave_NDVI) > Threshold	None 0.00
9	arctan(Ann_Max_NDVI/Ann_Min_NDVI) >= Threshold AND Ann_Min_NDVI < Threshold AND Ann_Max_Refl < Threshold	74.0 deg. 0.15 25.0
10	Ann_Max_Refl < Threshold	10.5 %
11	Ann_Min_NDVI > Threshold	0.44
12	Ann_Max_Ref2 > Threshold	28.0 %
13	Ann_Min_Refl < Threshold AND	3.75 %

Fig. 4. Decision tree classification method.

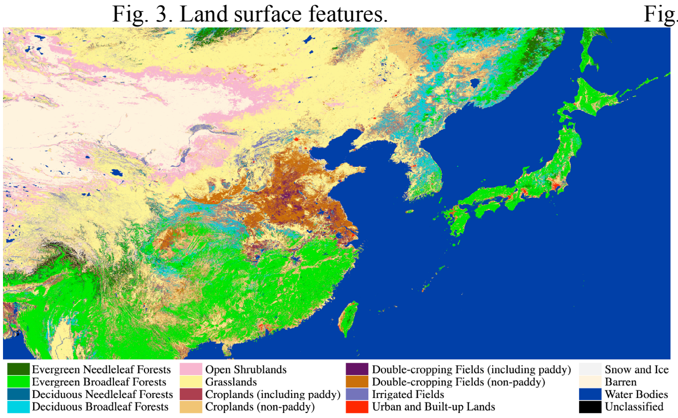

Fig. 5. Classification result.

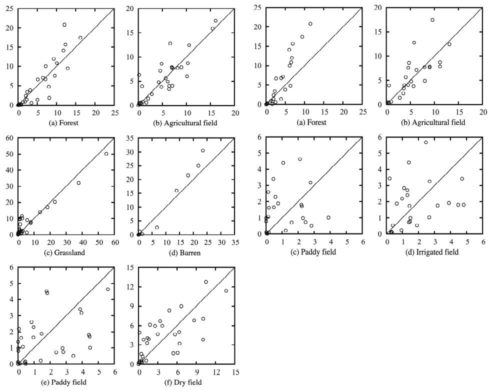

Fig. 6. Comparison to reference data.

4. Change detection using AVHRR

4.1 Production of AVHRR data set

Time series of AVHRR data for 20 years has been being produced from HRPT, LAC and GAC data with 1 km resolution. HRPT was supplied by Kitsuregawa Laboratory [5], University of Tokyo, and LAC and GAC were downloaded from CLASS, NOAA [6]. The radiometric calibration is applied using time varying calibration coefficients to derive the top of atmosphere reflectance for channel 1 and 2. Channel 3 to 5 are converted to blightness temperature by non-linear calibration method[7-10]. In geometric calibration, initial correction is applied by means of Two-Line Element orbital information [11] followed by precise correction based on the ground control points (GCPs) derived from MODIS product. Precise correction is composed of orbital correction and attitude correction. Orbital correction is applied daily several paths at the same time for the purpose to keep the number of available GCPs, and attitude correction is applied by each path in order to allow the frexibility of attitude. Optimized orbital information and attitude angles are derived by least square estimation.

The HRPT data is not available especially in the western region around upstream of the Yellow River, because it is outside of the receivable range of University of Tokyo receiving station. Therefore, GAC is used as base product and HRPT and LAC are overlaid if these are available, though the spatial resolution of GAC is lower as 4 kilometers. The outline of the overlay is shown in figure 7.

4.2 Preliminary study using Pathfinder AVHRR Land Data Set

Change detection method was applied for Quingtongxia and Hetao irrigation districts as the feasibility study by means of 8 kilometers resolution AVHRR data set, Pathfinder AVHRR Land data set. Annual maximum NDVI (Ann_Max_NDVI) is derived by averaging of second to sixth maximum NDVI among the daily data for one year. Time series of regional distribution of Ann_Max_NDVI for both irrigation districts are shown in figure 8. Ann_Max_NDVI has been increased gradually in both districts through 20 years. The trend is slightly different, that is, widely distributed Ann_Max_NDVI has been concentrated to higher value in Quingtongxia districts, and lower Ann_Max_NDVI has been totally increased in Hetao district. The reason of these increase seems to be the increase of agricultural fields, however, the detail of the change is not interpreted from 8 kilometer resolution data set.

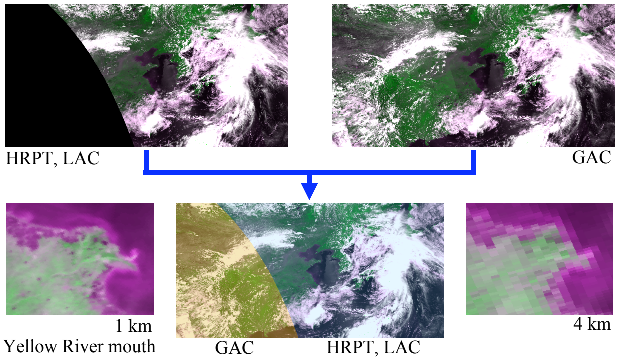

Fig. 7. Overlay of HRPT, LAC (1 km) and GAC (4 km).

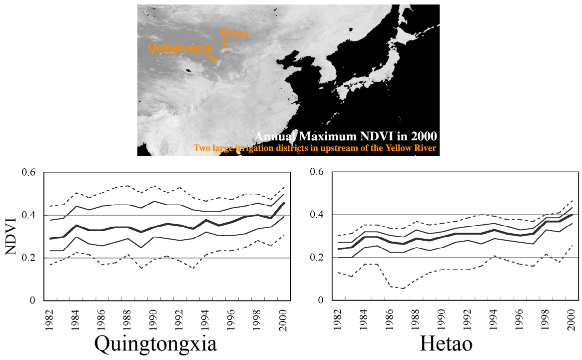

Fig. 8. Time series of the distribution of the annual maximum NDVI for two irrigation districts.

5. Detailed analysis using Landsat

The change of the Ann_Max_NDVI in irrigation districts has been analyzed in detail using higher resolution data, 1 kilometer resolution AVHRR combined with Landsat. The method of analysis is shown in figure 9. Ann_Max_NDVI over Quingtongxia districts in 1999 was derived from 1 kilometer daily AVHRR data described in section 4. Land cover map was derived by simple decision tree classification using Landsat/ETM+ acquired on 12th Aug. 1999 when the status of the vegetation is most active. The data was downloaded from GLCF, University of Maryland [12]. Since the spatial resolution of AVHRR and ETM+ is about 1 kilometer and 28.5 meters respectively, 1 pixel of AVHRR corresponds to 32 by 25 pixels of ETM+. Therefore, fraction of agricultural area (Frac_Agri_Area) in one AVHRR pixel is calculated from the land cover map of ETM+. Finally Frac_Agri_Area is estimated from the Ann_Max_NDVI.

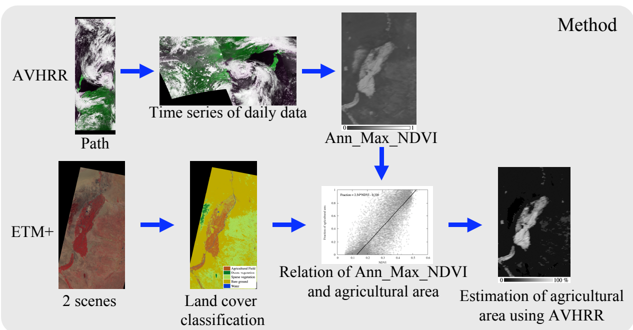

Fig. 9. Method of the analysis.

The decision tree classification method applied to ETM+ is shown in figure 10. NDVI, reflectance in band 5 and digital elevation model GTOPO30 [13] were used to categorize the pixel into the five types of land cover. The classification result is shown in figure 11. As the assessment of the classification accuracy, only agricultural field is compared to county based census value, that is, agricultural area in each county is extracted using county mask (figure 12) and it is compared to the sowing area in 1999 recorded in the Statistical Yearbook of Ningxia province. The result is shown in figure 13. The overestimated counties are located in midstream of the district, and relatively underestimated counties are in downstream. Excess underestimated county is Yanchi county, which is located outside of the irrigation districts.

Ann_Max_NDVI in Quingtongxia district is shown in figure 14. The relation of Ann_Max_NDVI and Frac_Agri_Area is shown in figure 15. The linear equation of [Frac_Agri_Area = 2.54 * Ann_Max_NDVI - 0.33] is derived from the least square regression. The Frac_Agri_Area estimated from AVHRR using this equation is shown in figure 16. The mountainous area was masked by GTOPO30. Figure 17 shows the county based comparison of agricultural area with ETM+ classification. This figure indicates that AVHRR estimation is comparable to the ETM+ estimation in county base. This method is specialized to irrigation districts in arid region where the contrast of the NDVI in agricultural area and background is high. The method will be applied to the time series of AVHRR for detecting the seamless change of the land cover in irrigation districts.

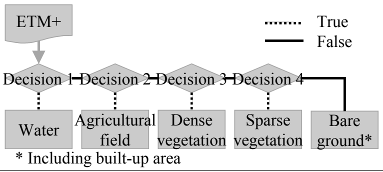

Decision	Criteria	Thresholds
1	NDVI < Threshold AND	0.400
	Ref5 < Threshold	3.75 %
2	Elevation < Threshold AND	1800 m
	NDVI > Threshold AND	0.350
	Ref5 < Threshold	25.0 %
3	NDVI > Threshold	0.375
4	NDVI > Threshold	0.250

Fig. 10 Classification method.

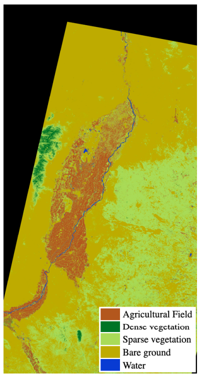

Fig. 11. Land cover map.

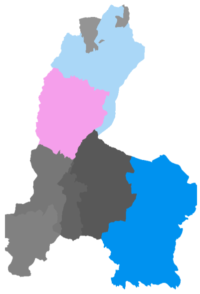

Fig. 12. County mask

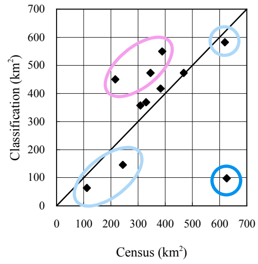

Fig. 13. Comparison result.

Fig. 14. Ann_Max_NDVI

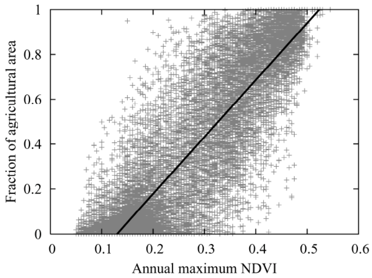

Fig. 15. Relation of Ann_Max_NDVI and Frac_Agri_Area.

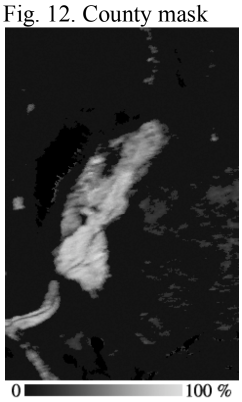

Fig. 16. Frac_Agri_Area. derived by AVHRR

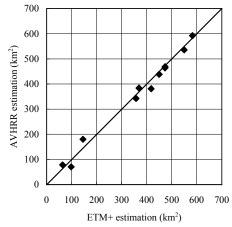

Fig. 17. Comparison

6. Conclusions and future plans

The land cover monitoring on the Yellow River in China is in progress under the hydrological project. Land cover map in 2000 was produced using 250 meter MODIS product and it is used as the base map of the hydrological model. The time series of AVHRR for 20 years has been being produced from HRPT, LAC and GAC with the spatial resolution of 1 km. Land cover change especially concerned with the agricultural field will be detected using this data combined with Landsat.

Acknowledgement

This study has been carried out as a part of the Research Revolution 2002 project supported by the Ministry of Education, Culture, Sports, Science and Technology (MEXT) in Japan.

Authors appreciate the valuable distribution of HRPT by Kitsuregawa Lab., LAC data by Comprehensive Large Array-data Stewardship System, Landsat by Global Land Cover Facility, and GTOPO30 by USGS.

References

[1] The Yellow River Studies. (2003). http://www.chikyu.ac.jp/yris/.
[2] CASW Data Technology, 1 km land-use & land cover raster data of China, http://www.casw.com.cn/.
[3] Chinese Forest Science Data Center website, http://www.cfsdc.org/.
[4] National Bureau of Statistics of China website, http://www.stats.gov.cn/.
[5] Kitsuregawa Laboratory, http://www.tkl.iis.u-tokyo.ac.jp/english/.
[6] NOAA's Comprehensive Large Array-data Stewardship System, http://www.class.noaa.gov/nsaa/products/welcome.
[7] Kidwell, K. B., "NOAA Polar Orbiter Data Users Guide" (November 1998 revision), http://www2.ncdc.noaa.gov/.
[8] Goodrum, G., et al., "NOAA KLM User's Guide" (September 2001), http://www2.ncdc.noaa.gov/.
[9] Agbu, P.A., and M. E. James. (1994). "The NOAA/NASA Pathfinder AVHRR Land Data Set User's Manual", Goddard Distributed Active Archive Center, NASA, Goddard Space Flight Center, Greenbelt.
[10] Ouaidrari, H., et al. (2002). " Land surface temperature estimation from AVHRR thermal infrared measurements An assessment for the AVHRR Land Pathfinder II data set", Remote Sensing of Environment vol. 81, pp. 114-128.
[11] Celes Track, http://www.celestrak.com/.
[12] Global Land Cover Facility, University of Maryland. http://glcf.umiacs.umd.edu/data/.
[13] GTOPO30 Global 30 Arc Second Elevation Data Set http://www1.gsi.go.jp/geowww/globalmap-gsi/gtopo30/gtopo30.html.

ANALYSIS OF POPULATION DENSITY DISTRIBUTION WITH IMAGE SATELLITE

Ketut Wikantika[1,2], Farid M. Rahman.[1], Andri Hernandi[2], Hadi, F.[1,2]

[1]Expertise Group on Remote Sensing and Geographical Information Science
[2]Center for Remote Sensing
Faculty of Civil Engineering and Environment, Institut Teknologi Bandung
Jl. Ganesha 10 Bandung (40132), Indonesia
Telp. 022-2530701 Ext. 3644, Fax. 022-2530702
Email : ketut@gd.itb.ac.id

ABSTRACT

Current demographic data from Badan Pusat Statistik (BPS) is only calculated and displayed based on administrative boundary without knowing the actual density. This make the derived information is not complete, tend to be homogenuous and is not represent the real facts. In the regional planning, demographic aspect is one of the most important aspect because planning is basically for and by the citizen itself. Remote sensing technology currently provide alternative solution on the problem of time-series spatial data. The excellence of remote sensing which can provide continuous data can be utilized to study population distribution on certain area. This research studies the role of remote sensing to analyze the population distribution in several villages in Bandung with Quickbird satellite images. The method in this research is land use density according to least square principles. The output of this method is a new thematic map which describe population density distribution on a more informative map and have the ability to represent the actual condition.

Keywords: distribution, population density, *land use density*, least square principles

1. INTRODUCTION

Data on current population density from Badan Pusat Statistik (BPS) is only calculated and displayed based on administration area. Due to this condition, the information is not complete, tend to be homogeneous and visually not represent the real condition. While in the planning of an area or city, demographic aspect is one of the important components because planning is designed for and by the citizen itself.

Every steps taken by the government during the development process is basically to improve the citizen's wealthiness. Information on population density is one of the most important data in the regional planning. Due to this reason, there is a need to search for new techniques that produce information with a better quality.

This research utilize a high spatial resolution imagery, Quickbird, to analyze population density distribution in several villages in Bandung. Land use density method with least square principle was chosen as the research method (Min et al., 2002).

2. DATA AND STUDY AREA

Data used in this study consists of Quickbird satellite imagery acquired on August 2003, GPS point that were taken in 2004, administrative boundary with 1:25.000 scale from topographic map and Bandung statistical data of the year 2003. Six villages chosen as study case are Cipedes, Sukabungah, Pasteur, Cipaganti, Pajajaran and Pamoyanan. These six villages area assumed to represent several type of land in Bandung.

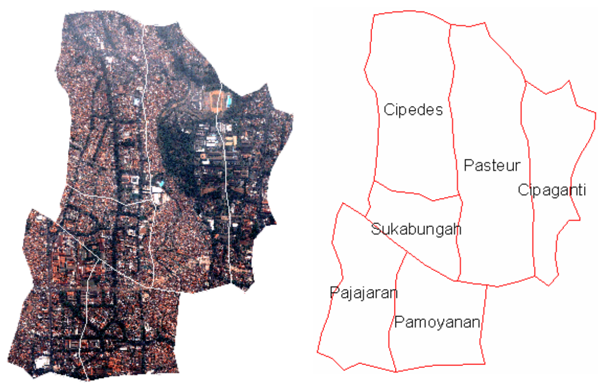

Figure 1. Quickbird satellite image (left) and village administration boundary (right)

3. METHODOLOGY

The research methodology consists of several steps:

a. Reference study, covers study on fundamental theories and methods which will be used to analyze population density distribution with satellite images.
b. Secondary data collection.
c. Data processing which includes image geometric correction, population density calculation, digitization and result displays.
d. Research analysis and publication.

Validation step is carried out by taking picture on each habitation during the field check.

4. *LAND USE DENSITY METHOD*

In this method, population density assessment is obtained from land use type. The approach method is the presentation of population density represented by the different land use type, especially land habitation type. Mathematics model which is used as the approach (Min et al., 2002)

$$\boldsymbol{P} \sum_{i=1}^{n} (A_i D_i) \quad (1)$$

where:
P = total population
A_i = size area on each landuse type
D_i = population density on each landuse type

The land use type is obtained from different of population density. The flow of this method is: first, the inhabitation and the non-inhabitation is distinguished with remote sensing imagery. Every kind of inhabitation type is distinguished in inhabitation area. The boundary of every kind of inhabitation is measured. The area of every kind of inhabitation type multiplying corresponding population density from sample is the estimation population of every kind of inhabitation type. The total sum of every kind of inhabitation type is the total population in study area.

The excellence of the land use density method is it's idea and calculation is simple; the disadvantage of the method is that the selection of sampled region is much more difficult. Is there method the population density of every habitation type is estimated but the sampled region need not be selected. In some region, there is mathematical relation among the The advantage of this method is the relatively easy calculation process, while the difficult are in choosing the sample area and whether those areas will memenuhi population density formula or not.

Further description on this method is shown in the next paragraph below. Suppose there are j regions which the population is known, j = 1,2,...,m. The population sum of every regions is P_j. There are i kinds of habitation types, i = 1,2,..,n. The population density of every habitation type is D_i, then

$$\boldsymbol{P_j} \sum_{i=1}^{n} (A_{ji} D_i)$$

When several villages in the study area were sampled, the above formula is became to :

$$\begin{aligned} P_1 &= A_{11}D_1 + A_{12}D_2 + \dots + A_{1n}D_n \\ P_2 &= A_{21}D_1 + A_{22}D_2 + \dots + A_{2n}D_n \\ P_m &= A_{m1}D_1 + A_{m2}D_2 + \dots + A_{mn}D_n \end{aligned} \quad (3)$$

After those equation are rearranged in matrix type is like below :

$$P = A.D \quad (4)$$

where :

$$P = \begin{bmatrix} P_1 \\ P_2 \\ \dots \\ P_m \end{bmatrix} \qquad A = \begin{pmatrix} a_{11} & a_{12} & \dots & a_{1n} \\ a_{21} & a_{22} & \dots & a_{2n} \\ \dots & & & \\ a_{m1} & a_{m2} & \dots & a_{mn} \end{pmatrix}$$

$$D = \begin{bmatrix} D_1 \\ D_2 \\ \dots \\ D_m \end{bmatrix} \qquad (5)$$

When m > n, that is, the region count known population is more than habitation type count. The least square principle is used to calculate the best population density estimation of every kind of habitation which the errors of statistical population is least.

$$D = [A^T A]^{-1} . A^T P \qquad (6)$$

5. HABITATION DEFINITION

According to the WordNet which was released by Princeton University in 2001, the word habitation has three definition, (1) the native habitat or home of an animal or plant , (2) housing that someone is living in, (3) the act of dwelling in or living permanently in a place (said of both animals and men).

Indonesia uses none of these definition for classifying its human habitations. This result in no standard classification for human habitations. While in land use method, this definition is one of the needed parameter to assess the population density. As an example, China classifies its human habitation to several types such as high building, multilayer building, simple building and compositive building. The high building indicates a building with more than 7 layers. The multilayer building indicates a building with from 3 to 6 layers. The simple building indicate a building with less than 3 layers. The compositive building indicate a building which used for business and habitation.

Based on the definition above, the way to overcome this problem is to make some assumption which is relevant to the definition and to the study area. The assumptions which were chosen are:

a) Habitation is defined only to those building used as a place for permanent stays.
b) The building is not design for a work place
c) The building is not design for temporary stay such as hotels, motels and etc.
d) The building is not design to educate people

After the habitation type is defined, the next step is to carried out interpretation of satellite image. In this research, habitation is only divided into structured habitation and unstructured habitation.

6. RESULTS AND DISCUSSION

RGB composite Quickbird satellite image was used in this study. This image was firstly geometrically corrected with 9 GCPs that were distributed evenly in the study area. The accuracy of GCPs distribution was checked by independent check points (ICP). The value of RSME from ICP shows a value of 0,5 pixel. The datum that was used in the process of rectification is WGS 84 with map projection South UTM 48. Tranformation method that was used is first degree polynomial transformation with nearest neighbor as the interpolation method.

After the data on size area of each habitation and population are obtained, the next step is the data calculation with mathematic model to assess population density. The data which will be used in this calculation is shown in Table 1.

To make the process easier and to fit the concepts of population density calculation with the chosen mathematics model, the data in Table 1 is rearranged in matrix.

Tabel 1. Data for calculation of population density

No.	Village	Area (Km2)	Habitation type	Area (Km2)	Population (P)
1	Cipaganti	0,040357548	Structured habitation	0,040357548	11664
			Unstructured habitation	0	
2	Cipedes	0,593817838	Structured habitation	0,152017917	23698
			Unstructured habitation	0,441799921	
3	Pajajaran	0,298752457	Structured habitation	0,185674304	22242
			Unstructured habitation	0,113078152	
4	Pamoyanan	0,358116354	Structured habitation	0,167232574	9309
			Unstructured habitation	0,19088378	
5	Pasteur	0,663372739	Structured habitation	0,05785	19723
			Unstructured habitation	0,60552113	
6	Sukabungah	0,382620902	Structured habitation	0,125909076	25058
			Unstructured habitation	0,256711826	
Jumlah Total		2,337037838			111694

The calculation shows that the number of population density for structured habitation is approximately 89586 people / km2, while for unstructured habitation is about 24146 people/km2. By seeing these numbers, population density for structured habitation has higher number. This is not because of the wrong data or calculation but arise as the result of calculation from least square principle. This analysis is reasonable because when the calculation is retaken in the reverse direction by using D value on the mathematical model, the total value of P and total value of Pc is nearly the same, 111.694 and 104138, 3155 people. The difference is about 7556 people or about 6,8 % from statistical data.

The foundations of population density assessment with this method is the dividing of each administrative region into several habitatation types. After that, each habitation on every administration region is further classified and united into one tipe of habitation. The number of habitation will influence the detail of information that we will have. The more class of habitation, the more class of population density that will be derived and this will result in the better quality of population density information.

By using this method, we can provide a new presentation model to describe the population density distribution. The population density is visualized not just by translating numeric data into administrative boundary but also visualized by its density on each administrative region.

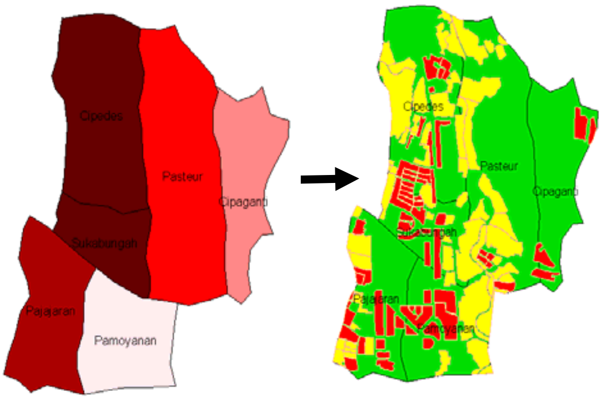

Figure 2. Conversion of
presentation model on population density

The difference between the use of previous way and this model in describing population density information is that by using land use density method the presentation is more representing the real condition.

7. CONCLUSIONS

Based on the result and analysis, there are several conclusions :

a. The population density method with land use density can not be used on low spatial resolution satellite image due to the need of detail classification process.

b. The information on population density that will be gained by this method is depended on the number of habitation classes. There is no standard habitat classification in Indonesia, so the application of this method is difficult.

c. Satellite image can be applied in the social mapping research as a data resource to calculate and to present information on condition and social characteristic of certain region.

RECOMMENDATION

There is a need to make a standard habitation classification in Indonesia. If this classification exist, it will be easier to define the type of human settlement from satellite images.

REFERENCES

Min, Lu An., Ming, Li Cheng, Jian, Li-zhong, 2002. Modelling Middle Urban Population Density With Remote Sensing Imagery. Proceedings of ISPRS Symposium on Geospatial Theory, Processing and Applications, Ottawa, Canada

WordNet, **www.answers.com/library/WordNet** (2001)

Mapping soil degradation by topsoil grain size using MODIS data

Jieying Xiao[1], Yanjun Shen[2], Tateishi Ryutaro[1]

[1] Center for Environment Remote Sensing, Chiba University, 1-33, Yayoi, Inage, Chiba 263-8522, Japan

Tel: 043-290-2964; Fax: 043-290-2963 Email: xiaojy@graduate.chiba-u.jp

[2]Institute of Industrial Science, the University of Tokyo, 4-6-1 Komaba, Meguro, Tokyo 153-8505, Japan

Abstract:

MODIS BRDF reflectance data at the end of April 2004 was selected to make a desertification map base on topsoil grain size by using Gain Size Index at arid and semiarid Asia. After data processing, GSI was applied into desertification mapping, and we find that high GSI area distributed at the desert and its' marginal area, degraded grassland, desert steppe. The desertification map was output according to the correlation between GSI and grain size distribution, the classification of desertification is no desertification, light desertification, middle desertification, and severe desertification. The result can manifest the soil degradation very well.

1 Introduction

Desertification is land degradation, manifested by “desert-like” conditions in dryland areas. Climatic conditions together with geomorphologic processes help to mould desert-like soil surface features in arid zones. The identification of these soil features serves as a useful input for understanding the desertification process and land degradation as a whole (Shrestha et al,. 2005). Soil degradation mapping is very useful for land management and soil evaluation, the changing of soil properties like texture**,** organic matter (OM), pH, phosphorus and potassium is important for the world because it has close relation with the food and living condition for human being. Grain size distribution is one of important characteristics of soil texture, and coarsen of the soil surface is an indicator of soil degradation.

Soil reflectance spectra have a direct relationship with soil texture, as well as to other parameters such as soil moisture, and organic matter. Remote sensing technique is proved as an available method for detecting and monitoring the change of land cover. Analysis of remotely sensed data involves identifying features and correlating ground-based measurements with recorded reflectance or emittanee values (Mattikalli, 1997). Earlier studies have identified significant relationships between some of these properties and spectral reflectance of soils in the visible and near infrared portions of the electromagnetic spectrmn (e.g., Gerbermam et al., 1979; Stoner anti Baumgardner, 1981; Horvath et al., 1984; Baumgardner et al., 1985; Jeyasingh, 1986; Mattikalli, 1997). And recently, also many studies concern about this topic, Shrestha et al (2005) analyzed absorption feature parameters in the spectral region between 0.4 and 2.5 μm wavelengths and correlated with soil properties such as soil colour, soil salinity, gypsum content and applied Linear unmixing and spectral angle matching techniques to assess their suitability in mapping surface features for land degradation studies. Chikhaoui et al., (2005) characterized the state of land degradation in a small Mediterranean watershed using ASTER data and ground-based spectroradiometric measurements, developed land degradation index, and applied this index for assessing and mapping land degradation.

Very few studies concerned about soil degradation mapping by topsoil grain size in arid and semiarid area, even recently there isn't one grain size distribution map or a desertification map base on the topsoil grain size. And it cost time and resource to obtain the map of soil physical properties in regional or continental scale using traditional method, in this study, it will become very quick and economical to get the topsoil grain size content map. The present study will apply the grain size index which base on the field survey and laboratory analyses, to the mapping of soil degradation by manifesting the topsoil grain size distribution using remote sensing images.

2 MODIS data and processing

2.1 MODIS data

In the present study, the surface reflectance data production name MODIS/TERRA Nadir BRDF-Adjusted Reflectance 16-DAY L3 Global 1 KM SIN Grid Product (MOD43B4 NBAR) were chosen for mapping the soil degradation in arid and semiarid area of central east Asia. Every 16 days, the MODIS BRDF/Albedo Product (MOD43B) algorithm relies on multidate, atmospherically corrected, cloud-cleared data and a semiempirical kernel-driven bidirectional reflectance model to determine a global set of parameters describing the Bidirectional Reflectance Distribution Function (BRDF) of the land surface. These one kilometer gridded parameters are then used to determine directional hemispherical reflectance, bihemispherical reflectance, and nadir BRDF-adjusted reflectance (NBAR) for seven narrow spectral bands and (in the case of albedo) three broad bands. Since the parameters of the simple kernel-based BRDF model (RossThickLiSparseR) are also provided, along with extensive quality information, the MODIS BRDF/Albedo Product offers members of the global observation and modeling community the additional flexibility to derive reflectance and albedo measures particularly suited to their specific applications. MOD43B is a MODLAND Level 3 Product and is provided globally as discrete 1200 by 1200 element tiles in an Integerized Sinusoidal Grid projection in a HDF-EOS format. MOD43B1 provides the BRDF model parameters, MOD43B2 provides an alternative set of model parameters, MOD43B3provides the black-sky albedo (at a solar zenith angle of 45 degrees) and the white-sky albedo, and MOD43B4 provides the NBAR value at the mean solar zenith angle of the 16 day period (source from: http://edcdaac.usgs.gov/modis/mod43b4.asp).

The BRDF gives the reflectance of a target as a function of illumination geometry and viewing geometry. The BRDF depends on wavelength and is determined by the structural and optical properties of the surface, such as shadow-casting, mutiple scattering, mutual shadowing, transmission, reflection, absorption and emission by surface elements, facet orientation distribution and facet density. (Lucht, http://geography.bu.edu/brdf/brdfexpl.html, last updated: 1, Aug 2000)

MOD43B4 NBAR Product is computed for each of the MODIS spectral bands (1-7) at the mean solar zenith angle of each 16-day period. Since the view angle effects will have been removed from the directional reflectance, this will result in a more stable and consistent product. NBAR values could be directly used as the primary input to the advanced technique classifiers used in the production of the global MODIS Land Cover Product. It is expected that the user community will be quick to take advantage of the NBAR data for those situations where composited surface reflectances may have been traditionally used (Schaaf et al., 2002 and http://geography.bu.edu/brdf/userguide/nbar.html, last update, Apr 2004). The Original Data Set Characteristics are:
Area = ~ 10 x10 lat/long
Size = 1200 x1200 rows/columns
Volume = ~31MB
Resolution = 1 kilometer
Projection = Integerized Sinusoidal
Data Type Reflectance = 16-bit Signed Integer
Data Type Quality = 32-bit Unsigned Integer
Data Format = HDF-EOS

Science Data Sets (SDS) = 2 (http://edcdaac.usgs.gov/modis/mod43b4.asp last update at 13 June, 2005)

2.2 Data processing

The data set is come from Land Processes Distributed Active Archive Center (LPDAAC) of NASA's Earth Observing System (EOS). The chosen area showed by the MODIS/TERRA Nadir BRDF- Adjusted Reflectance 16-DAY L3 Global 1 KM SIN Grid Product by RGB color composition, the date range of this image is 10-25, June 2004, Fig.1, vegetation cover is in green color while the desert, sandy land and bare ground is in pink, orange or thistle. The location is at arid and semiarid area of Asia, including China, Mongolia, Kazakhstan, Uzbek, Turkmen, Afghan, Pakistan, Tajikistan, Kyrgyzstan and so on. Most of these countries in this area suffering the severe land degradation, especially China. The images for GSI and soil texture mapping were from 23, April to 8, May in 2004.

The original data set was preprocessed before using, including into image mosaic one by one by using MODIS reprojection tool (MRT) software, and then change the original Integerized Sinusoidal projection into geographic Latitude and Longitude WGS 84. Geometric correction was done to the images, Landsat ETM$^+$ images were used and considered as a reference. Landsat ETM$^+$ images were downloaded from Global Land Cover Facility Earth Science Data Interface of University of Maryland (http://glcfapp.umiacs.umd.edu: 8080/esdi/index.jsp). The images are georeferenced to Geographic map projection for WGS84 Reference datum. (The work of mosaic, reprojection and geometric correction has been done by Al-Bilbisi et al., 2005). And then made a spatial subset to the image to choose arid and semiarid area of Asia only using ENVI software.

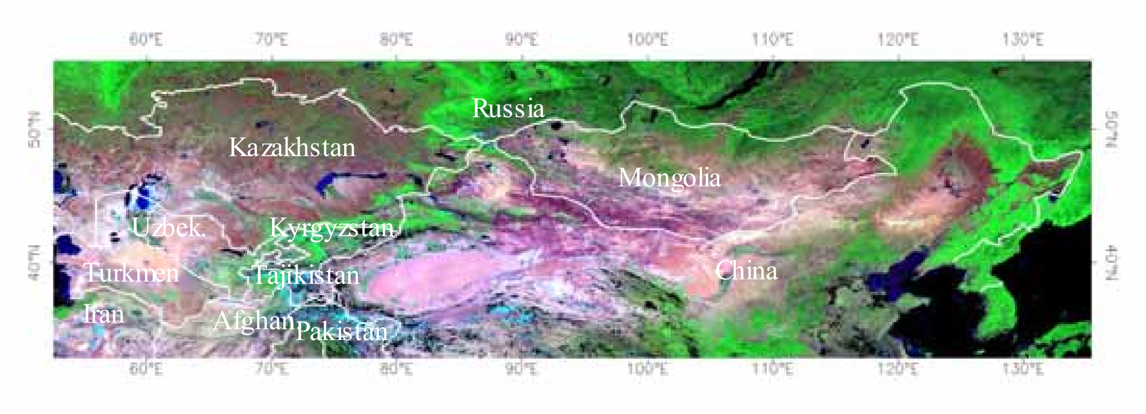

Fig. 1 Arid and semiarid area in Asia.

There are some fill values in this data set, so the mask was applied into the images to delete noisy, and then calculated the reflectance data of every band for the preparation for the calculation of GSI. In this study, the data of 23 Apr to 8 May 2004 was chose from MOD43B4 NBAR data set for desertification mapping.

3. Soil degradation mapping by using GSI

Topsoil Grain Size Index (GSI) was developed by Xiao et al in 2005, it is base on the field survey and laboratory analyses. After the analyses of the correlation between grain size distribution and reflectance data of topsoil samples, we found that the reflectance data changing accompany with the changing of grain size distribution, especially fine sand content and clay+silt content. Then GSI was applied into local area, we obtain the GSI map of the local area, high GSI area means fine sand rich area. Then according to the correlation between GSI and fine sand content, fine sand content distribution map was output as the result, it could manifest the fine sand content very well.

It is calculated by the equation (1):

$$GSI=(R-B)*(R+B+G) \quad (1)$$

Where R, G, B, mean the red, green, and blue visible band of MODIS image that band 3, 4, and 1. In this study, GSI will be applied into the arid and semiarid area of Asia to describe the land degradation of this area.

4. Result

Grain size of topsoil is one of the important characteristics of the soil, and coarsen of the topsoil manifested the soil degradation turning serious. In this study, the fine sand (0.0075-0.425mm in diameter) content of topsoil was obtained by using the GSI map in arid and semiarid Asia.

GSI was classified into seven classes according to the value (Fig.2), and higher GSI value points concentrated at the desert area and sandy land while the highest value points are not located at the large area desert. From the GSI map of 2004, the white color area (GSI is in the range of 0.1-0.15) is only lies on the North part of China and the South part of Mongolia, while it can be found at the south part and some part of Taklimakan desert in China.

Also the desertification maps based on the GSI map were drawn in this study. The Grain Size Index was coming from the correlation between the reflectance and the grain size content, so in this study, the fine sand percentage was found through calculating the reflectance, classified into <15%, 15-30%, 30-45%, and >45%. Then the desertification map were made according to the content of fine sand, classified into no desertification, light, middle and severe desertification, showed by Fig.3, the desertification map manifested the content of the particle which grain size from 0.0075mm to 0.425mm in diameter of arid and semiarid Asia in 2004. From the desertification map, we can find the severe desertification area (in gray color) is in desert area and northeast part and north part of Inner Mongolia, China, some south part of Mongolia and north part of Tibet high plateau of China. If long-term data are possible, change detection can be conducted. In addition, this desertification map can be used for other analyses. It will benefit for analyzing the correlation between desertification and other contributing factors.

This is the first desertification map which base on the topsoil grain size. It is very easy to find the topsoil grain size content in large scale by very economical and quick way. The topsoil grain size map can be used as a tool for land degradation process assessment and change detection.

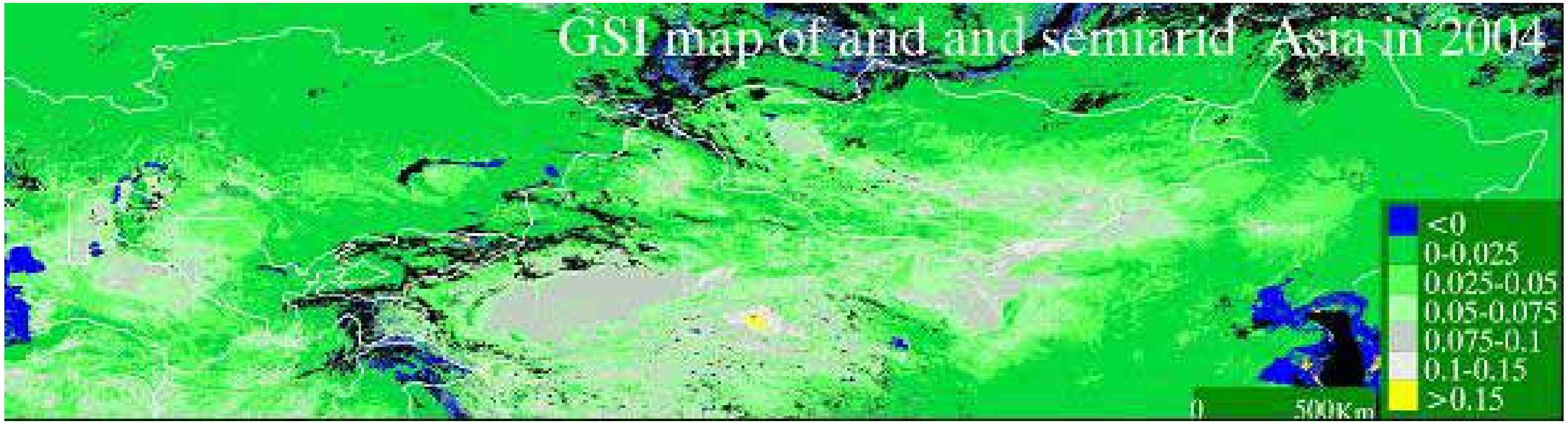

Fig. 2 GSI map of arid and semiarid area of Asia at 2004

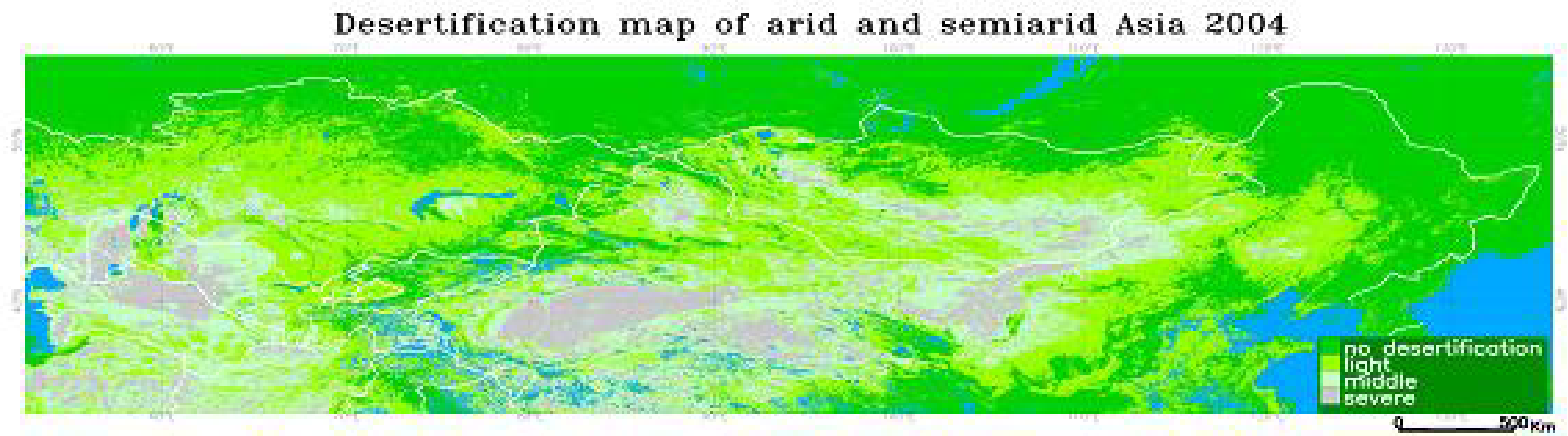

Fig. 3 Desertification map of arid and semiarid area of Asia at 2004

Reference:

Shrestha D.P., Margate D.E., Meer F., Anh H.V. 2005, Analysis and classification of hyperspectral data for mapping land degradation: An application in southern Spain. International Journal of Applied Earth Observation and Geoimformation. Volume 7, Issue 2, pp85-96.

Gerbermann, A. H., and Neher, D. D. 1979, Reflectance of varying mixture of clay and sand. Photogramm. Eng. Remote Sens. 45, pp1145-1151.

Stoner, E. R., and Baumgardner, M. F. 1981, Characteristic variations in reflectance of surface soils. Soil Sci. Soc. Am. **J.** 45, pp1161-1165.

Horvath, E. H., Post, D. F., and Kelsey, J. B. 1984, The relationships of Landsat digital data to the properties of Arizona rangelands. Soil Sci. Soc. Am. J. 48, pp1331-1334.

Baumgardner, M. F., Silva, L. F., Biehl, L. L., and Stoner, E. R. 1985, Reflectance properties of soils. Adv. *Agron.* 38, pp1-44.

Jeyasingh, V. K. tt. 1986, Development of a technique of modeling and predicting soil characteristics based on spectral reflectance. Ph.D. thesis, Indian Institute of Technology, Powai, Bombay.

Chikhaoui M., Bonn F., Bokoye A.I., Merzouk A., 2005, A spectral index for land degradation mapping using ASTER data: Application to a semi-arid Mediterranean catchment. International Journal of Applied Earth Observation and Geoimformation, Volume 7, Issue 2, pp 140-153.

http://modis.gsfc.nasa.gov/about/

http://modis.gsfc.nasa.gov/about/specifications.php

Lucht, http://geography.bu.edu/brdf/brdfexpl.html, last updated: 1, Aug 2000

Schaaf, C. B., Gao F., Strahler, A. H., Lucht W., Li X., Tsang T., Strugnell N. C., Zhang X., Jin Y., Muller J.-P., Lewis P., Barnsley M., Hobson P., Disney M., Roberts G., Dunderdale M., Doll C., d'Entremont R., Hu B., Liang S., and Privette J. L., First Operational BRDF, Albedo and Nadir Reflectance Products from MODIS, Remote Sens. Environ., 83, 135-148, 2002.

http://geography.bu.edu/brdf/userguide/nbar.html, last update, Apr 2004

http://glcfapp.umiacs.umd.edu: 8080/esdi/index.jsp

Al-Bilbisi Hussam, Tateishi Ryutaro, Rokhmatulah and Arihara Kota, et al., 2005, Pre-processing of global MODIS data form USGS, Proceedings of the 39thConference of the Remote sensing society of Japan (submitted).

Mattikalli, N, M., 1997, Soil color modeling for the visible and near-infrared bands of Landsat sensors using laboratory spectral measurements. Remote Sensing of Environment, Volume 59, Issue 1, pp14-28.

http://edcdaac.usgs.gov/modis/mod43b4.asp last update at 13, June 2005

xiao, J, Y., Shen, Y.J., Tateishi R. Development of topsoil grain size index for monitoring desertification in arid land using remote sensing. International Journal of remote sensing, (conditional accept, 2005).

Land cover change and land use of oases surrounding Taklimakan Desert in Xinjiang Uyghur, China derived from satellite images

T. Ishiyama*, N. Saito*, S. Hujikawa** and H. Ohkawa**

*Center for Environmental Remote Sensing, Chiba University, Japan
**Geotechnos Co. Ltd, Japan

Abstract

Land cover change of the oases surrounding Taklimakan Desert in Xinjiang Uyghur in the past 40 years was examined by means of satellite images. From the results of the analysis of these images, the following have been explained. The farmland utilization ratio in average stands at 0.28 in the northern edge of Taklimakan Desert. In the meantime, the ratio stands at 0.13 in the southern edge, whereas 0.31 in the western edge. It is revealed that in the northern edge, area of the irrigation land is vast enough to be utilized. Small oases are much noticed generally in the southern edge, and accounted for usually less than 0.15 resulting in lowness in the utilization ratio of the farmland. However the smaller the value of the said ratio is, the higher the potential of the farmland development is. It is explained that the vegetation land is slightly expanded in the upper reaches of the river in the small oases in the northern edge, but the vegetation land is drastically changed to barren land in the lower reaches of the river. On the other hand, it is explained that the vegetation regions are being expanded year by year in the oases in the northern edge. Especially in Aksu, the farmland area was expanded accompanied with increase of the number of the development settlers.

1. Introduction

In recent years, it is reported that wide area of the land has been rapidly converted into sandy sites in the edges of the oases in Taklimakan Desert in the northern part of Xinjiang Uyghur, China and is suffering from violence of dust storms. Although the cause of the land being converted into sandy sites are not yet explained, it is widely conceived that overlapped actions between the change of weather or climate and human activities, e.g. overgrazing of livestock, outrageous lumbering, land degradation brought about by execution of inadequate irrigation onto farmland, etc. are the causes.

To explain how the land cover change in the regions surrounding Taklimakan Desert is, analysis was made by using the data of the earth observation satellites with the investigation of the distribution of the oases surrounding Taklimakan Desert and the land cover change in Pishan Oases in the southern edge and in the vicinities of the Aksu Oases in the northern edge, especially with the fluctuation in the vegetation regions.

2. Distribution of the oases in Taklimakan Desert and the district surrounding them

The oases of Takilamakan Desert comprise the river water from the mountains in the vicinities of the desert and a tiny amount of the underground water, and change of the horizontal distribution of the vegetation density of the farmland of the oases and desert regions is quite drastic. In Fig. 1, a distribution map of the vegetation indices of the Takilamakan Desert obtained by analyzing TERRA/MODIS data is shown. Great oases are noticed on an alluvial fan in the western end on Pamir Plateau and Tianshan Mountains in the western end and northern edge of Takilamakan Desert. On the other hand, the oases on the southern edge that have developed on an alluvial fan of Qunlun Mountains are relatively small in comparison with the one referred to above. Thus it is understood that the longitudinal width is shorter than the one of the western edge and of the northern edge.

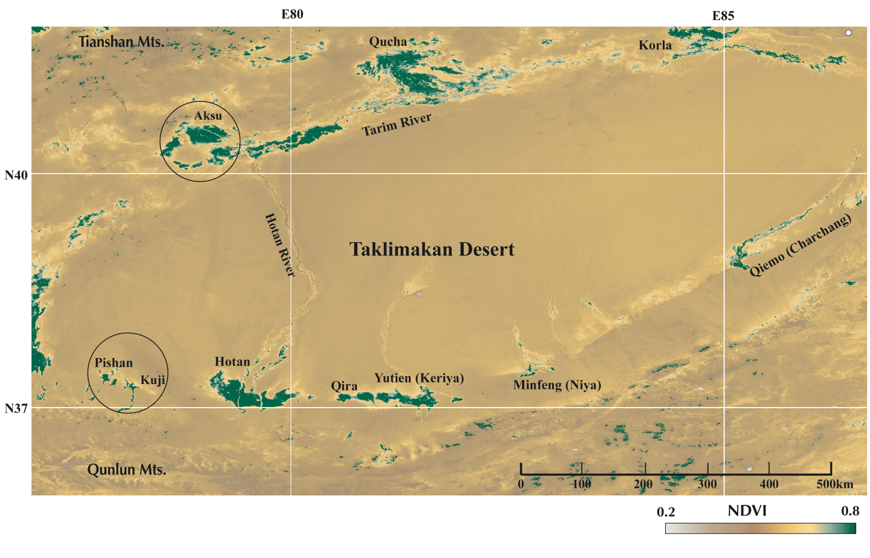

Fig. 1. Distribution of vegetation index of whole Taklimakan Desert derived from TERRA/MODIS data (May 1, 2000). The circles indicate the test sites.

Table 1. Areas of cultivated (NDVI; 0.4-0.8) and irrigation (HD-NDVI; 0.6-0.8) land of oases around Taklimakan Desert derived from MODIS data.

Oasis	Cultivated Land	Irrigation Land	Delta	Ratio of NDVI
(Northern)	(km^2)	(km^2)		
Aksu	2,830.3	486.6	969	0.17
Awat	709.9	549.0	160.9	0.78
Qucha	4,114.0	378.0	3736	0.09
Korla	843.3	340.6	502	0.40
Yuli	1,539.9	260.1	1280	0.17
				Average 0.32
(Western)				
Yarkand	3,290.7	1,277.4	2014	0.399
Kashgar	3,017.8	670.9	2347	0.222
				Average 0.31
(Southern)				
Qiemo	846.5	97.6	749	0.115
Yutien	1,060.2	125.5	934	0.118
Qira	421.4	68.7	352	0.163
Hotan	2,464.9	365.9	2099	0.148
Pishan	296.9	41.9	255	0.141
				Average 0.14

In Table 1, the area of the oases surrounding Takilamakan Desert that is calculated from MODIS data is shown. The area in question is obtained from the number of the pixels of the vegetation indices calculated from the satellite data. As the introduction equation of the vegetation indices, normalized vegetation indices (NDVI) were used. At this stage, NDVI (0.4-0.9) takes up the district ranging from a region of open vegetation to a region with high vegetation density as an objective. In this study, the regions shall be expressed as cultivatable land. On the other hand, the vegetation indices (HDNDVI: high density NDVI, 0.6-0.9) indicates an inner oases farmland with high vegetation density. The area ratio of both the former and the latter can be expressed as farmland utilization ratio (= irrigation land/cultivatable land). The values of the land utilization ratio in average are 0.28 on the northern edge of Takilamakan Desert, 0.13 on the southern edge, and 0.31 on the western edge, according to Table 1. Akus and Qucha in the northern edge and Yarkand and Kashgar in the western edge are oases exceedingly immense, and the utilization area of the irrigation land is shown to be particularly vast. On the contrary, oases rather small in comparison with those in the northern or western edge are generally found in the southern edge. The ratio of the area of the individual oases is usually lot less than 0.15, and the utilization ratio of the farmland is very low. However the smaller the value of the ratio is, the higher the potential of the farmland development is. It is made known that the utilization of the farmland is also low in Hotan in the southern edge, which is a relatively great oasis.

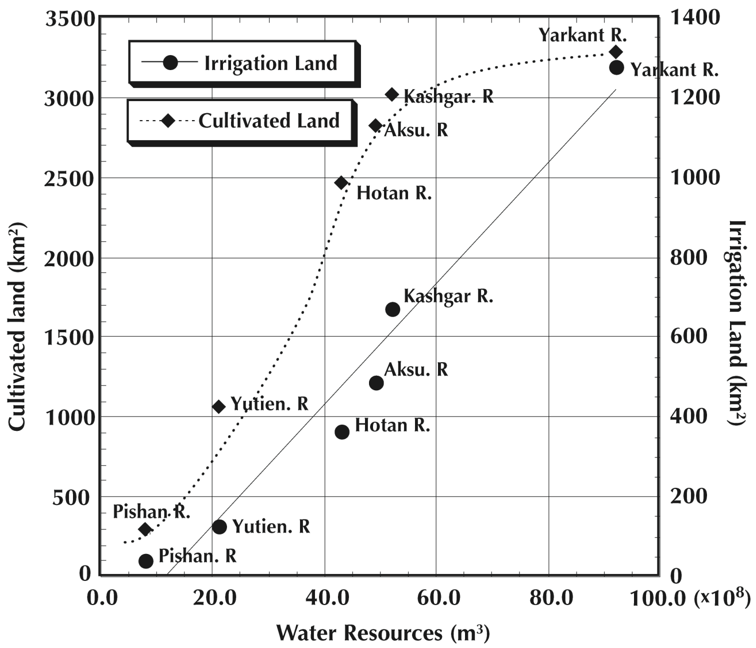

Fig. 2. Relationship among total water resources and irrigation, cultivated land in drainage of Taklimakan Desert. The areas of irrigation and cultivated land derived from MODIS data.

Needless to say, the oasis utilization ratio is dependent on the amount of the water supplied from rivers and on the volume of the underground water. In Fig. 2, a relation among the total amount of the water resources of the principal rivers forming the oases, cultivatable land shown in Table 1, and irrigation land is shown. The irrigation land area and total amount of the water resources are almost in a linear relation. However with correlation between the cultivatable land (including natural vegetation land) and total amount of the water resources, it is noticed that the both factors are in a linear relation to the extent that the total amount of the water resources is almost 5 billion cubic square kilometers. However when the amount exceeds the said value, the cultivatable land is saturated. On condition that all the water resources are utilized with good efficiency, it is to be expected that the cultivatable land will also be increased accompanied with expansion of the irrigation land. However as a matter of fact, no increase can be seen with the cultivatable land despite the fact that the riverside district is enlarged as seen in Yarkand and Kashgar in the southern edge. This might mainly stem from the reason that in these regions, under development of the irrigation channels and inferiority in water control technology compel the water resources to be wasted exceedingly purposelessly. Also the land where salts were accumulated owing to inadequate irrigation laws is much seen in Yarkand, Kashgal, Akus, etc. This is linked with the difficulty to develop cultivatable land because of the lowness of the level of the area.

3. Land cover change in the southern and northern edges in Takilamakan Desert

3.1 Land cover change in the oases in the southern edge

To examine the land cover change in the southern edge in Takilamakan Desert, comparison was made among the different images obtained from the earth observation satellite launched into space in 1972 at the time of observation. However in the northern edge, almost none of regions with great land cover change that was vast enough to be identified from the images of the satellite could be extracted. However on-the-spot investigation reports that the tiny land cover change that is hardly discernible from images of the satellite, e.g. invasion of the sand of moving dunes into the oases or erosion of the vegetation regions by domestic animals is found. On the other hand, expansion of the farmland by irrigation or enlargement of vegetation by afforestation is seen. Thus it can safely be said that change of the land surface is a quite complicated one owing to complexity of natural phenomena and human activities(1, 2).

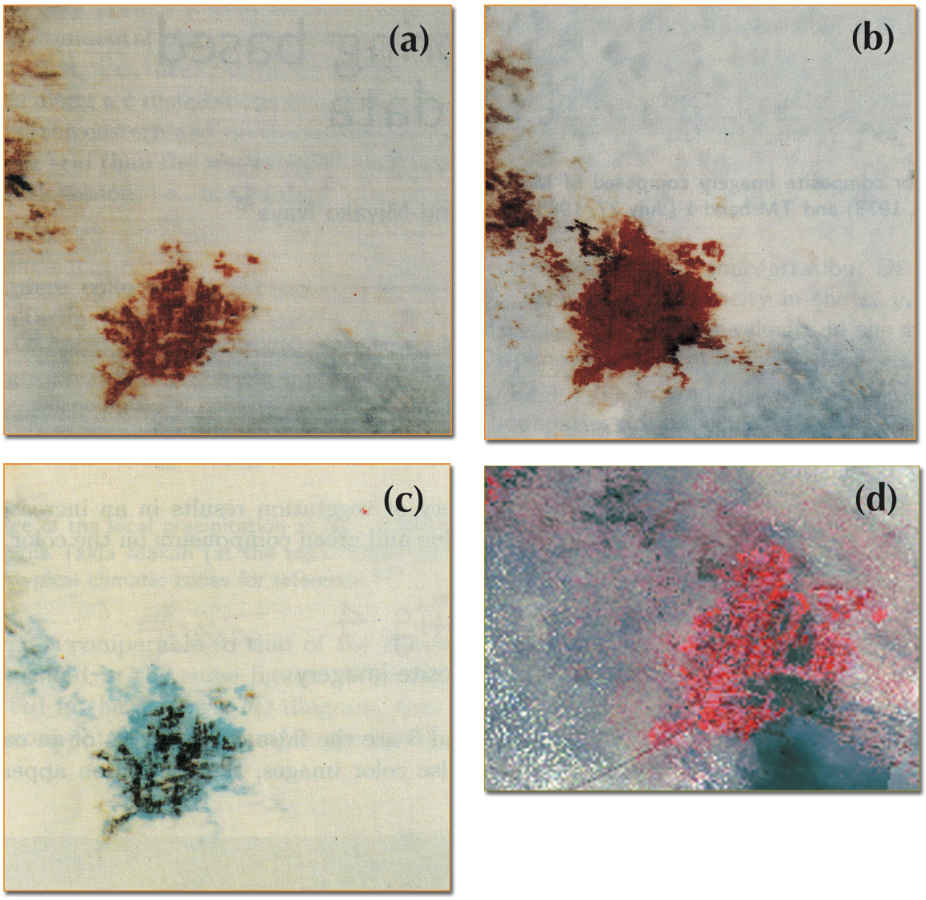

Fig. 3. Comparison of land cover condition of the small oasis of eastern edge of Lop based on Landsat MSS(1973), TM(1988) and Terra/ASTER (2001).Fig. 3 (a). Landsat/ MSS on July 24, 1973., Fig. 3 (b).LANDSAT/ TM on July 27, 1988., Fig. 3 (c). The extraction of 56% rise in vegetation areas (light blue) derived from composite imagery composed of MSS band 4 image (July 24,1973) and TM band 1(July 27, 1988), (d). The land cover condition derived from TERRA/ ASTER on April 27, 2001.

In Fig. 3, change of small farmland in the eastern edge of Lop District, Hotan City is shown. The figure reveals that the city is separated from Lop District as is seen in Fig. 3a (Landsat MSS, 1973), but it is explained from the analytical result that Lop District is partially connected with the vegetation region in 1988, i.e. 15 years after the separation as is seen in Fig. 3b

(Landsat TM). Thus it is made known that the area of the connected part is expanded as widely as 56% (Fig. 3c). Furthermore it is explained from comparison of ASTER image in 2001 in the same region with Landsat TM in 1988 referred to above that Lop District is again divided, but the vegetation region is increased 7% in a downstream direction (Fig. 3d). Thus at least in the southern edge of Takilmakan Desert as seen above, change of land surface situation complicated enough to repeat expansion and shrinkage of the vegetation region in the oases is shown. In the oases developed along a great river, such districts where vegetation regions are being expanded accompanied with expansion of the farmland or afforestation are also in existence. Land degradation as seen in conversion into desert rather appears outwardly to be in a state of stagnation.

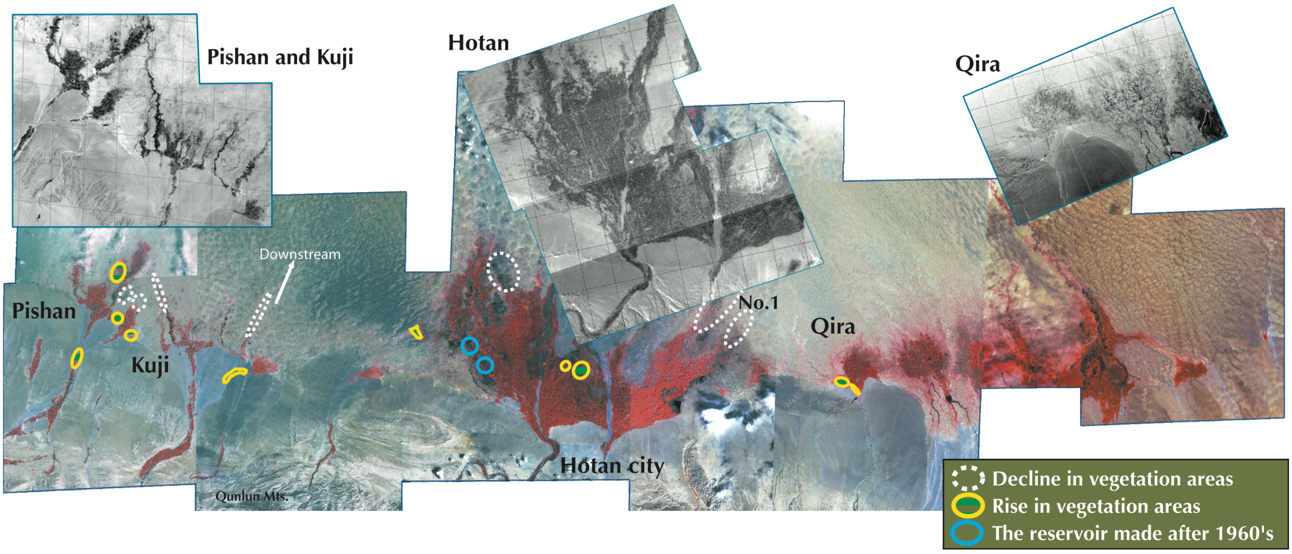

Fig. 4. Comparison of CORONA photographic image (1960) and ASTER image (2001) in land cover condition of southern edge of Taklimakan Desert. Top gray scale images are shown CORONA satellite image.

In Fig. 4, an outline is shown with the change of the land cover of the whole of the southern edge of the newest TERRA/ASTER images taken place after 40 years in the same region where the images of CORONA satellite (KH-4B resolution: 15m) manifested itself in the primary period of 1960. The result obtained by visually discerning both the types of the images is depicted on the image of ASTER. It is ascertained from the depiction that with the small oases such as Pishan or Muji on the districts surrounding the boundary on the desert, vegetation regions are in a declining trend. Meanwhile on the upstream district of these oases or on the place close to the irrigation canal, situations are quite reverse and the vegetation region is expanded. In the north of Lop Region (No. 1, district) of Hotan City in Fig.4, sand of the dunes rushed to these districts starting from the beginning of 1980. The farmland could not but be deserted because of such rush of sand, according to the local farmers. However in Moyu located in the west of Hotan City, the farmland was developed by introducing the water from 5 irrigation cisterns situated along Karakash River. The area of the said 5 irrigation cisterns is the greatest in the southern edge. On the other hand, it is also made known from the on-the-spot investigation in September 1991 that sand protection by means of afforestation in recent years prevents the dunes from being invaded. In Fig. 5, geographical positions of the change of the area of the vegetation region of the oases in the southern edge are shown. From the figure, it is made plain that regression of the vegetation region is remarkable in the downstream part of the oasis. On the other hand, it is understood that the great expansion of the vegetation region seen in the center of the figure is dependent on the existence of large cisterns in the vicinity of Moyu District, Hotan City.

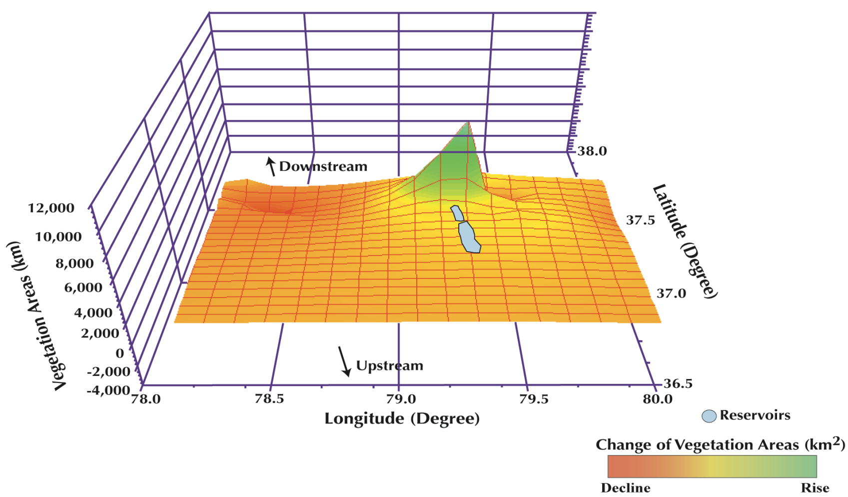

Fig. 5. Three dimensional image of distribution of fluctuation of vegetation areas during 1960's and 2001 around southern edge of Taklimakan Desert.

3.2 Distribution of the land cover change on a district surrounding Pishan

Comparison between ASTER image of the CORONA satellite in the beginning of 1960 and the one obtained 40 years later made it possible to extract the change regions where land cover was in progress. The extraction was in accordance with the following method. The CORONA image, which was printed on 70mm monochrome film, was digital-converted by means of a scanner. The image in question, in which the geometrical distortion brought about during the observation is contained, was deprives of its geometrical distortion by referring to the GCP (ground control point) obtained from ASTER image in the same region with which geometrical correction is made. The images obtained in this manner were classified into 10 clusters in accordance with the ISODATA classification method (Non supervisor classification). From all the clusters, the clusters believed to be in vegetation region were extracted by visually discerning them. By the extracted clusters, which were furthermore re-classified into the ones in the vegetation region and the ones in the non-vegetation region, extraction of the vegetation region was successfully made at the final stage. On the other hand, the area of the vegetation region, barren land, etc. were respectively calculated from the number of the pixels of the analyzed satellite images.

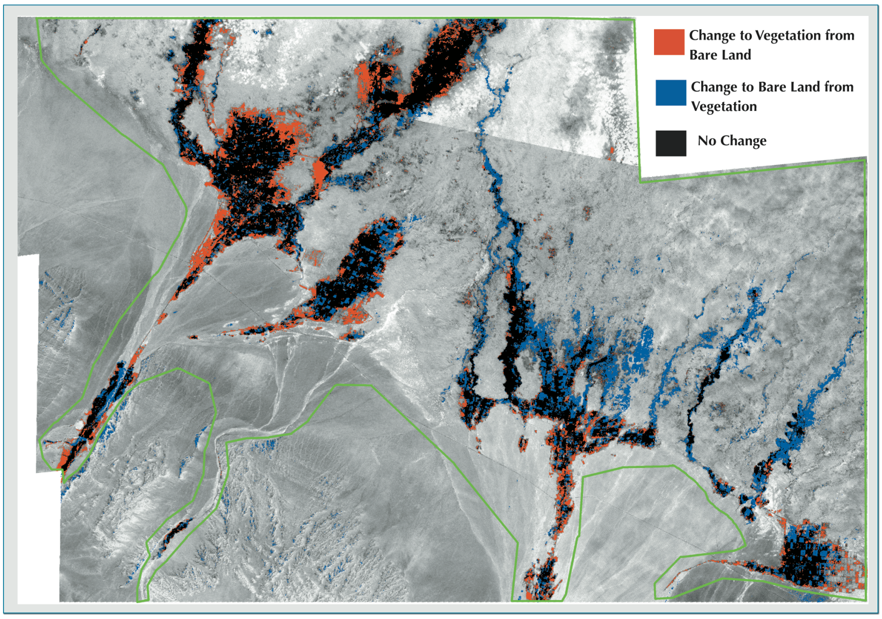

Fig. 6. Distribution of the land cover change on the district surrounding Pishan was obtained from the images of ASTER image of the CORONA satellite in the beginning of 1960 and the one obtained 40 years later. The green line shows border of the test site in this study.

Table 2. Land cover change in Pishan oasis of during 1960 and 2000 derived from CORONA and ASTER data.

Fluctuations	Pishan (km^2)
Change to Vegetation from Barren Land	75.0
Change to Barren Land from Vegetation	106.9
No Change (Vegetation)	161.5
No Change (Barren Land)	1680.3

Distribution of the land cover change on the district surrounding Pishan that was obtained from the images of the 2 periods referred to above (Fig. 6) is shown. With the small oases such as Pishan, Muji, etc. expanding on the fan of Qunlun Mountains, slight expansion of the farmland owing to existence of the small-sized irrigation cistern and irrigation channel was noticed as a result of the analysis of the satellite images. Expansion of the farmland was seen in the upper reaches of the small rivers, but contrarily vegetation is in regression on the down reaches of these rivers. A single piece each of small cistern is respectively in existence in Pishan and Muji at present, but each of them appear to have been not constructed around 1978. For this reason, a sufficient amount of irrigation water was not provided in the lower reaches and expansion of farmland is believed to have been a difficult one. Especially on the tip of the oasis, invasion of sand from dunes plunges the oases into a crisis of being converted into desert. Meanwhile on the southern edge, Hotan that developed on the alluvial fan of the Karakax River, the largest river, and the Yurunkaxi River are blessed with utilizable water in comparison with Pishan.

Several large-sized cisterns were constructed, and they contribute to expansion of farmland (Fig. 4). Area of the 40-year-old change of the land cover that is obtained from satellite data is shown in Table 2. In Pishan or Muji, things are dependent on the small rivers and a tiny amount of underground water. However such water of the rivers and underground water are very scanty in their absolute amount, and therefore expansion of farmland will be hard to be accomplished in future as well. In such an environment, there is a possibility that the pressure applied onto the agriculture in the lower reaches and land degradation will be expedited. It can safely be said that Xinjiang Government's water resources control, e.g. adequate distribution of water to the regional residents, will be a key factor to promote a countermeasure for oases to be converted into desert.

3.3 Aksu in the northern edge

The oases in the northern edge are blessed with the utilizable river water derived from the Tiansian Mountains. The area is vast enough generally in comparison with that of the oases in the southern edge. Especially Aksu is the largest oasis in the northern edge.

The satellite data used for this study are CORONA (KH-4B, Aug. 8, 1969) and multi-temporal Landsat images, whereas the sensors are MSS, TM, and ETM. The Landsat data were converted from the digital number to brightness value by referring to the meta-data of the individual sensors. Composite images were formulated from the blue, red, green, and near-infrared bands of the obtained brightness values, and the images obtained in a manner the same as that of the CORONA images are classified into 10 clusters in accordance with the ISODATA classification method (Non supervisor classification). A cluster believed to be in the vegetation region is visually discerned to be extracted from all the clusters, and furthermore is re-classified into the ones in the vegetation region and in the non-vegetation region. Thus at the final stage, the one in the vegetation region was extracted. The images of the 3 scenes in a district surrounding Aksu were mosaic-processed to cut out the range as wide as the CORONA image. Thus the vegetation cover area was calculated. The vegetation region extracted from the CORONA image of 1969 is shown in Fig. 7(a), whereas the vegetation regions of 1976, 1990 and 2002 extracted from the Landsat image are shown in Fig. 7(b), Fig. 7(c) and Fig. 7(d). It is understood from these that the cover area of vegetation is continuously increased every year starting from 1969. It is also understood that the area is being expanded especially along the district surrounding Aksu City and its eastern side. The developing farm is expanded from the left bank of the Aksu River to Aral to reach the Tarim River. This corresponds to the vegetation region as the farmland extracted from the satellite image. In Table 3, aging (year variation) of the vegetation cover area is shown.

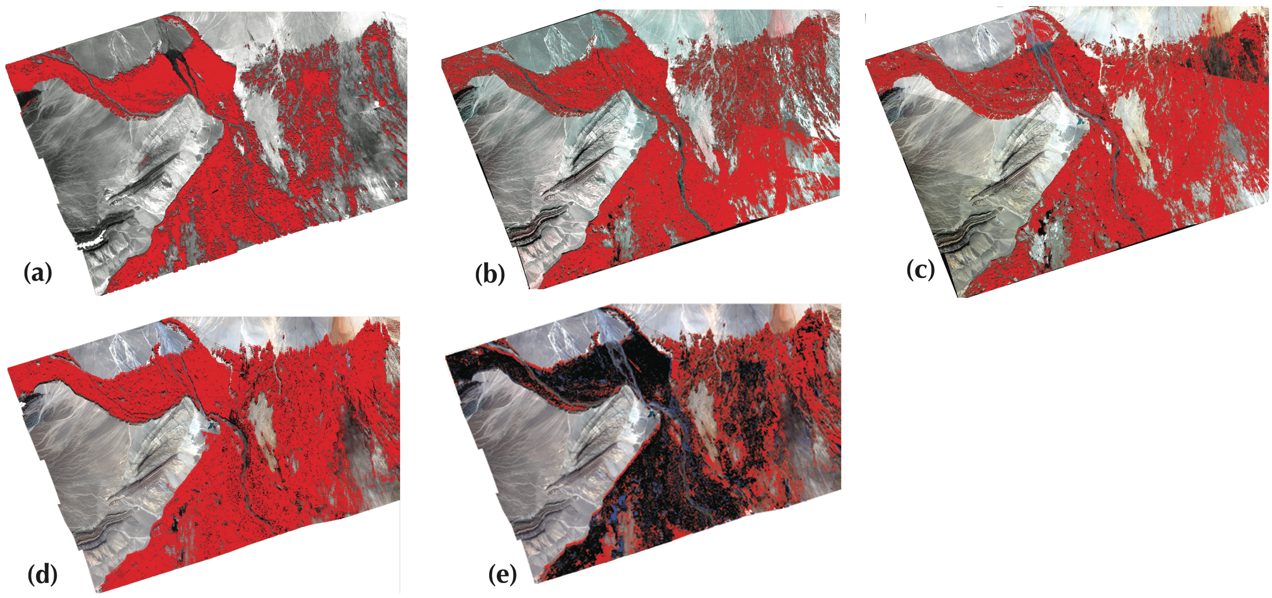

Fig. 7. The vegetation region extracted from multi temporal satellite images in Aksu, the CORONA image of 1969 in Fig. 7(a), whereas the vegetation regions of 1976, 1990 and 2002 extracted from the Landsat image in Fig. 7(b). Fig. 7(c). and Fig. 7(d). , Fig. 7(e) is shown the land cover change of Aksu obtained from composite of the image of CORONA satellite in 1969 and Landsat image 33 years later.

Table 3. Fluctuation of vegetation areas in Akus oasis derived from satellite data.

1970	**2386.1** (km^2)
1976	**2321.3**
1990	**2712.0**
2002	**2718.6**

The population that was changed in Takilamakan Desert in recent 40 years, which was 3,047,300 in 1949, was 1,104,200 as the whole of the northern edge(3). However the values referred to above were reversed in 1980 to be 5,138,600 in the southern edge and 6,919,400 in the northern edge. Meanwhile in Fig. 8, population fluctuation in Aksu City in recent years is shown. It is understood from this that the population of 7,000,000 in 1953 was increased to reach 1,500,000. Furthermore the population became 1,715,900 in 1990. The population increase starting from the middle of 1900 was brought about owing to the fact that the Chinese Government shifted the development settlers from the other regions for the purpose of farmland development in the northern edge. It is comprehended that aging of the vegetation cover area shown together with the change curve of the population well corresponds to the increase in population. Shown in Fig. 7(e) is the land cover change of Aksu obtained from composite of the image of CORONA satellite in 1969 and Landsat image 33 years later on the region the same as that of the former. It is comprehended from the figure that the vegetation region is increased in the left coast of the Aksu River, whereas the vegetation region remains almost unchanged in the right bank in the vicinity of Awat the same as in 1969. Contrarily to the above, the region where the vegetation region is in regression was also observed.

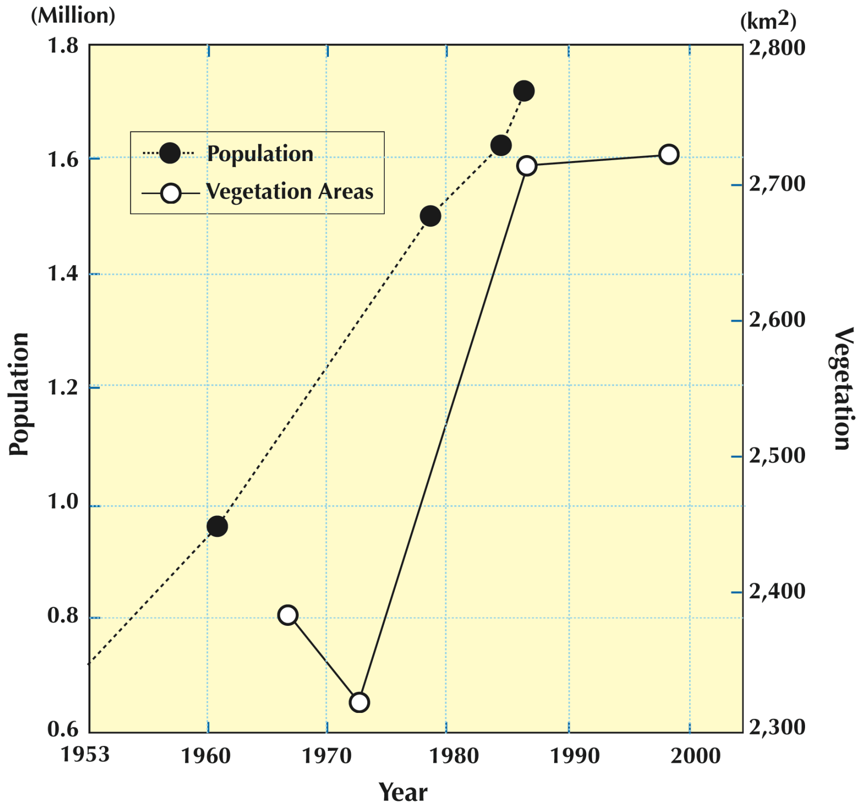

Fig. 8. Recent fluctuations of population and vegetation areas in Aksu oasis.

4. Conclusions

Papers concerning the study on land degradation such as conversion of oases into desert in Takilamakan Desert are publicized mainly by Chinese researchers. However very few papers describing change of the land cover throughout the whole of Takilamakan Desert quantitatively are available. In this paper, land cover or land use in oases surrounding Takilamakan Desert was analyzed by using satellite data. On the other hand, quantitative analysis was made with the change of land cover of the representative oases in the southern and northern edges of Takilamakan Desert. Thus several fruitful outcomes have been obtained. This is the first report concerning the land cover and land use on the district surrounding the oases in the whole of Takilamakan Desert.

With the change of land cover and land use in a vast region where natural condition is very severe as seen in Takilamakan Desert, the whole situation cannot be grasped until analysis is successfully made with satellite data that can make observation of wide region for a long-term. Conversion of oases into desert makes progress not only by climate change but also by human environmental change. Concurrently with this, it is also possible to prevent such progress from being accomplished to a certain degree of extent. However with the oases dependent on small rivers or a tiny amount of underground water, it is exceedingly difficult to prevent the sand from dunes from invading to the oases when the social foundation such as irrigation cisterns, water course, windbreaks, etc. are poorly provided. This can commonly be said especially with the oases in the southern edge that are short of river water and underground water.

Environmental dynamics in Takilamakan Desert is considerably complicated, and long-term and multi-temporal observation is required. In this region as well in recent years, frequency of dust storm is increased resulting in severe damage in humans or livestocks. On the other hand, more than 90% of water resources are supplied from glaciers. Thus when global warming is intensified in future resulting in shrinkage of the glaciers in Qunlun Mountains, Tianshan Mountains, and Pamil Plateau, drastic change of the environment will be caused in the oases and their surroundings.

(Acknowledgment)

Part of this study was supported under the auspices of a subsidy for Japan society for the promotion of science.

(References)

(1) Sugihara,S., T. Ishiyama and M. Naya: Desertification monitoring based on the satellite data., RIKEN Review, No. 5, April, p. 15-16, 1994.

(2) Ishiyama, T., S. Fujikawa, H. Ohkawa and S. Tanaka: Observation of vegetation distribution of Hotan oasisd in southern part of Xinjiang Uyghur, Proceedings of the 13th conference of Japanese association for arid land studies, pp. 66-67, 2002. (Text in Japanese)

(3) Yoshino, M., : Desertification in China, Published by Aichi University , pp.301., 1997 . (Text in Japanese)

Ice breakup dates on 18 Eurasian lakes estimated by MODIS data from 2001 to 2005.

Takashi NONAKA[1], Tsuneo MATSUNAGA[2], and Akira HOYANO[3]

[1] PASCO Corporation

[2] National Institute for Environmental Studies

[3] Tokyo Institute of Technology

Abstract

Ice breakup date is one of the important indices showing climate changes, and we had developed the ice breakup date estimation method using satellite data to infer the ice breakup date of the lakes with no available in-situ data. In this study, ice breakup dates on 18 Eurasian lakes from 2001 to 2005 were estimated using water temperature trend derived from MODIS data. The annual changes of the ice breakup dates were different by the location, elevation, local climate, and so on. In the next stage, we evaluated the relationships between ice breakup dates and mean air temperature. The result showed that 1 day change of the ice breakup date represented the 0.2 ℃ changes of the mean air temperature.

1. Introduction

Snow and ice is widely taken up as one of the important indices showing climate change (IPCC 2001). It is reported that the ice breakup date of lake and river has become early about fewer weeks over the past century (Magnuson *et al*. 2000). Here, the ice breakup date means that a first day when a specific area of lake surface is completely free of ice. However, few ice breakup date data of the lakes on the central part of the Eurasian continent, for example Lake Baikal (Shimaraev *et al*. 1994), are recorded. We have developed ice breakup date estimation method using water temperature trend derived from satellite thermal infrared data to obtain the information for the lakes with no available records (Nonaka *et al*. accepted). In this study, we estimated the ice breakup date on 18 Eurasian lakes from 2001 to 2005 using Moderate Resolution Imaging Spectroradiometer (MODIS) data. From the time series analysis, the relationships between ice breakup dates and local climates were also discussed.

2. Ice Breakup Date Estimation Method

The ice breakup date estimation method we developed was based on Bussieres *et al*. (2002), and using the water temperature trend. The method uses the slow seasonal lake surface temperature variation, and ice breakup date is estimated by going back from a time series of the surface temperature data derived from satellite thermal infrared data (Fig. 1).

Fig. 2 shows the flowchart of the developed ice breakup date estimation method and used data when the ice breakup date is estimated by MODIS data. It consists of two parts, the threshold surface temperature estimation and water temperature trend analysis. First, the surface temperature when the lake surface is completely free of ice (threshold surface temperature, T_{TH}) is determined. The surface temperature data of the lake are derived from the Sea Surface Temperature (*SST*) products (Brown and Minnett 1999). In the process, we use the reflectance data of near infrared band as well as SST data. Secondly, lake surface temperature data on a clear day are derived using the cloud mask, and the surface temperature (*ST*) is plotted against date (*t*). In the next stage, *ST* data after snow and ice on the lake is completely melted and *ST* rises are selected, and expressed as a quadratic regression equation by *t*

$$ST = at^2 + bt + c \tag{1}$$

where *a*, *b*, and *c* are coefficients determined by least square fit. Finally, the intersection of the regression equation and T_{TH} is the ice breakup date.

The accurate T_{TH} estimation is important for the method because 1 ℃ change of the T_{TH} corresponds to more than 10 days change of the ice breakup date for some study lakes. The estimated T_{TH} for freshwater was 2 ℃, while that for seawater was 0.5 ℃ (Nonaka *et al.* accepted). When we evaluated the developed method using in-situ data of Saroma-ko Lagoon and Lake Baikal, the accuracy was better than 3 days.

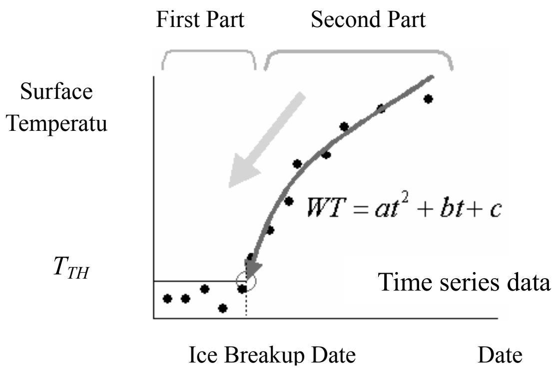

Fig. 1. Schematic of the ice breakup date estimation method using water temperature trend.

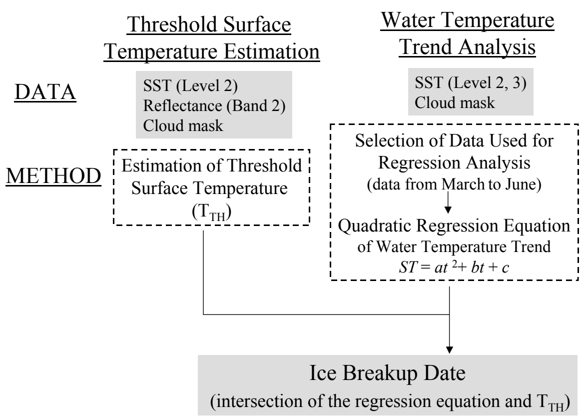

Fig. 2. The flowchart of the ice breakup date estimation method and used data when ice breakup date is estimated by MODIS data.

3. Ice Breakup Date on 18 Eurasian Lakes from 2001 to 2005

3.1 Used Data

Satellite sensor data are generally only useful for estimating ice breakup dates if the satellite has a short revisiting time. When using sensors with thermal infrared bands, such as the MODIS and the Advanced Very High Resolution Radiometer (AVHRR) satisfy this condition. In this study, we rely on MODIS data to estimate the ice breakup dates in order to take the advantages of thoroughly prepared information on products such as cloud mask, SST, and so on.

The sensor performs quite well estimating SST, with an estimation accuracy of 0.25 ˚C within the range of -2 ˚C to 32 ˚C (Evans 2002). Our estimation of the ice breakup dates on the 18 lakes investigated in this study were performed using MODIS Level 3 mapped SST data products with 4.89 km resolution collected during daytime from 2001 to 2005.

3.2 Study Lakes

Using ILEC (2001), we selected 18 freshwater lakes (Table 1, Fig. 3) in the central part of the Eurasian continent for investigation in this study. All of the lakes are larger than about 2000 km^2. Some are manmade reservoirs, and one is partially saltwater (the east part of Lake Balkhash).

Table 1. Features of the 18 Eurasian lakes investigated in this study.

No	Lake	Country	Latitude, Longitude	Elevation (m)	Volume (10^3 km^3)	Surface Area (km^2)
1	Peipsi	Russia/ Estonia	58.4 ^{o}N, 27.4 ^{o}E	30	25	3558
2	Ladoga	Russia	60.5 ^{o}N, 31.2 ^{o}E	5	908	18135
3	Onega	Russia	61.5 ^{o}N, 35.2 ^{o}E	35	280	9890
4	Rybinsk	Russia	58.0 ^{o}N, 38.5 ^{o}E	102	25	4550
5	Tsimlyansk	Russia	48.2 ^{o}N, 43.1 ^{o}E	36	24	2702
6	Volgograd	Russia	50.2 ^{o}N, 45.4 ^{o}E	15	31	3120
7	Kuibyshev	Russia	54.5 ^{o}N, 49.4 ^{o}E	53	57	5900
8	Kama	Russia	58.3 ^{o}N, 56.1 ^{o}E	109	12	1910
9	Balkhash	Kazakhstan	45.4 ^{o}N, 76.2 ^{o}E	341	106	18200
10	Chany	Russia	54.5 ^{o}N, 77.4 ^{o}E	106	4	2010
11	Zaisan	Kazakhstan	48.0 ^{o}N, 83.5 ^{o}E	341	53	5510
12	Krasnoyarsk	Russia	54.5 ^{o}N, 91.4 ^{o}E	243	73	2000
13	Khubsugul	Mongolia	51.0 ^{o}N, 100.2 ^{o}E	1645	Not obtained	2760
14	Bratsk	Russia	54.4 ^{o}N, 102.1 ^{o}E	402	169	5478
15	Baikal	Russia	53.4 ^{o}N, 106.4 ^{o}E	456	230000	31500
16	Vilyuisk	Russia	62.5 ^{o}N, 111.1 ^{o}E	244	36	2170
17	Zeya	Russia	54.2 ^{o}N, 128.1 ^{o}E	315	68	2119
18	Khanka	Russia	44.5 ^{o}N, 132.2 ^{o}E	69	18	4190

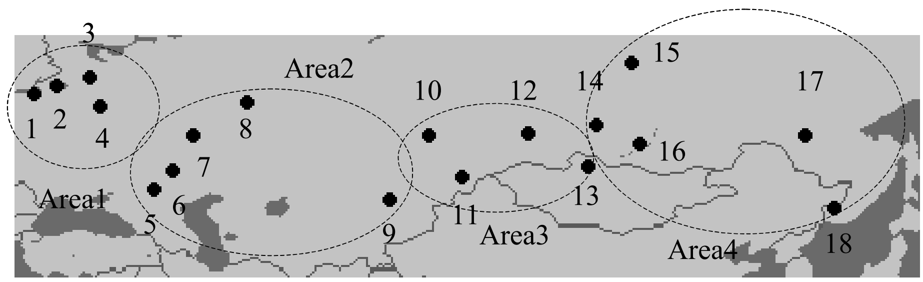

Fig. 3. The location of the study lakes. The each number correspond to the lake in table 1.

3.3 Results

The ice breakup dates on the 18 Eurasian lakes were estimated using the developed method (Fig. 2). The threshold of all of these lakes was assumed to be 2.0 ˚C, the estimated value for freshwater lakes (in the case of Lake Balkhash, only the western freshwater was selected), and the daily Level 3 mapped SST data from March to June were used for all estimation, and the water temperature trend was evaluated as a quadratic equation (1) for each lake (coefficients *a*, *b*, and *c* of each lake are not reported). Surface temperature was defined as the mean value of 3 × 3 pixels at the center of each lake.

Fig. 4 shows the ice breakup dates (Julian day) of these lakes for 5 years. The ice breakup dates in 2002 and 2004 are relatively earlier for some of the study lakes, especially lakes in area 1 and area 2). In contrast, the ice breakup date in 2005 is earlier than in 2004 for Lake Chany, Zaisan, Vilyuisk and Zeya in area 3 and 4. Moreover, clear trend of the time series is not observed for lakes at high elevation of area 3, except Lake Khubusgol. We postulate these features are mostly related with the air temperature trend in spring, so the relationships between ice breakup dates and mean air temperature is dealt in the next section.

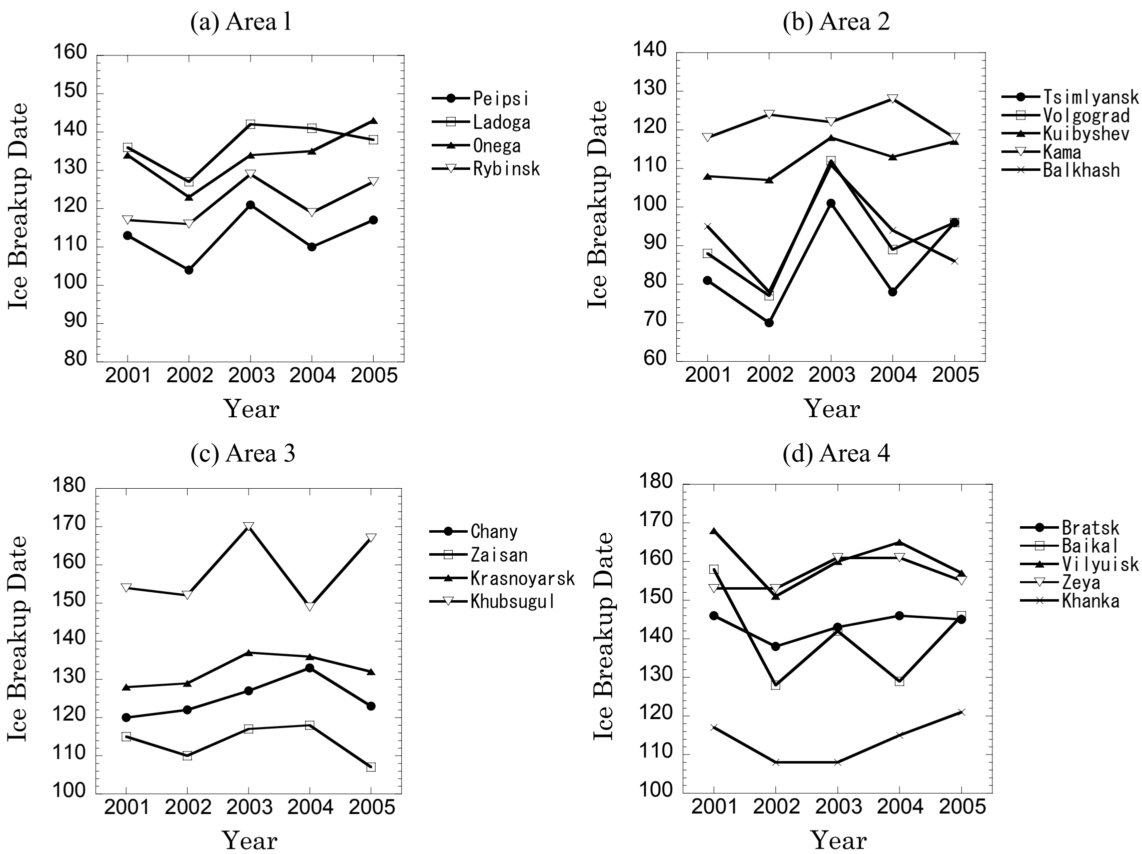

Fig. 4. Ice breakup dates of 18 study lakes on the Eurasian continent from 2001 to 2005.

3.4 Relationships between ice breakup dates and air temperature

The relationships between ice breakup dates and local air temperature are discussed in this section. Air temperature data were derived from National Center for Environmental Prediction/ National Center for Atmospheric Research (NCEP/NCAR) data set (Kistler *et al.* 2001). It is noted that the effects of air temperature is different by the time of the ice breakup dates. Palecki and Barry (1986) showed that the ice breakup date is correlated most with air temperature in previous month. Accordingly, we used the mean values from March to May in this study taking into consideration of the ice breakup date of study lakes.

Fig. 5 shows the time series of the mean air temperature for each area from 2001 to 2005. The air temperature was averaged for the all lakes of each area. We can see that the air temperature in 2002 and 2004 are relatively higher than other years in area 1, corresponding to the ice breakup dates. Further, the fact that the ice breakup dates in 2005 is earlier than in 2004 for some of the lakes in area 3 and 4 can be explained from the increase the air temperature from 2004 to 2005.

Fig. 6 shows the relationships between ice breakup dates (*IB*) and mean air temperature (*T*). The linear regression equation was expressed as:

$$T = 27.05 - 0.20\,IB \tag{2}$$

The correlation coefficients of the equation (2) were –0.93, and the rms error was about 1.8 ˚C. This equation means that a day change of the ice breakup date corresponded the 0.2 ℃ changes of the mean air temperature from March to May. These results suggest that annual changes of the ice breakup date mostly can be explained from the mean air temperature.

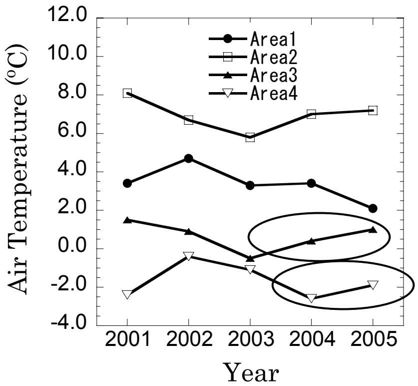

Fig. 5. Time series of the mean air temperature for each area from 2001 to 2005.

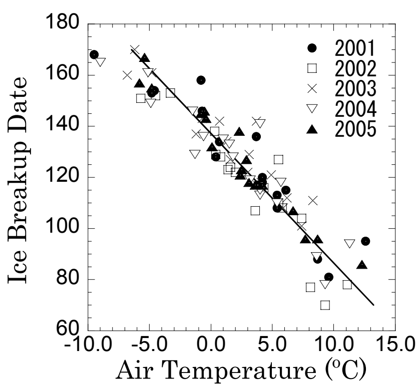

Fig. 6. The relationships between ice breakup date on 18 Eurasian lakes and mean air temperature for each year.

4. Summary

Ice breakup dates on 18 Eurasian lakes from 2001 to 2005 were estimated using water temperature trend derived from MODIS data. The annual changes of the ice breakup dates were different by the location, elevation, local climate, and so on. In the next stage, we evaluated the relationships between ice breakup dates and mean air temperature. The result showed that 1 day change of the ice breakup date represented 0.2 ℃ changes of the mean air temperature from March to May. We need long term of the ice breakup dates to grasp the relationships between ice breakup dates and local climate more detail, and it is left for future studies.

Acknowledgements

The authors are grateful to GES DAAC for providing MODIS SSC data, cloud mask data, and reflectance data.

References

Brown, O., and Minnett, P., 1999. MODIS infrared sea surface temperature algorithm theoretical basis document version 2.0, April 30, 1999, pp. 91. Available online at: http://modis.gsfc.nasa.gov/data/atbd/atbd_mod25.pdf.

Bussieres, N., Verseghy, D., and MacPherson, J., 2002. The evolution of AVHRR-derived water temperatures over boreal lakes. Remote Sens. Environ., 80, 373-384.

Evans, R., 2002. MODIS sea surface temperature (SST) products. http://podaac.jpl.nasa.gov:2031/DATASET_DOCS/modis_sst.html ".

ILEC, 2001. World lakes database. http://www.ilec.or.jp/database/database.html.

IPCC, 2001. Climate Change 2001: The Scientific Basis. Cambridge University Press, Cambridge UK, pp.

Kistler, R., Collins, W., Saha, S., White, G., Woollen, J., Kalnay, E., Jenne, R., and Fiorino, M., 2001. The NCEP–NCAR 50–Year Reanalysis: Monthly Means CD–ROM and Documentation, Bulletin of the American Meteorological Society: Vol. 82, No. 2, 247–267.

Magnuson, J., Robertson, D., Benson, B., Wynne, R., Livingstone, D., Arai, T., Assel, R., Barry, R., Card, V., Kuusisto, E., Granin, N., Prowse, T., Stewart, K., and Vuglinski, V., 2000. Historical trends in lake and river ice cover in the northern hemisphere. Science, 289, 1743-1746.

Nonaka, T., Matsunaga, T., and Hoyano, A., Estimating ice breakup dates on Eurasian lakes using water temperature trend and threshold surface temperature derived from MODIS data. Int. J. Remote Sens. accepted.

Palecki, M., and Barry, R., 1986. Freeze-up and break-up of lakes as an index of temperature changes during the transition seasons: A case study for Finland. *Journal of Climate and Applied Meteorology, 25,* 893-902.

Schimaraev, M., Verbolov, V., Granin, N., and Sherstyankin, P., 1994. Physical limnology of Lake Baikal: A review. Baikal International Center for Ecological Research, Irkutsk.

Estimation of Miyakejima volcanic gas hazards using vegetation index images

Naoko Iino[1], Kisei Kinoshita[2], Toshiaki Yano[3] and Shuichi Torii[4]
[1] Faculty of Engineering, Kagoshima University, Japan
E-mail: iino@mech.kagoshima-u.ac.jp
[2] Research and Development Center, Kagoshima University, Japan
[3] Kagoshima University, Japan
[4] Faculty of Engineering, Kumamoto University, Japan

Abstract

The eruptive activity of Miyakejima volcano started on 8 July 2000, and the ejection of enormous amounts of sulphur dioxide (SO_2) has been continued since August 2000. The Tokyo Metropolitan Government started monitoring volcanic gas concentrations at the foot of the volcano from the end of 2000. We studied the seasonal and regional characteristics of high concentrations of SO_2 using the data. In order to estimate the volcanic gas hazards for the whole Miyakejima, a hazard mapping method using the Normalized Difference Vegetation Index (NDVI) images is proposed.

1. Introduction

Volcanic gases and aerosols released into the atmosphere have adverse impact on air quality, vegetation, animals, and human health. Miyakejima volcano, about 170 km south of Tokyo (Fig. 1), has been ejecting enormous amounts of sulphur dioxide (SO_2) from the summit (775 m a.s.l.) since mid-August 2000.

The Tokyo Metropolitan Government stated the monitoring of volcanic gas concentrations from the end of 2000 at three gas-monitoring stations at the foot of the volcano, and expanded into fourteen stations as of April 2004 (Fig. 2 and Table 1). We have been analyzing the SO_2 concentrations to investigate the mechanism of high concentration occurring at the volcano. The following results were obtained from our previous studies (Iino et al., 2003, 2004a, b). (i) High SO_2 concentrations at the ground surface on Miyakejima are mainly caused by downdraft owing to strong wind. (ii) The seasonal and regional characteristics of high SO_2 concentrations correspond well to the 925 hPa wind observed at Hachijyojima, the nearest upper air observatory from Miyakejima (Fig. 1). (iii) There is notable difference of environment of SO_2 concentrations owing to a slight directional difference from the crater. This should be considered in making a volcanic gas hazard map at the volcano. (iv) The frequency distribution of high SO_2 concentration events corresponds well to the distribution of vegetation shown in an image of Terra/ASTER.

In this study, we propose a method to estimate the volcanic gas hazards for the whole Miyakejima using satellite imagery which shows the distribution of vegetation before and after the 2000 Miyakejima eruption. The resultant hazard map is examined by comparing with the occurrence frequency of high SO_2 concentrations at each gas-monitoring station and with the ground observations by visible (VIS) or near-infrared (NIR) cameras. Here, the NIR photographs are obtained based on our previous studies (e. g., Kinoshita et al, 2003).

In addition, we briefly discuss the long-term trend and the seasonal and regional characteristics of the occurrence frequency of high SO_2 concentrations, defined above 0.1 ppm and 10 ppm, using SO_2 concentration data during January 2001 - September 2005

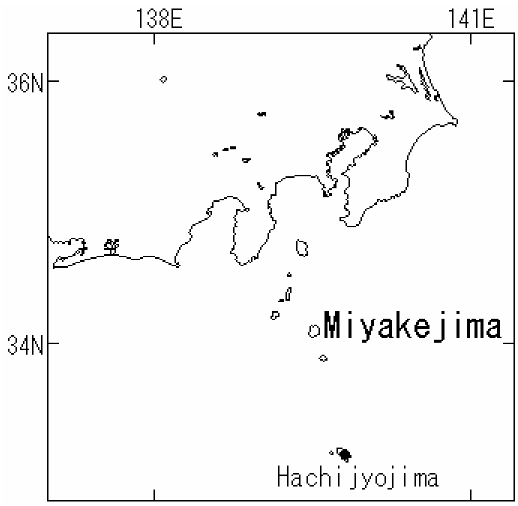

Fig. 1 Location of Miyakejima volcano.

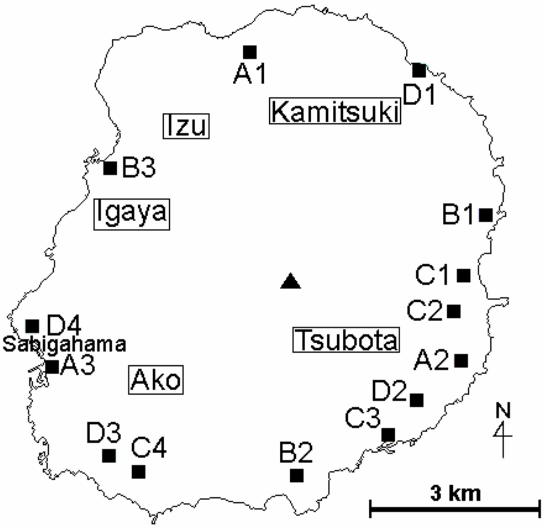

Fig. 2 Locations of volcanic gas-monitoring stations on Miyakejima as of April 2004 (■), the summit vent (▲), and the district names.

Table 1 Gas-monitoring stations

Symbol	Station name	Abbreviation	Observation start (month/year)
A1	Branch Office	BO	12/2000
D1	Mimoi	MM	04/2004
B1	Ainohama	AH	09/2001
C1	Miike	MI	03/2002
C2	Yakuba	YK	05/2002
A2	Airport	AP	12/2000
D2	Mitake-Jinjya	MJ	04/2004
C3	Tsubota	TS	03/2002
B2	Akacocco	AC	09/2001
C4	Usugi-Namakon	UN	03/2002
D3	Usugi-Bus Stop	UB	04/2004
A3	Ako	AK	12/2000
D4	Furusato	FU	04/2004
B3	Igaya	IG	09/2001

2. Sulphur dioxide concentrations at Miyakejima

Figure 3 shows occurrence frequency of high SO_2 concentrations of all gas-monitoring stations since January 2001. The environmental standard of SO_2 concentration, which was prescribed by the Ministry of Environment in Japan, is less than 0.1 ppm for one-hour averaged value. However, much higher concentrations, several ppm, were often recorded at Miyakejima. Thus, we defined here the two standards of high concentration levels of SO_2 as 0.1 and 1 ppm. In each figure, solid and dotted lines indicate the high concentrations frequencies of 0.1 and 1 ppm, respectively.

The occurrence frequency of high SO_2 concentrations is not in the obvious decreasing trend though five years have passed since the Miyakejima 2000 eruption. The seasonal and regional characteristics of high concentrations derived from a ten stations analysis (Iino et al., 2004b) are essentially the same as the results including four stations, which were added from April 2004. These are summarized as follows. (i) The stations located between east and east-southeast directions from the vent, C1, C2 and A2, observe very high rate in winter. (ii) At east-northeast station, B1, the rate of high concentrations is high not only in winter but also in summer. (iii) At southwest stations, C4 and D3, the rates of high concentrations are relatively high throughout a year. (iv) At north and southeast stations, A1 and C3, respectively, the high concentrations rates are not high.

Here, we focus on the four stations added in April 2004, D1-D4. The Mimoi station, D1, located at northeast is interesting, because there had been no continual gas-monitoring station though southwesterly wind is dominant in spring and summer. As expected from the wind, the rate of high concentrations defined as 0.1 ppm at the station is high in spring and summer, while low in autumn and winter (Fig. 3b). Whereas the rate of high concentrations defined as 1 ppm, the rate of high concentrations is low though in spring and summer. It may depend on the characteristics of wind of which the rate of strong wind in summer is lower than that in winter. For the Mitake-Jinjya station, D2 (Fig.3g), located at southeast, the characteristics of high concentrations is similar to the Airport station, A2 (Fig. 3f), but the rate is obviously lower, about one third. The characteristics of the Usugi-Bus Stop station, D3 (Fig.3k), located at southwest and near the Usugi-Namakon station, C4 (Fig. 3j) is similar to the tendency and frequency levels of the C4 station. For the Furusato station, D4 (Fig. 3m), located at west-southwest near the Ako station, A3 (Fig. 3l), the tendency of high concentrations is similar to the A3 station but the levels are about one half.

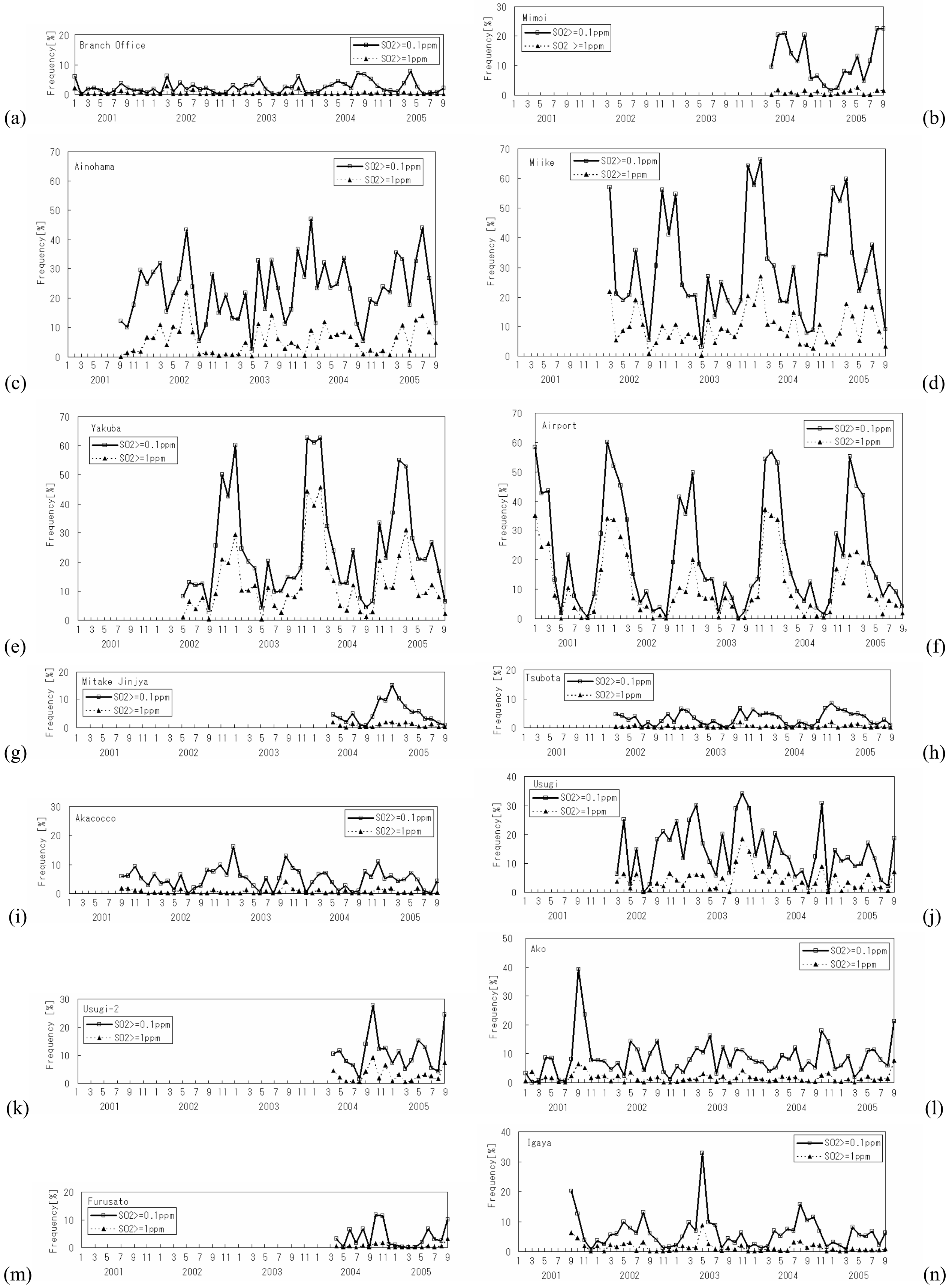

Fig. 3 The occurrence frequency of high SO_2 concentrations during January 2001 - September 2005.

3. Hazard mapping for high sulphur dioxide concentrations

In order to estimate the volcanic gas hazards for the whole Miyakejima, we propose a new hazard mapping method using the Normalized Difference Vegetation Index (NDVI) images. This method is based on a hypothesis that the distribution of vegetation at Miyakejima volcano well reflects the influence of volcanic gases. The satellite data used are as follows. Before the 2000 Miyakejima eruption is JERS-1/OPS on 3 April 1994, while after the eruption is Terra/ASTER on 7 April 2003. We selected the same season data to eliminate the effect of seasonal change in vegetation.

First, the JERS-1/OPS was corrected geometrically to fit to Terra/ASTER data, by taking eight GCP-points. Second, the NDVI is calculated as the difference between the near-infrared and visible reflectances divided by the sum of the two. The NDVI images of JERS-1/OPS (OPS-NDVI) and Terra/ASTER (ASTER-NDVI) are shown in Figs. 4a and b, respectively. As shown in Fig. 4a, Miyakejima had been covered with vegetation except for the lava or artificial areas. After the 2000 Miyakejima eruption shown in Fig. 4b, the east and southwest regions are shown as dark-colour areas, that is the area with low NDVI values. Therefore, it can be considered that vegetation there was damaged by volcanic gases. The difference between OPS-NDVI and ASTER-NDVI was calculated to visualize the relative change in vegetation, and classified into four steps of hazards by referring with one-year averaged value of SO_2 concentrations at each station (Table 2), during May 2002 - April 2003. Finally, originally less vegetation areas, such as open water, the lava, artificial areas, were masked by using near-infrared image of JERS-1/OPS though the mask is not enough, e.g., for the areas of airport or crater. The resultant volcanic gas hazard map is shown in Fig. 4c. The color image of Fig. 4c is shown at our web site (in Japanese). http://ese.mech.kagoshima-u.ac.jp/miyake/.

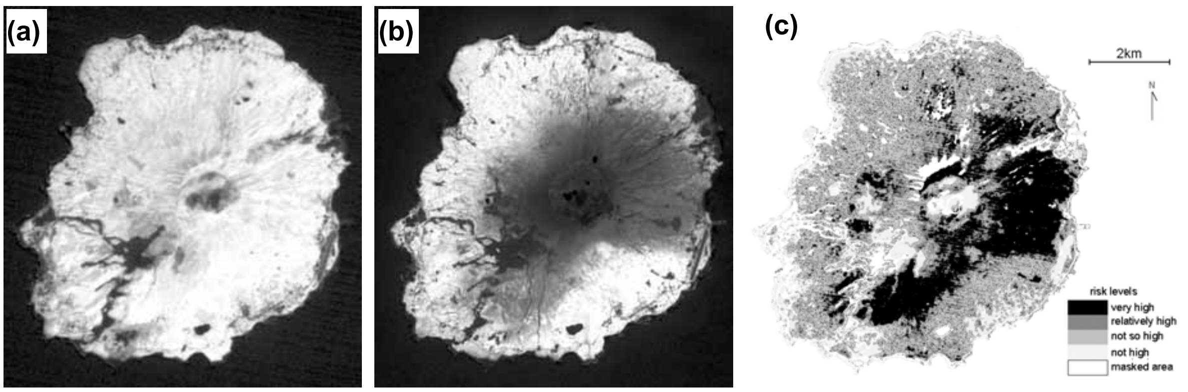

Fig. 4 NDVI images. (a) JERS-1/OPS on 3 Apr. 1994, (b) Terra/ASTER on 7 Apr. 2003. (c) Volcanic gas hazard map.

Table 2 The one-year averaged SO_2 concentrations during May 2002- April 2003.

Gas-monitoring station	SO_2 concentrations [ppb/year]
Branch Office	11
Ainohama	143
Miike	279
Yakuba	280
Airport	166
Tsubota	17
Akacocco	29
Usugi-Namakon	120
Ako	46
Igaya	40

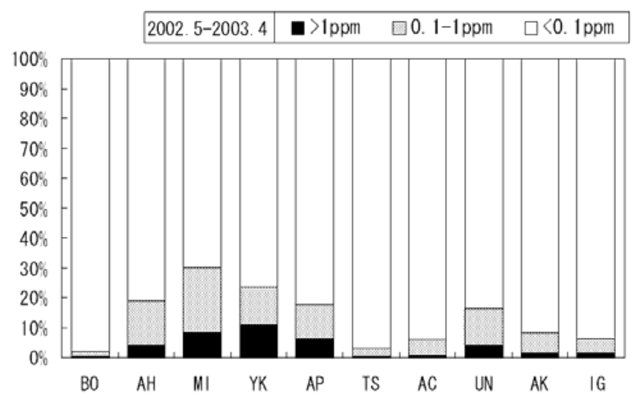

Fig.5 The rate of SO_2 concentration levels during May 2002 - April 2003.

In Fig. 4c, the difference of NDVI values becomes large with the decrease of the vegetation, that is, the gas hazard level is evaluated to be high. Figure 5 shows the rate of SO_2 concentration levels at each station during May 2002 - April 2003. At the foot of the volcano, the gas hazard levels, e.g., the highest level is seen in east and followings is in southwest, correspond well to the environment of SO_2 concentrations shown in Fig. 5. It is also found that the hazard level becomes higher at the mountainside near the crater.

4. Ground observations

Figure 6 shows ground observations in May 2005 from the coastal loop-line road around Miyakejima and from a ship with visible (VIS) and near-infrared (NIR) cameras. Vegetation is shown as dark in VIS images (Figs. 6a-c), and as white in NIR images (Figs. 6d-f). In the high volcanic gas concentration districts, Tsubota in the east (Fig. 6a) and Ako in the southwest (Fig. 6b), many wilted trees were observed at the foot of the volcano. In contrast, vegetation in other districts (e.g., Figs. 6d-f) was almost normal at the foot of the volcano, except for some wilted Japanese cedar. We confirmed that the volcanic gas hazard map (Fig. 4c) is consistent with ground observations of Miyakejima island. The observation results containing animation files are displayed at our web site mentioned above.

(a) Tsubota high concentration district (VIS)

(b) Ako high concentration district (VIS)

(c) Izu-Kamitsuki (VIS)

(d) The Tsubota station, C3 (NIR)

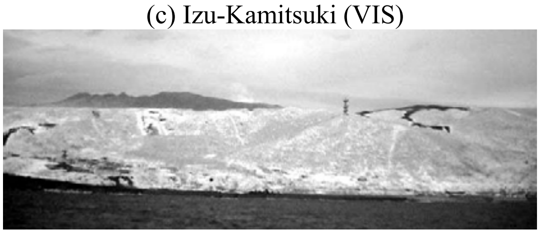

(e) Ako-Sabigahama (NIR)

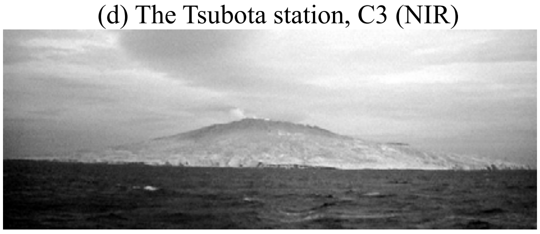

(f) Igaya-Izu (NIR)

Fig.6 Ground observations from the coastal loop-line road around Miyakejima, (a)-(d) and from a ship, (e)-(f). Figs 6(a)-(c) are visible photographs. Figs. 6(d)-(f) are near-infrared photographs by SONY DCR-TRV30 with night-shot mode and Fujifilm IR84 and Kenko ND400. The district names are shown in Fig.2.

5. Concluding remarks

In order to estimate the volcanic gas hazards for the Miyakejima island as a whole, a hazard mapping method using the Normalized Difference Vegetation Index (NDVI) images was proposed. The resultant hazard map was consistent with the occurrence frequency of high SO_2 concentrations at ten gas-monitoring stations as of 2003, and with the ground observations by visible or near-infrared cameras.

However, it should be noted that volcanic gas behaviour depends on the wind around the crater and that the high concentrations have the seasonal characteristics as shown in Fig. 3. Therefore, the volcanic gas hazard map should be used together with the meteorological information. In order to improve and complete the Miyakejima volcanic gas hazard map, further studies will be done in near future.

Acknowledgements

We thank very much to the Tokyo Metropolitan Government for providing the SO_2 measurement data in Miyakejima. Terra/ASTER data by ERSDAC, Japan, was provided as a part of ASTER-AO activity. N. Iino is grateful to Mr. C. Kanagaki for technical supports of the NIR-camera observation, and to Mr. T. Shiba for collaborative works on hazard mapping.

References

Iino, N., K. Kinoshita, M. Koyamada, C. Kanagaki and A. Terada, 2003. Analysis of high volcanic gas concentrations at the foot of Miyakejima volcano, Japan, J. Natural Disaster Science **25** (2), 85-91.

Iino, N., K. Kinoshita, T. Yano and S. Torii, 2004a. Dispersion of volcanic clouds at Miyakejima and gas concentrations at surface stations, CD-ROM Proc. 1st Int. Symp. Micro&Nano Tech., Honolulu, USA, Mar. 2004, XXIII-C-01, pp.1-6.

Iino, N., K. Kinoshita and T. Yano, 2004b. Regional characteristics of high concentration events of volcanic gas at Miyakejima, J. JSNDS **23** (4), 505-520 (in Japanese with English Abstract).

Kinoshita, K., C. Kanagaki, A. Minaka, S. Tsuchida, T. Matsui, A. Tupper, H. Yakiwara and N. Iino, 2003. Ground and Satellite Monitoring of Volcanic Aerosols in Visible and Infrared Bands, Proc. CEReS Int. Symp. Remote Sensing, Chiba, Japan, Dec. 2003, pp.187-196.

Vegetation and Water Quality Analyses of Industrial Waste Using Remote Sensing

Wenhui ZHAO [1], Takanori SASAKI [2] and Shigetaka FUJITA [3]
[1, 2, 3] Division of Electrical and Electronic Engineering, Graduate School of Engineering,
Hachinohe Institute of Technology
E-mail: d05202@hi-tech.ac.jp

Abstract

After an illegal dumping site was found on the border between Iwate and Aomori Prefectures, an environmental monitoring system using artificial satellites and ground observation apparatus was established to constantly monitor and analyze environmental changes. In this study, the data collected using this system, including satellite data, on-site, infrared camera images, and water quality data, was analyzed to establish the level of on-site contamination and state of recovery. Some SPOT images were compared to establish the on-site vegetation changes using the NDVI (Normalized Difference Vegetation Index). The relationship between changes in water quality and rainfall was established. It was confirmed that the removal of fluid waste and extensive work carried out on the site reduced the alkalinity of the water.

Key Words: industrial waste, remote sensing, vegetation analysis, water quality

1. Introduction

One of the biggest illegal dumping sites in Japan was found on the border between Iwate and Aomori Prefectures. Its area is 27 hectares, and the total amount of waste is about 820,000 m^3. It caused major social problems such as environmental contamination [1)]. Fig. 1 is an aerial photograph taken on April 25, 2005 showing the state of the illegal site and the various methods used to treat the waste. The waste is taken away in trucks, but this will take several years to complete. In the meantime, the waste has been covered with tarpaulins to avoid pollution spreading before disposal. Waterproof walls will be set up around the site. An environmental monitoring system was established to collect and analyze the environmental data on-site. The satellite data such as multispectral SPOT image was analyzed for environmental analyses in the wide area, and the data from on-site sensors was analyzed in detail. This system is very useful for establishing the level of contamination and state of recovery on and around the site.

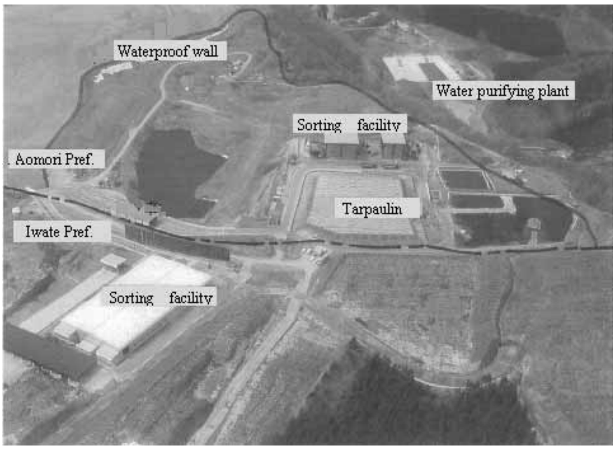

Fig. 1 Aerial photograph of illegal dumping site (April 25, 2005)

2. Remote sensing systems and analysis methods

Artificial satellites and ground observation apparatus were used in this environmental monitoring system. Data from NASA's Terra-1 and Aqua EOS satellites was received directly by an antenna installed on the roof of a building on our campus. SPOT images, DEM (Digital Elevation Model) data, and Quickbird images were analyzed by ENVI software. Two high spatial resolution SPOT images were compared to establish the changes in on-site vegetation using the NDVI (Normalized Difference Vegetation Index).

Five water quality analyzers, weather measuring equipment, and two infrared cameras were set up at the dumping site. Data was then transmitted to the monitoring PC in the university every three minutes. The items measured were pH, electric conductivity, temperature, flow rate, wind direction, wind velocity, air temperature, and rainfall. Fig. 2 shows an example of an on-site image taken by infrared cameras that can be operated remotely. Environmental changes and on-site work progress can be checked using this data. This ground observation system and field work back up the satellite images for better accuracy.

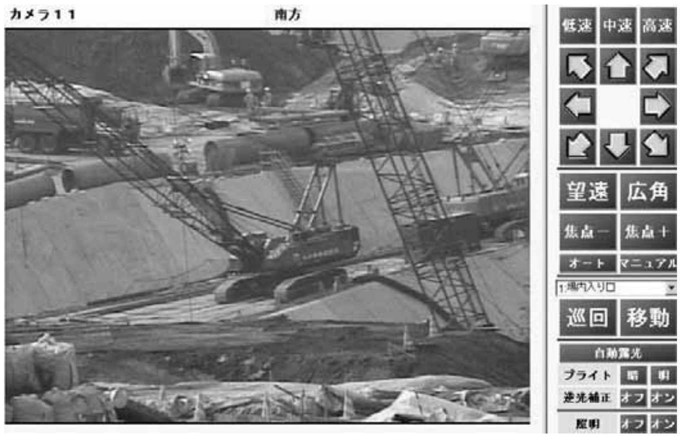

Fig. 2 Image from infrared camera (November 4, 2005)

3. Result and discussion

3.1 Vegetation analysis using SPOT images

Two high spatial resolution SPOT images were analyzed in this study. One is a SPOT 2 image of 20 m spatial resolution taken on July 20, 1992, and the other is a SPOT 5 image of 10 m spatial resolution taken on June 17, 2004. The NDVI was used to transform multispectral data into a single image band representing vegetation distribution [2]. The NDVI values indicate the amount of green vegetation present in the pixel — near-infrared radiation minus visible red radiation divided by near-infrared radiation plus visible red radiation [3]. This formula is called the Normalized Difference Vegetation Index. Written mathematically, the formula is: NDVI = (NIR - RED)/ (NIR + RED). For SPOT data, NIR represents Band 3 (0.78-0.89 μm) and RED represents Band 2 (0.61-0.68 μm).

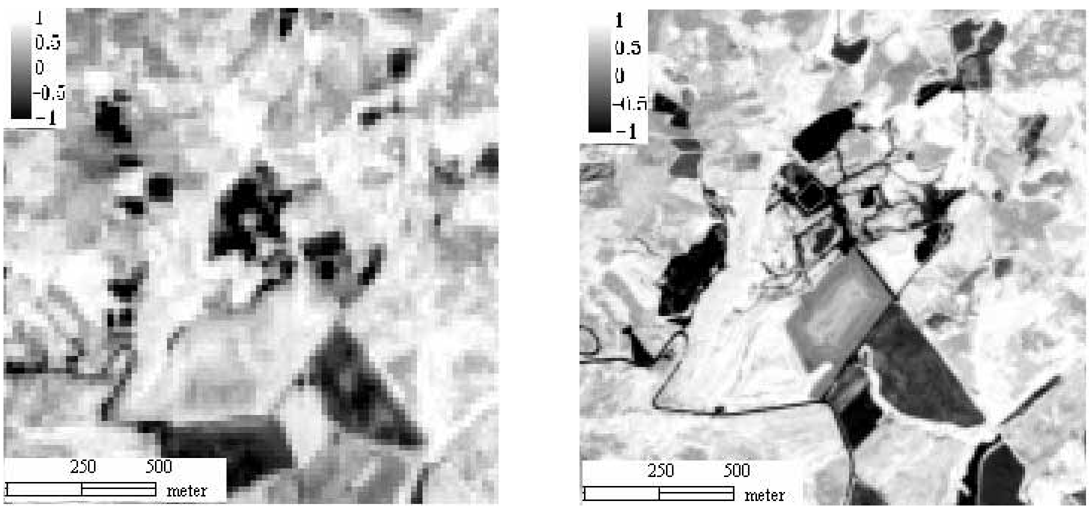

(a) July 20, 1992 (b) June 17, 2004

Fig. 3 Changes in NDVI data on dumping site

Fig. 3 (a) shows the on-site vegetation on the site before the waste was dumped and Fig. 3 (b) shows the on-site vegetation after the waste was dumped. Very low NDVI values (0.1 and below) correspond to barren areas of rock, sand, or water. Moderate values (0.2 to 0.4) represent shrub and grassland, while high values (0.6 to 0.8) indicate forest. The on-site NDVI value was lower, meaning that there was less on-site vegetation than in the surrounding area. There are signs of human activity such as narrow paths in Fig. 3 (b), in contrast to the natural montane vegetation shown in Fig. 3 (a). Furthermore, these figures show a reduction in vegetation, and we can determine those areas that had changed in that period. This vegetation analysis will be a useful tool for identifying and confirming illegal dumping sites.

3.2 Analysis of water quality using ground observation apparatus

Water quality data plays an important role in observation and analysis of the level of on-site contamination. Five water quality analyzers were installed at the former water supply source (Point 1), the new water supply source (Point 2), in the vicinity of the Kumahara River (Point 3), at the intake (Point 4) and the outlet (Point 5) of the water purifying plant as shown in Fig. 4 [4]. Fig. 5 shows the changes in water quality in September 2005. In this figure, the pH and electric conductivity of on-site water (Point 4 and 5) were higher than normal water (Point 1, 2, and 3), and the pH at Point 4 reduced on rainy days (September 2, 7, 14, and 22).

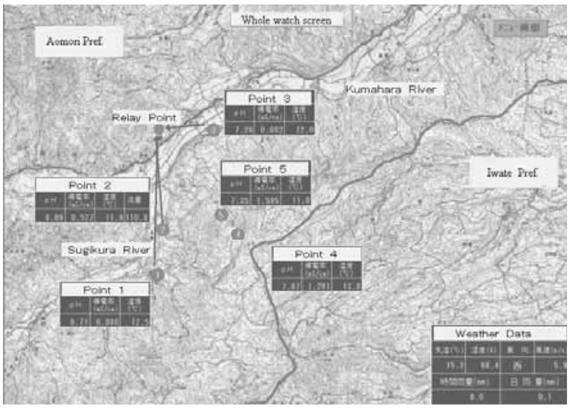

Fig. 4 Distribution of water quality analyzers

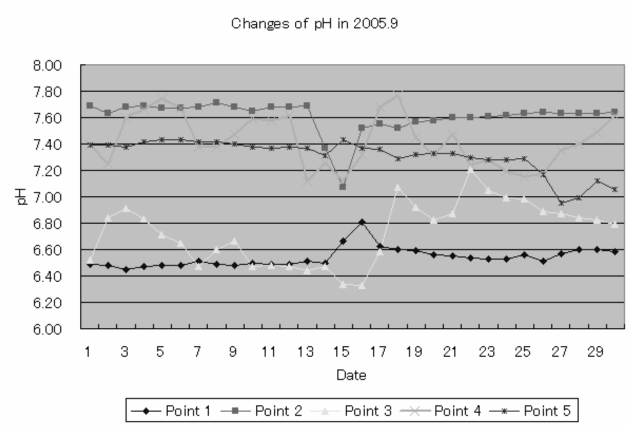

Fig. 5 Changes of pH in September 2005

The removal of waste began in September 2004, and 34,428 tons of waste (26,668 tons of solid waste and 7,760 tons of fluid waste) was removed by November 2005. Although only 4% of the total waste in Aomori Prefecture has been removed, almost all the fluid waste has been removed. Furthermore, the extensive work carried out as mentioned above has improved the water quality. The changes in pH at Points 4 and 5 are shown in Table 1. We found that the alkalinity of the water was reduced by the water purifying plant — the mean pH in September 2004 fell from 7.92 (Point 4) to 7.41 (Point 5), and in September 2005 fell from 7.34 to 7.18. The mean pH at Point 4 also fell from 7.945 (September and October 2004) to 7.46 (September and October 2005).

Table 1 Changes in water quality (pH)

	September 2004	October 2004	September 2005	October 2005
Point 3 (Kumahara River)	7.34	7.15	6.93	6.48
Point 4 (entrance of the water purifying plant)	7.92	7.97	7.34	7.58
Point 5 (exit of the water purifying plant)	7.41	7.27	7.18	6.85

In addition, it is thought that the water quality will improve further after waterproof walls are built around the dumping site as shown in Fig. 1.

4. Conclusions

A remote sensing system was established to monitor and analyze the environmental data at the illegal dumping site on the border between Iwate and Aomori Prefectures. In this paper, the data collected using this system, including satellite data, images from on-site infrared cameras, and water quality data, was analyzed to establish the level of on-site contamination and state of recovery.

Multispectral SPOT images of high spatial resolution were analyzed using the NDVI to establish changes in vegetation at the dumping site. We found signs of human activity such as narrow paths and a substantial reduction in on-site vegetation when the waste was dumped. This system will help identify and confirm other illegal dumping sites. Changes in water quality are important in assessing contamination and were analyzed, along with rainfall, as the waste was removed. The removal of waste and other on-site work reduced the alkalinity of the water. In the future, new satellite data and ground data will be sequentially collected by this system. This will be compared with current data to understand and forecast environmental changes.

References

1) S. Fujita et al.: Environmental monitoring using remote sensing technology, Abstracts of International Symposium on APGC, p. 308, (2004).

2) Research Systems Inc: ENVI Tutorials, Research Systems Inc. pp. 668-670, (2004).

3) Garguet-Duport, B., et al.: The Use of Multiresolution Analysis and Wavelets Transform for Merging SPOT Panchromatic and Multispectral Image Data, Photogrammetric Engineering and Remote Sensing, Vol. 62, no. 9, (1996).

4) Wenhui Zhao, Takanori Sasaki and Shigetaka Fujita: Environmental Monitoring of Industrial Waste using Satellite and Ground Observation Apparatus, Proceedings of International Conference on Materials Engineering for Resources, pp. 332-335, (2005).

Satellite image presentation system for education SiPSE based on DEM data

Kisei KINOSHITA[1], Nobuya TOMIOKA[2] and Hirotsugu TOGOSHI[3]

[1] Research and Development Center, Kagoshima University, Kagoshima 890-0065, Japan

[2] Learning Information Center, Kagoshima City Board of Education, Kagoshima 890-0816, Japan

[3] Oumaru Junior School, Kawanabe-cho, Kagoshima 897-0131, Japan

E-mail: *sipse-adm1@edu.kagoshima-u.ac.jp*

Abstract

A data set for 3D presentation of the LANDSAT image for any part of Japan and its viewer are provided by the SiPSE homepage via the Internet. The digital elevation model data covering Japan with 50 m resolution are embedded in the data set. In addition to the on-line system described in Japanese for the domestic use, off-line systems are developed with larger file size and other functions for research and international uses. The 3D images are compared with aerial and ground photographs especially with near-infrared mode.

1. Introduction

In order to drive a satellite 3D image in real time movement as a flight simulator in a personal computer, the SiPSE system has been developed [1-3], where SiPSE is an abbreviation of the Satellite image Presentation System for Education. The SiPSE homepage in Japanese started in September 2000 covering Kyushu, Okinawa and Izu Islands, and extended to cover Japan in 2001, with the address *http://sipse.edu.kagoshima-u.ac.jp/sipse/* .

SiPSE off-line systems have been also developed for research purposes so as to include new functions: Some of them are covering submarine topography, embedding the volcanic eruption cloud, simulation of the sea level rise and so on [2]. For the international use, the CD packages of the viewer in English and some data have been tested in China, The Philippines, Australia, U.S.A., and Italy.

The satellite image for 3D presentation may be selected from true or natural color, and single band modes. Especially, monochromatic view of TM band-4 is very useful to recognize water and land areas, to see the vegetation coverage and mountainous topography, and to compare with aerial and ground photographs with near-infrared (NIR) mode.

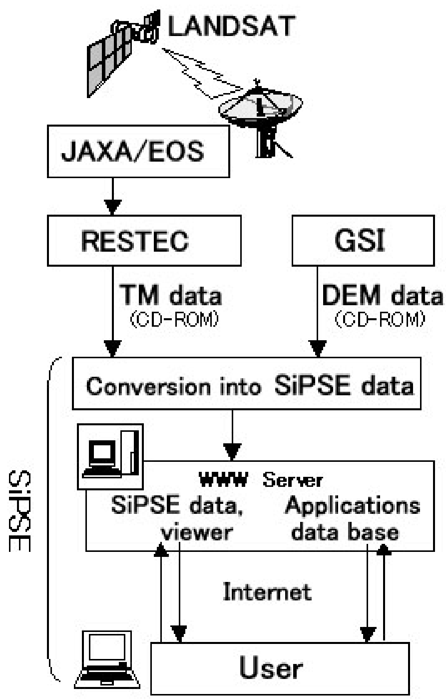

Fig. 1.

The construction of the SiPSE system.

2. The SiPSE system

The data set, called **the SiPSE data**, is composed of digital elevation model (DEM) data and the satellite data of the land coverage, as shown in Fig. 1. The land coverage data is obtained from the LANDSAT TM 1-4 data with the pixel size 28.5 m by reducing the brightness from 8 bits into 4 bits. The reduction of the TM data and the discard of the bands 5-7 are done so as to reduce the file size for the Internet use. The land coverage is expressed by the true-color mode with TM 1, 2 and 3, or by the natural-color mode with TM 1, 2+4 and 3 corresponding to B, G and R, respectively. TM 4 is also utilized for the gray scale presentation of the NIR image. This form of the land-cover data in pre-processed form for the web use started in 1996 as the SiNG data covering Kagoshima area in southern Japan [4], where TM 6 was maintained converting into the temperature scale.

Geographical Survey Institute (GSI) provides the DEM data with the spatial resolution 50 m covering Japan in CD-ROMs. In the SiPSE data, the DEM information is converted to fit with the land-cover data with higher spatial resolution by linear interpolation.

The SiPSE data can be handled by means of **the SiPSE viewer**, which is also provided via the Internet. The 3D presentation in a Windows computer with a selected land-cover image of a scene can be done in still or motion modes, specifying ways and the speed of the motion. The vertical/horizontal ratio of scales in a 3D image can be adjusted, as well as the overall scale. The standard size of a scene is 512 pixels with 512 lines corresponding to 15 km squared, while it is 1024 * 1024 corresponding to 30 km squared for specially registered users. Wider areas up to six times in length can be obtained by lowering the spatial resolution. The viewer has other functions such as free drawing on the land-cover image, measuring a distance between specified points and the size of a specified area.

3. Volcanic topography and land coverage

There are a lot of beautiful volcanic sceneries in Japan, which are nice subjects of the SiPSE imagery [2, 3]. Let us visit Unzen volcano located in the center of Shimabara peninsula in western Kyushu, Japan, as shown in Fig. 2. The volcano started eruption in November 1990, and a lava dome developed at the Fugen-dake summit accompanied with pyroclastic flows endangering lives of the inhabitants during 1991-1995. We see the lack of vegetation on the dome and the passages of the flows very clearly both in the true color and NIR images. We may see the topographic structure of the volcanic complex, including old volcano Mayu-yama on the east side of the main peak, by changing the viewing direction. Thus, the SiPSE system may be utilized for the prevention of the volcanic disasters with respect to the improvement of the understanding of the topographic situation.

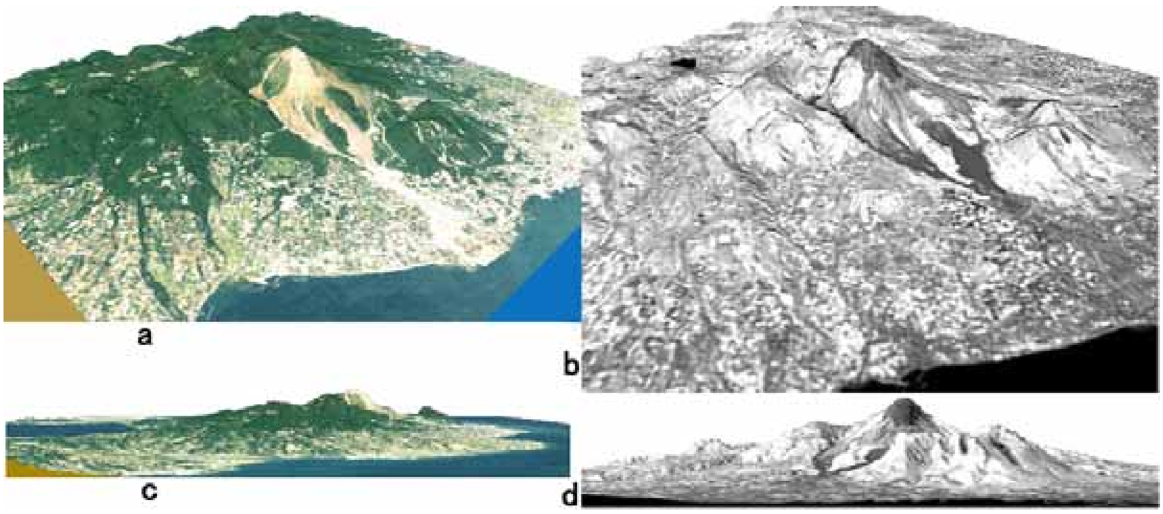

Fig. 2. Unzen volcano observed from south-eastern sky in true-color and NIR images (a and b), from the south in true-color image (c), and from the east near the horizon in NIR image (d), respectively. LANDSAT: 1998.10.4.

4. NIR images of SiPSE-3D and aerial photographs

In a NIR image of rather flat scene in daytime, we may distinguish vegetated area, bare land and water areas as light gray, dark gray and almost black, respectively, such as shown in Fig. 3, which is a SiPSE-3D NIR image of three big rivers in the west of Nagoya city pouring into Ise Bay, seen from eastern sky. In this image, urban areas of Nagoya, Ogaki and other cities are relatively dark. In the areas of Suzuka and Ibuki mountains with rich vegetation in the upper part of the figure, mountainous topographies can be observed by the shadows of the sunshine. The old battlefield Sekigahara can be found in between the two mountainous areas.

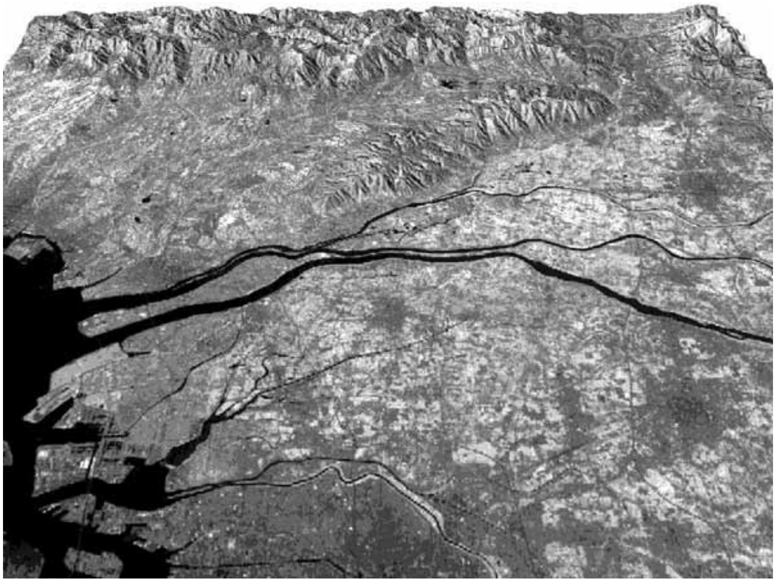

Fig. 3. A SiPSE-3D NIR image of three big rivers, Ibi-, Nagara- and Kiso-gawa, from top to down pouring into Ise Bay, seen from eastern sky. Original LANDSAT data: 1997.10.21.

Fig. 4 is an aerial NIR photograph toward the north from above Ise Bay. We may clearly see the three big rivers, and the difference of the vegetation in urban and rural areas. In such a slant view near the horizon, we may see very wide NIR view comparable to a full scene of LANDSAT data, while conventional visible image is usually very much obscured by aerosol and moisture. See [5] for more about NIR photographs.

Fig. 4. An aerial NIR photograph toward the north from above the center of Ise Bay, by the night-shot mode of Sony DSC-V3 with IR84 filter of Fuji-film on 4 Nov. 2005 at 12:17. Shin-Nagoya airport is seen on the down right.

In Fig. 5, we compare southern part of Kyoto basin in true-color and NIR images by SiPSE-3D observed from southern sky (a and b), and a mosaic of NIR photos from northern sky (c). In two SiPSE-3D images (a and b), plains and mountainous areas exhibit opposite brightness in true-color and NIR owing to the difference in vegetation, while the rivers are clearly seen in both images as relatively dark lines. Three big rivers, Kazura-gawa from the north, Uji-gawa from the east and Kizu-gawa from the south, join together into Yodo-gawa that flows down toward south-west into Osaka Bay through the Osaka plains. Kamogawa, joining Kazura-gawa, is also seen clearly in Fig. 5a.

(a) SiPSE-3D true-color image

(b) SiPSE-3D NIR image (LANDSAT data: 1989.5.31)

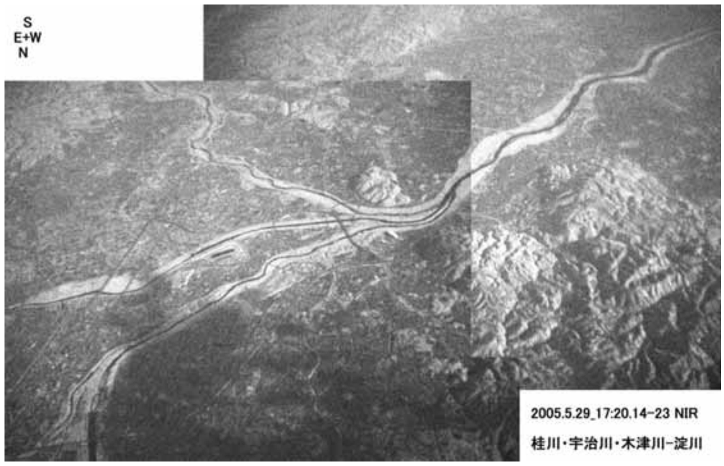

(c) A mosaic of NIR photographs by the night-shot mode of Sony DCR-TRV30 with Fuji-film IR84 and Kenko ND400.

Fig. 5.
Southern part of Kyoto basin observed from the southern sky (a, b), and northern sky (c).

The NIR photograph (c) is very similar to the satellite-based image (b), except for the directions of the observation and the sunlight. In Fig. 5c, we may see big bridges crossing the rivers, and also the shadow of the clouds in the downside of the picture.

It is interesting to note that we may find big battlefields decisive to Japanese history in Fig. 5: On 13 June 1582, Mizuhide Akechi was defeated by Hideyoshi Hashiba at the decisive Yamasaki battle around the upstream of Yodo-gawa, and Hideyoshi turned out to be the governor of Japan. On 3 January 1868, the battle of Toba-Fushmi started around the down streams of Kazura-gawa and Uji-gawa, and ended after three days resulting the collapse of the Tokugawa regime. Topographical importance of these areas to become historical scenes may well be understood by the satellite 3D images.

5. Estimate and simulation of volcanic eruption cloud heights

The height determination of volcanic eruption cloud is very important for the dispersion forecasts of ash clouds so as to avoid the airline hazards. In order to improve the pilot reports of the cloud height observed, two methods have been developed as off-line systems. One of them is to estimate the cloud height of an aerial photograph by the simulation of the land topography with a height scale [6], and the other one is to embed a model of eruption cloud as a 3D object in a SiPSE 3D image, such as shown in Fig. 6. By changing the cloud height, the wind direction and the viewpoint in the latter case, we may simulate various situations for the training.

Fig. 6. A model of eruption cloud as a 3D object embedded in a SiPSE 3D image of Sakurajima volcano. The box of parameter control buttons is shown on the left hand side.

6. Unification of land and submarine topographies

Marine Information Research Center provides the submarine topography data around Japan in a CD-ROM with the resolution 1 km. In order to join with the land topography and land-cover data with much higher spatial resolution, special care is necessary for the handling of the coastal lines. Instead of the sea surface data or some coverage data of the sea bottom, it may be reasonable to use the sea depth data with a graduation scale. Fig. 7 is a scene of Amami, Tokara and Kumage Islands up to the southern Kyushu observed from southern sky, thus constructed.

Fig. 6. From Amami Islands to southern Kyushu, Japan, observed from southern sky. Relatively big islands from the top to the down are Tanegashima, Yaku-shima, Amami-Oshima, Tokunoshima, Okinoerubu-jima and Yoron-jima. This SiPSE-3D image is composed of the true-color image for the land and the sea depth graduation image, with the DEM information. Equi-depth lines are also drawn on the sea. Horizontal scale is enhanced by the facter 5.

In Fig. 6, we may see a part of very deep Nankai Trough on the right-hand side as very dark blue area. This 3D presentation with submarine topography is developed as an off-line system with special handling of the data.
In general, we may try new approaches in off-line systems, while we should keep the constancy of the format in the on-line system open to public through the Internet.

7. Concluding remarks

In order to construct a land image database of a satellite for the 3D presentation, a large archive of the original data is necessary so as to obtain cloudless scenes. To avoid the snow-cover in northern areas is also an important requirement for the scenes. The SiPSE database is thus constructed during 1996-2001, by selecting relatively new scenes if available.
In order to unify neighboring LANDSAT scenes to get wide images, it is better to use the original data with similar seasons and years. However, this requirement is not always easy to fulfill, because of the clouds and/or snow-cover. Handling of very wide scenes is investigated as an off-line activity of the SiPSE group.

Acknowledgements

We are grateful to JAXA (previously NASDA) for allowing the use of LANDSAT data in the SiPSE format, and GSI for the use of the DEM data of Japan in the SiPSE database.

References

[1] H. Togoshi, N. Tomioka and K. Kinoshita, Development of 3D image presentation system for education using digital elevation model and remote sensing data, Proc. 27th Japanese Conf. Rem. Sens., 1999, p.273-274 (in Japanese with English abstract).

[2] K. Kinoshita (ed.), Construction and application of the satellite image providing and presentation system for education, Kagoshima Univ., 2004, 141p. (in Japanese).

[3] K. Kinoshita, N. Tomioka and H. Togoshi, “How to create and see 3D satellite images by SIPSE system, - Observation of landscapes of Japan from the sky –“, Kokon-shoin, 2005, 126p. (in Japanese:
木下・冨岡・戸越， SiPSE による 3D 衛星画像の作り方と読み方－日本の自然を空から見る，古今書院，2005.).

[4] N. Tomioka, K. Takayama, A. Minaka and K. Kinoshita, Construction of Satellite Image Providing System for Education on the Internet, Proc. 22nd Japanese Conf. Rem. Sens., 1997, p.215-218 (in Japanese with English abstract).

[5] K. Kinoshita, C. Kanagaki, A. Minaka, S. Tsuchida, T. Matsui, A. Tupper, H. Yakiwara and N. Iino, Ground and Satellite Monitoring of Volcanic Aerosols in Visible and Infrared Bands, Proc. CEReS International Symposium on Remote Sensing, Monitoring of Environmental Change in Asia, Chiba, Japan, pp. 187-196, 2004.

[6] K. Kinoshita, C. Kanagaki, N. Iino, M. Koyamada, A. Terada and A.C. Tupper, Volcanic plumes at Miyakejima observed from satellites and from the ground, Proc. SPIE 4891(2003), Optical Remote Sensing of the Atmosphere and Clouds III, part of SPIE's 3rd Int. Asia-Pacific Environmental Remote Sensing Symp., October 2002, Hangzhou, China, 227-236

Hydrologic image interpretation on small-scale on farm pond using high resolution satellite imagery

Kenji SUZUKI [1] and Yukiyo YAMAMOTO [2]
[1, 2] Japan International Research Center for Agricultural Sciences
E-mail: suzukik@jircas.affrc.go.jp

Abstract
This paper describes the use of satellite image interpretation for analysis of small-scale on-farm ponds in northeastern Thailand based on field knowledge of hydrology and water use. Image interpretation on high-resolution QuickBird satellite imagery revealed that 1) the type of pond can be categorized visually from the viewpoint of its location, 2) the catchment location in relation to the pond can be estimated from the intake point of water and the layout of the pond. Through a series of image interpretations, the effectiveness of high-resolution satellite imagery for field sciences and investigations was confirmed.
Keywords: Field sciences, Image interpretation, Northeastern Thailand, QuickBird

1. Introduction

In field science, which focuses on the survey of actual sites, a technique of juxtaposing field study observations with interpretations of aerial photography or high-resolution satellite imagery is effective in the investigation of area-specific phenomena. For example, in a study of river engineering, aerial photographs of the area around the channel taken immediately after flooding provided invaluable information when combined with the site survey and hydraulic model tests (Miwa *et al*., 2003).

High-resolution imagery produced typically by IKONOS or QuickBird satellites provide images that are as detailed as aerial photographs, with a resolution of up to 1 m. Since these satellite images became available, some researchers have been testing them for use in surveys of relatively small areas in so-called site-based field studies (Suzuki *et al*., 2005a).

This paper describes an example of image interpretation regarding the hydrological location of small-scale ponds using field knowledge and high-resolution satellite imagery.

2. Overview of the study area and data used

For this study, we selected the village of NS in Ban Haet District, Khon Kaen Province, in northeastern Thailand. The village is located about 30 km south of the city center of Khon Kaen. The area is characterized by a gently undulating terrain. Paddy fields dominate the lower site, the valley, while the upper site features sugar cane and cassava farms.

The soil is sandy with poor water retention capacity and nutrient content, and is susceptible to erosion. Heavy rain often causes soil erosion in the upper site, where the lands are practically bare. The wet seasons and dry seasons are distinct in northeastern Thailand. Precipitation is minimal in the dry season. In the wet season, the precipitation is variable because the timing of seasonal onset and the amount of rainfall are unstable. The rain generally comes in the form of localized squalls, contributing to the uneven temporal and spatial distribution of water resources. As a result, agricultural productivity has remained low and unstable.

Under such circumstances, there have been many small-scale water resources developments. Small ponds adjacent to cultivated fields, such as paddy fields and farmlands, and irrigation weirs built in small rivers are typical examples of such measures. The study site, the village of NS, has already had more than 260 ponds developed in the area, and is known to have more ponds than other areas (Suzuki *et al*., 2005b).

This study used panchromatic images (60 cm/pixel) and multispectral images (2.4 m/pixel) taken by QuickBird in the dry seasons of April 2002 and January 2004 for visual interpretation. In addition, we conducted field surveys in the subject area over the period from 2002 to 2005 to facilitate the observation of precipitation and water levels.

3. Examples of interpretation and application

3.1 Identification of types of ponds

Farmers own small-scale ponds adjacent to their farms, and take water primarily by pump for a variety of uses, including rice planting and drought relief, as well as for fish farming and vegetable growing. The ponds in the study area are roughly divided into 2 categories according to their location and construction methods.

The most common ponds in the lower site are made of earth bunds built in the lowest part in the valley bottom (Photo 1). The bunds run for lengths of some 60 to 80 m. Water levels available for storage are less than 1.5 m, although some ponds have their upstream side dug down somewhat deeper. Since there is little precipitation during the 6-month dry season, the water level keeps falling during this time due to an evaporation rate of about 5 mm/day. These ponds usually remain wet even without stored water because they are situated in the valley. However, their water budget suggests that water may not be available year-round because of their inherently shallow storage depth.

Contrastingly, the ponds in the upper site are predominantly dug into the ground by heavy machinery. One side of the pond runs about 20 to 30 m in length. The total height of the surrounding embankment and the depth of the dug-out pond provide the storage depth, which can be as high as 3 m (Photo 2). Many of these ponds have water available for use year-round because sinking them into the ground ensures a sufficient storage depth. Some of these ponds are replenished by shallow subsurface water.

On the images, the bunds of the ponds that dominate the lower site are visually identifiable. The images taken in the dry season in particular often present the ponds in an irregular shape that reflect falling water levels (Fig. 1). On the other hand, the in-ground ponds in the upper site retain their rectangular shape, and do not change even when their water level falls. The embankments surrounding these ponds are also recognizable in the images (Fig. 2). These differences presented by high-resolution satellite imagery provide the possibility of identifying the type of pond from the images. For convenience, this study refers to these respective types of ponds as the “lower ponds” and the “upper ponds”.

Many of these ponds are of a rectangular shape, with the short sides normally running parallel to the direction of the grade. The paddy fields are also rectangular and laid out in a similar orientation. This layout reduces the difference in water levels in ponds (and in paddy fields) when the water is stored on a sloped terrain. Nevertheless, even this layout may cause unevenness, especially in paddy fields, if the land is not leveled sufficiently. Accordingly, the layout of ponds and paddy fields (the orientation of the short sides) provides clues which make it possible to estimate the direction of the surface grade at the site.

Photo 1 Typical pond in the lower site

Photo 2 Typical pond in the upper site

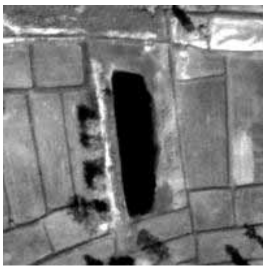

Fig. 1 Typical pond in the lower site
(QuickBird, Panchromatic, 0.6 m/pixel)

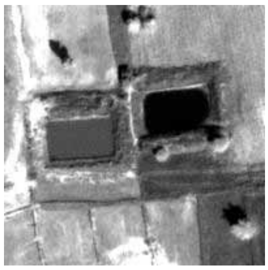

Fig. 2 Typical pond in the upper site
(QuickBird, Panchromatic, 0.6 m/pixel)

3.2 Identification of intake points in the upper ponds

The water level may vary among a number of ponds present within a small watershed even with the same usage of water. What factors regulate the difference in the water levels of the upper ponds? Figure 3 illustrates the concept of the water budget of a pond. Because there is little difference between the ponds in terms of their surface area, factors such as precipitation and evaporation are virtually the same. On the other hand, factors such as surface flow, lateral inflow (and outflow), and seepage loss of the ponds may vary depending on their location. The lateral inflow (and outflow) and seepage loss are relatively small. Consequently, the inflow of surface water from the catchment area regulates the water budget of the ponds, and is the biggest factor causing locational differences.

Substantial rainfall in the wet season causes a rapid rise in the water level (Fig. 4). Especially, a daily rainfall of more than 100 mm raised the water level by more than 55 cm in a day in mid-September. Subtracting the 10 cm of direct rainfall on the pond surface, the water level rose by 45 cm. Assuming that 40 cm of this rise was due to surface inflow from the catchment area, and that the runoff ratio was 0.4, a calculation-based water budget estimates the size of the catchment area to be 10 times as large as the surface area of the pond.

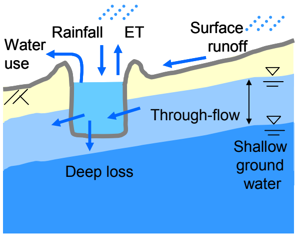

Fig. 3 Concept of water budget of upper ponds

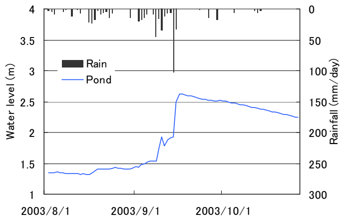

Fig. 4 Observed changes in water level of an upper pond

If the inflow of water depends on the size of the catchment area, farmers will be motivated to secure the catchment area. Many of the upper ponds are equipped with an intake point or a small channel to secure an inflow of water from their catchment area. The passage of water, however, makes the ground around the intake point prone to erosion. If the volume of water passing is too high, there is a risk that the embankment near the intake point may collapse. Furthermore, if farmlands or bare lands occupy a large portion of the catchment area, and these lands are adjacent to a pond directly, sedimentation from the inflow of sediment-laden surface water becomes a problem.

An examination of images identified some ponds with recognizable sedimentation indicating the location of their intake points. Figure 5 is a satellite image that provides a relatively clear view of the area near the intake point. The area marked by the dotted line indicates the extent of the sedimentation, presented as a triangle with its apex at the intake point in the upper right corner. Photo 3 is a photograph of the intake point of this pond and the actual condition of the sedimentation, confirming how well the satellite image corroborated them.

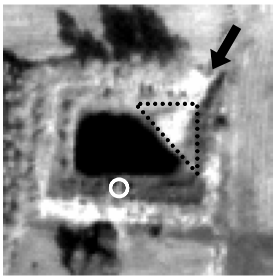

Fig. 5 Sedimentation around intake point of water (QuickBird, Panchromatic, Jan. 2004, Arrow: intake point, Dotted line: sedimentation, Photograph taken from position marked ○)

Photo 3 Sedimentation around intake point of water (Photograph taken from position marked ○ in Fig. 5 in July 2005; Arrow: intake point, Dotted line: sedimentation)

A comparison of images taken at 2 different times also confirms the process of sedimentation over time. The white area in Fig. 6a is a newly constructed pond. The embankment and the periphery of the new pond are presented as a bright white area in contrast to the surroundings as it is bare land covered by dry soil. Another image of the same pond taken 2 years later (Fig. 6b), however, shows a clear sign of sedimentation due to the inflow of sediment.

(a) 2002

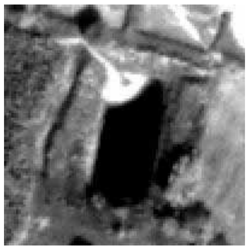

(b) 2004

Fig. 6 Process of sedimentation in a pond (QuickBird, Panchromatic, 0.6 m/pixel)

Figure 7a shows an upper pond in a rare dried-up condition, which provides us an opportunity to make close observation of the condition of its bottom. Examining the bottom surface of the pond indicates that its intake point is located at the lower right corner. The sediment-laden water flowed into the pond from this point, but has since dried, appearing in white in the image. The 2004 image of the same pond (Fig. 7b) shows a higher water level than is shown in the 2002 image (Fig. 7a). The shape of the water surface clearly confirms the area of sedimentation in the lower right corner of the pond. The intake point itself is not very clear in Fig. 7b. If the water level were slightly higher, the sedimentation would have been hidden beneath the water surface, making it difficult to identify the intake point. In other words, the presence of sedimentation provides convincing evidence of the location of the intake point. Accordingly, the sedimentation on the bottom of a pond exposed by low water level supports the identification of the location of the intake point.

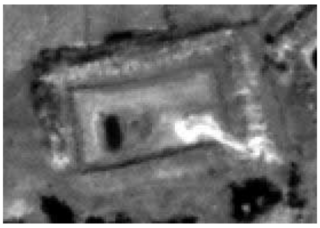

(a) 2002

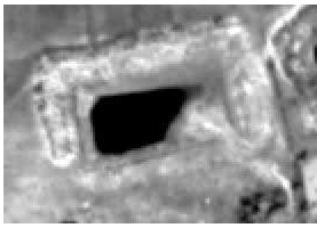

(b) 2004

Fig. 7 Observed sedimentation at low water levels (QuickBird, Panchromatic, 0.6 m/pixel)

4. Conclusion

This study examined hydrological information that can be extracted from visual interpretation of high-resolution satellite images of small-scale ponds in northeastern Thailand. It was found that (1) it was possible to classify the ponds according to their location or their type (ponds in the upper site, and in the lower site); (2) for some of the ponds, it was possible to estimate the location of the main catchment from the layout of the ponds and the location of the intake point. These interpretation techniques are believed to provide valid information when conducting an investigation of suitable locations for irrigation ponds.

With respect to the collection of hydrological information using remote sensing methods, the role of visual interpretation is very important from the point of view of region-specific information (Kondo, 2003). To this end, a researcher must possess sufficient understanding of local conditions and expert knowledge of the visual interpretation of satellite imagery. A future task is to accumulate examples to further develop and refine the analytical techniques that utilize field knowledge.

References

Kondo, A., 2003. Application of remote sensing and GIS technology to hydrology; *Geography Review*, 76(11), pp. 788–799, *in Japanese*.

Miwa, H., Kurashima, E., 2003. Present situation and cause analysis of diversion dam failures in Japan, *Paddy and Water Environment*, 1(4), pp. 207–214.

Suzuki, K., Y. Yamamoto, M. Ando, C. Ogura, 2005a. Evaluation of land and water resources in rainfed agricultural areas using high-resolution satellite data and GIS, *Journal of the Japanese Agricultural Systems Society*, 21(3), *in press*.

Suzuki, K., Y. Yamamoto, M. Ando, 2005b. Evaluation of small-scale on-farm ponds in northeast Thailand using hydrologic model and GIS, *Journal of the Japanese Agricultural Systems Society*, 21(1), pp. 59–64.

Processing and interpretation of JERS-1 Synthetic Aperture Radar (SAR) image of Cepu and its surrounding areas, Central Java Province, Indonesia

Wahyudi W. PARNADI[1], Salim RUSLI[1], Ketut WIKANTIKA[2], Josaphat TETUKO S. S.[3]
[1] Department of Geophysical Engineering, Institute of Technology Bandung
[2] Department of Geodetic Engineering, Institute of Technology Bandung
[3] Center for Environmental Remote Sensing, Chiba University
E-mail: wparnadi@bdg.centrin.net.id

Abstract
Geological as well as lithological interpretations of subsurface condition from Radar image are of great interest. Conventionally, geological features are derived visually from the images. Patterns associated with geological structures/ features are recognized. Attempts to interpret lithological as well as structural geological features deeper than 1 - 10 meters are of course challenging. This research is in the early stage of an attempt to derive lithological and geological features from Radar image conducted in the Department of Geophysical Engineering of Institute of Technology Bandung, Indonesia. In this stage, we tried to derive geological structures and other features visually from JERS-1 SAR data from Cepu area in Central Java Province, Indonesia, in which a huge oil reservoir located. Conventional image processing flows applied on the data could improve data quality that lead to more interpretability of the data. Eleven anticlinal folds and one faulted anticlinal fold were detectable. These folds could be identified based on their characteristics: coarse textures and high brightness values, folded form or horizontally folded and symmetrical or repetitive patterns. Shear fault structures could also be identified based on the appearance of lineaments intersecting folds. A small difference in structure orientation interpretation from image-derived structures and the geological structure map could be resulted from the error in the process for geometric correction, especially for structures located outside ASTER image coverage acting as geometrical correction reference. Even for structures inside the ASTER image coverage, Digital Elevation Modeling (DEM) technique should be incorporated in the processing for better results in the determination of structures orientation.

1. Introduction

Interpretation of subsurface condition from Radar image is of great interest, covering surface as well subsurface features with resolution much higher than resolution offered by radar technique. Lithological as well as geological informations extracted from the image could be of higher value. Conventionally, geological features are derived visually from Radar images (Sabins, 1997). Patterns associated with geological structures/features could be detected. Oil seeps occurrence under ocean could also be recognize in radar image. This leads sometimes to the discovery of oil and gas fields in frontier areas.

In nature, Oil and gas were trapped at a depth below 400m – 700m. In Indonesia, their occurrence could be in shallow reservoir at a depth of 200m-500m and in reservoir at deeper depth. In other side, informations extracted from remote sensing data provide just some 10 centimeters – 1 meter thick subsurface condition. That makes remote sensing data used only in the reconnaissance survey. Traditionally, seismic technique is the only primary method applied for oil and gas exploration. However, some fieldworks recognize the use of remote sensing data in the late stage of oil and gas exploration for some purposes. Seismic surveys, which are the routine method for defining drilling prospects can not be carried out in the most of Petroleum Prospecting Licenses (PPL) operated by Chevron Corporation in Papua New Guinea for two reasons: (1) inaccessibility and rugged topography causing expensive exploration, and (2) scattering of seismic energy which results in very poor data (Sabins, 1997). It is therefore better to incorporate remotely sensed data in late stage of exploration. An attempt to interpret lithological as well as structural geological features deeper than 1 - 10 meters is therefore a challenging task. That depth is, in the first approximation, appropriate for geotechnical and environmental purposes. This could more likely be carried out using correlation between remotely sensed data and data derived from surface measurement. Another better method would be derivation of physical mechanisms between electromagnetic waves and their interaction with subsurface media. We are now in the early stage of our attempts to obtain techniques that make deeper interpretation of radar data possible.

In this research, we tried to derive geological structures and other features visually from JERS-1 SAR data from Cepu area, Central Java Province, Indonesia, in which a huge oil reservoir located. Figure 1 and figure 2 show the study area and its geological structures. The study area located in the coordinates 6˚ 29' 14.09" S – 7˚ 17' 39.42" S and 111˚ 27' 4.32" E – 112˚ 18' 9.19" E. This area comprises of part of Randblatung and Rembang zones. This zone is geologically dominated by anticlinal folds structure with East-West orientation. In this zone is more than 20 oil fields, which are developed since 1893, located. This zone has potentially the biggest hydrocarbon accumulation among other zones in the surrounding areas. The use of geological map is intended to get better understanding of geological features and structures that could be recognized in the Radar image. Since we are still in the first stage to work with radar data, we applied conventional image processing flows. We hope that such image processing flows are sufficient to improve data quality that lead to more interpretability of the data.

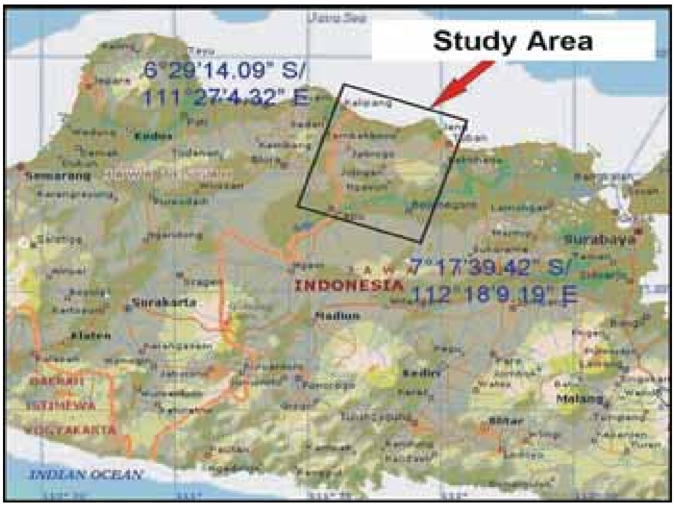

Fig. 1: Cepu Study Area is located in Central Java Province, Java Isle, Indonesia, in the coordinates 6˚ 29' 14.09" S – 7˚ 17' 39.42" S and 111˚ 27' 4.32" E – 112˚ 18' 9.19" E. A huge oil and gas reservoir was found to be at 200-400 m depth.

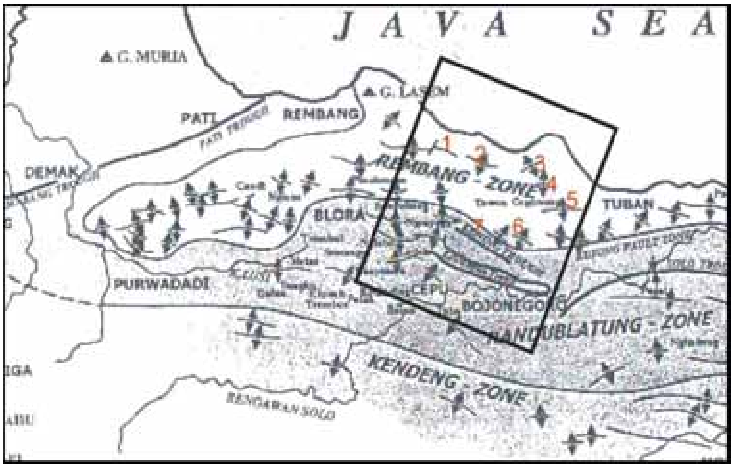

Fig. 2: Geological Structure Map of study area showing anticlinal folds and their orientations (Darman & Sidi, 2000). The study area is located in some part of Randublatung and Rembang areas. This zone has potentially the biggest hydrocarbon accumulation among other zones in the surrounding areas.

2. Data and Data Processing

JERS-1 as well as ASTER images for this research were available from Remote Sensing Research Center - Panditho Panji Foundation, Bandung – Indonesia and ERSDAC of Japan. Combining with data from field observation, we processed the JERS-1 image using following data processing flows: radiometric correction (speckle reduction) with low-pass filtering, geometric correction (image rectification) with least-square polynomial regression, image sharpening with linear contrasting and high-pass filtering. Speckle reduction was carried out using two types of filters: 3x3 and 5x5 median filters. Beside visual appearance, we used ratio between deviation standard σ and statistic mean μ (= σ/μ ratio) as other criteria. Images with the smallest σ/μ ratio were taken to further processes. Geometric corrections were applied with image rectification. ASTER image was acted as reference image in this process. Objects which clearly identified in the images were selected as ground control points (GCPs). Distribution of GCPs as well as their correspondence points in the SAR image could be easily done since we marked all the points during field observations. Image sharpening was carried out through 2 consecutive techniques: image contrasts sharpening and special filtering. Autoclip transform was adopted for the image contrast sharpening. 3x3 high-pass filtering was then applied after image contrast sharpening. All these processing steps were conducted using ER Mapper 6.4 software available in our Department. Figure 3 shows raw image of study area. The area is quite easily accessible. Rectangle in red denotes area used for comparison in speckle reduction processing step. Geometric correction is applied using JERS-1 SAR and ASTER images. For this purpose, distribution of control points in the JERS-1 SAR image and their reference points in the ASTER image is shown in the figure 4. Figure 5 shows processed JERS-1 SAR image after image sharpening. Image histogram after application of high-pass filtering is shown in the right side of the figure.

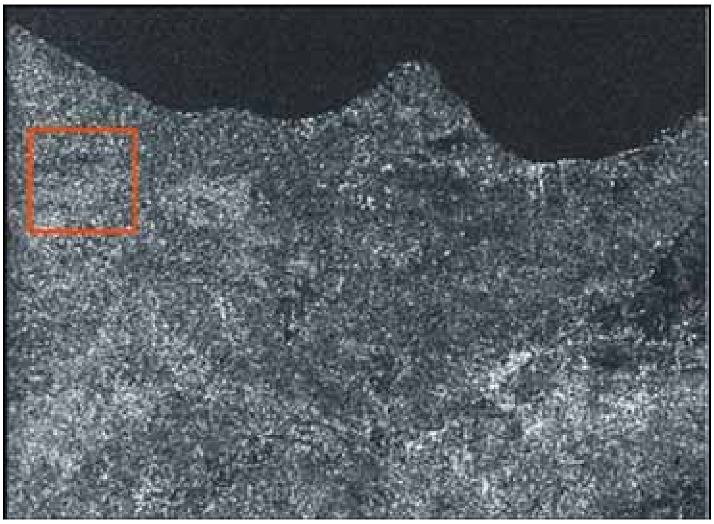

Fig. 3: Raw SAR image of study area. Area for speckle reduction processing step is shown in red rectangle.

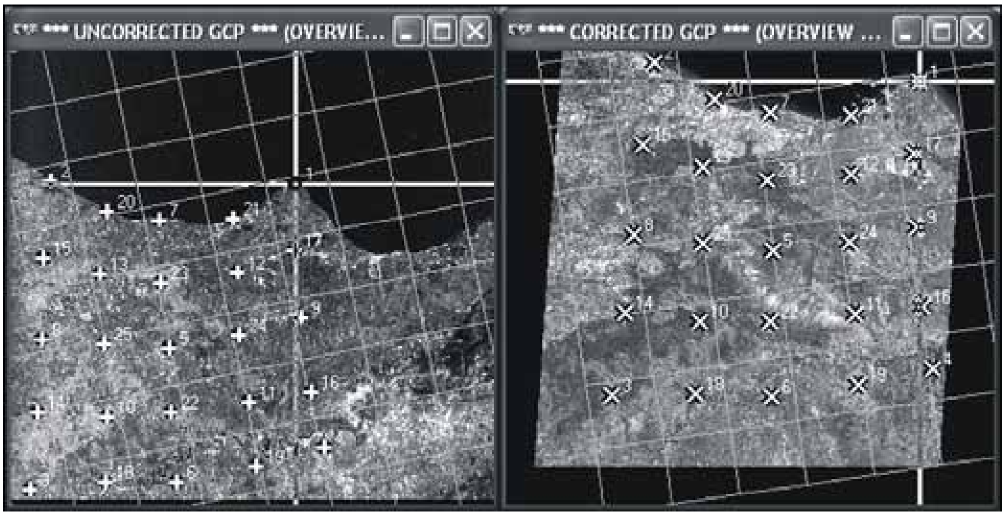

Fig. 4: Distribution of ground control points (GCPs) in the JERS-1 SAR image (left) and their reference points in the ASTER image (right) for image rectification in the geometric correction processing step. These points could be easily recognized in field observation.

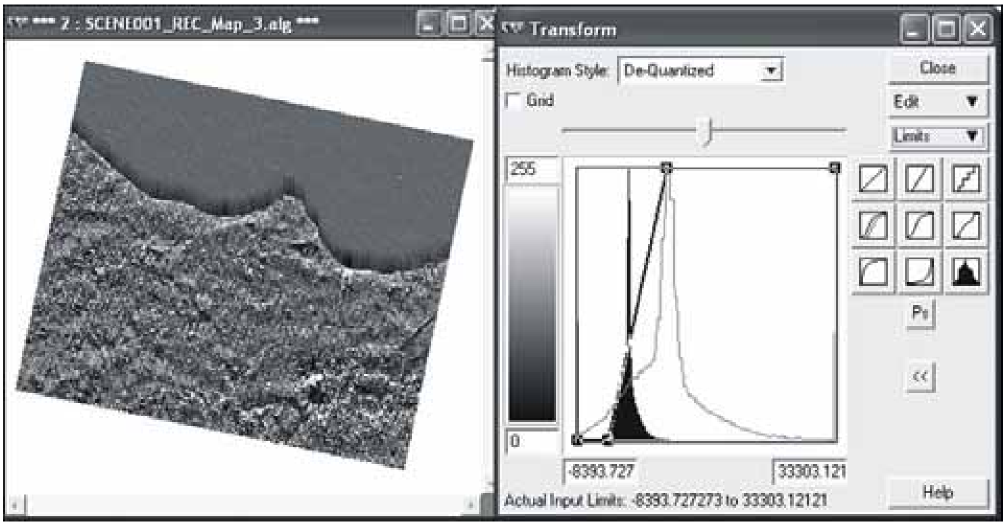

Fig 5: processed JERS-1 SAR image after image sharpening (left) and an example of applied parameter for this image sharpening. Data histogram of the image after high-pass filtering is shown (right).

3. Data Interpretation

Processed image combining with geological structures map were available in the interpretation stage. Two types of geological structures were identifiable in the processed image: anticlinal folds and faults. Eleven anticlinal folds and one faulted anticlinal fold were detectable. Four and five anticlinal structures have NW-SE and SW-NE orientation respectively. Only 1 anticline was found with W-E orientation. These folds were identified based on their characteristics, i.e. coarse textures and high brightness values, folded form or horizontally folded and symmetrical or repetitive patterns. Figure 6 shows interpreted anticlinal folds and fault. White solid lines denote fold structures and white dashed line denotes shear fault. Identification of these anticlinal structures was quite easily carried out in the images.

Shear fault structure was identified based on the appearance of lineaments intersecting folds. Figure 7 is image fraction showing area in the adjacent of interpreted fold no. 1 and shear fault. Symmetrical axes are denoted by blue arrows. These results have been compared with geological structure map. Based on this comparison, 3 anticlinal structures, i.e. anticline 4, 5, 6, were found to be declined from their orientations in the geological structure map. The difference in structure orientation interpretation from image-derived structures and the geological structure map is more likely resulted from the error in the process for geometrical correction, especially for structures located outside ASTER image coverage acting as geometrical correction reference. Moreover, for structures inside the ASTER image coverage, Digital Elevation Modeling (DEM) technique should be incorporated in the processing flows in order to get better results in the determination of structures orientation.

4. Conclusion

Interpretation of subsurface condition from Radar image is of great interest, either structurally/geologically or lithologically. In conventional way, geological features and structures are derived visually from the Radar images. Patterns in the image are tried to be identified and recognized as objects associated with geological structures/features. Attempts to interpret lithological as well as structural geological features from the images for subsurface media deeper then, say 1-10 meters are of course challenging. This 1-10 meters range is, in the first approximation, suitable for geotechnical and environmental purposes. This research is in the early stage of an attempt to derive lithological and geological features from Synthetic Aperture Radar (SAR) image conducted in the Department of Geophysical Engineering of Institute of Technology Bandung, Indonesia. In this stage, we tried to derive geological structures and other features visually from JERS-1 SAR data from Cepu Area, in which a huge oil reservoir located. Cepu area situated some part in the Randublatung and other part in the Rembang zones. This zone is well-known as a zone which has potentially the biggest hydrocarbon accumulation among other zones in the surrounding areas. Application of conventional image processing flows on the data has improved data quality that lead to more interpretability of the data. Eleven anticlinal folds and one faulted anticlinal fold were then detectable. These folds were identifiable based on their characteristics: coarse textures and high brightness values, folded form or horizontally folded and symmetrical or repetitive patterns. Shear fault structures are also be identifiable based on the appearance of lineaments intersecting folds. A small difference in structure orientation interpretation from image-derived structures and the geological structure map was found. This could be resulted from the error in the process for geometric correction, especially for structures located outside ASTER image coverage acting as geometrical correction reference. In order to provide better results in the determination of structures orientation, even for structures inside the ASTER image coverage, Digital Elevation Modeling (DEM) technique should be incorporated in the processing steps.

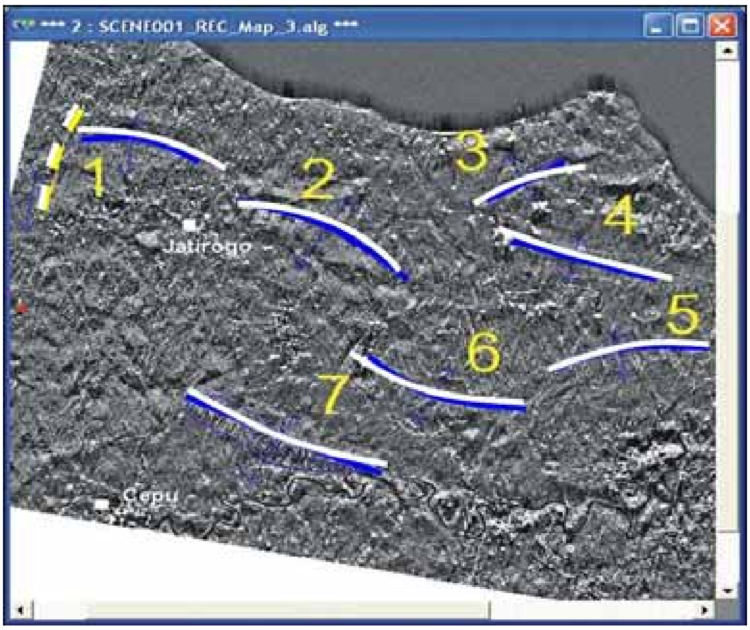

Fig. 6: Interpreted folds (denoted by white solid lines) and fault (white dashed line) in the study area. These anticlinal folds are some of 11 anticlines structures found in the study area. Most anticlines have E-W orientations.

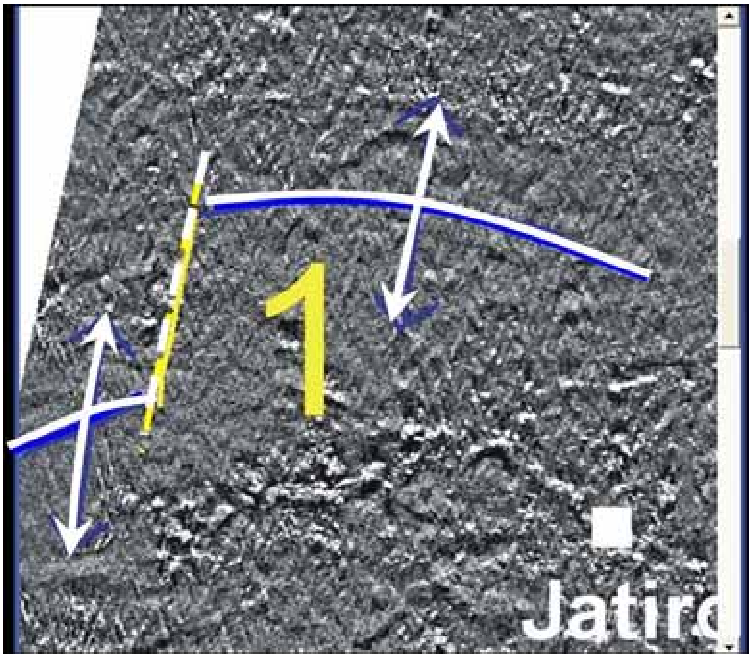

Fig. 7: Image fraction showing more detailed area in the adjacent of interpreted fold no. 1 and shear fault. Arrow signs denote symmetrical axes.

References

[1] Darman. H. and Sidi, H. (eds.), 2000. An outline of The Geology of Indonesia : Indonesian Assoc. Geologists (HAGI), Jakarta.

[2] Jensen, J., 1986, Introductory to Digital Image Processing: A Remote Sensing Perspective: Prentice-Hall, New Jersey, USA.

[3] Permana, T. W., 2003, Analysis of Soil Backscattering Value using Transmission Lines Approach and Data Processing of JERS-1 SAR Data (in Indonesian language): BSc. Thesis, ITB, Bandung.

[4] Rimayanti, A., 2001, Geological Mapping with fusion method of SPOT-HRV and JERS-1 SAR Data (in Indonesian language): BSc. Thesis, ITB, Bandung.

[5] Sabins, F. F., 1997, Remote Sensing, Principles and Interpretation: W. H. Freeman and Company, New York, 3rd ed.

[6] Tateishi, R., Al Bilbisi and J. Tetuko S. S., 2003, A Technique to Estimate Topsoil Thickness in Arid and Semi-Arid Areas of North-Eastern Jordan using Synthetic Aperture Radar Data: Int. J. Remote Sensing, 25, No. 19.

[7] Tetuko S. S., J, Tateishi, R. And Takeuchi, N., 2003, Estimation of Burnt Coal Seam Thickness in Central Borneo using JERS-1 SAR Data: Int. J. Remote Sensing, 24, No. 4.

Acknowledgment

We thank Remote Sensing Research Center - Pandhito Panji Foundation of Indonesia and ERSDAC of Japan for providing the JERS-1 SAR and ASTER image data.

Impacts of the sea surface temperature anomaly in the Pacific and Indian Oceans on the Indonesian climate

Bannu[1,2], Hiroaki Kuze[1], Nobuo Takeuchi[1] and D.A. Suriamihardja[2]

[1] Center for Environmental Remote Sensing, Chiba University,
1-33 Yayoi-cho, Inage-ku, Chiba 263-8522, Japan

[2] Center for Environmental Studies (CES), Hasanuddin University,
Makassar 90245, South Sulawesi, Indonesia

Abstract: Impacts of the El Niño-Southern Oscillation (ENSO) and Indian Ocean Dipole (IOD) events on the Indonesian rainfall were studied using observational data and the NCEP/NCAR reanalyzing global data. ENSO and IOD variability in the time-periods are detected by using wavelet analysis, and we attempt composite analysis of the rainfall amounts over Indonesia during ENSO and IOD events. The correlation between strong El Niño intensities and several regions in Indonesia with rainfall below normal (< 85%) are high, but when the intensities are weak the correlation becomes low. In this case other phenomena such as IOD can contribute to drought in Indonesia. Our analysis also indicates that during El Niño and positive IOD events, the southeast monsoon (Australian monsoon) over Indonesia is intensified, causing the dry season longer than rainy season.

Keywords: NCEP/NCAR reanalyzing data, observational rainfall data, ENSO, IOD, and wavelet analysis.

1.Introduction

Sea surface temperature (SST) variability in the tropical Pacific Ocean such as El Niño-Southern Oscillation (ENSO) phenomena is associated with drought and flooding in many parts of globe. El Niño (La Niña) represents the warm (cool) phase of the ENSO cycle. The term El Niño (La Niña) refers to a periodic warming (cooling) in SST across the central and east-central equatorial Pacific (**Fig. 1**).

Recently it has been pointed out that conditions in the Indian Ocean might also affect climate variability in Indonesia. The El-Niño like temperature anomaly in the Indian Ocean is called the Indian Ocean Dipole, or IOD (Saji et al., 1999, Webster et al., 1999; Hendon, 2003). The IOD event has raised a number of new questions about its generation and possible interactions with other climate phenomena. During a positive IOD event, the SST drops in the southeastern part of the Indian Ocean, off the northern coast of Australia, the eastern coast of Japan and throughout Indonesia. At the same time, the SST rises in the western equatorial Indian Ocean and off the eastern coast of Africa. This SST increase leads to heavy rainfall over the east Africa and severe droughts/forest fires over Indonesia (**Fig.2,** left). The negative IOD event, on the other hand, is in effect the reversal of the positive IOD (**Fig.2**, right).

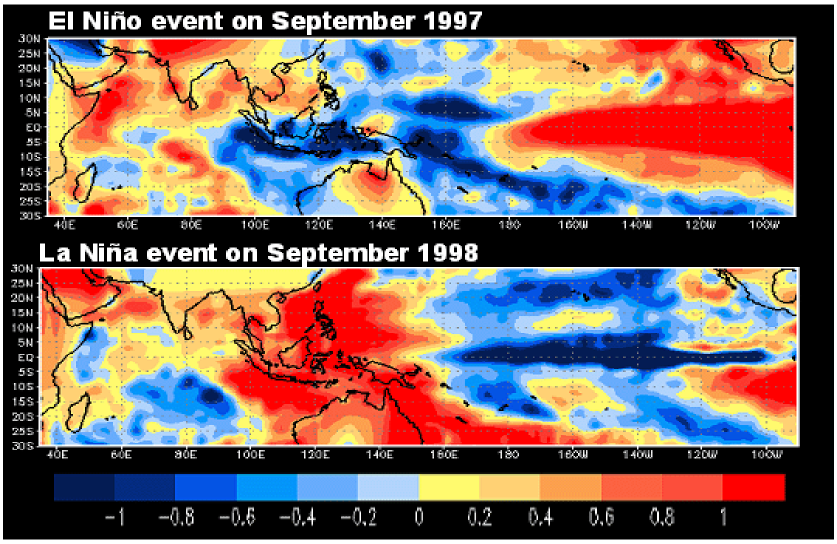

Fig.1 Sea surface temperature anomaly pattern on the El Niño and La Niña events.

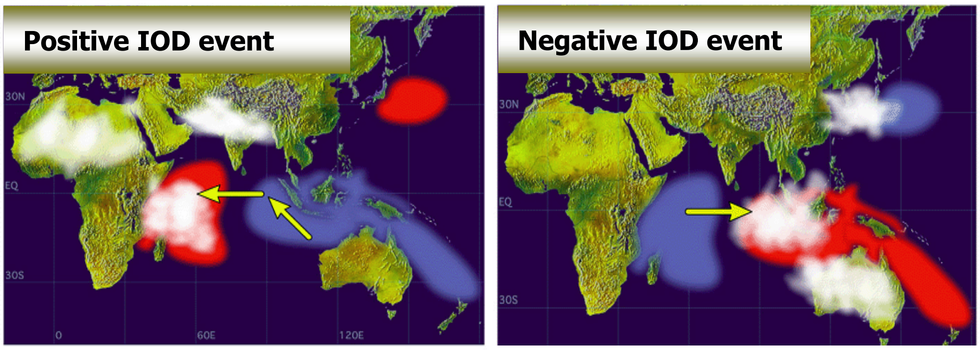

Fig.2 Illustrative of the sea surface temperature pattern on the positive IOD and the negative IOD events (source: http://indianocean.free.fr/links.htm)

A number of studies have reported that Indonesian rainfall is strongly affected by the ENSO phenomena (Philander, 1990; Hendon, 2003), and also by the IOD event (Saji et al., 1999; Webster, et al, 1999; Hendon, 2003). Geographically, Indonesia is not a country that seriously suffers from droughts. However, when affected by the warm episode of ENSO and IOD, rainfall becomes much lower than the normal amount.

In this paper we demonstrate the clear impact of the ENSO and IOD events on the Indonesian rainfall. Wavelet analysis is used to analysis the time-periods of ENSO and IOD variability, and we attempt composite analysis of the rainfall amounts over Indonesia during ENSO and IOD events.

2.Data and methodology

For sea-surface temperature (SST), wind and rainfall, we use monthly data in this study. The ENSO index is measured by the area-average SST anomaly in Niño 3.4 region (5^{o}S–5^{o}N, 120^{o}–170^{o}W), and obtained from the NOAA Climate Prediction Center web site (http://www.cpc.ncep.noaa.gov/). The IOD index as reported by Saji et al (1999) is defined as the SST anomaly difference between the tropical western Indian Ocean (10^{o}S–10^{o}N;50^{o}–70^{o}E) and the tropical south-eastern Indian Ocean (10^{o}S–Eq;90^{o}–110^{o}E). The global data on SST, rainfall and surface wind are derived from the NCEP-NCAR reanalysis data. For validation of result, rainfall data from ground observations at 7 meteorology stations in Indonesia (in **Fig.7**) are used in this analysis (Indonesian Meteorology and Geophysics Agency (BMG), 2002, personal communication).

To detect the time-periods, the ENSO and IOD indices are analyzed with wavelet transform. Wavelet analysis is a useful tool for analyzing time series with many different timescales or changes in variance. Here we employ the Morlet wavelet (MW), and the transform is performed in Fourier space using the method described in Torrence and Compo (1998). The MW consists of a complex exponential function modulated by a Gaussian. The wavelet power spectrum (WPS) is defined as the square of the absolute value of the wavelet transform, giving a measure of the time series variance at each period and at each time. To study the non-stationary change of a variance, it is most appropriate to choose the global wavelet spectrum (GWS). The GWS is equivalent to the Fourier power spectrum smoothed by the Morlet wavelet function in the Fourier domain. The steps involved in the wavelet analysis are given as a schematic flow chart below:

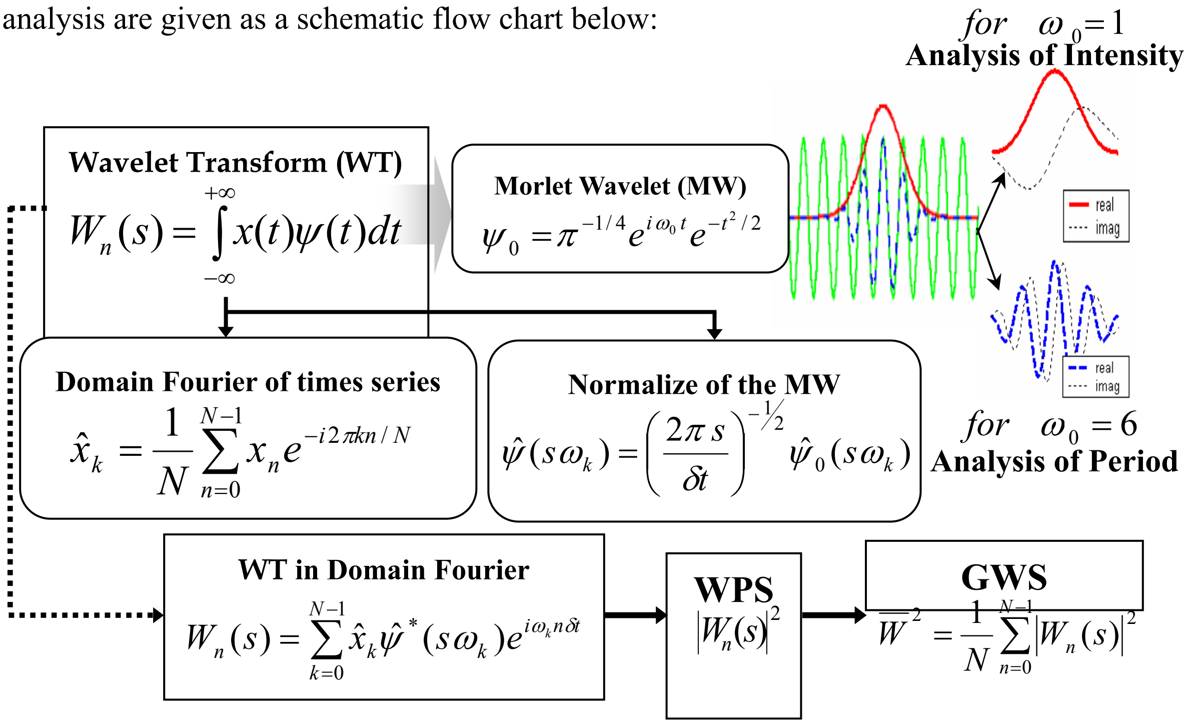

Fig.3 Flow chart of the Wavelet analysis

3. Results and discussion

Since the ENSO and IOD indices are non-orthogonal (Yamagata et al, 2002), it would be reasonable to investigate the possible interactions between ENSO and IOD. Bannu et al, 2005 has reported that the ENSO and IOD events show the strong 2 – 8 year inter-annual cycles. This result suggested that some IOD events coincide with some ENSO events. Using wavelet analysis, we find that three of the major warm ENSO events (i.e., those in 1972, 1982, 1997) are accompanied with positive IOD events (**Fig. 4a** and **4b**).

Accordingly, WT analysis can detect variations of power spectrum by decomposing the ENSO/IOD indices into time–periods. As a result, one can determine the dominant modes of variability and understand how those modes vary in time.

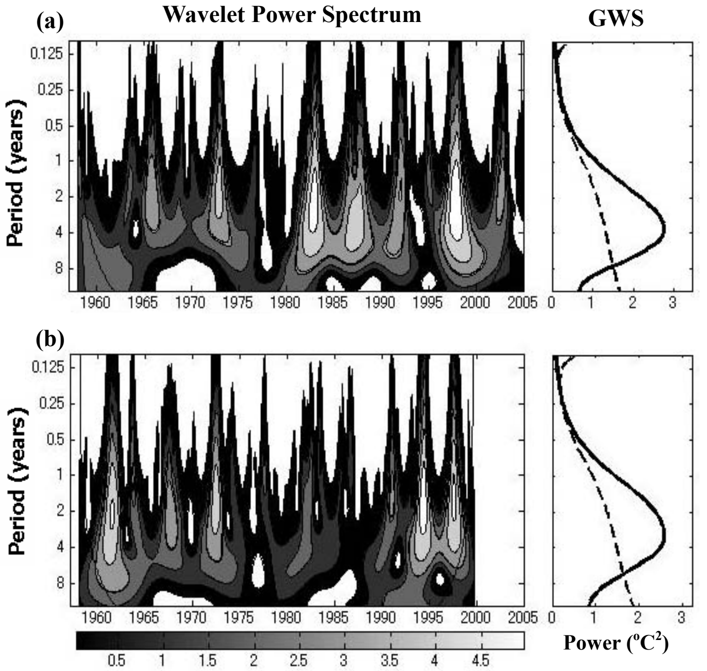

Fig.4 Wavelet power spectrum and Global Wavelet Spectrum (GWS) for: (a) ENSO index and (b) IOD index.

In Indonesia, drought conditions during the dry season (June – November) typically occur in conjunction with the development of El Niño in the Pacific. This is typically represented by cold anomalously SST around Indonesia while warm anomalies develop in the eastern Pacific and western Indian Oceans. Conversely, enhanced Indonesian rainfall during the dry season often occurs during the development of La Nina, with SST anomalies opposite to those of El Niño. Seasonal relationships between Indonesian rainfall throughout the Indo-Pacific basin are explored by calculating seasonal anomaly. In contrast to the IOD 1994 event where the dipole is prominent only in the Indian Ocean (**Fig.5**, left), a similar phenomenon in 1997 was accompanied by another dipole pattern in the Pacific due to the co-occurrence of the well-known El Niño event (**Fig.5**, right). The correlation between strong El Niño intensities and several regions in Indonesia with rainfall below normal (< 85%) are high, but when the intensities are weak the correlation becomes low. In this case other phenomena such as IOD can contribute to drought in Indonesia. Our analysis also indicates that during El Niño and positive IOD events, the southeast monsoon over Indonesia is intensified (**Fig.8**), causing the dry season longer than the rainy season (**Fig.6** and **Fig.7**).

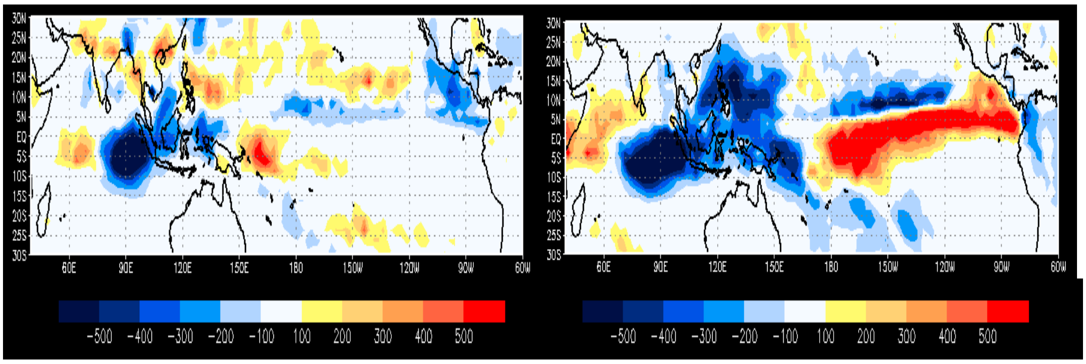

Fig.5 Anomalies of the rainfall on September – November, for 1994 (left) and 1997 (right). Values are in ($mm.month^{-1}$).

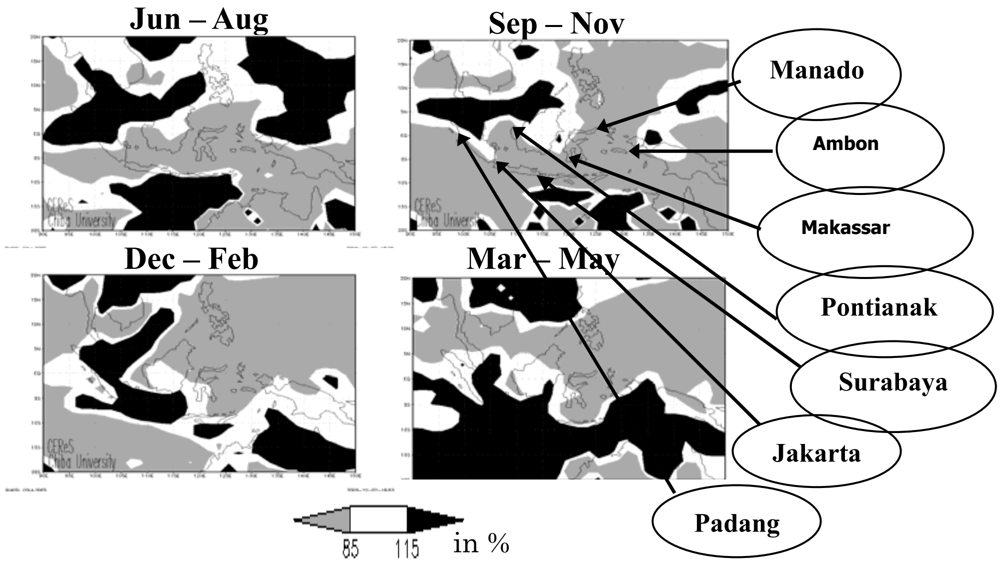

Fig.6 Seasonal rainfall percentage during ENSO and IOD events. Below normal (< 85%), normal (85 – 115%), and above normal (>115%).

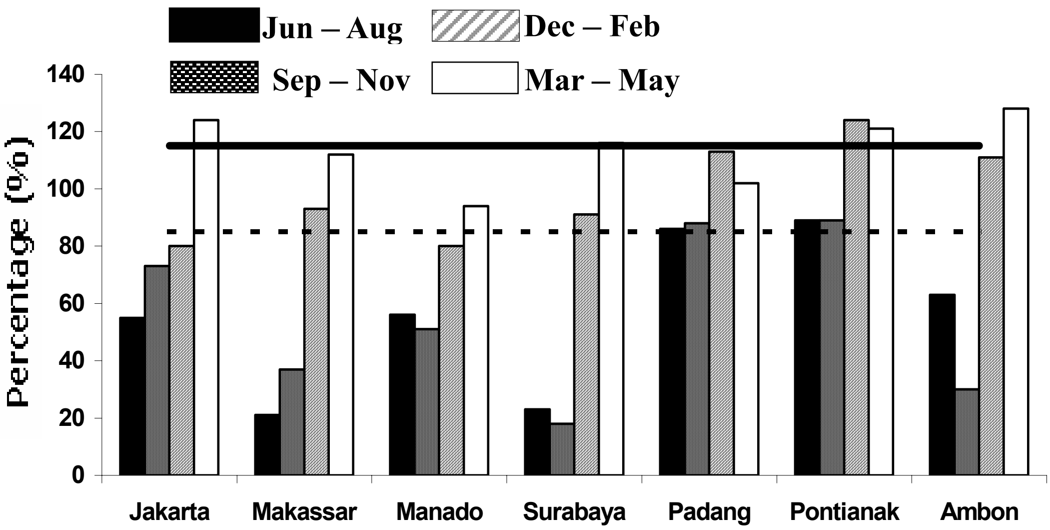

Fig.7 Seasonal rainfall percentages for ground observations data during ENSO and IOD events. Below normal (85%; dotted line) and above normal (115 %; solid line).

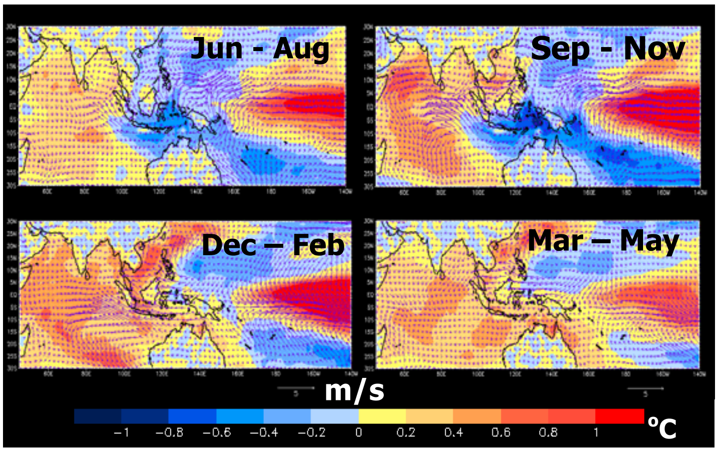

Fig.8 Composite analysis of the SST and surface wind anomaly during El Nino and positive IOD events.

Interestingly, the positive IOD and the warm episode of ENSO have opposite influences in the Far East including Japan (**Fig. 2a** and **2b**); positive (negative) IOD events give rise to warm and dry (cold and wet) summer owing to enhancement of downdraft in the troposphere (Yamagata et al, 2002). The Indian summer monsoon rainfall (ISMR) is enhanced (decreased) during positive (negative) IOD events; the recent weakening of ENSO-ISMR relation may be interpreted in terms of frequent occurrence of the positive IOD in the recent decade (Ashok et al., 2001).

References:

Ashok, K., Z. Guan, and T. Yamagata, 2001: Impact of the Indian Ocean Dipole on the Decadal relationship between the Indian monsoon rainfall and ENSO. Geophysics Research Letter, **28**, 4499-4502.

Bannu, D. Sudiana, H. Kuze, N. Takeuchi, M.A. Ratag, and B. Tjasyono, 2005, Analysis on the impacts of ENSO, IOD, and monsoon over the Maritime Continent of Indonesia, Proceedings of the 2005 Autumn Meeting of the Meteorology Society of Japan.

Hendon, H.H, 2003, Indonesian rainfall variability: impacts of ENSO and local air-sea interaction, J. Climate, **16**, 1775-1790.

Philander, S.G., 1990, El Niño, La Niña, and the Southern Oscillation, Academic Press, Inc. New York, USA.

Saji, et al, 1999, A dipole mode in the tropical Indian ocean, Nature, **401**, 360-363.

Torrence, C. and G.P. Compo, 1998, A practical guide to wavelet analysis, Bull. Amer. Meteor. Soc., **79,** 61-78.

Yamagata, T., S.H. Behera, S.A. Rao, Z. Guang, K. Ashok, and H.N. Saji, 2002, The Indian Ocean Dipole; a Physical Entity, CLIVAR Exchanges: selected research papers, **24**, 1-6.

Webster, P.J., A.M. Moore, J.P. Loschnigg, and R.R. Leben, 1999, Coupled ocean-Atmosphere Dynamics in the Indian Ocean during 1997-98, Nature, **401**, 356-359.

Identification of the climate control factors on carbon cycle variations of tropical forests combined analysis of ground and satellite observations

Shin NAGAI[1], Kazuhito ICHII[2] and Hiroshi MORIMOTO[1]
[1] Graduate School of Environmental Studies, Nagoya University
E-mail: s010116d@mbox.nagoya-u.ac.jp
[2] San Jose State University

Abstract
An estimation of the responses of tropical rainforests for climate changes is important problem to evaluate the terrestrial global carbon cycle. In the present study, we analysed the cross-correlation functions of vegetation indexes to climate parameters for the satellite-based global scale data in the southeastern Asia and the ground-observed point data at Bukit Soeharto, Borneo. Cross-correlation functions show various signals for the regional and temporal scale. Our conclusion is that tropical rainforests in the southeastern Asia have spatio-temporally various responses for climate variations.
Keywords: NDVI, tropical rainforests, climate change, southeastern Asia, cross-correlation function

1. Introduction

Tropical forests play an important role in the global terrestrial carbon cycle. Identification of the response of vegetation activities for climate changes needs to estimate the tropical ecosystem. In special, tropical rainforests are significant. There are three methods to evaluate the relationship, that is, (1) terrestrial ecosystem model (e.g. Nemani *et al*. 2003), (2) field measurement study (e.g. Potts 2003) and (3) analysis using satellite-based data (e.g. Nagai *et al*. 2005). Nemani *et al*. (2003) show that radiation is the most important climate factor. On the contrary, Potts (2003) presents that a severe drought due to strong El Niño events restricts vegetation activities. Nagai *et al*. (2005) detect that interannual variations in NDVI (Normalized Difference Vegetation Index) are inclined to decrease in El Niño events due to dryness. A reason for different interpretations is that tropical rainforests have no distinct phenology and the climate system consists of various time scale modes. Although ground-based data provide a good explanation, there are few field stations. Therefore, we need an analysis using the satellite-based global scale data.

In the present study, we evaluated the responses of tropical rainforests for climate variations in the southeastern Asia using the cross-correlation functions for the satellite-based global scale data, and compared with the analysis of ground-based point data.

2. Data

2.1 Study area

Our target area is the tropical rainforests in the southeastern Asia, where includes the field station Bukit Soeharto (0°51’41″S, 117°02’41″E) (Figure 1). We made two conditions to select tropical rainforests that the vegetation map of DeFries *et al*. (1998) shows evergreen broadleaf forests and monthly mean precipitation from 1971 to 2000 is over 100 (mm). We roughly divided the southeastern Asia into seven areas as shown in Figure 1.

The flora of Bukit Soeharto is secondary tropical rainforests recovered from the forest fires in 1983 and 1998 due to severe droughts. There is a dry season from July to October (Gamo 2003).

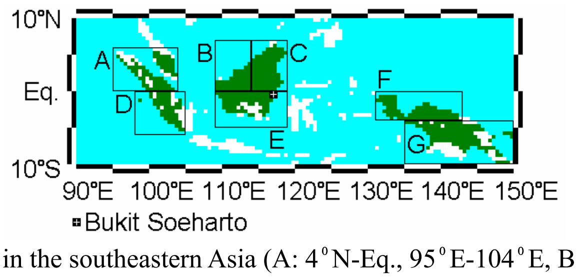

Figure 1. Our study areas in the southeastern Asia (A: 4°N-Eq., 95°E-104°E, B: 7°N-Eq., 109°E-114°E, C: 7°N-Eq., 114°E-119°E, D: Eq.-6°S, 98°E-105°E, E: Eq.-5°S, 109°E-119°E, F: Eq.-4°S, 131°E-143°E and G: 4°S-10°S, 135°E-150°E).
The selected tropical rainforests colour black. A cross marker shows the field site Bukit Soeharto.

2.2 Global scale data

We used the Global Inventory Modeling and Mapping Studies (GIMMS) NDVI data (Pinzon 2002, Pinzon *et al*. 2004, Tucker *et al*. 2005) distributed by the ISLSCP Initiative II data archive (Hall *et al*. 2005) with a 0.25° spatial resolution. Precipitation and temperature data based on ground observations are the Climate Research Unit (CRU) TS 2.0 data with a 0.5° spatial resolution (Mitchell *et al*. 2004). Incoming surface solar radiation data derived from satellites is the Goddard Institute for Space Studies (GISS) downwelling shortwave full sky at surface radiative flux data with a 2.5° spatial resolution (Rossow and Schiffer 1999). We used monthly composite data from January 1984 to December 2000.

2.3 Ground observation data

The LAI (Leaf Area Index) calculated from attenuation of PAR (Photosynthesis Active Radiation), soil water content at 10 (cm) underground, air temperature at 30 (m) above ground, and PPFD (Photosynthesis Photon Flux Density) data from January 2001 to December 2004 with a 30 minute temporal resolution were used. We reconstructed weekly composite data from the daily average of soil water content and temperature, and the daytime (8:15-17:45) average of LAI and PPFD. Deficit data were complemented by an autoregressive model.

3. Method

The cross-correlation functions of NDVI to climate parameters were calculated as shown in equation (1) after applying three month moving average for each data to remove high frequency components.

$$C_{\text{NDVI}-\text{climate parameter}}(k) = \frac{1}{N}\sum_{t=k+1}^{N} \text{NDVI}(t)\ \text{climate parameter}(t-k) \quad (1)$$

where N is the length of time-series.

In the same way, we evaluated the cross-correlation functions of LAI to climate factors for the ground-based point data after applying four week moving average.

4. Results and discussion

We compared the monthly average of NDVI with the ground-observed LAI at Bukit Soeharto to test the seasonal variation in the satellite data. Although NDVI data in tropical rainforests include noise components due to cloud contamination (e.g. Kobayashi and Dye 2005), the seasonal cycle of NDVI coincides with those of LAI well.

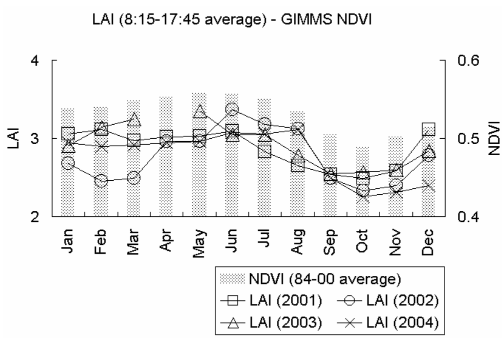

Figure 2. The monthly average of NDVI from 1984 to 2000 (bar) and ground-observed LAI (thin line) from 2001 to 2004 at Bukit Soeharto. We extracted the NDVI data from a grid (0°50' S-0°75' S, 117°00' E-117°25' E). The LAI data show daytime (8:15-17:45) average.

Figure 3 shows the cross-correlation functions of NDVI to climate parameters. Tropical rainforests have various responses for climate factors with different lag time and there are regional differences. We can roughly divide five groups, that is, (1) Malaysia (area A, B and D), (2) the northern Borneo (area C), (3) the southern Borneo (area E), (4) the northern New Guinea (area F) and (5) the southern New Guinea (area G). NDVI has higher positive correlations with temperature and radiation with no lag time in Malaysia and the northern Borneo. On the contrary, NDVI has a higher positive correlation with precipitation with some lag time in Malaysia, the southern Borneo and the northern New Guinea. In the northern Borneo, precipitation has no correlation with NDVI. NDVI-temperature and radiation show higher positive correlations with some lag time in New Guinea. These results mean as following sensitivities of tropical rainforests to climate parameters. Temperature and radiation are important at a point of time in Malaysia, which coincides with Nemani *et al*. (2003). However, precipitation is significant with some lag time in Malaysia, the southeastern Borneo and the northern New Guinea. It presents that water stress restricts vegetation activities, which is consistent with such as Gamo (2003), Potts (2003) and Nagai *et al*. (2005).

Similarly the cross-correlation functions of LAI to climate parameters at Bukit Soeharto are shown in

Figure 4. The correlation of LAI-soil water content denotes the same tendency of the NDVI-precipitation in the southern Borneo (area E), while those of LAI-temperature and PPFD are different from the NDVI-temperature and radiation respectively. It's assumed that ground-based point data include the local meteorology, in special, variations of amount of cloud cover. However, this result means that water stress limits vegetation activities, and agrees with the estimation of the satellite-based global scale data.

We detect that tropical rainforest in the southeastern Asia have different responses to climate parameters spatio-temporally. However, we should be concerned that the climate of southeastern Asia has variations due to the interaction between ENSO and Asian monsoon. More detailed analysis is necessary.

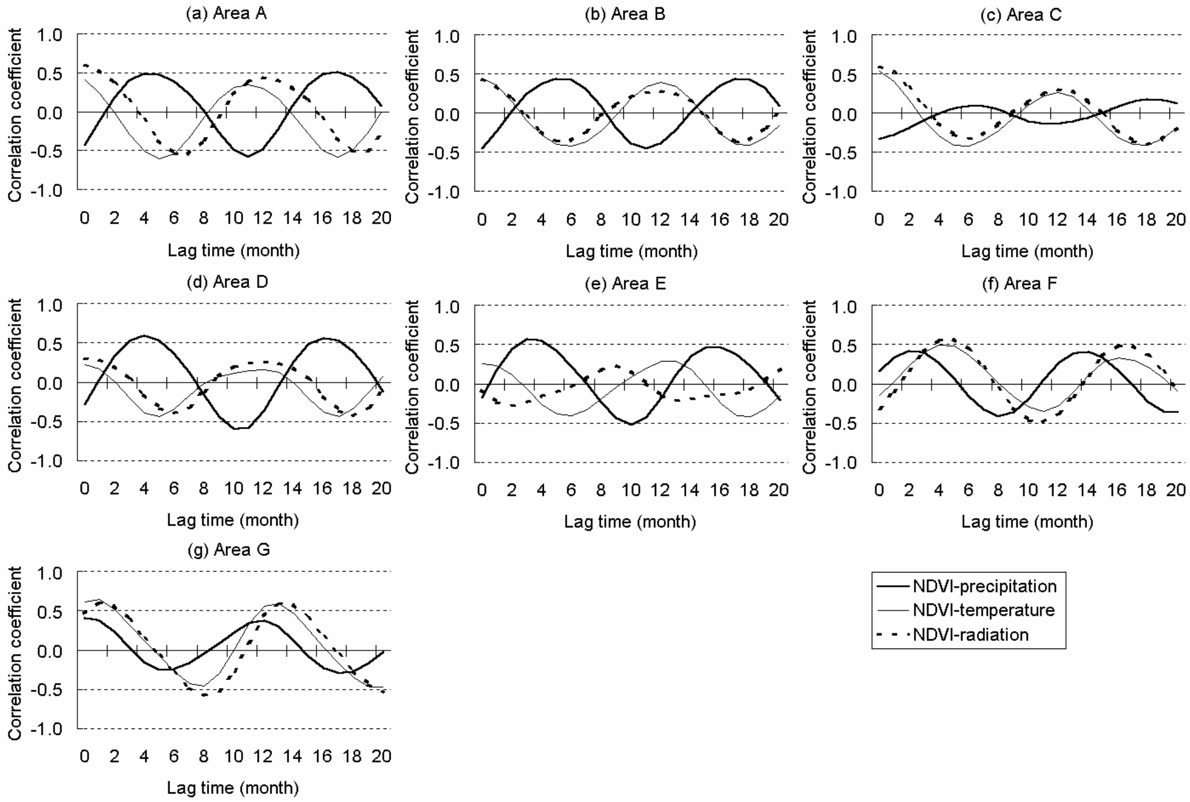

Figure 3. Cross-correlation functions of NDVI to precipitation (bold line), temperature (thin line) and radiation (dotted line) for selected tropical rainforests regions (a: area A, b: area B, c: area C, d: area D, e: area E, f: area F and g: area G).

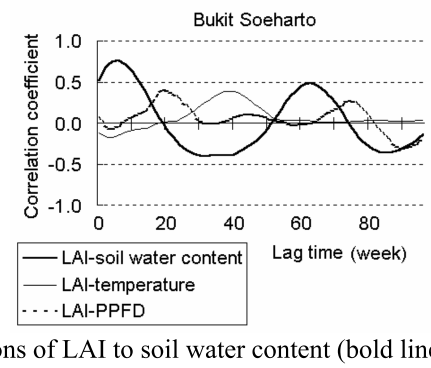

Figure 4. Cross-correlation functions of LAI to soil water content (bold line), temperature (thin line) and PPFD (dotted line) at Bukit Soeharto.

Acknowledgement
We wish to express our gratitude to Dr. Gamo, National Institute of Advanced Industrial Science and Technology (AIST), Japan, for providing the ground-based point data and constructive advice. A grant from the Ministry of Education, Culture, Sports, Science and Technology, Japan (Dynamics of the Sun-Earth-Life Interactive System, No.G-4, the 21st Century COE Program) supported our study.

References
DEFRIES, R.S., HANSEN, M., TOWNSHEND, J.R.G. and SOHLBERG, R., 1998, Global land cover classifications at 8km spatial resolution: the use of training data derived from Landsat imagery in decision tree classifiers. *Int. J. Remote Sens.*, **19**, pp. 3141-3168.

GAMO, M., 2003, CO_2 balance in the secondary tropical rain forest, available online at http://staff.aist.go.jp/old-gamo/2003.3a/3-2index.html.

HALL, F.G., COLLATZ, G., LOS, S., BROWN DE COLSTOUN, E. and LANDIS, D., (Eds.), 2005, ISLSCP Initiative II. NASA, DVD/CD-ROM (USA: NASA, 2005).

KOBAYASHI, H. and DYE, D.G., 2005, Atmospheric conditions for monitoring the long-term vegetation dynamics in the Amazon using normalized difference vegetation index. *Remote Sensing of Environment*, **97**, pp. 519-525.

MITCHELL, T.D., CARTER, T.R., JONES, P.D., HULME, M. and NEW, M., 2004, A comprehensive set of high-resolution grids of monthly climate for Europe and the globe: the observed record (1901-2000) and 16 scenarios (2001-2100). *Tyndall Center Working Paper*, **55**, available online at http://www.tyndall.ac.uk/publications/working_papers/wp55.pdf.

NAGAI, S., ICHII, K. and MORIMOTO, H, 2005, Relatinoship between interannual variations in satellite-based vegetation index and ENSO phase over tropical forests, *J. Agri. Meteorol.*, **60**(6), pp. 1211-1214.

NEMANI, R.R., KEELING C.D., HASHIMOTO, H., JOLLY, W.M., PIPER, S.C., TUCKER, C.J., MYNENI, R.B. and RUNNING, S.W., 2003, Climate-driven increases in global terrestrial net primary production from 1982 to 1999. *Science*, **300**, pp. 1560-1563.

PINZON, J., 2002, Using HHT to successfully uncouple seasonal and interannual components in remotely sensed data, In *SCI 2002*, 14-18 July 2002, Orlando, Florida (Conference Proceedings).

PINZON, J., BROWN, M.E. and TUCKER, C.J., 2004, Satellite time series correction of orbital drift artifacts using empirical mode decomposition, In *Hilbert-Huang Transform: Introduction and Applications*, HUANG, N. (Ed.), pp. Chapter 10, Part 2. Applications (to appear).

POTTS, M.D., 2003, Drought in a Bornean everwet rain forest. *Journal of Ecology*, **91**, pp. 467-474.

ROSSOW, W.B. and SCHIFFER, R.A., 1999, Advances in understanding clouds from ISCCP. *Bull. Amer. Meteor. Soc.*, **80**, pp. 27.

TUCKER, C.J., PINZON, J.E., BROWN, M.E., SLAYBACK, D., PAK, E.W., MAHONEY, R., VERMOTE, E. and EL SALEOUS, N., 2005, An Extended AVHRR 8-km NDVI Data Set Compatible with MODIS and SPOT Vegetation NDVI Data. *Int. J. Remote Sens.*, in press.

TRMM OBSERVATIONS OF THE PRECIPITATION AROUND THE HIMALAYAN REGION

B. C. BHATT*, **A. HIGUCHI**** **and K. NAKAMURA***
**Hydrospheric Atmospheric Research Center, Nagoya University*
***Center for Environmental Remote Sensing, ChibaUniversity*
bhatt@hyarc.nagoya-u.ac.jp

Abstract

The climatological features of the diurnal cycle of precipitation are investigated around the Himalayas by utilizing hourly, 0.05 deg. x 0.05 deg. gridded, precipitation data from the Tropical Rainfall Measuring Mission (TRMM) satellite for each meteorological season of the five-year period 1998-2002. The horizontal and vertical distribution of precipitation are investigated in the context of diurnal cycle. There is substantial seasonal and diurnal variation of precipitation over the southern slopes of the Himalayas. There is midnight-early morning peak of precipitation in the summer monsoon season. This peak migrates southward over the southern slopes of the Himalayas.

1. Introduction

It is generally said that atmospheric convection in the Himalayas and Tibetan Plateau plays an important role in sustaining the monsoon through the release of latent heat. Therefore, it is important to understand the variability of convective activities in this region. To the authors knowledge, precipitation regime has not been well studied around the Himalayas, where annual precipitation is as much as 300-400 cm over the southern slopes of the Nepal Himalayas (Shrestha 2000; Barros et al. 2000) and there appears strong variability over the diurnal cycle with nocturnal peak in rainfall during the summer monsoon season (Barros et al. 2003).

Ever since the launch of the Tropical Rainfall Measuring Mission (TRMM) in 1997, tremendous interest has arisen in the field of using these remotely sensed data to establish a global precipitation climatology. The non-synchronus orbit of TRMM has potential for documenting the diurnal cycle. The TRMM produces data from unique sensors like TRMM Microwave Imager (TMI) and Precipitation Radar (PR). TMI is a nine-channel passive microwave sensor desinged to provide quantitative rainfall information. The PR is capable of measuring the detailed, three-dimensional structure of precipitation with horizontal resolution of 4.3 km. The PR measurement has a very high accuracy, whether taken over land or ocean. More description of TRMM sensors can be found on Kummerow et al. 1998.

Here, we would like to demonstrate one of the remarkable precipitation characteristics observed by TRMM: the diurnal variation of rainfall. Areas of emphasis include: horizontal and vertical variation of the diurnal cycle of precipitation.

2. Data and Method

We mainly used PR products (e.g., PR2A25, PR2A23) to investigate precipitation distribution. The main data included are the attenuation-corrected radar reflectivity factor and near-surface rainfall rate. 'Near-surface rainfall rate' was accumulated and binned to hourly local times for the grid size of 0.05 deg. x

0.05 deg. for each meteorological season for the 5-year period 1998-2002. We adopted similar procedure for the radar reflectivity factor and storm height datasets. Additionally, we choose rainrate threshold of <=5 mm h^{-1}(120 mm day $^{-1}$) as light rain and >5 mm h^{-1} as moderate to heavy rain. This selection was based on the precipitation histogram tendency around the Himalayas. Refer to Bhatt and Nakamura, 2005 for more details.

3. Results and Discussion

3.1 Horizontal distribution

The spatial variability of storm height around the Himalayas is shown in Fig. 1a. It shows a difference of the peak (maximum) storm height between June-July-August (JJA) and March-April-May (MAM). Actual storm height used in our analysis is the top of the precipitation column above the ground level instead of mean sea level. There is an increase of peak storm height over the southern slopes of the Himalayas, and decrease over the northern Indian subcontinent and the Tibetan Plateau in the premonsoon season. These results suggest that there is significant difference among the storm height distribution over the Tibetan Plateau, northern Indian subcontinent and southern slopes of the Himalayas.

The storm height characteristics over the southern slopes of the Himalayas are unique. We next present area-averaged 3-hourly diurnal cycle of rainfall occurrence in three climatic divisions (refer Bhatt and Nakamura, 2005) over the Himalayas (Fig. 1b). These plots show normalized percentage of rainy grids in three climatic divisions of the Himalayas. An inspection of the diurnal cycle of precipitation reveals an afternoon maximum during the premonsoon season and midnight-early morning maximum during the summer monsoon season. Other noted features include: daytime peaks during September-October-November (SON) and December-January-February (DJF). As a unique feature, midnight-early morning southward progression of precipitation is noticed during JJA over the southern slopes of Himalayas.

3.2 Vertical distribution

As anticipated from our earlier discussion on horizontal variability, the vertical profiles of radar reflectivity factor could show relatively similar geographical variability over the Himalayas. We selected radar reflectivity factor data above the terrain and gridded for 0.05 deg. x 0.05 deg. over three climatic divisions of the Himalayas. Figure 2 shows the climatological diurnal cycle of the radar reflectivity factor and its vertical distribution averaged over the 82.5E-85.0E longitudinal belt during JJA. The white dashed contours represent the vertical velocity from GAME reanalysis dataset, which provide some idea on the upward motion. We observe, daytime northward migration of precipitation denoted by 'A' and midnight-early morning southward one denoted by 'B'. At the extreme high elevations, daytime precipitation cells are enhanced as denoted by 'C'. There is trailing stratiform precipitation in this region. The brightband altitude appears approximately at 5.5 km MSL. There is relatively deep but small precipitation system in the foothills of the Himalayas at 3-6 LT. We also studied the climatological diurnal cycle of radar reflectivity factor for MAM over the same region. We found that vertical profiles depicted isolated deeper precipitation cells (not shown) than in the summer monsoon season with no brightband. Overall, the analysis of precipitation does confirm substantial diurnal and seasonal variability.

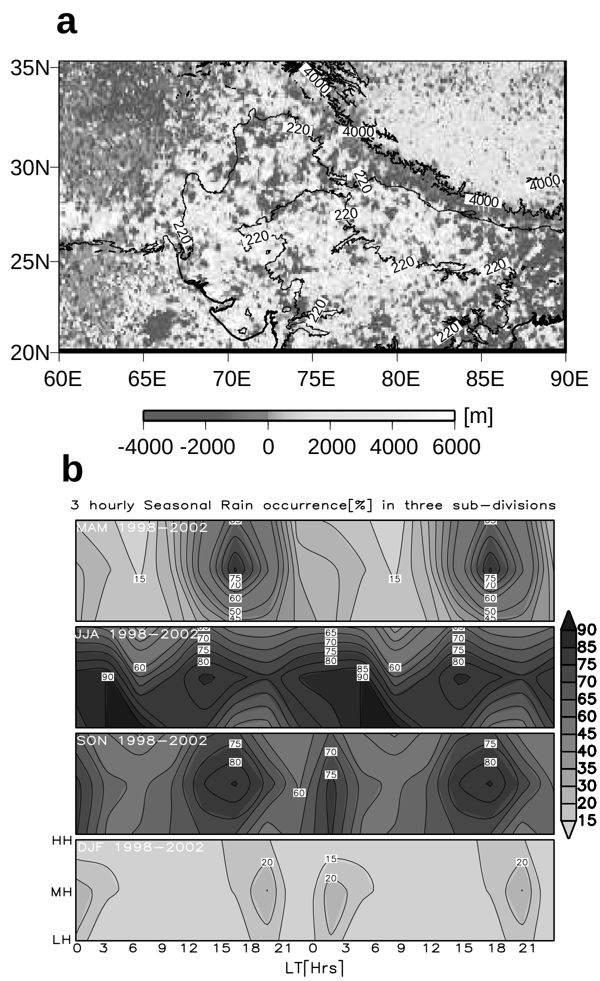

Figure 1: (a) Horizontal distribution of peak storm height difference between JJA and MAM. The topographic contours are also shown. (b) Areal representation of the seasonal variation of the diurnal cycle of rainfall occurrence in three climatic divisions over the Himalayas for eight time periods of a day. The LH, MH, HH in y-axis stand for the lower, middle and high Himalayas, respectively. See text for explanations.

4. Concluding Remarks

The climatological features of the diurnal cycle are investigated using high resolution PR data. An inspection of the diurnal cycle of precipitation appeared in PR observations reveals an afternoon maximum during the premonsoon season and midnight-early morning maximum during the summer monsoon season over the southern slopes of the Himalayas. Unlike the horizontal distribution of precipitation, the vertical distribution of precipitation shows almost similar geographical variability over the southern slopes of the Himalayas. The vertical profiles of the radar reflectivity factor reveals trailing stratiform precipitation regime over the southern slopes of the Himalayas in the summer monsoon season.

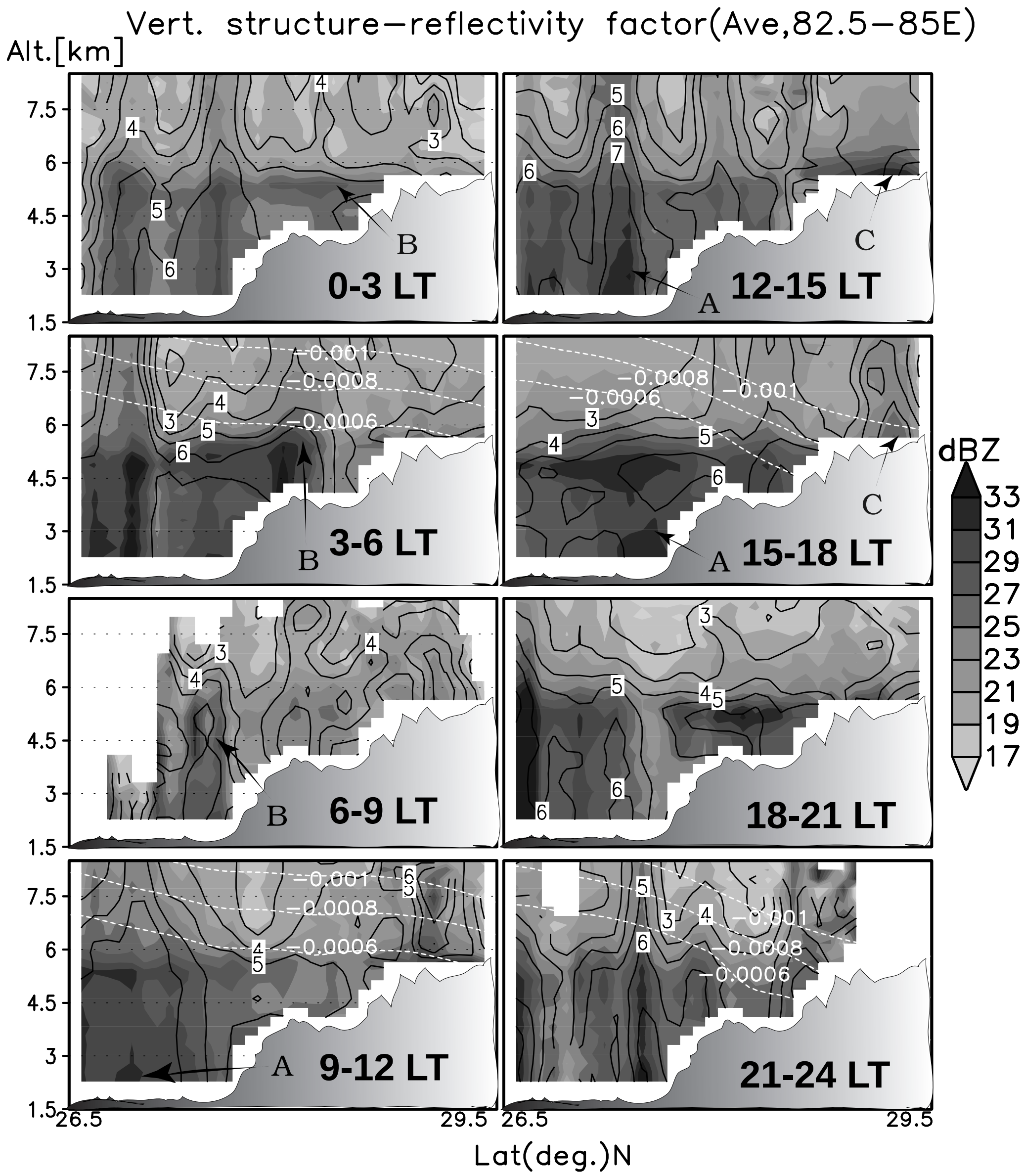

Figure 2: The diurnal variation of the vertical profiles of radar reflectivity factor averaged over 82.5°−85.0°E longitudinal belt from PR during JJA of 1998-2003. The solid contours represent standard deviation, label by label for each 250 km by 5 km segments from south to north. The white dashed contours represent climatological mean vertical velocity (m s^{-1}) averaged over 80°−85°E longitudinal belt from GAME reanalysis. For more explanations, refer to text.

References

[1] Barros A. P., Joshi M., Putkonen J. and Burbank D. W., 2000: A study of the 1999 monsoon rainfall in a mountainous region in central Nepal using TRMM products and rain gauge observations. *Geophy. Res. Lett.,* **27(22)**, 3683-3686.

[2] Barros, A. P., and T. Lang, 2003: Monitoring the monsoon in the Himalayas: Observations in central Nepal, June 2001. *Mon. Wea. Rev.,* **131**, 1408-1427.

[3] Bhatt, B. C., and K. Nakamura, 2005: Characteristics of monsoon rainfall around the Himalayas revealed by TRMM Precipitation Radar, *Mon. Wea. Rev.,* **133**, 149-165.

[4] Kummerow C., Barnes W., Kozu T., Shuie J. and Simpson J., 1998: The Tropical Rainfall Measuring Mission (TRMM) sensor package. *J. Atmos. Oceanic Technol.,* **15**, 809-816.

[5] Shrestha, M. L., 2000: Interannual variation of summer monsoon rainfall over Nepal and its relation to the southern osciallation index. *Meteor. Atmos. Phys.,* **75**, 21-28.

Comprehensive evaluation of Leaf Area Index estimated by several methods— LAI-2000, SunScan, Fish-eye, and littertrap —

Midori Kurata[1], G.A.Sanchez-Azofeifa[2], Wang Quan[1]*, Yoshitaka Kakubari[1]

[1] Faculty of Agriculture, Shizuoka University

E-mail: zoorin@agr.shizuoka.ac.jp

*E-mail: wangquan@agr.shizuoka.ac.jp

[2] Earth & Atmospheric Sciences University of Alberta,Canada

Abstract

The leaf area index (LAI), was estimated in mountaineous beech forest stands different estimation techniques. The effective LAI (Le) was estimated optically by measurements with the gap fraction instrument LAI-2000, SunScan, and Fish-eye. The aim of this study was to find out the most reliable estimation technique in mountaineous beech forest stands.

1. Introduction

Leaf Area Index (LAI) is a key biophysical variable influencing land surface processes such as photosynthesis, transpiration, and energy balance and is a required input for various ecological models. LAI is defined as the projected area of leaves per unit ground area. There are several techniques for estimating LAI. Remote sensing offers the possibility of providing relatively accurate estimations of LAI at a reasonable cost for most regional projects. However, remotely sensed vegetation indices at present need site- and stand-specific calibration against ground-based measurements of LAI and still do not yield suitable results for complex canopies such as forests with a high LAI. It is necessary to rely first on ground-based LAI estimates if remotely sensed vegetation indices need cross-calibration.

Direct and indirect methods are used to estimate LAI in the field. Direct methods mainly include destructive sampling, application of allometric equations based on tree diameters (and tree height), and leaf litter fall collection. On the other hand, LAI can also be estimated indirectly from the measurement of light transmission through plant canopies. This method takes use of a number of commercially available instruments, such as LAI-2000, DEMON, TRAC, hemispherical photography and so on.

The aim of this study is to establish a practical technique for LAI estimation suitable to mountaineous beech forest ecosystems.

Table 1 structural description of each sites

type	old-beech							mix-wood					young-beech	
site name	**1500k**	**1500y**	**1300y**	**900X3**	**700n2**	**600k**	**550k**	**1200y**	**1100y**	**900y**	**900X4**	**700n**	**900X1**	**900X5**
altitude (m)	1500	1500	1300	900	700	600	550	1200	1100	900	900	700	900	900
age of stands (yr)	300	300	300	150	200	250	260	250	250	250	150	200	70	85
†DBH (cm)	17.6	13.8	11.5	28.9	36.9	30.2	37.1	20.0	11.8	16.6	15.8	16.0	23.1	17.3
mean tree height (m)	22	20	20	22	30	27	34	20	19	31	21	31	21	21
stand density (trees ha-1)	450	229	250	383	361	433	246	539	625	535	829	425	1033	1400
basal area (m2/ha)	30	21	31	42	52	46	36	35	54	45	31	31	51	46
percent of *Fagus Crenata* (%)	71	72	86	59	82	74	86	33	38	41	28	31	94	74
	○	○	○	○			○		○	○		○		

† DBH, diameter at breast

○; destructive sampling were made in 1970s

Table 2 Mean and standard deviation values of LAI based on direct methods

type	old-beech							mix-wood					young-beech	
site name	**1500k**	**1500y**	**1300y**	**900X3**	**700n2**	**600k**	**550k**	**1200y**	**1100y**	**900y**	**900X4**	**700n**	**900X1**	**900X5**
altitude (m)	1500	1500	1300	900	700	600	550	1200	1100	900	900	700	900	900
allometric equation	3.6	2.3	3.1	4.9	6.1	5.5	4.6	3.6	5.3	5.4	4.5	3.8	7.4*	7.5*
litter collection	4.1	-	-	-	5.3	5.4	4.6	5.9	-	-	4.9	-	4.9	5.2
(standerd deviation)	0.7	-	-	-	0.4	0.7	0.7	0.9	-	-	0.6	-	0.2	0.7

* is calculated by Eq.(3), LAI of the other sites are calculated by Eq.(2).

2. Method

2.1 Study site

Measurements were made on the northern slope of the Naeba Mountain (2145m, 36° 51'N, 138° 41'N), located in southern Niigata Prefecture of the Japan Sea side of central Honshu in Japan. 14 sites (Table 1) were deployed along the altitude gradient from 550 to 1500m, the beech dominates the forest over range from 550m to 1550m. In all these sites, the canopy upper layers are consisted mainly by beech (*Fagus Crenata*) with occasional mixture of a small number of other species. These 14 sites are roughly categorised into 3 types by stand ages and the ratio of understory trees (old-beech, young-beech and mix-wood).

Seven sites of them are permanent sites (since 1960's) at different altitudes, as one of the IBP/PT programs (Table 1). Among these sites, destructive samplings were made for parameterising allometric at each altitude (see Table 3).

2.2 Estimating LAI by direct methods

2.2.1 litter collection

5-10 litter traps were set randomly at 8sites respectively (Table 2). And they were collected occasionally through the whole season. The traps had a circular area ($0.25m^2$) and were placed about 1 m above the ground. Collected litter was separated into leaves and other non-leafy materials such as branches. They were air dried out and weight. Some of each the collected litters were taken sampled for area and dry weight, which SLA is calculated as;

$$SLA = \Sigma A_i / \Sigma w_i \qquad (1)$$

where SLA is the specific leaf area, A_i is the one-sided projected area of the given leaf "i", and W_i is the dry weight of it. LAI was then calculated by multipulying SLA with the dry weight.

2.2.2 allometric aquation

The stand leaf area was estimated based on allometric correlations between leaf area and D^2H or $D\pi$. The allometric equation was as following ;

$$\log F = h \log (D^2H) + K \qquad (2)$$

$$F = 0.006 \times (D\pi)^2 + 0.4656 (D\pi) \qquad (3)$$

where F is the total leaf area of each tree, while, D is diameter at breast height and H is its tree height. *h* and *K* are fitted coefficients of the equation (Table 3). Then, summation of leaf area of all trees and devided is by the plot area to get LAI of each site. Eq.(2) is used for old-beech and mix-wood, while Eq.(3) is used for young-beech.

Table 3 Coefficients (h and K) of Eq.(2) used for the calculation of leaf area at different altitudes

Altitudes(m)	h	k	Sources
1500	0.656	-0.793	Kakubari *et al.* (1970)
1300	0.629	-0.684	Maruyama and Yamada (unpublished)
1100	0.709	-1.152	Kakubari (unpublished)
900	0.594	-0.466	Yamada and Maruyama (1962)
700	0.669	-0.852	Maruyama *et al.* (1970)

2.3 Estimating LAI by indirect methods

The effective LAI (LAIe) was estimated indirectly by using LAI-2000, SunScan, and Fish-eye. All of them are optical instruments, measuring radiation based on gap fraction and calculating LAI from the Beer-Lambert extinction law. LAI-2000 and SunScan measure both incoming radiation and transmitted through the canopy.

For both instruments, 10~25 sample points were set in each site. Measurements were made onetime at the peak of the growing season (August and September) in order to estimate the maximum PAI (Plant Area Index), and repeated again after leaf fall for WAI (Wood Area Index). Then LAI was calculated from the following equation ;

$$LAI = PAI - WAI \tag{4}$$

2.3.1 LAI-2000

The Plant Canopy Analyser, LAI-2000 (LI-COR Inc. , USA) uses a fish-eye light sensor to measure the diffuse radiation below 490nm. The simplest way is to measure below- and above-canopy radiation is to use two cross-calibrated sensors simultaneously. However, we have only one sensor to work with. Below- and above-canopy measurements were made with view caps of 22.5° and 90° . Although LAI-2000 is compact and easy to use in the dumpy forest, it requires a diffuse radiation environment which eventually determined by the weather condition.

2.3.2 SunScan

The SunScan Canopy Analysis System (Delta-T Devices Ltd, UK) measures the incident photosynthetic active radiation (PAR) above canopy and the transmitted PAR through the canopy. The SunScan probe can also be connected to a Beam Fraction Sensor (BFS) measuring both direct and diffuse incident radiation above the canopy and simultaneously connected to the common logger of the linear probe. In this way, it is available in all weather conditions. But in forest stands, the cable length becomes alimiting facter.

2.3.3 Fisheye

Hemispherical photograghs were taken in overcast sky condition by using digital cameras(COOLPIX990, 3.34 megapixels, Nikon) with Fisheye converter (FC-E8, Nikon). This method does not require above-canopy measurements. From the digital images, gap fraction and canopy openness were calculated by a specific software Hemiview (Delta-T Devices Ltd, UK). PAI and WAI were calculated by equation according to Norman and Campbell (1989).

3. Results and Discussion

3.1 Estimated LAI by direct methods

The relations between LAI estimated by the litter collection and by allometric equation are shown in Fig 1. For the

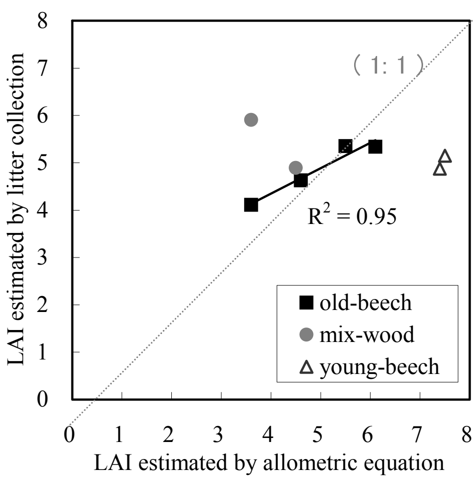

Fig. 1 Relationships between LAI estimated by allometric equation and by litter collection.The dotted line is 1:1

old-beech forest, the relationship was almost 1:1. However, big deviations were found for mixed and young beech forests. This may partly due to the less destructive samplings in these types. Moreover, the leaf fall from the understories in the mix-wood stands may contribute to the total leaf collection which finally level to the large LAI values in these stands.

One of the most reliable methods the LAI estimation is to collect leaves in litter traps as made in this study. And from the above result, allometric equation is also reliable if there are enough data and use that equation in similar stands.

In this study, LAI determined from litter collection was treated as true values, from which all other methods were compared and validated. The destructive sampling was made for sites with no litter traps, from which the estimated values then used as ground truth.

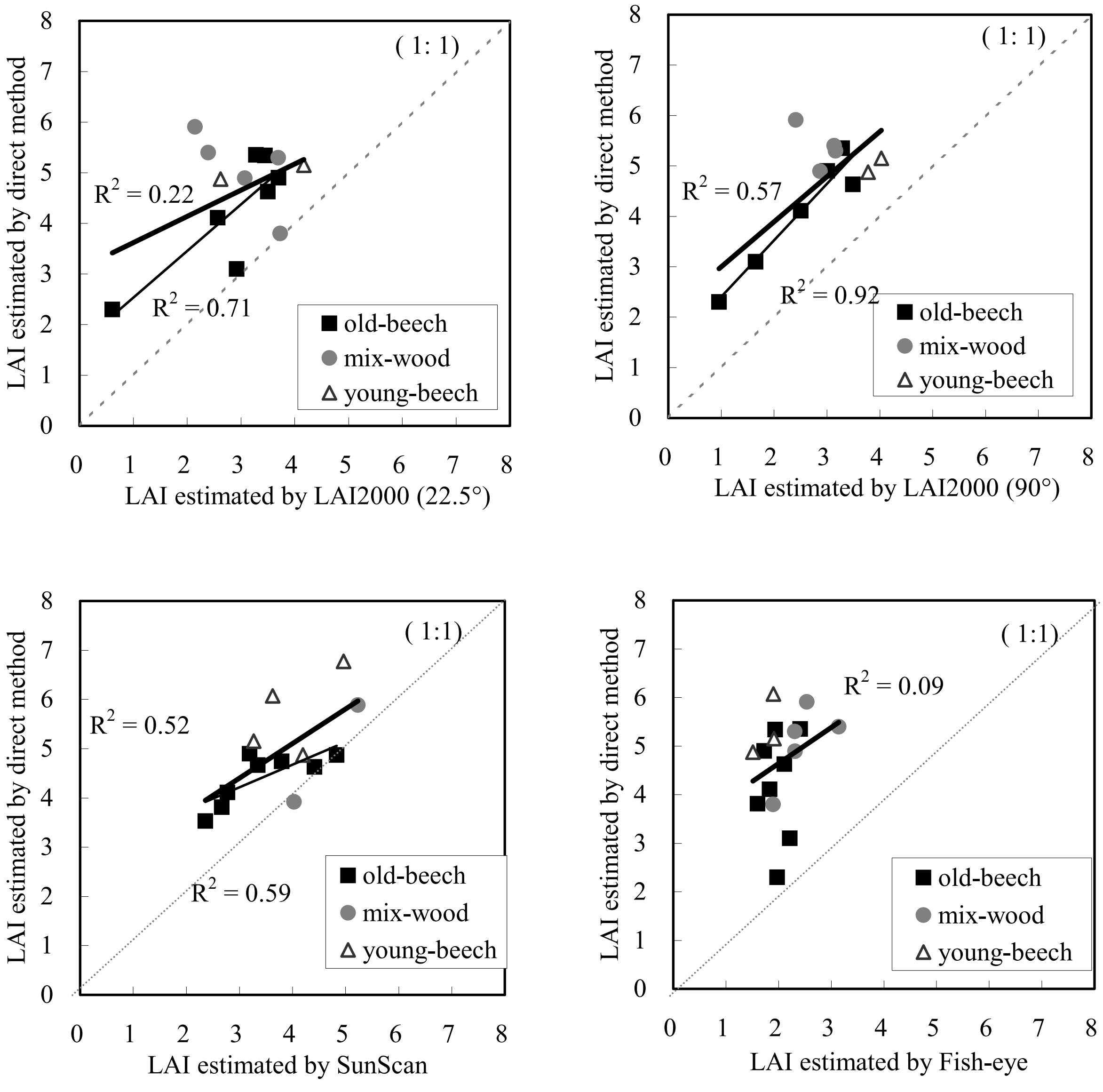

Fig. 2 Relationships between LAI based on direct methods and LAIe estimated by LAI-2000, SunScan and Fish-eye. Thick line shows the correlation of all samples, while thin line only for old-beech.

3.2 Estimated LAI by indirect methods

Fig. 2 shows the relationships between LAI based on direct methods and LAIe estimated by LAI-2000, SunScan and Fish-eye. Among these indirect methods, LAI-2000 has the strongest correlation with the direct estimated LAI, Especially for the LAIe from LAI-2000 with 90° view-cup. In this sense, wide field-of-view is much desired for the heterogeneous radiation environment as below canopy.

Although LAI-2000 estimated LAIe has strong linear relationship with the direct methods derived LAI, it was underestimated. Therefore, it needs connection before it can be used.

SunScan estimated LAIe of old-beech has the linear relationship to direct LAI, although in young-beech LAIe was underestimated.

LAIe estimated by Fisheye is saturated around LAIe =2. Classification of images involves using digital image process to distinguish canopy opening from foliage, which is achieved by determining a threshold intensity value.

4. Conclusion

We found that the method based on LAI-2000 was suitable for LAI estimation in mountain beech forests. And broad view angle is required for measuring. In addition, it usually underestimates LAI and thus needs conection before it can be used.

Although it is very portable, Fish-eye measuring requires more technique. SunScan is hard to use in the forest stands if the cable is connected to BFS. However, SunScn is resistant to weather changes and can keep measuring under versatile weather conditions.

Reference

Campbell GS. 1986. Extinction coefÆcients for radiation in plant canopies calculated using an ellipsoidal inclination angle distribution. Agricultural and Forest Meteorology 36, 317-321. sunscan

Norman JM, Campbell GS. 1989. Canopy structure. In: Pearcy RW, Ehleringer JR, Mooney HA, Rundel PW, eds. Plant physiological ecology: feld methods and instrumentation. London: Chapman and Hall, 301-325. hemiview

Applying the Remote Sensing in a Decision Support Tool for Food Security

Eleonora RUNTUNUWU, Fadlullah RAMADHANI, and Setyono HARI ADI
Indonesian Agroclimate and Hydrology Research Institute
Email: runtunuwu2001@yahoo.com

Abstract

One of the most significant challenges for improved the national food security programme is availability of timely, up-to-date, and accurate data for planners and decision makers. Such information needs to be available to concerned government official, regulators, donors, NGO and other interested organizations in a comprehensive, consistent, regular, and easy to understand format. This research attempts to (1) develop a food security database system included an analytics instrument to improve the quality of paddy field data using remote sensing and GIS technologies, (2) compute the food balance of each region using DSS model, and (3) design the web-based food security information system. Remote sensing (RS) technology and geographical information system (GIS) have been used to delineate the crop area for estimating paddy yield based on cropping areas and productivity. Integrating all kind of spatial, both image and vector as well tabular data in a database system, then transformed into information to enhance the knowledge based as a basis for decision making for food security are discussed in this paper.

1. Introduction

The concept of food security has developed over the past three decades. Concerns about food security up to the end of the 1970s were directed more at the national and international level, and concerned the ability of countries to secure adequate food supplies. Only later did the level of analysis shift to include a focus on food security at local level, even down to households and individuals (Young, *et al.,* 2001). In this paper, the food security was discussed for sub national level and it possible to scale up to national level.

In Indonesia, there are many institutions concerned in food security data, which each institution has own analytical tools and methods to determine the food security parameters; therefore, we often find a dissimilar published data for a same parameter such as the paddy field area of a certain province. In addition, it takes time for collecting the historical data from local until national levels; consequently, it is awfully difficult to access the real time food security information.

Therefore, this research attempts to develop an analytics instrument to improve the quality of paddy field data using remote sensing technology and geography information system. Integrating all kind of spatial, both image and vector with tabular data in a database system, then transformed into information to enhance the knowledge based as Decision Support System (DSS) model for food security are discussed in this paper. Although definitions of a DSS are abundant and varied, there is a basic consensus that a DSS must be a helpful system for decision makers (Freeland, 1999). In Choi *et al.* (2002) and Bohanec (2002), the decision support area has been defined as the development of approaches for applying information systems technology to increase the effectiveness of decision makers in situations where the computer can support and enhance human judgment in the performance of tasks that have elements which cannot be specified in advance. Several researches that utilized DSS in food security are Young (1998), Young *at al.* (2001), and Young (2001).

2. Data and methodology

The procedure began with collection and pre-processing of required digital image layers (Figure 1). The type of satellite imagery data used here is selected Landsat 7 ETM in planting time of 2002-2004 period. To allow the web-based food security information system development, the method was defined in three main steps (Figure 2).

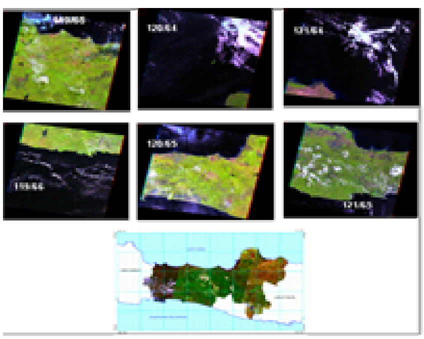

Figure 1. The path/row Landsat 7 ETM of study area

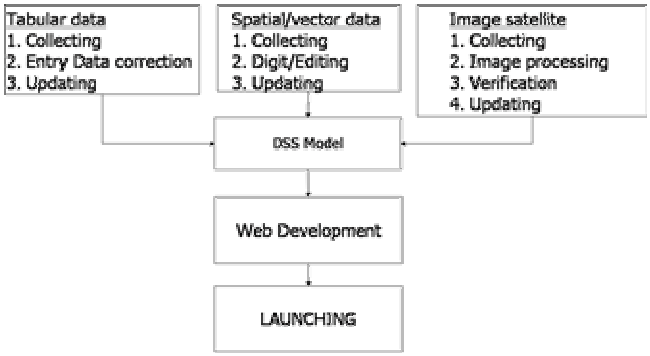

Figure 2. Schematic procedures used on this research.

The first is food security database system development. It included also the modified the quality of paddy field data by using RS technologies, Global Positioning System (GPS) and theodolite measurements. In this case, we found the relationship between the remote sensing to GPS as well to theodolite results using regression analysis. The samples were obtained from various classes of slope, there is: <8, 8-16, 16-45, and >45%. The relationships were then utilized to calculate the paddy field area in order to get more accuracy data.

The second step is development of DSS model to calculate the food balance of each region using the remote sensed paddy field as well the population data. The estimated paddy area (ha) was converted to rice yield (kg) – as supply – by multiplying it with productivity (kg/ha). The population data have been used to estimate the rice requirement of a certain district (as demand), Figure 3. by comparing the supply and demand data, the food balance could be identified (surplus, deficit or sufficient of each region. All these data and results were then designed in a web-based food security information system.

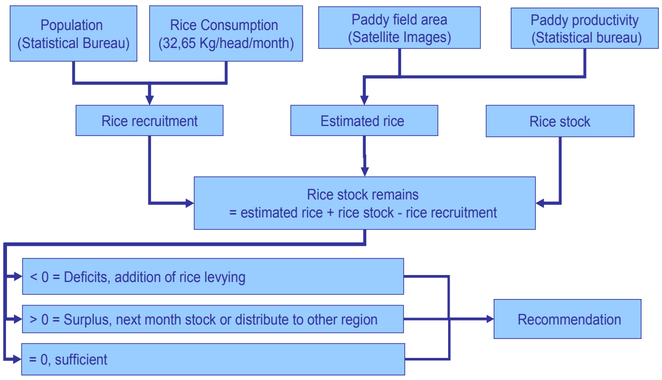

Figure 3. The DSS model to calculate the food balance

3. Result and Discussion

a. The food security database development

The first result of this research is food security database system on district level. The database can be divided into five main groups, are (i) Geographic data such as administrative boundary, road, river, etc; (ii) biophysics data such as, land use/land cover distribution; (iii) Food commodities data such as production, harvesting area, productivity, etc; (iv) Civilization and agriculture infrastructure data; and (v) Socio-economic data such as population; The feature of food security DSS model is strongly depended on quality and quantity of data input. All of those parameters is related each other and could be modified depend on technology and essential purpose in the future.

Beside developed the food security database system, this study tried to develop an analytics instrument to improve the quality of paddy field data using remote sensing and GIS technologies. The regression result of RS vs Theodolite and GPS vs theodolite are illustrated in Figure 4 and Table 1, respectively.

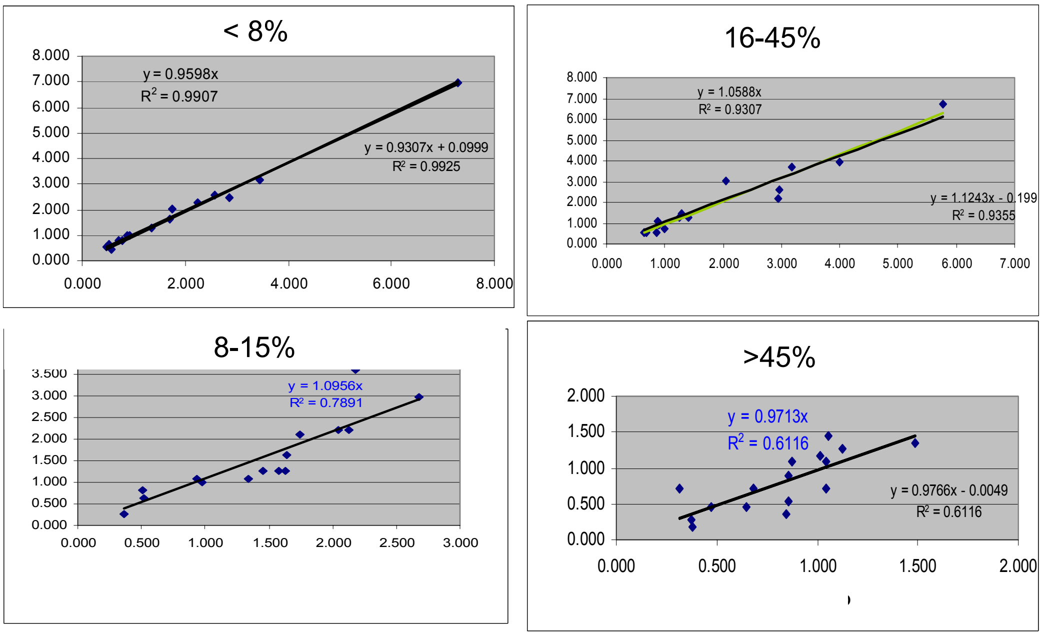

Figure 4. The regression analysis between RS and theodolite

Based on the Figure 4 and Table 1, the remote sensing technology using Landsat 7 ETM have been successfully used to estimate the paddy field area (range of R^2 is 60-99%) for all groups of slope (<8%, 8-16%, 16-45%, >45%). On the next analysis, we used the RS and theodolite relationship equation.

Table 1. The recapitulation of regression analysis: RS vs theodolite and GPS vs theodolite

No	Slope (%)	a constan		Corelation Coeficeint (R^2)	
		RS	GPS	RS	GPS
1.	< 8	0.9598	0.9667	0.9907	0.9874
2.	8 - 16	1.0956	1.1072	0.7891	0.8106
3.	16 - 45	0.9419	1.0588	0.9658	0.9307
4.	> 45	0.9713	0.9242	0.6116	0.7710

b. DSS model for food balance analysis

Figure 5 shows the one example of estimated the paddy field area in Sragen Distric of Central of Java Province for 4 phase of paddy growth (water, vegetative, generative, harvest phases). The area of each phase could be used to estimate the harvest area for one or two months later, and then were converted to paddy yield (as supply, for two months later. Table 2 shows some examples that the paddy field area have been converted to paddy yield (kg) by multiply the RS area (ha) to rice productivity (kg/ha) around 6000-7000 kg/ha depended of season and area.

The population data could be used to estimate the rice requirement as demand in food balance analysis. The DSS model, in this case, was focused on examine the rice stock recommendation of each district of each month. By applying the DSS model in Figure 3, the food condition in each district could be identified: surplus, sufficient, or deficit. This DSS is very useful for decision makers to make a decision. For deficit area, it has to increase the rice stock from other district; otherwise for the surplus area, it could be used for the next month stock or transfer to another district.

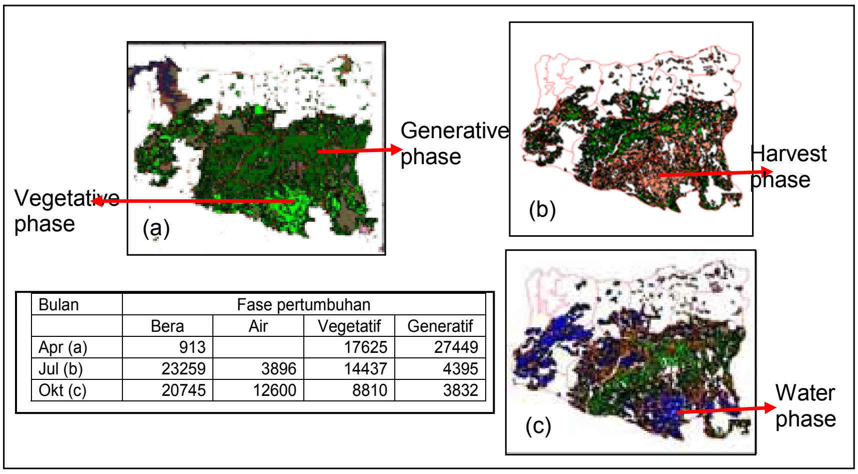

Bulan	Fase pertumbuhan			
	Bera	Air	Vegetatif	Generatif
Apr (a)	913		17625	27449
Jul (b)	23259	3896	14437	4395
Okt (c)	20745	12600	8810	3832

Figure 5. The analysis estimate of paddy field area on four phases of crop growth

Table 2. The area paddy area and estimated paddy field

NO	Location	Distric	Slope (%)	GPS (ha)	Theodolite (ha)	RS (ha)	Paddy yield (kg)
1	Dukuh Karya	Karawang	0-8	6.960	7.295	6.972	393.74
2	Karya Mulya	Karawang	0-8	2.456	2.865	2.477	143.85
3	Karang Jaya	Karawang	0-8	1.880	1.735	2.018	101.49
4	Pagadungan	Karawang	0-8	2.503	2.247	2.293	127.41
5	Ciranggon	Karawang	0-8	2.603	2.565	2.569	166.66
6	Campaka	Purwakarta	8-15	0.510	0.520	0.642	38.06
7	Cikumpay	Purwakarta	8-15	2.312	2.125	2.202	130.55
8	Nagri Tengah	Purwakarta	8-15	1.787	1.745	2.110	125.09
9	Sawah Kulon	Purwakarta	8-15	2.024	2.045	2.202	130.55
10	Pasawahan	Purwakarta	8-15	1.523	1.625	1.260	74.70
11	Kerta Mukti	Padalarang	16-45	2.272	2.055	3.060	181.41
12	Karang Layung	Padalarang	16-45	1.404	1.395	1.260	74.70
13	Babakan Sari I	Purwakarta	16-45	0.830	0.895	0.900	53.36
14	Sampay	Cianjur	16-45	1.341	1.255	1.260	74.70
15	Warung Jambe	Padalarang	16-45	2.308	2.945	2.160	128.06
16	Cikondang	Padalarang	>45	1.216	1.125	1.260	74.70
17	Babakan Sari II	Purwakarta	>45	0.281	0.375	0.270	16.01
18	Lingga Mukti I	Purwakarta	>45	0.593	0.645	0.450	26.68
19	Lingga Mukti II	Purwakarta	>45	0.425	0.475	0.450	26.68
20	Marga Asih	Padalarang	>45	0.516	0.685	0.720	42.69

c. Web based food security information system development

In order to deliver the food security information to numerous users, the system should be launched by using internet facility. Figure 6 shows the capture of web based food security information system. The system is user friendly, therefore, everybody will be able to access the information.

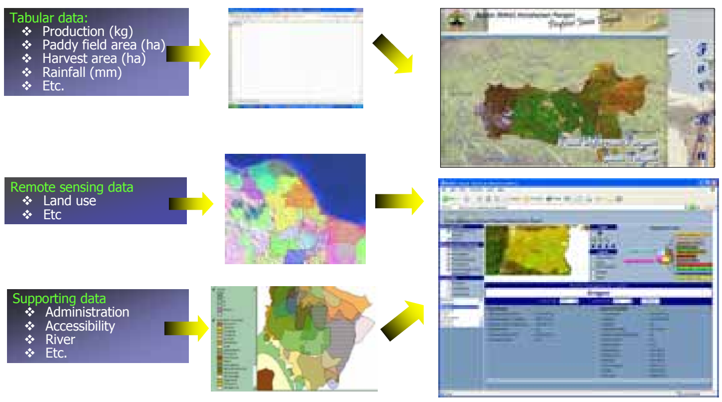

Figure 3. Illustration of food Security system information development

3. Conclusion

One of the most strategic challenges in Indonesia is how to achieve food security through optimization of the available resources. For this purpose, quantification of the characteristic of resources and the magnitude of events both spatially and temporally in the best quality and format is imperative. Satellite imagery with broad coverage and timely information can be fully utilized for multi purposes programs with multiple stakeholders to develop a decision tool.

Food security has to be achieved at national, local and household levels by securing the access to food by the population and to information by policy makers. The decision support system (DSS) for food security that has been developed for Central Java province was carried out in three main phases: i. e. (a) identify and develop required variable in the database such as demographical, statistical, satellite data, etc; (b) estimate paddy production of each district using high resolution images and compute food balance based on the supply and demand, and (c) design and operate the information delivery system to multiple users.

With the DSS the different variables and criteria commonly used by various institutions dealing with food security can be standardized. The utilization of multi-spectral and multi-temporal satellite imagery integrated in geographic information system as components of the DSS will facilitate the efforts of all the institution as well as minimizing the cost.

Furthermore, the DSS is very useful to formulate strategic policy in achieving food security; avoid duplication in program and budget; and develop monitoring system to ensure food availability. When expanded to cover national or regional level as ASEAN the system can promote inter-regional trade. Considering the different peak of harvest of rice crop (March in the southern hemisphere and November-December in the north), the trade will be mutually beneficial. The trade will provide the consumers with freshly produced food and minimize cost of storage as well as getting better price to the producers.

References

Bohanec, Marko, 2002, What is Decision Support?, Department of Intelligent systems, Jožef Stefan Institute, Ljubljana, Slovenia.

Choi, J Y, B. Engel, J. Harbor. 2002. GIS and Web-based DSS for Preliminary TMDL Development. In Total Maximum Daily Load (TMDL) Environmental Regulations: Proceedings of the ASAE Publication Number 701P0102, ed. Ali Saleh. March 11-13, 2002 Conference, (Fort Worth, Texas, USA) Publication Date March 11, 2002. Pp. 477-484

Freeland, N, 1999, Malawi: Review of food security information systems, Masdar Technology Ltd, UK.

Sean B. EOM, 2002, Decision support systems, Southeast Missouri State University, USA.

Young H, 1998, Food Security Assessment In Emergencies; Theory And Practice Of A Livelihoods Approach, Paper, London, UK.

Young, H, 2001, Food-security assessments in emergencies: a livelihoods approach, DS Print & ReDesign, Enfield, London.

Young H, S. Jaspars, R. Brown, J. Frize and H. Khogali, 2001. Food-security assessments in emergencies: a livelihoods approach. Network Humanitarian Practice Network (HPN). No 36. 40 pages.

The environmental problem of the Dead Sea using remote sensing and GIS techniques

Ahmad Al-Hanbali[*1], Hussam Al-Bilbisi[*2], and Akihiko Kondoh[*2]

[*1]Graduate School of Science and Technology, Chiba University, Yayoi 1-33, Inage, Chiba, 263-8522, Japan

[*2]Center of Environmental Remote Sensing, Chiba University, Yayoi 1-33, Inage, Chiba, 263-8522, Japan

E-mail: ahmad@graduate.chiba-u.jp

Abstract

The objectives of this research are to detect the changes of the areas of the Dead Sea (DS) surface water and evaporation ponds during the past 31 years, and to emphasize the effect of DS area changes on the surrounding groundwater body. A subset of each of the Landsat (MSS), Landsat (TM), and ASTER (VNIR), acquired in 1973, 1987 and 2004, respectively, were used in this study. By comparing only the DS area with the evaporation pond area in the last 31 years and with the aid of the GIS tools to represent the changes spatially, the evaporation pond area has increased from 32.5 km^2 in 1973 to 231.3 km^2 in 1987, and then reached to 244.6 km^2 in 2004. On the other hand, the DS area has declined from 922 km^2 in 1973 to 671.7 km^2 in 1987, and then to 641.3 km^2 in 2004. DS is hydraulically connected with the lower aquifer system of the surrounding groundwater basins. Thus, any drops in the DS water level will have a direct effect on the surrounding groundwater body, letting the groundwater to flow toward the DS due to its position at the lowest point on earth, therefore, causing for the shared countries to loose every year millions of cubic meters of water from its groundwater storage, which may create a serious environmental problem in the DS region.

Keywords: Dead Sea, Evaporation Pond, Change Detection, GIS, Groundwater

1. Introduction

Remote sensing provided valuable information that has a wide range of applications in water resources management. The monitoring of land use/cover changes over time has been widely used within the scientific communities. Land use/cover change detection using remote sensing and geographic information system (GIS) technologies were approved to be powerful tools for evaluating the environmental conditions and human activities in different ecosystems.

For more than 40 years Dead Sea (DS) (Figure 1) was facing an environmental problem due to the continuous drop of its sea level. During this period the amount of water which was used to flow into the DS was estimated to be 1980 million cubic meter per year (MCM/year), but due to the projects done by shared countries (Israel, Jordan, and Syria) in the DS catchment's area during the last 4 decades this amount was reduced to around 617 MCM/year. The largest amount of water resources consumption has been done by Israeli government by preventing about 500 MCM/year of lake Tiberias from flowing into the Jordan river which was considered the major source of feeding the DS, beside hundreds of MCM/year, which were diverted or dammed by the same country, coming from west side wadis near Jordan river and DS's west coast.

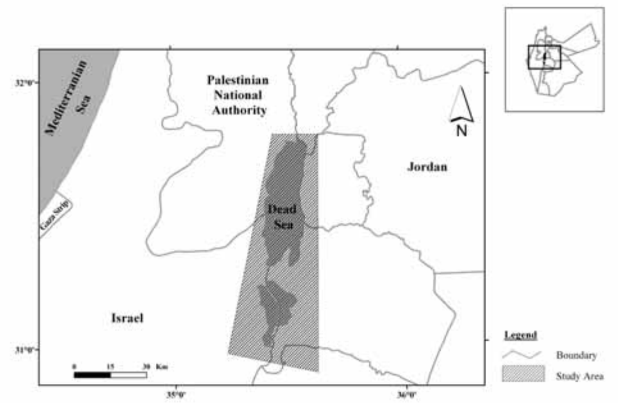

Figure 1. Location map of the study area

The 617 MCM/year mentioned earlier was still without taking into consideration the new dams, which were constructed in Jordan during the last 4 years such as Mujeb dam and Wala dam with capacities 35 MCM/year and 9 MCM/year, respectively. The 44 MCM/year of storage quantity of these new dams should be subtracted from 617 MCM/ year mentioned above to be 573 MCM/year.

DS was consisted of two parts the deep northern part with maximum depth 728m bsl and the shallow southern part with an average depth does not exceed 10m. A drop of more than 1000 MCM/year of water inflow into the DS was able to let the southern part of the DS to become dry, which was converted totally after that into a huge evaporation ponds used for industrial work to extract the valuable minerals such as potassium, magnesium, calcium, and bromine. This process is still making unbalancing of the DS's water resources by utilizing every year an average net amount of water around 300 MCM/year, which means that the net amount of water reaches the DS now is equal 273 MCM/year.

Landsat Multi-Spectral Scanner (MSS), acquired in January 1973, Landsat Thematic Mapper (TM), acquired in August 1987, and ASTER visible and near infrared radiometer (VNIR) image, acquired in September 2004, were employed for evaluating the land use/cover change in the DS region.

There are two main objectives of this study, the first one was to study the DS area change detection, and the second objective was to emphasize the effects of the changes of DS area on the surrounding groundwater body especially from Jordanian side.

2. Methodology:

2.1 Geometric Correction:

A subset of each of the Landsat Multi-Spectral Scanner (MSS), with 57 m spatial resolution, acquired in January 1973, Landsat Thematic Mapper (TM), with 28.5 m spatial resolution, acquired in August 1987, and ASTER visible and near infrared radiometer (VNIR) image, with 15 m spatial resolution acquired in September 2004 were used for evaluating land use/cover change detection of the DS region. The digital images were geometrically rectified to each other to facilitate their comparison, which was georeferenced to UTM map projection (Zone 36), and WGS84 ellipsoid. The resultant root mean square error (RMSE) was less than 0.5 pixels, indicating an excellent registration. The nearest neighbor resampling method was used to avoid altering the original pixel values of the image data.

2.2 Image Classification:

To map changes that had occurred between the three dates, Landsat MSS, TM, and ASTER images were individually used as input for supervised classification using maximum likelihood classifier. A modified version of Sato-Tateishi Land Cover Guideline (ST-LCG) (Sato and Tateishi, 2002) was adopted and used as a classification scheme design for this study. In total, five land use/cover classes were included in the scheme: urban, vegetation, water, evaporation pond, and bare land. The spatial distributions of all five classes were extracted from each of the land use/cover maps of 1973, 1987 and 2004 (Figure 2).

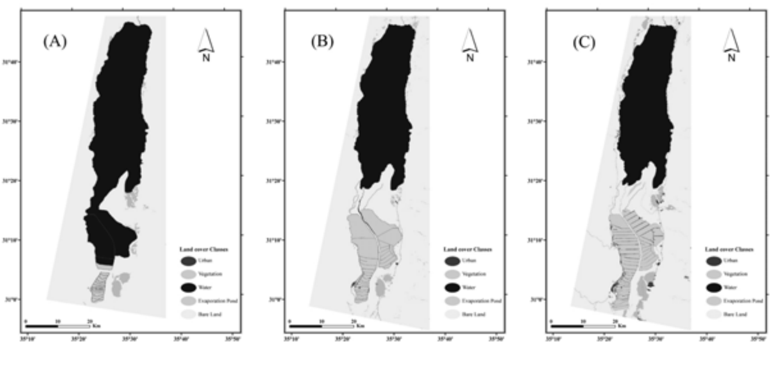

Figure 2. Land use/cover classification map of the Dead Sea region based on (A) analysis of Landsat MSS 1973 (B) Landsat TM 1987 (C) ASTER VNIR 2004

3. Results and Discussion:

3.1 Change Detection:

For this study, the post-classification comparison change detection approach was employed. Among the five land use/cover classes (Table 2); there are two major classes of interest in DS region: water and evaporation pond. Water class represents the DS water and a very small part of the Jordan River water, while the evaporation pond class represents all the evaporation ponds used by Potash companies in both sides, Jordan and Israel, for minerals extraction purpose.

Table (2) Land use/cover change for the studied area as extracted from the digital images

	1973		1987		2004	
Class	**Class Area (Km^2)**	**Class (%)**	**Class Area (Km^2)**	**Class (%)**	**Class Area (Km^2)**	**Class (%)**
Urban	8.8	0.3%	16.8	0.6%	40.4	1.5%
Vegetation	49.3	1.9%	40.0	1.5%	68.8	2.6%
Water	922.3	35.7%	678.9	25.3%	644.4	24.0%
Evaporation Pond	34.8	1.3%	233.7	8.7%	245.6	9.2%
Bare Land	1567.8	60.7%	1714.3	63.9%	1680.7	62.7%

By comparing only the DS area, where a significant change has occurred (Table 3), the results show that the DS area has a continuing decline. In 1973, there were 922 km^2 of the water-covered area declined to 671.7 km^2 by 1987, and then to 641.3 km^2 by 2004, thus representing a decrease of 30.1% in water-covered area between 1973 and 2004. On the other hand, the evaporation pond class has increased from 34.8 km^2 (or 1.3%) in 1973 to 233.7 km^2 (or 8.7%) in 1987, and then reached to 245.6 km^2 (or 9.2%) in 2004, thus representing an increment in the evaporation pond class is more than 7 times in land area.

Table (3) a comparison between the areas of the Dead Sea and Evaporation Pan as extracted from Land use/cover maps 1973, 1987, and 2004

	1973	1987	2004
Dead Sea area (Km^2)	922.0	671.7	641.3
Evaporation Pond area (Km^2)	34.8	233.7	245.6

The main reasons of DS declination, as mentioned in (section 1), was due to the reduction in the amount of water resources which was used to flow into the DS, since most of these water was diverted or dammed by the three shared countries (Jordan, Syria and Israel), and due to the usage of the DS water itself by Potash companies (at both sides of Jordan and Israel) for the extraction of its minerals.

For both classes of interest (water and evaporation pond) and by using the digital data of the three periods, with the aid of the GIS tools, the changes which have occurred in the DS were represented spatially during

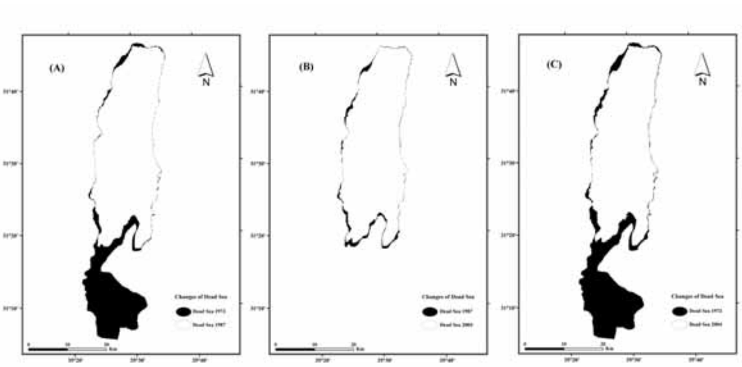

Figure (3) The spatial changes of the Dead Sea area (A) 1973-1987, (B) 1987-2004, and (C) Total changes 1973-2004

the periods (1973-1987), (1987-2004) and (1973-2004) as shown in (Figure 3). During these periods, it was clear that the changes have occurred in the southern and western parts of the DS region (Fig. 3B) due to the shallow depths in these regions.

In 1973 the evaporation pond was occupied only the end of the southern basin of the DS in the Israeli side, but during the period (1973–1987) when the southern part of the DS became dry, Israel expanded its industry and increased the number of evaporation ponds towards the north direction. In addition to that Jordan constructed the potash company and evaporation ponds at the end of 1970s, which means, the southern basin of the DS had been totally converted into an industrial area as shown in (Figure 4A). During the period from (1987–2004) both countries increased the number of evaporation ponds, Israel towards the southern direction and Jordan towards the northern direction of the evaporation ponds reaching by this its maximum area 244.6 km^2 as shown in (Figure 4B).

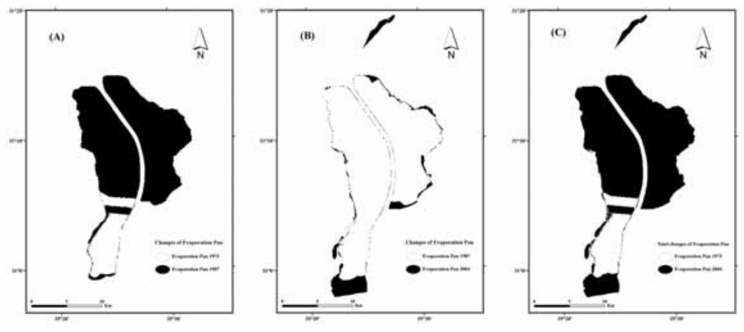

Figure (4) The spatial changes of the evaporation pan area (A) 1973-1987, (B) 1987-2004, and (C) Total changes 1973-2004

3.2 The effect of Land use/cover changes on the groundwater:

The land use/cover change detection showed how the DS was shrinking due to the decreasing in its water level, resulted from the reduction in the amount of surface water, which was used to feed the DS, beside with the utilizing of the DS water for mineral extraction. This is not only the apparent problem of the DS, but there is also another major problem due to the effects of this phenomenon on the surrounding groundwater body. Because the DS is hydraulically connected with lower aquifer system, which is composed of Kurnub/Zarqa aquifer and Ram/Disi aquifer especially from Jordanian side, the continuous decrease in the DS water level is causing an increase in the hydraulic head between the DS and the groundwater, which consequently, leading to continuous flow of groundwater toward the DS since the latter is the lowest point (Figure 5). Thus, flowing of groundwater from the surrounding lower aquifer toward the hyper-saline water of the DS is causing for the shared countries to loose every year millions of cubic meters of fresh water from its groundwater storage (Salameh and El-Naser, 2000, and JICA, 2001). For that reason more care should be taken into consideration to not let the DS water level decrease more, otherwise, the groundwater which is considered a major water supply for Jordan will be lost due to the intensive use of the DS water for industrial work, which may lead in the future to increase the water crisis in this region.

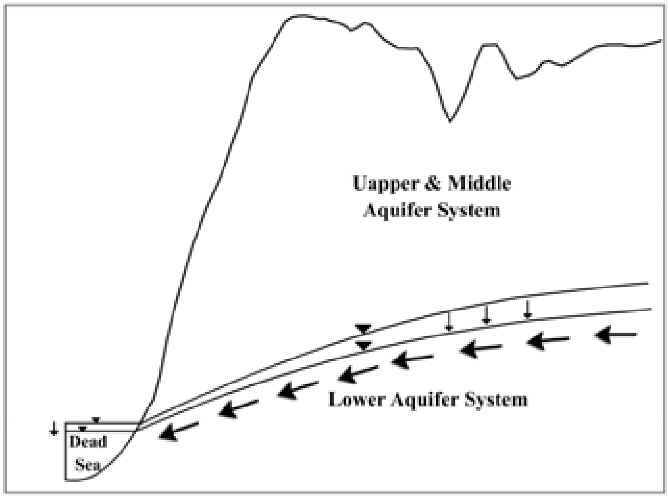

Figure 5. The continuous decrease of the DS water level is leading to increase the groundwater flow toward DS.

References:

1. JICA, 2001, The Study on Water Resources Management in the Hashemite Kingdom of Jordan, final report.
2. Salameh, E. and El-Naser, H. (2000): Changes in the Dead Sea level and their impacts on the surrounding groundwater bodies, Acta hydrochim. hydrobiol., 28, pp 24–33.
3. Sato, H. and Tateishi, R. (2002): Proposal for global land cover guideline legend based on FAO's LCCS, Asian Journal of Geoinformatics, vol. 3, No.2, December 2002, pp 35-46.

Experimental study on the effect of Cheong-gye stream restoration on urban environment

(Long-path measurement of atmospheric pollutant species with an obstruction flashlight)

Yohei Shiraki, Ippei Harada, Hiroaki Kuze

(Center for Environmental Remote Sensing, Chiba University)

Toshiaki Ichinose (National Institute for Environmental Studies)

Yingjiu Bai (Tohoku University of Community Service and Science)

1. Introduction

The expressway was dismantled in Seoul in July, 2003, and the municipal river (Cheong-gye stream) was restored in October, 2005. In this study, it is intended that the atmospheric pollutant data and the air temperature data are accumulated in the proof of the relaxation effect of the heat island phenomenon in Cheongecheon.

In the monitoring of atmospheric pollutant species such as NO_2, SO_2 and O_3, conventional point measurements at ground sampling sites lead to concentrations for local environments. It is also valuable to obtain additional information of regional concentrations measured over a certain distance, e.g., several hundred meters to several kilometers. Differential optical absorption spectroscopy (DOAS) in the visible and near-UV region is more suitable to monitor horizontally averaged concentrations of pollutants (Edner *et al*., 1993).

In the conventional long-path DOAS method, a continuously emitting light source is employed, and the source (or occasionally a retroreflector) is placed at a certain distance from the observation site. Then the combination of a monochromator and a detector such as a photomultiplier, photodiode arrays, or a charge-coupled device (CCD) serves to spectrally analyze the transmitted light. In the present paper the Center for Environmental Remote Sensing, Chiba University, reports a novel DOAS spectrometer based on a white flashlight source and a compact CCD spectrometer (Yoshii *et al*., 2003). The motivation of this study is to utilize white flashlights (obstruction lights) installed on tall constructions such as towers, bridges, and stacks for the DOAS measurement. Such white flashlights are widely used for the safety of aviation traffic in many countries. In Japan, it is mandatory for tall constructions (higher than 60m) to operate highly illuminant (more than 2×106cd) white flashlights during the daytime that are detectable in every direction from several kilometers away. Normally, xenon lamps are used for this purpose, giving a strobe emission every 1.5s. Compared with the conventional DOAS measurements, the advantage of the present scheme is evident; if one can find an appropriate obstruction light, as is the case in cities or industrial areas, the DOAS measurement can be carried out without bothering to prepare light sources. After transmission in the atmosphere, the spectral analysis is easily attained by use of a commercially available CCD spectrometer, which enables us to measure the spectrum of the pulsed signal.

Additional advantages associated with the present pulsed DOAS are as follows. First, the background from the sky radiation is easily subtracted because the spectra with and without the strobe flash are distinguished straightforwardly from the difference in the observed intensity. Second, simultaneous observation of several trace gas species is feasible if the relevant spectral features fall within the considered wavelength interval of the lamp and the CCD. Third, when the spectral intensity of the flashlight is known at the strobe site, the transmitted spectra bring about the information on the aerosol extinction along the optical path.

The purpose of this study is twofold. First, we compare the long-path result with the point data simultaneously measured at ground-based monitoring stations. Second, we analyze quantitative evaluation of the effect of Cheong-gye stream restoration on air quality.

2. Study area and Experiment

2.1 Study area

Seoul city is located in the northwest of Korea. The area of the city is 605.52km^2, and its population about 10,000,000 inhabitants. The topography of the study area is steep range of hills mountain land. In short, ups and downs of land are steep. The study area is around restored a cheong-gye stream in 1 October, 2005. The cheong-gye stream flowing from west to east in the city center of Seoul was an inner-city river with the length of 10.92 km joining to the Han-gang river.

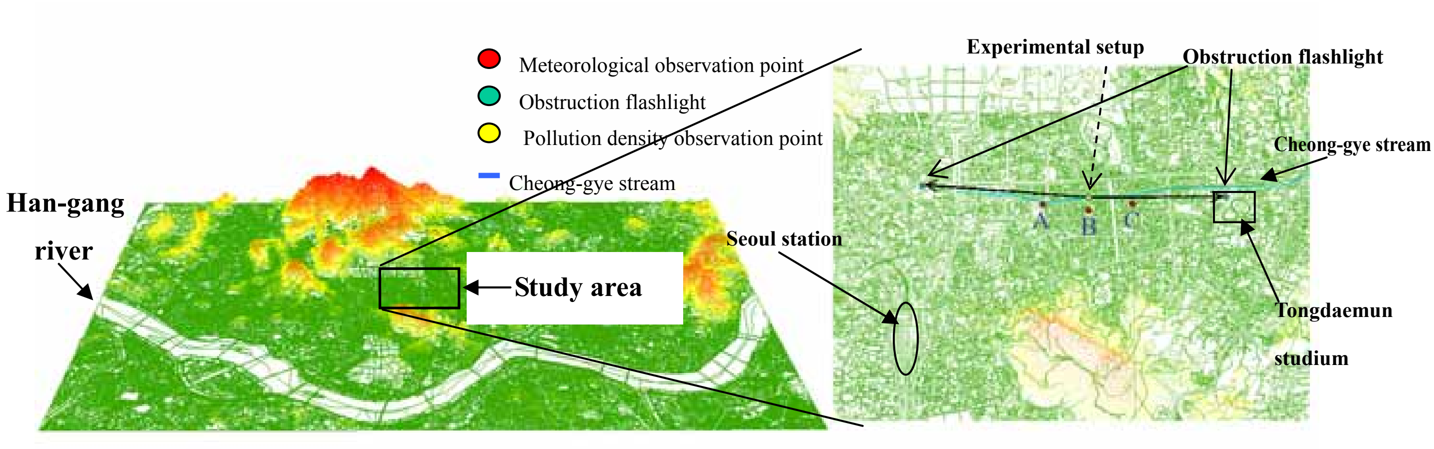

Fig. 1 Study area (Seoul city)

2.2 Experimental method

(a) Measurement of atmospheric pollution

Fig. 2 shows a schematic of the experimental setup. An astronomical telescope (Meade, DS-115), with an aperture diameter of 115 mm and a focal length of 910 mm, is employed to focus the image of a point light source located at a far distance. The image is formed near the eyepiece location (the eyepiece itself is removed from the telescope) where the entrance slit (1 mm high and 5 μm wide) of a CCD spectrometer (Ocean Optics, USB2000) is placed. The CCD consists of 2048 elements and is sensitive in a wavelength range of 200-800 nm, resulting in an average resolution of 0.3 nm/pixel. This CCD spectrometer is composed of a fixed grating and a linear CCD array with a mechanically stable, crossed Czerny-Turner design. No moving parts are incorporated, resulting in high reliability and compactness (89 mm wide × 63 mm deep × 34 mm high). The CCD gate duration is set at 300 ms in the experiment. Between successive gate periods, there exists a time lag of 7 ms, in which each spectral data is sent to a personal computer (PC) through the universal serial bus. The data acquisition can be attained successfully even when no trigger (synchronous with the flashlight) is applied to the CCD spectrometer, though this relatively long gate time as compared with the flashlight duration (about 0.5ms) causes somewhat increased amount of the background skylight. For the measurement in the center of Seoul, we made use of a xenon strobe install at the top of Doosan tower as a light source. The lamp height is about 160m above the ground level. According to the regulation, the light intensity is diminished at dusk and dawn, and during the nighttime blinking red lights replaces the flashlights. Thus, the DOAS measurement is limited to the daytime, around 7 a.m. to 6 a.m. during the summer and autumn. In the west direction 2.0km from the source, a DOAS system was installed in a Cheong-gye stream at Cheongae-3ga (Fig .1).

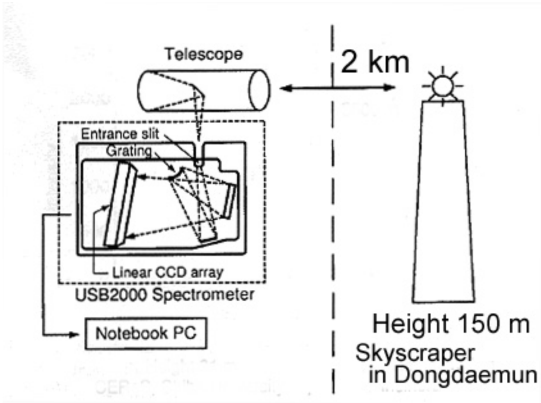

Fig. 2 Experimental setup for measuring NO_2

(b) Meteorological observation

In September 24th 2005, an observation data of air temperature at 19:30-20:30 was used in Cheongecheon. The goal of the observation was to know change in air temperature at sunset. All the observation points are on the paving of asphalt.

3. Result

3.1 Analisis of the DOAS spectrum

The quantitative analisis of trace compounds is based on Lambert Beer's law (e.g., Fuqi, 2005).

$$I_1 = I_0 \cdot \mathrm{e}^{-\alpha LC} \tag{1}$$

Here I_1 and I_0 denote the light intensity at a specific wavelength with and without absorption, respectively. In addition, α,L and C denote the absorption coefficient, the length of open path, and the mixing ratio of trace gas, respectively. Since the broad band absorption has little spectral structure, the DOAS technique only considers the narrow band structure. Therefore, for the derivation of concentrations, the differential cross sections ($\Delta\alpha$) over several wavelength channels are taken into account. The cross sections for the wavelengths (gases) of interest has been pre-recorded by the manufacturer and stored in the analyzer's memory. The strength of absorption for each trace gas however, varies as a function of wavelength. Thus, to optimize the detectibility of each gas for the DOAS system, wavelength region of the strongest absorption was selected and used for each gas such as: 265.7-304.4 (O_3), 280.7-319.3 (SO_2), and 406.2-444.2 nm (NO_2).

An example of this approach is shown in Fig. 3. that shows the two data spectrums compared in the analysis. In this case, we employ the DOAS spectrum on 28 September 2005 (9:35-9:40) as the clear-day spectrum. Then a spectrum observed on 29 September 2005 (16:00-17:00) is divided by the clear-day spectrum. The intensity of observed spectrum was very small, therefore the intensity of observed during 16:00 to 17:00 was performed integration. The difference in the bias level between the two spectra is ascribed mainly to the difference in the aerosol optical thickness.

Fig. 4 shows monthly average of NO_2 during January, 2001 to October, 2005. However, the air quality standards of NO_2 in Seoul is 0.05 ppm (the value of annual average); the value of NO_2 in Chongae 4 ga is more than 0.05 ppm during July 2003 to June 2005. The influence of construction is stronger than the influence of the autoexhaust. However, it is worth observing atmospheric pollutant species, since the value of NO_2 in Chongae 4 ga is low after restored a cheong-gye stream (October 2005).

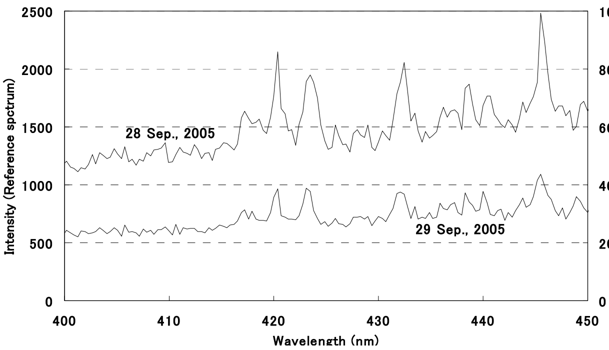

Fig. 3 Observed spectrum (28 September, 2005 16:00-17:00 JST) and reference spectrum (29 September, 2005 9:35-9:40 JST).

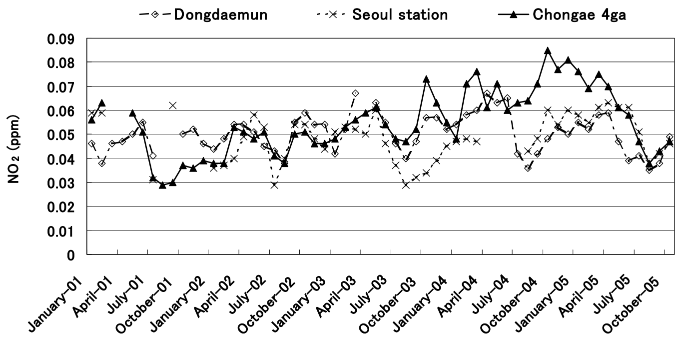

Fig.4 Monthly average of NO_2 around the road.

3.2 Relation of building form and air temperature

Fig. 5 (North-South) and Fig. 6 (East-West) show the change in air temperature obtained according to the air temperature measurements. At first the decreases in the air temperatures are seen in Cheongecheon according to Fig. 5. In general, there is relaxation effect of air temperature in the river, and away from the river, the air temperature tends to be high. Next, the air temperature of point A is the lowest according to Fig. 6. It is thought that the density in the building influences the air temperature.

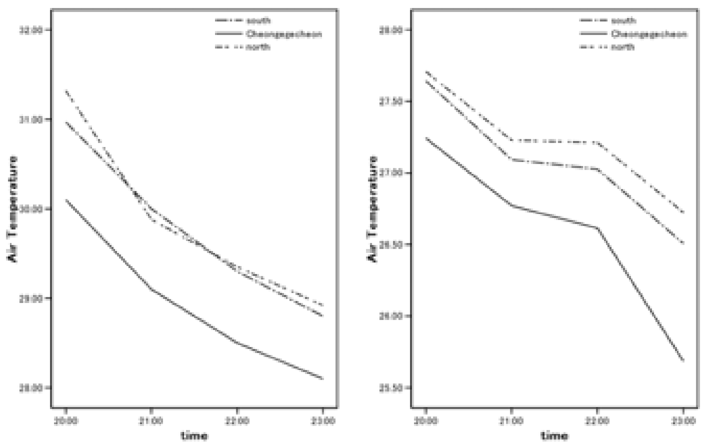

Fig. 5 Daily variation of air temperature (Left:2004, Right:2005) (North-South)

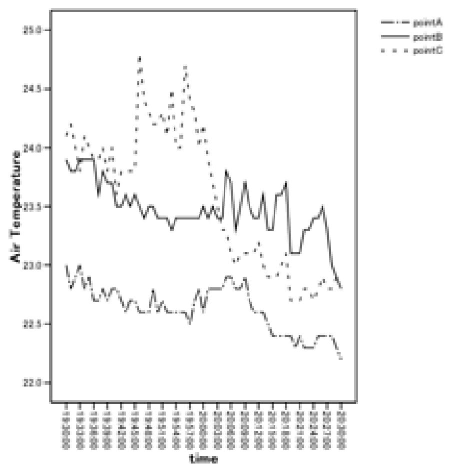

Fig. 6 Daily variation of air temperature (2005) (East-West)

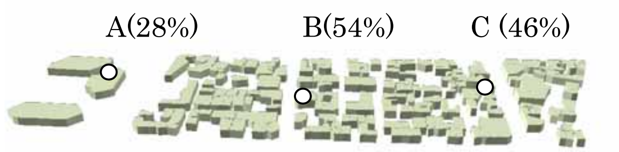

Fig. 7 Pattern diagrams of building (Density in the building of 120m in radius from observation point).

Radiant quantities R from the ground surface when there is an obstacle are shown by the next formula.

$$R = \sigma T^4 - \gamma\ \sigma T_1^4 - (1-\gamma)\Gamma\ \sigma T_\alpha^4 \quad \cdots (2)$$

Here, σ: Stefan constant, T: Ground surface temperature, T_1: Ground surface temperature of obstacle, T_a: Air temperature, Γ: The emission absorption quantity by the atmosphere and the emission absorption quantity by the planckian radiator ratio, γ: The spatial ratio which the obstacle occupies.

In addition, $0 < \gamma < 1$ and $0 < \Gamma < 1$ is. At the early morning of the city, it is thought $T_1 > Ta$ and $T > Ta$. If the value of R decreases, cooling rate of the ground level becomes small. As a result, ground surface temperature of the city becomes high in comparison with suburb. In addition, when altitude of the building is high, in order to reflect multiplex with the wall surface, the structure of the city is likely to be heated (e.g.Kawamura, 1964). In this study, it thought about the relation of the density of the building and the air temperature.

As a result, there is a proportional trend between the air temperature and the density in the building, in other words when the air temperature is high the density of the building is also high, and vice versa. It is necessary to investigate an accurate architectural form in order to examine the relation of a detailed architectural form with the air temperature in the future.

The atmospheric pollutant species observation and the meteorological observation in Seoul will be studied, and the relaxation effect of the heat island phenomenon of the municipal river will be clarified. Thus, it is possible to contribute to the creation of the municipal river and the promotion of maintenance in Asian cities.

References

KAWAMURA, T. (1964): Some prospect concerning component of city temperature in Kumagaya City, Geogr. Rev. Japan, 37, 560-564.

Edner, H., Ragnarson, P., Spannare, S., and Svanberg, S. (1993): Differential optical absorption spectroscopy (DOAS) system for urban atmospheric pollution monitoring, Applied, Optics, 32, 327-333.

Yoshii, Y., Kuze, H., Takeuchi, N. (2003): Long-path measurement of atmospheric NO2 with an obstruction flashlight and a charge coupled device spectrometer, Applied Optics, 42, 4362-4368.

Fuqi, S., Kuze, H., Yoshii, Y., Nemoto, M., Takeuchi, N., Kimura, T., Umekawa, T., Yoshida, T., Hioki, T., Tsutsui, T., and Kawasaki, M. (2005): Measurement of regional distribution of atmospheric NO_2 and aerosol particles with flashlight long-path optical monitoring, Atmospheric Environment, 39, 4959-4968.

Study the effect of green covering on the land value of Tokyo Metropolis using geographic information system (GIS)

Ippei Harada[1] and Akihiko Kondoh[2]

[1]Graduate school of Science and Technology, Chiba University (E-mail:ippei@graduate.chiba-u.jp)

[2]Center for Environmental Remote Sensing, Chiba University (E-mail:kondoh@faculty.chiba-u.jp)

Abstract

The city environmental element was extracted using Geographical Information System (GIS). The influence of the city environmental element was correlated with the formation of land values and analyzed using multiple linear regression analysis. Multiple linear regression analysis was used to analyze the factor of the green environmental impact on the formation of land value. It was not be able to explain the influence of the vegetation impact on the land value of the area through the meso-scale in 70km range from the center of Tokyo, but this influence was clarified through the area of a local scale within a radius of 4.4 km range from the city of Tokyo metropolis as considered one of the elements that the vegetation could influence the formation of land.

1. Introduction

1.1 Background

The urbanization around the center of Tokyo was expanded due to the increasing population of Tokyo region (Tokyo, Chiba prefecture, Saitama prefecture, Kanagawa prefecture). The housing establishment and city traffic have developed the suburbs which were before an agricultural land and mountainous area. The rapid expansion of Tokyo from the end of 1980s till the beginning of 1990s due to the impact of the economic bubble have increased the land and stock values, thus increased the problem of urban environment, and it is difficult to evaluate the effect of the expansion of Tokyo metropolis on the city environment.

A land price in a city is a comprehensive value which is controlled by many environmental and other related functions, local economical structure and their close interrelation. Moreover, it is an important factor to which the land value has specified the spatial pattern of various elements which constitute time and spatial change of an internal structure of city (Wakita, 1976).

Geographic Information System (GIS) and remote sensing technologies provide potential opportunities for quantifying and monitoring urban environments. For instance, medium resolution remote sensing data (e,g, Landsat Thematic Mapper) have been widely utilized in mapping urban land use and land cover through classification algorithms (Harris & Ventura, 1995 and Treitz *et al.*, 1992).

1.2 Purpose

The natural conditions of land specifications, such as convenience, comfortable nature, economical efficiency inhabitation or a production activity may determine the land value. The purpose of this research verifies whether a city consists of some various elements which the geographical feature and the green environment, are being reflected in a land value, in order to evaluate the expansion of Tokyo metropolis during the bubble economic term from the center of Tokyo to its suburbs.

2. DATA AND STUDY AREA

2.1 Data

(a) 10m Grid Land use of Metropolitan Area (in 1984 and 1994)

(b) Land classification map of 1:500000 scale (Chiba prefecture, Saitama prefecture, Tokyo prefecture, Kanagawa prefecture)

(c) Official announcement of land price in 1985 and 1997.

(d) 2 scenes of Landsat TM data acquired during daytime August 3rd, 1985 and July 19th, 1997（Path：107 / Row：35）

2.2 Study Area

Tokyo is the center of major activities and developments of Japan. The impacts of the changes took place in Tokyo was large even outside its periphery and that has resulted in the land value increase in the nearby prefectures also. These prefectures include parts of Tokyo metropolis, Chiba prefecture, Saitama Prefecture, and Kanagawa Prefecture.

Figure 1. Tokyo region

Table 1. Analyzed city

Analyzed city	Latitude	Longtitude	Altitude(m)
Kumagaya	36°06.8′	139°23.0′	30
Kuki	36°05.0′	139°38.4′	12
Hatoyama	35°58.2′	139°15.4′	44
Urawa	35°52.4′	139°35.4′	8
Koshigaya	35°53.4′	139°47.6′	5
Tokorozawa	35°46.2′	139°25.0′	119
Ome	35°47.2′	139°19.0′	155
Nerima	35°44.0′	139°40.2′	38
Hachioji	35°39.8′	139°19.2′	123
Fuchu	35°40.9′	139°29.2′	58
Tokyo(Otemachi)	35°41.2′	139°45.9′	7
Shinkiba	35°38.0′	139°50.5′	6
Abiko	35°52.5′	140°02.0′	20
Funabashi	35°43.7′	139°59.8′	24
Chiba	35°36.0′	140°06.4′	4
Kisarazu	35°22.5′	139°55.3′	5
Ebina	35°26.0′	139°23.2′	18
Yokohama	35°26.2′	139°39.4′	39

3. The analysis method

3.1 Land use/cover change in Tokyo metropolis

The extent of Tokyo metropolis is about 100 km and there are many cities existed also on the fringe of Tokyo. It is necessary to understand the land use change in Tokyo metropolitan area, in order to examine the influence of this change on the environment. 1984 and 1994 were selected since during this period the economic bubble has took place and there was serious change in the land use of Tokyo metropolitan area.

3.2 Extracted city environmental elements using GIS

(a) Relation between land value and spatial distance from Tokyo station

Wakita (1976) described that the negative correlation between a spatial distance and the land value is an index of the accessibility to the center of Tokyo metropolitan.

(b) Relation between land value and landform

Topography is a major natural factor that affects the valuation of residential lands because land surface properties are closely related to hazard vulnerability and amenities for human living. Supposed disaster damages especially those due to floods are evaluated as negative profits, resulting in the decline of the land value. The influence of topography on residential land value has been evaluated by deriving land value functions of which major explanatory variables are topographic and geographic attributes of each residential land. As a result, the land value of lowland was evaluated at about 85 % of that of upland (Mizutani, 2000).

The land price data were classified into four classes based on geographical features (lowland, upland, hilly land, reclaimed land). Using the land classification map of 1:50000 scale with the aid of GIS, a new factor of city environment was extracted

3.3 Relation between land value and green environment

Two Landsat TM data were used for the present study. Of these one was acquired before bubble economy period (August 3rd, 1985), and the other was after the bubble economy (July 19th, 1997). The vegetation indices were extracted based on the following equation (1).

$$NDVI = (NIR\ (TM\ band\ 4) - Red\ (TM\ band\ 3))\ /\ (NIR\ (TM\ band\ 4 - Red\ (TM\ band\ 3)) \quad (1)$$

The area where the value of NDVI was larger than 0.1 was assumed to be a vegetated region, therefore, the value (0.1) of NDVI was used generally as a threshold of the vegetation region and non-vegetation region (e.g. Kondoh, 2004). The ratio of green covering around the analytical point (within a radius of 4.4 km from the analytical point) was calculated. The average area of an administrative district in Tokyo metropolitan area becomes about 60 km^2, and corresponds to the area of the concentric circle of 4.4km in the radius that centers on the analyzed city.

3.4 Multiple linear regression analysis

The influence of the city environmental element was correlated with the formation of land values and it was analyzed using multiple linear regression analysis.

Regression equation that evaluates the effect of city environment onto the land value is indicated in equation (2):

$$P(z)=f\cdot(Z1+Z2+Z3+,\dots,+Zn) \quad (2)$$

Where, Z1 is the spatial distance from Tokyo station, Z2 is the spatial distance up to near station, Z3 is the building structure (reinforced concrete, steel framework, timbered), Z4 is the with or without of town gas, Z5 is the with or without Sewerage, Z6 is the with or without Water supply, Z7 is the land area, Z8 is the building coverage ratio, Z9 is the building capacity ratio, Z10 is the land form (hilly land, upland, lowland, reclaimed land) and Z11 is the green covering ratio.

Multiple linear regression analysis was used to analyze the factor of the green environmental impact on the formation of land value in 70 km range from the center of Tokyo (meso-scale) and in 4.4 km range from the city of Tokyo metropolis (local-scale).

Official announcement of land price data of the local scale was classified into four areas:

1. Nerima, Tokyo (Otemachi) and Shinkiba in Tokyo city area located within a radius of 20 km from Tokyo station.
2. Funabashi, Urawa, Koshigaya, Fuchu and Yokohama around Tokyo city area located within concentric circles of 20～30 km from Tokyo station.
3. Abiko, Chiba, Kisarazu and Tokorozawa in suburban 1 area located within concentric circles of 30～40 km from Tokyo station.
4. Kumagaya, Hatoyama, Kuki, Hachioji, Ome and Ebina in suburban 2 area located within concentric circles of 40～70 km from Tokyo station.

4. Results

4.1 Land use/cover change in Tokyo metropolis

The outskirts of Tokyo (Otemachi) which is the city center of Tokyo have a small change of land use. However, it is clear that change of land use is large in the area around Koshigaya and Urawa of Saitama Prefecture from northwest to northeast within a 40 km of the city center of Tokyo.

Land uses of mountain area and paddy field have decreased since the residential area and community facilities have increased from 1984 to 1994. Urbanization has progressed in the suburbs and it has grasped spatially that the city is expanded in a suburb from the center of Tokyo. However, the land use area of park and green space increased not only in the center of Tokyo but also in the suburbs.

Table 2. The percentage of changes of land use from 1984 to 1994

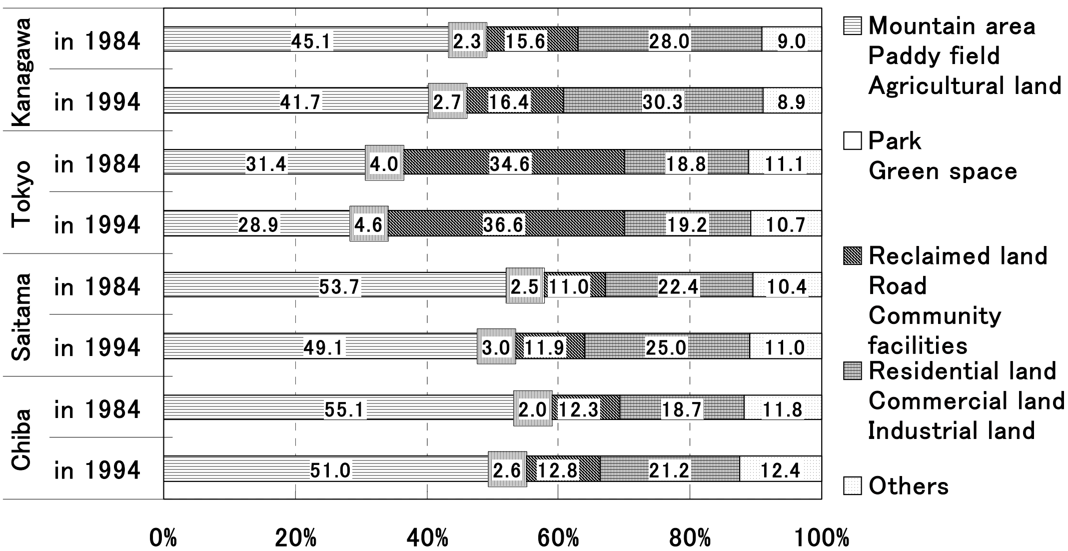

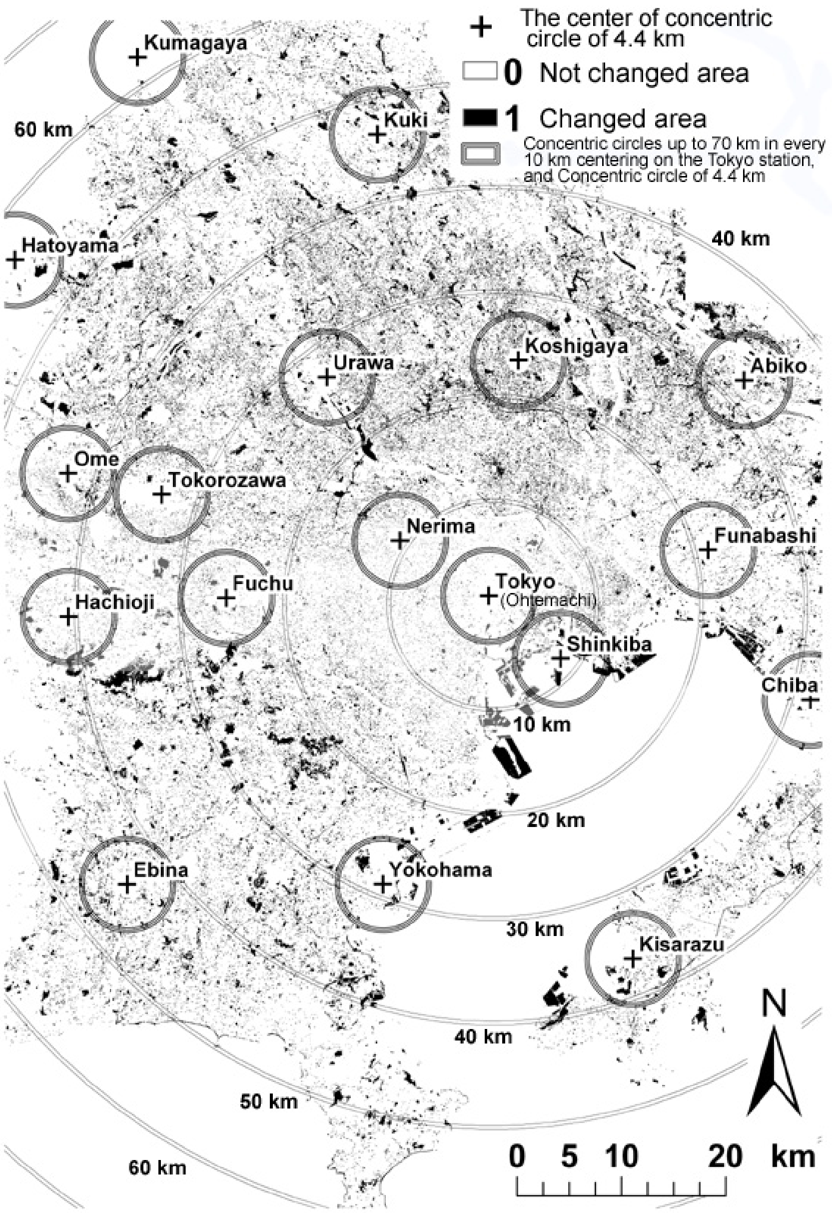

Fig 2. Land use change of Tokyo metropolitan during the period 1984-1994.

4.2 Multiple linear regression analysis

Table 3. Determining factors of land values by regression analysis of the meso-scale

Multiple linear regression analisis (Land value in 1984 and in 1997)		
Year	in 1985	in 1997
Explaining variable 1	Spatial distance from Tokyo station	Building capacity ratio
Explaining variable 2	Sewarage	Spatial distance from Tokyo station
Explaining variable 3	Spatial distance up to near station	Sewarage
Explaining variable 4	Land form (hillyland>upland>lowland>reclaimed land)	Spatial distance up to near station
Explaining variable 5	Town gas	Building structure (reinforced concrete>steel framework>timbered)
Explaining variable 6	Building coverage ratio	Land form (hillyland>upland>lowland>reclaimed land)
Explaining variable 7	Building structure (reinforced concrete>steel framework>timbered)	Building coverage ratio
Explaining variable 8	Building capacity ratio	Town gas
Explaining variable 9	Green covering ratio	Green covering ratio
Multiple correlation coefficient	0.81	0.92
Contribution ratio (%)	64.5	85.0

Table 4. Determining factors of land values by regression analysis of the local-scale

Multiple linear regression analisis (Land value in 1984 and in 1997)		
Year	in 1985 (Tokyo city)	in 1997 (Tokyo city)
Explaining variable 1	Spatial distance from Tokyo station	Building capacity ratio
Explaining variable 2	Green covering ratio	Spatial distance up to near station
Explaining variable 3	Building capacity ratio	Building structure
Explaining variable 4	Building coverage ratio	Green covering ratio
Explaining variable 5	Spatial distance up to near station	Land form
Explaining variable 6	Land area	Land area
Explaining variable 7	-	-
Explaining variable 8	-	-
Explaining variable 9	-	-
Multiple correlation coefficient	0.647	0.894
Contribution ratio (%)	28.3	79.5

Multiple linear regression analisis (Land value in 1984 and in 1997)		
Year	in 1985 (around Tokyo city)	in 1997 (around Tokyo city)
Explaining variable 1	Sewarage	Building capacity ratio
Explaining variable 2	Spatial distance up to near station	Spatial distance up to near station
Explaining variable 3	Green covering ratio	Green covering ratio
Explaining variable 4	Town gas	Sewarage
Explaining variable 5	-	Land form
Explaining variable 6	-	Building structure
Explaining variable 7	-	Building coverage ratio
Explaining variable 8	-	Town gas
Explaining variable 9	-	Spatial distance from Tokyo station
Multiple correlation coefficient	0.708	0.883
Contribution ratio (%)	48.6	77.4

Multiple linear regression analisis (Land value in 1984 and in 1997)		
Year	in 1985 (suburban 1)	in 1997 (suburban 1)
Explaining variable 1	Sewarage	Sewarage
Explaining variable 2	Spatial distance up to near station	Building capacity ratio
Explaining variable 3	Land form	Spatial distance up to near station
Explaining variable 4	Building structure	Green covering ratio
Explaining variable 5	Building capacity ratio	Spatial distance from Tokyo station
Explaining variable 6	Green covering ratio	Building structure
Explaining variable 7	-	Building coverage ratio
Explaining variable 8	-	Land form
Explaining variable 9		
Explaining variable 10	-	-
Multiple correlation coefficient	0.861	0.865
Contribution ratio (%)	71.4	73.6

Multiple linear regression analisis (Land value in 1984 and in 1997)		
Year	in 1985 (suburban 2)	in 1997 (suburban 2)
Explaining variable 1	Green covering ratio	Building capacity ratio
Explaining variable 2	Sewarage	Green covering ratio
Explaining variable 3	Spatial distance up to near station	Sewarage
Explaining variable 4	Land area	Building structure
Explaining variable 5	Building coverage ratio	Spatial distance up to near station
Explaining variable 6	Building structure	Spatial distance from Tokyo station
Explaining variable 7	Spatial distance from Tokyo station	Town gas
Explaining variable 8	Town gas	Land area
Explaining variable 9	-	Building coverage ratio
Explaining variable 10		Land form
Multiple correlation coefficient	0.842	0.868
Contribution ratio (%)	67.3	74.2

5. Conclusions

Multiple linear regression analysis was used to analyze the effect of the green environmental impact on the formation of land value. It was not be able to explain the influence of the vegetation impact on the land value of the area through the meso-scale in 70km range from the center of Tokyo, but this influence was clarified through the area of local scale in 4.4km range from the city of Tokyo metropolis as considered one of the elements that the vegetation could influence the formation of land value.

References

Harris, P.M. and Ventura, S.J. (1995): The integration of geographic data with remotely sensed imagery to improve classification in an urban area, *Photogrammetric engineering and remote sensing*, 61, 8993-8998.

Kondoh (2004): Vegetation and land cover change detection by global remote sensing and its causal analyses, *J.Japan soc. hydrol. & water resour*, 17(5), 459-467.

Mizutani, T. (2000): Statistical analysis of the influence of topographic factors on residential land value, *Transactions, Japanese geomorphological union*, 22(1), 43-58.

Treitz, P.M., Howarth, P.J. and Gong, P. (1992): Application of satellite and GIS technologies for land cover and land use mapping at rural-urban fringe, *Photogrammetric engineering and remote sensing*, 58, 4439-4448.

Wakita, T. (1976): *Land price formation in a Metropolis*, Taimeido, 164p.

The relationship between PAL NDVI and land use changes in semi-arid regions, China

Hajime OSADA[1*] and Akihiko KONDOH[2]

[1]Graduate School of Science and Technology, Chiba University,

[2]Center for Environmental Remote Sensing, Chiba University

*E-mail: osada_hajime@graduate.chiba-u.jp

Abstract

The land-cover or -use over the semi-arid regions, such as the Northeastern China, was rapidly changed in the last twenty years. To detect the environmental changes such as land use, the long term monitoring by the space-borne sensors is useful as a big heritage. The objective of this study is to detect the environmental changes of last twenty years by satellites and maps based on the local survey. We focused on the changes in the Northeastern China. A time series of the Pathfinder AVHRR Land data (PAL) was used for this study. Land use maps based on local survey, conducted 1980's and 1990's, were also used as evidences. Results ware summarized as follows: (1) NDVI was on the rising or roughly no changes in most areas . (2) High positive tendency of NDVI could express the land use change to cultivated land from grassland in this area. (3) The change pattern of NDVI is different depending on the pattern of land -cover or -use change. Satellites could detect the land use changes in local scale.

1. Introduction

The land-cover or -use over the semi-arid regions, such as the Northeastern China, was rapidly changed in the last twenty years. For example, the cultivated lands of Inner Mongolia autonomous region decreased by 15.4% from 1978 to 1987, while they increased by 22.1% from 1987 to 1996 (Yang and Li, 2000). This region has been desertification, induced by unsuitable land use, such as overcultivation, overgrazing of livestock, and excessive gathering of fuel wood (Zha and Gao, 1997). To explore suitable land use management or assessment, it is essential to monitor the environmental changes continuously in time.

To detect the environmental changes, the long term monitoring observed by the space-borne sensors is one of the important issues. Since operation of NOAA series satellites started in July 1981, the techniques to detect the global changes of vegetation and land cover have been developed. There are a lot of studies about the relationships between global changes of NDVI and climate factor, such as temperature, precipitation, and radiation (e.g. Nemani *et al.*, 2003, Yu

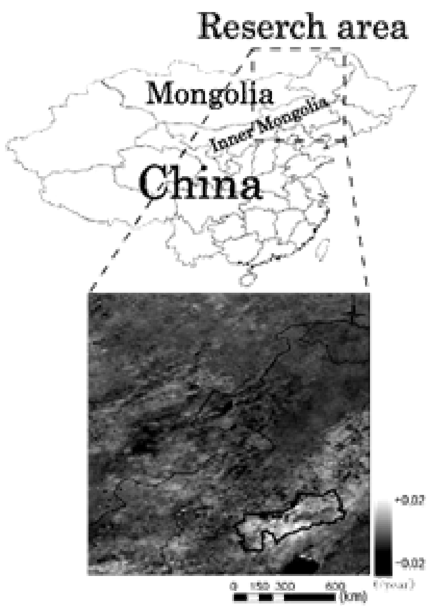

Figure 1 Research area and the distribution of linear trend of NDVImax. The area framed in by thick line is extracted as the area showing characteristic trend of rising.

et al., 2003, Kondoh *et al.*, 2002). To detect environmental changes, Kondoh (2004) adopted 5 indicators obtained by AVHRR data, as categorizing surface condition. He showed that the signal of environmental changes could be extracted by using the techniques in local scale. However, there are few studies to detect the environmental change by human activity in local scale. The objective of this study is to detect the environmental changes of last twenty years by satellites and maps based on the local survey in semi-arid regions in china.

2. Study area and method

2.1 Study area

Study area is located in the semi-arid regions, northeast part of China (110~125° E, 40~55° N) (Figure 1). Steppe grassland is extensive in this area. The average annual precipitation is about 200 ~ 500 mm.

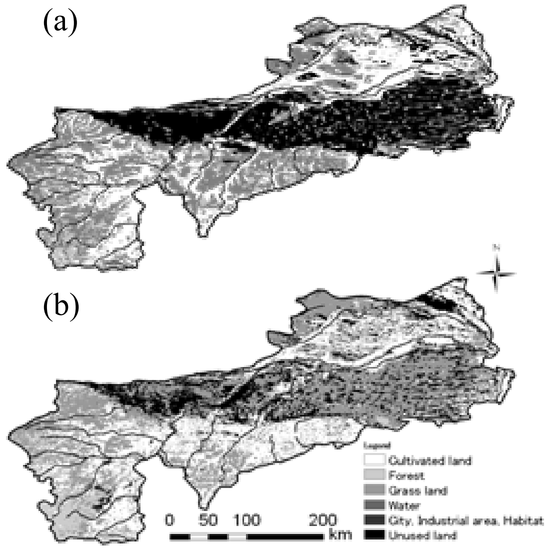

Figure 2 Land use map of 1980s (a) and later 1990s (b).

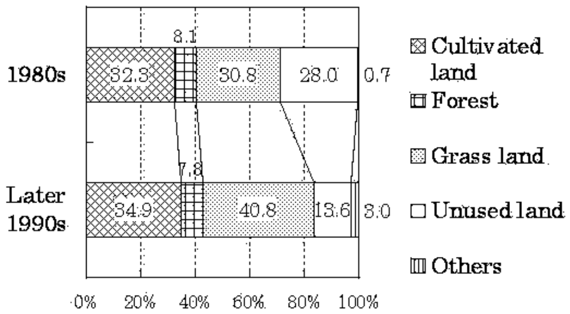

Figure 3 Composition of land use types, 1980s and late 1990s.

2.2 Pathfinder AVHRR Land Data

For this study, the 10-day composite Pathfinder Advance Very High Resolution Land data set (hereafter, PAL) was used. The period examined is from 1982 to 1999. NDVI (Normalized Difference Vegetation Index) was calculated from channel 1 and 2. Surface temperature calculated from channel 4 and 5 using sprit window method. The indicators for detecting environmental change are annual maximum value of NDVI (NDVImax), annual integrated value of NDVI (iNDVI), annual maximum temperature (Tmax), and annual slope of trajectory on Ts (surface temperature)-NDVI space (TRJ) (Nemani and Running, 1997). They were admitted the availability for detecting environmental changes (Kondoh , 2004).

2.3 Land use maps

Land use map of China, 1:1000000 and 1km mesh Land-use map of China were used for evidences of land-cover or change. The period covered of the former is from 1981 to 1987, and it was used as the data of 1980s. The period covered of the latter is from 1996 to 2000, and it was used as the data of later 1990s. Both maps are based on local survey. The names of the types in the two maps were different. They were classified into six types, such as cultivated land, forest, grassland, unused land (e.g. sandy land, sandy desert, and saline-alkali land), city-industrial area-habitat, and water.

2.4 Method

To extract the area through characteristic change, the linear trend of NDVImax of PAL is obtained from 1982 to 1999. In the area extracted by above mentioned, land-use or cover change based on the 2 land use maps was compared with the changing trend of each indicator.

3. Results and discussions

3.1 Long term change analysis in large scale

Figure 1 shows the linear trend of NDVImax in the whole study area. It shows that rising or roughly no change in most areas. Its rising may mean that annual production of vegetation in most areas. The characteristic signal that investigates increasing production of vegetation, was extracted in southeastern area of Inner Mongolia.

3.2 Land use change

Figure 2 shows the Comparison between the 1980s and the later 1990s. It indicates that the land use has been changed significantly in this area. In southeastern part in the area, large unused land changed to grassland. In south part of the area, grassland changed to cultivated land. Figure 3 shows the composition of the area of land use types in 1980s and later 1990s. The cultivated land increased by 10.0 %, and grassland decreased by 14.4 %. The change must indicate that large area of unused land turned into grassland.

3.3 Comparison of PAL data and land-cover changes

Figure 4 shows temporal changes of indicators in the area where changed grassland from unused land, and cultivated land from grassland. NDVImax is on the rise in both areas. The slope of linear regression, where changed cultivated land from grassland, is higher than where changed grassland from unused land. In the area changed cultivated land from grassland, iNDVI is also on the rising. But in the area changed grassland from unused land, iNDVI isn't on the rise on the after 1990, when it reaches at the maximal value in 1990. The change pattern of Tmax is similar in the 2 areas. The differences between the two areas is 5.2 ℃ in 1996 at the maximum value. It indicates that the differences of land cover produced the difference of temperature.

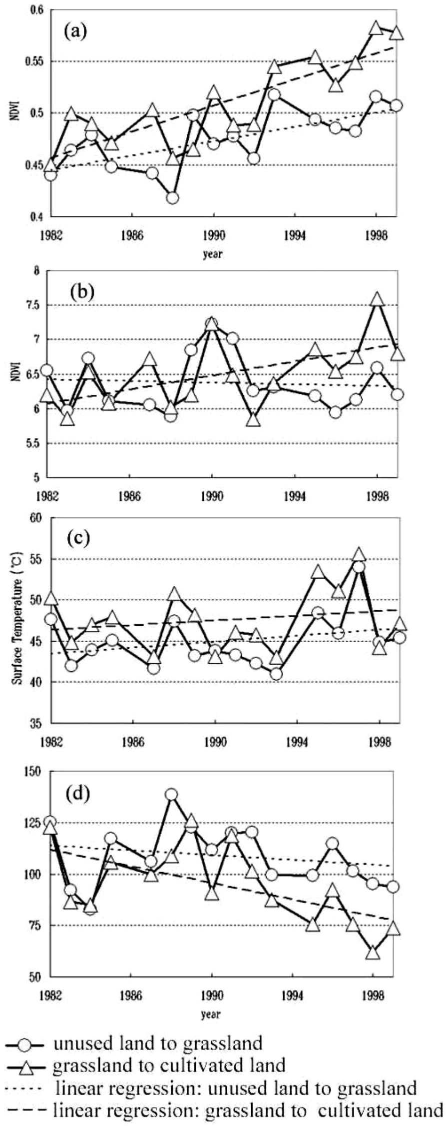

Figure 4 Temporal changes of indicators at the area where the land-cover changed (a): NDVImax. (b): iNDVI. (c): Tmax. (d): TRJ

Figure 5 shows Difference of the average value of indicators between 1982-1987 and 1996-1999. The signal of the change to cultivated land from grassland on south part could be extract by NDVImax, iNDVI, and TRJ. NDVImax corresponds best with the changes of land-cover in 4 indicators. In the area changed from unused land to grassland, the coincidence of a distribution with land-cover or -use change was not obtained. In the Tmax , non-random spatial patterns are obtained. But the distributions don't correspond to the change patterns of land-cover or -use changes.

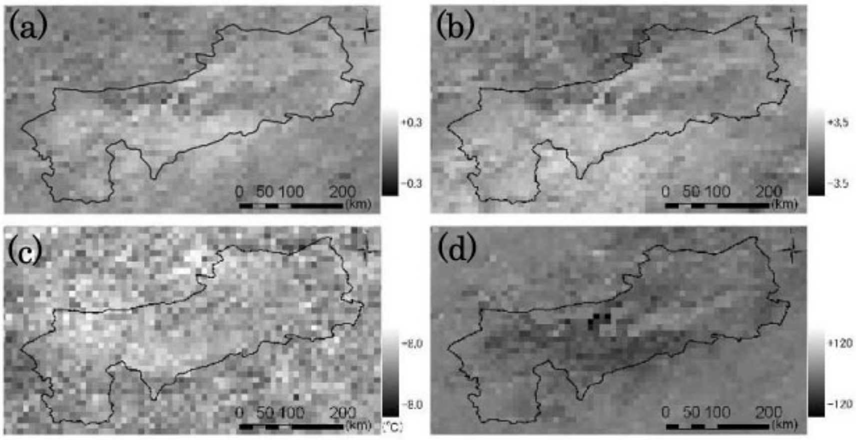

Figure 5 Difference of the average value of the indicators between 1982-1987 and 1996-1999. (a): NDVImax. (b): iNDVI. (c): Tmax. (d): TRJ. Positive value means increasing.

4. Conclusion

In this research, the area implied characteristic change was extracted by using PAL. The relationship between the indicators by using PAL and land-cover or -use changes, was examined in the extracted area. It is found that the change of land-use or cover can explain the some extracted signal of characteristic change by using PAL in local scale. The intensity of the environmental change signal is different depending on the pattern of land -cover or -use change. To detect the environmental changes in semi-arid regions, it is difficult to explain the land cover changes by using only the variation of NDVI. In the future, it is necessary to examine the relationship among the patterns of more detailed land covering changes, remote sensing data, and several causes of changes, such as human activity and climate-driven.

References

Zya, Y. and Gao, J. (1997), Characteristics of desertification and its rehabilitation in China, *Journal of Arid Environments*, **37**, 419-432.

Yu, F., Price, K. P., Ellis, J., and Shi, P. (2003), Response of seasonal vegetation development to climatic variations in eastern central Asia, *Remote Sensing of Environment*, **87**, 42-54.

Kondoh, A., Tateishi, K., Runtunuwu, E., and Park, J. (2002), Relating vegetation activity to climatic variation and atmospheric CO_2 content, *J.Japan Soc. Hydrol. & Water Resour.*, **15** (2), 128-138.

Kondoh, A., (2004), Vegetation and land cover change detection by global remote sensing and its causal analysis, *J.Japan Soc. Hydrol. & Water Resour.*, **17** (5), 459-467.

Nemani, R.R. and Running, S. W., (1997), Land cover characterization using red, near-IR, and thermal-IR data from NOAA/AVHRR, *Ecological Applications*, **7**, 79-90.

Nemani, R. R., Keeling, C. D., Hashimoto, H., Jolly, W. M., Piper, S. C., Tucker, C. J., Myneni, R. B., and Running, S. W., (2003), Climate-driven increases in global terrestrial net primary production from 1982 to 1999, *Science*, **300**, 1560-1563.

Yang, H. and Li, X., (2000), Cultivated land and food supply in China, *Land use policy*, **17**, 73-88.

The characteristics of water resources in XinJiang Uyghur Autonomous Region, China, using GIS and remote sensing

Dilnur Aji [1),] Akihiko Kondoh [2)]

[1)] Graduate School of Science and Technology, Chiba University

[2)] Center for Environmental Remote Sensing, Chiba University

Email: dilnuraji@graduate.chiba-u.jp and kondoh@faculty.chiba-u.jp

Abstract

Lakes and rivers are the most important water resources in XinJiang Uyghur Autonomous Region, China, since there are little precipitation and melted-snow water from high mountains, which are limited in summer season. This research describes the characteristics of water resources through analyzing the water area changes of main closed lakes using multi-temporal satellite data, and mapping the meteorological observations of the main rivers outflow for the past 50 years. Land cover change of Lake Ebnur region and its vicinity from 1972 to 2003 were analyzed by comparing the land cover classification images. As a result, some remarkable changes of water resources in XinJiang were produced. It is supposed that from 1950 until the second half of 1980, the changes of the water resources in XinJiang have been affected by human activities. On the contrary, from the second half of 1980 until present, the water resources have been affected by climatically fluctuation strongly. The detected land use /cover change of Lake Ebnur region from 1972 to 2003 shows that water area of the lake were governed by these changes.

Key words: water resources, satellite image, GIS, lake area, river outflow

1.Introduction

Satellite remote sensing and geographical information system (GIS) are useful techniques for monitoring the environmental changes at local, regional, and global scales.

In XinJiang Uyghur Autonomous Region, China, since the initiation of open policy in 1978, and especially in recent years, because of rapid economic development, water resources have drastically changed. Many researchers have engaged in environmental change studies in Xinjiang, and it have been thought that there is a lack of water resources since the population rate increases as well as the water resources decrease, beside with the climatic conditions becomes dry with time in XinJiang. Looking at the outflow of the rivers, the area of the lakes, and the land cover change around the Lake Ebnur region, we can see that the long time range is not always connected with the decreasing of water resources in XinJiang. In this research, the characteristics of water resources in XinJiang were discussed specifically . Multi-temporal satellite images covering some main closed lakes and meteorological observations of main rivers were used to analyze the changes of water resources. Water area changes of each lake were carried out by threshold method using the normalized difference vegetation index (NDVI).

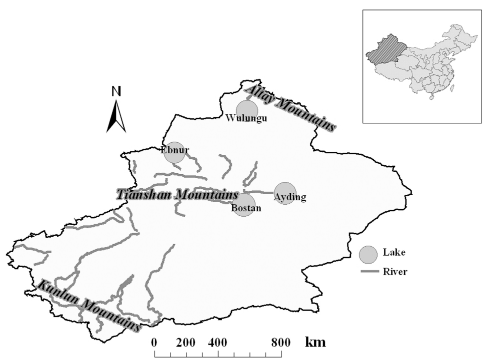

Fig.1 Lakes and rivers distribution in XinJiang

Meteorological observations were used for mapping the distribution of rivers outflow changes. Land cover change around the Lake Ebnur region from 1972 to 2003 was analyzed through comparing the land cover classification images. Climatically fluctuation was studied using CRU TS2. 0 data set, and World Climate Data. Finally, the main factors governing water resources were analyzed from both human and natural dimensions by adding the socio-economic statistical data.

2.Object area

XinJiang Uyghur Autonomous Region is located in Northwest of China between the range of 34°25′N~49°10′N, and 73°40′E~96°23′E, including 4 main closed lakes, which chosen for this study such as Lake Wulungu, Lake Bostan, and Lake Ayding, Lake Ebnur, and 26 rivers (Fig1), which have sustained agriculture production of XinJiang as the important water resources. The 4 closed lakes cultivated by each river, which flow into each lake from high mountains. Large delta used for agricultural land is formed in each river mouth.

3.Used data and Methodology

3.1 Data

In this study, multi-spectral image data, multi-temporal meteorological observations of main rivers outflow for the past 50 years, and multi-annual socio-economic statistical data are used as an input data for evaluating the characteristics of water resources in XinJiang, and land use land cover change for Lake Ebnur region.

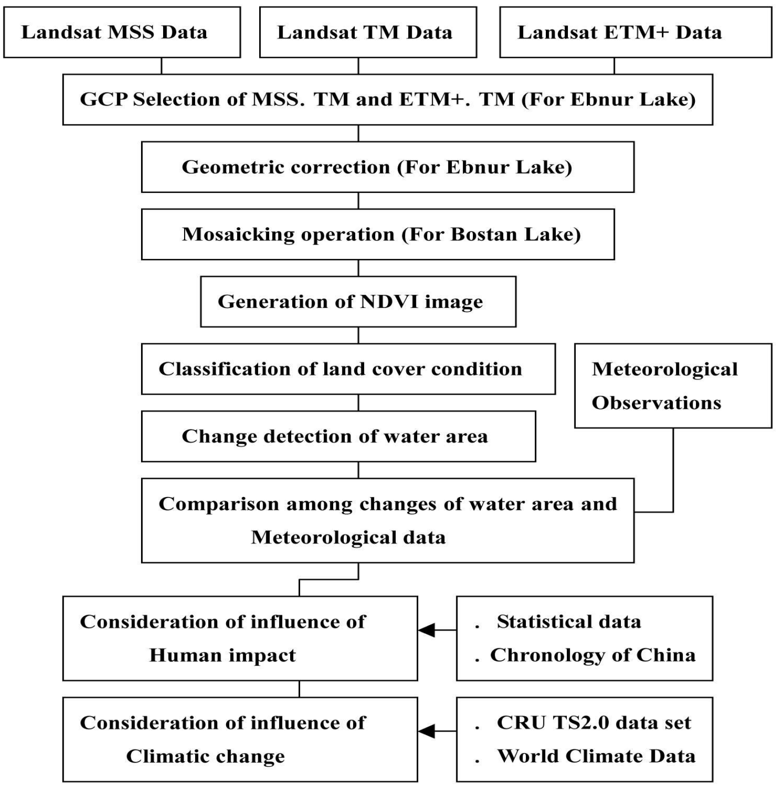

Fig.2 The flow of the analysis for water resources changes using time series satellite data, climatic data and other auxiliary sources

For analyzing the climatically change for study area, We extracted the precipitation and temperature data of XinJiang during the period 1951~2000 from CRU TS2. 0 data set, There are five variables supplied in CRU TS2. 0 data set, such as cloud cover, diurnal temperature rang, precipitation, and temperature, vapour pressure. The data is supplied on a 0.5-degree grid, covering the global land surface and supplied at a monthly time-step for 1901~2100. World Climate Data was used supplementing for after 1982, when the observational data cab be obtained.

3.2 Geometric Correction

A subset of each of the Landsat MSS digital images(1972, 1977), Landsat TM digital image(1990), and Landsat ETM+ digital image(2003), were used for evaluating water area change detection of Ebnur lake region. Only the TM and ETM+ images were used for another three lake regions. The digital images were geometrically calibrated to each other to facilitate their comparison for Ebnur lake region. The 1990 Landsat TM image, which was supplied by Earth Satellite Corporation, had already been rectified and georeferenced to UTM map projection (Zone 44), and WGS1984 ellipsoid. Then, this image was therefore employed as a reference scene to which the 1972 Landsat MSS scene, the 1977 Landsat MSS scene, and the 2003 Landsat ETM+ scene of Ebnur lake region were registered. Using image to image registration, the other 3 images (MSS of 1972, MSS of 1977, and ETM+ of 2003) were matched to the TM image with the total root mean square error (RMSE) of less than half-pixels. The nearest neighbor resampling method was used to avoid altering the original pixel values of the image data. The flow of data analysis is shown in Fig2.

3.3 Generation of NDVI image

Normalized difference vegetation index (NDVI) images was generated using visible and near-infrared bands of each satellite data as shown in the following equation:

$$NDVI=[(CH2-CH1)/(CH2+CH1)]\times a+b \qquad (1)$$

Where, CH2 is band 4 for both TM and ETM+ images, and CH1 is band 3 for the both images. For MSS images, band 7 was used as CH2, and band 5 as CH1. Land cover types of water, vegetation and another were discriminated with NDVI images by threshold method. Then, the water area was calculated of each lake region by multiplying the number of pixels and the area of each pixel together of each item. a and b are coefficients, and each of them was determined as 100.

3.4 Satellite image classification

To map changes of Ebnur lake region that had occurred between the four dates, Landsat MSS (1972, 1977), TM (1990) and ETM+ (2003) images were individually used as input for supervised classification purpose. Maximum likelihood classifier was employed to detect the land cover types. Land use map, which was published by the Chinese science publisher in 1990 with 1/1000000 scale, was used as an information data for classification.

3.5 Grid data differencing

To investigate the climatically changes in the second half of 1980s in XinJiang, the climate data during the period 1951~2000 was extracted from CRU TS2. 0 data set. This study was focused on the changes in precipitation and temperature in two periods in 1951~1990 and 1991~2000. To map the changes of precipitation and temperature between the two periods, grid data differencing was adopted for comparison and was performed on the generated dates of both periods. The differencing of precipitation and temperature were calculated as follows:

$$(1991\sim2000)-(1951\sim1990) \qquad (2)$$

4. Results and Discussions:

4.1 Water area of lakes

For this study, the changes in water area of each lake based on satellite data were extracted as shown in Fig3. The results show that the water area of each lake has a continuing growth from the end of 1980s. The area of lake Wulungu was increased to about 899km^2 in 2002 from 862km^2 in 1989(Fig3-A).

The water area of Lake Bostan was increased from about 980. 0 km^2 in 1990 to about 1230 . 2 km^2 in 2000(Fig3-B).

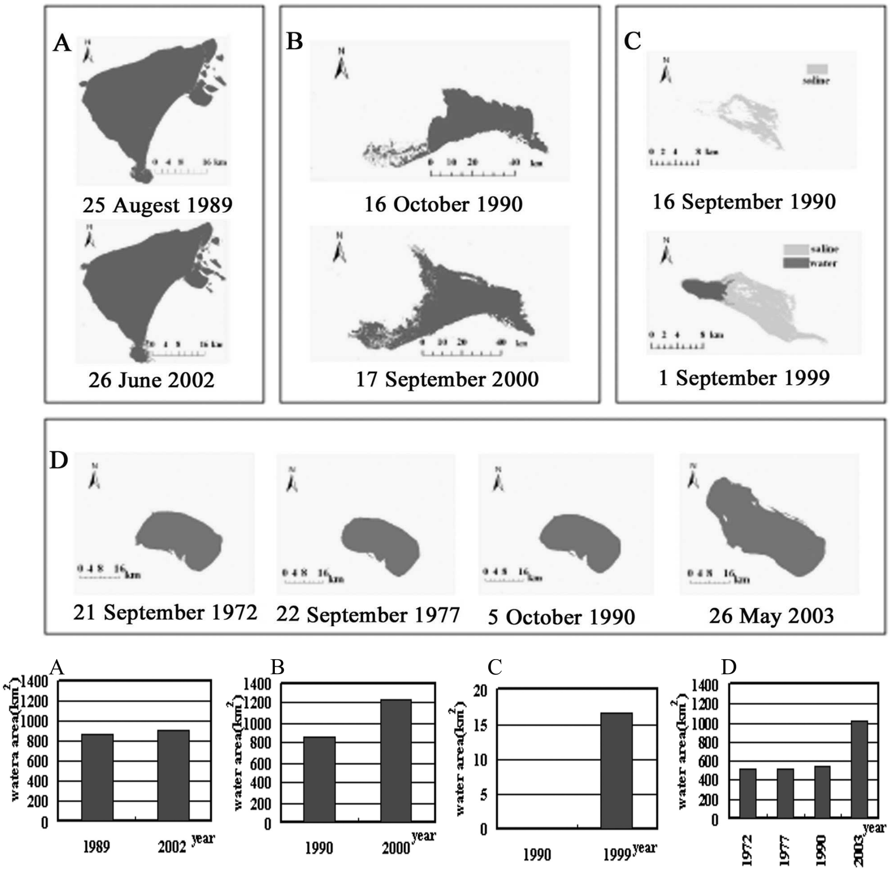

Fig.3 Change detection of water area of each lake

(A:Wulungu, B:Bostan, C:Ayding, D:Ebnur)

According to the previous investigation, the water area of Lake Ayding was about 152 km^2 in 1949, which was shrunk to about 22 km^2 in 1958. The result of this study shows that this lake was totally disappeared in 1990, and there was only about 34 km^2 of saline area around the lake. Then, the situation was changed for the same lake since its water area turned to increase about 16. 7 km^2 in 1999(Fig3-C).

By studying the Lake Ebnur area, it was found that the water area was 528. 2 km^2 in 1972, which decreased to 524. 8 km^2 in 1977, On the contrary, water area for the same lake has increased to 547. 6 km^2 in 1990, and then reached to 1029. 2 km^2 in 2003(Fig3-D).

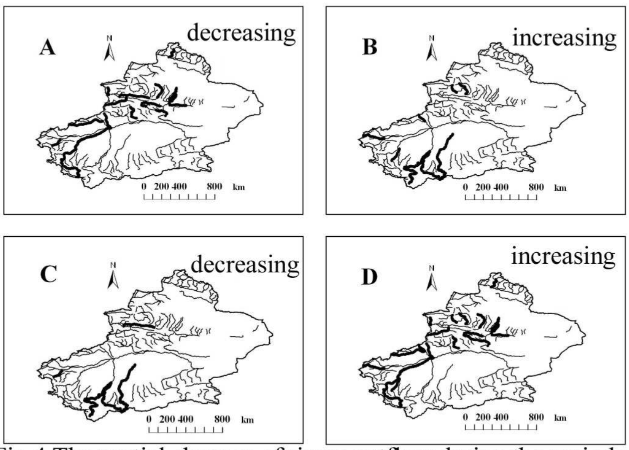

Fig.4 The spatial changes of rivers outflow during the periods 1956~1986(A,B) and 1987~2000(C,D)

4.2 Outflow changes of main rivers

By comparing the outflow changes of chosen main rivers in this study, it was found that the growth rate of these rivers outflow were –1. 6%, 5. 9%, and 7. 1%, in each period during 1956~1979, 1956~1986, and 1987~2000, respectively. It was shown that the water resources have a continuing increase in XinJiang after the second half of 1980. There were 65% of decreased rivers and 35% of increased rivers between the period of 1956~1986. Most of the decreasing processes were happened in north XinJiang, and most of the increasing processes were happened in south XinJiang in that period. On the contrary, there was a significant change, which has occurred during the period of 1987~2000, when the outflow of the 77% rivers have doubled, and the slight of outflow of the 23% rivers have decline. Remarkable increase was in north XinJiang and a slight decrease was in south XinJiang during the period of 1987~2000 as shown Fig4.

4.3 Change detection of land cover in Lake Ebnur region

There are four scenes of MSS (1972, 1977), TM (1990) and ETM+ (2003) images that include the Lake Ebnur region, and they were used for the post-classification change detection as shown in Fig5. Cultivated, and water, were the major land use/cover classes of interest in this study. Based on Fig5, cultivated area has a continuing increase, which increased from 54. 2 km^2 in 1972 to 127. 3 km^2 in 1977, to 267. 2 km^2 in 1990, and then to 734. 4 km^2 in 2003 for the studied area of Lake Ebnur region. The water class has also showed a significant change in this area. In 1972, there were 528. 2 km^2 of water area (or 12%), which declined to 524. 8 km^2 (or 11. 9%) by 1977(Table1). On the contrary, the water area has increased in 1990 from 547. 6 km^2 (or 12. 4%) to 1029. 2 km^2 (or 23. 4%) in 2003, which means, the water area changes of Lake Ebnur were governed by cultivated changes from 1972 to 1990. After 1990, water area has doubled without regard to even the growth of cultivated area.

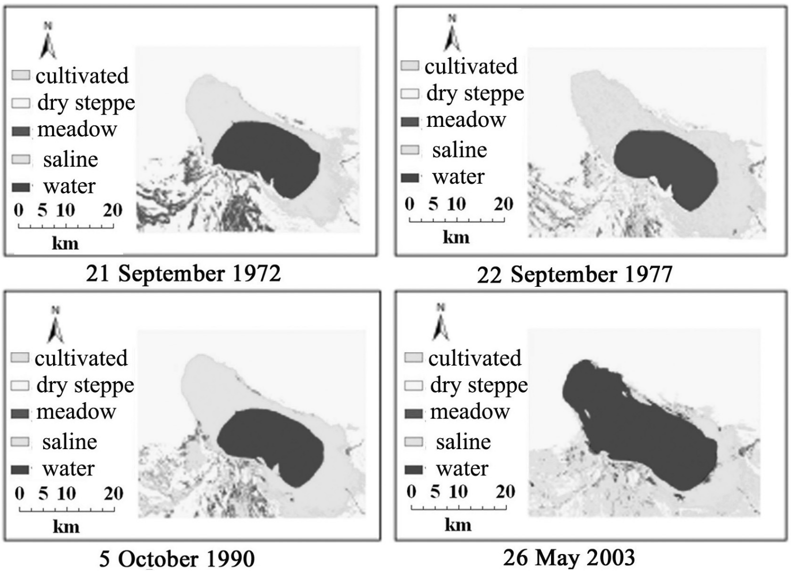

Fig.5 Land use/cover map of Lake Ebnur region from Landsat MSS/ TM /ETM+ dates

Table.1 Calculated area of land use/cover in Lake Ebnur region

Class Name	MSS1972		MSS1977		TM1990		ETM+2003	
	Area (km^2)	%	Area (km^2)	%	Area (km^2)	%	Area (km^2)	%
Cultivated	54.2	1.2	127.3	2.9	267.2	6.1	734.4	16.7
Water	528.2	12.0	524.8	11.9	547.6	12.4	1029.2	23.4
Saline	691.9	15.7	780.5	17.7	1072.9	24.4	418.8	9.5
Dry steppe	2844.9	64.7	2872.4	65.3	2371.0	53.8	2003.1	45.5
Meadow	279.1	6.3	94.9	2.2	145.7	3.3	214.5	4.9

4.4 Driving factors of the water resources

The changes of water resources was including the rivers outflow and lakes area that were governed by socio-economic and natural factors, such as population and the climatic change, etc. Fig6 shows that the temporal changes of population and cultivated area in each northern XinJiang and southern XinJiang. Each of these change was accorded with the fluctuation of rivers outflow from 1950s to the end of 1980s as shown Fig4.

The change in the situation of precipitation and temperature as shown in Fig8 indicated that the increase tendency was happened after the end of 1980s. Based on the Fig7, it was considered that the increasing of precipitation directly causes lakes area expansion and rivers outflow rising in the end of 1980s, the rising of temperature may make the melted-snow water, which flow into the rivers and lakes from high mountains.

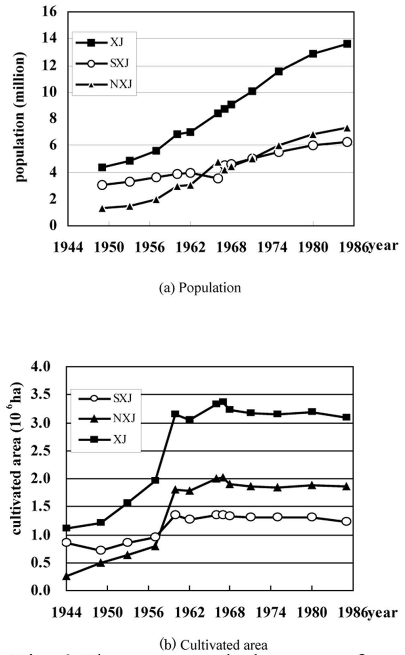

Fig.6 The temporal changes of population and cultivated area in Northern and Southern XinJiang

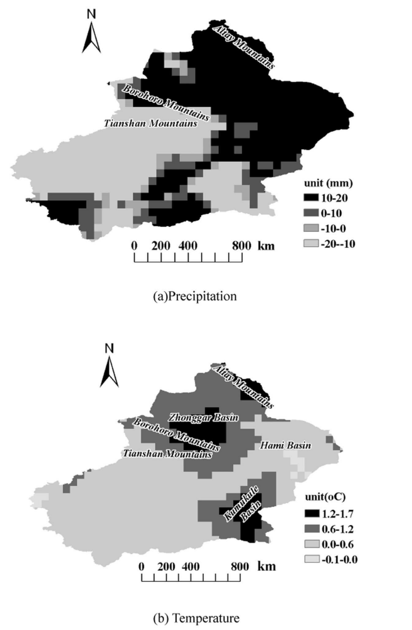

Fig.7 Difference of precipitation and temperature between the periods 1991~2000 and 1951~1990 using CRU TS 2.0 data set

The characteristics of water resources in XinJiang for the second half of the 1980s had some remarkable changes. It was presumed that the causes of water resources changes were not only due to the effect of human activities but also due to the effect of climatic fluctuation. It is supposed that from 1950s until the second half of 1980s, the changes of the water resources in XinJiang have been affected by human activities strongly. On the contrary, from the second half of 1980s until present, the water resources have been affected by climatic fluctuation strongly. The detected land use /cover change of Lake Ebnur region from 1972 to 2003 shows that water area of the lake were governed by these changes.

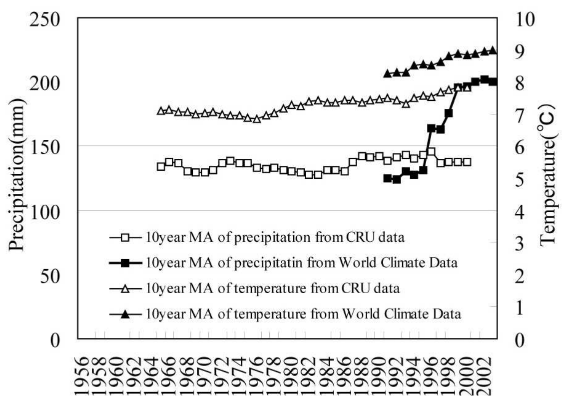

Fig.8 Variation of precipitation and temperature in XinJiang

References

Hietel, E. , Waldhardt, A. , 2004 : Analyzing land-cover changes in relation to environmental variables in Hesse, Germany, Landscape Ecology 19, pp. 473–489.

Nakayama,Y.,Tanaka,S.,Endo,K.and Suga,Y. (1993) : A change of Aral Sea's water area by satellite data, Proceedings of IGARSS, 1, pp. 194-196.

Micklin, P. , 1998 : Desiccation of the Aral Sea, Soviet Union, Science, 241, pp.1170-1176.

Information design for agricultural Plant Planning and Satellite based Remote Sensing Data Visualization

Tomoyuki SHIGETA, Takeshi SUNAGA,
Yutaka MUGISHIMA, Noriyuki YOYASU, Hironobu RYOU, Daigo YAMAZAKI,
Chiharu HONGO*,
Kazunari YOKOYAMA**

Information Design Department, Tama Art University
*Center for Environmental Remote Sensing (CEReS), Chiba University
**National Agricultural Research Center for Hokkaido Region

Abstract

This paper shows design and cooperative design process for agricultural plant planning system based on information Design point of view. The system allows farmers planning kinds and yields of vegetables for the coming year. Developing functionalities for plant planning, visualization of Satellite based Remote Sensing (SRS) data, interactions for operating the system and graphical user interface are concerned in the design. The design project consists of farmers and multidisciplinary researchers those are agricultural biologist, remote sensing researcher and information designers. The objective of the design project has been vegetable farming in Tokachi area of Hokkaido, Japan.

1. Introduction

The vegetable farmers deal with thirty hectare field on average and fifteen to twenty crops in Tokachi. For the planning at this moment of our survey, hand drawing maps of the field and hand writing names and quantities of crops that he planted in each year have been used as figure 1. And notes of manures and fertilizers are existed.

The design we proposed is an assistance for the planning as interactive system for the farmers. Basic functions of the system are browsing, planning and recording concerning to vegetable crops, several values of harvests, and records of insects and disease.

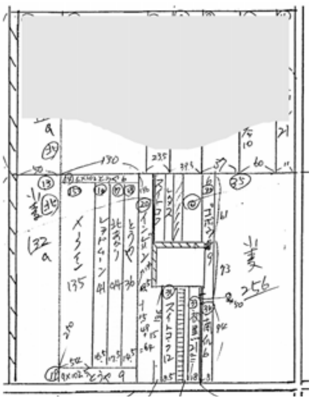

Fig. 1. A hand drawing map of fields, names and quantities of crops planned by farmer for 2005 (YM, 2005)

2. Planning Support System for Cropping and Fertilizing

2.1. Basic functions of the system

Following functions are designed in the Planning Support System. Those are (1) cropping for the next year, (2) fertilizing for the next year, (3) recording agricultural information concerning to this year that is listed in table 1, and (4) browsing past information about planning and recording in preceding years.

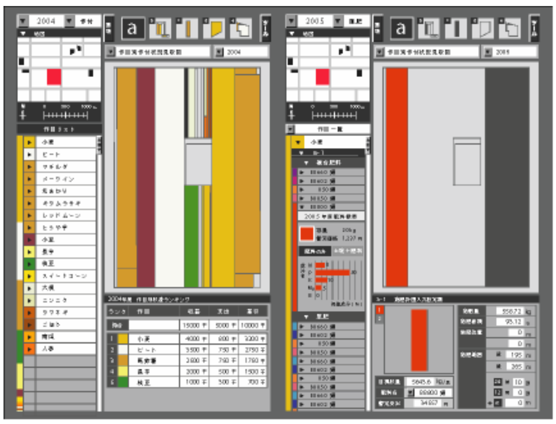

Fig. 2. A Screenshot of the Planning Support System for Cropping and Fertilizing

A main screen of the system is shown in figure 2. Left side of the screen is an area for planning crops on a plan of field where the farmer considers and right side is an area for browsing past information on same plans. Horizontal lists of the left area shows potential kinds of crops for the planning. The right area shows harvested kinds of crops with which the farmer deals.

Table. 1. Variables of agricultural information for the planning

a. Plan of Field for Cropping
b. Plan of Field for Fertilizing
c. Yields and productions
d. Starch-concentration (potato)
e. Sugar-concentration (beet)
f. Protein (wheat)
g. Nitrogen-content (soil)
h. Insects and diseases
i. Profit and loss

2.2. SRS data for the system

Variables of estimation for the system are followings. Those are calculated from SRS data.

j. Estimated yield of each crop
k. Estimated starch-concentration of potato on each field
l. Estimated sugar-concentration of beet on each field
m. Estimated protein of wheat on each field
n. Estimated nitrogen-content of soil on each field

2.3 Social system configuration for the planning support system

The planning support system is used by a number of farmhouses under management by a certain organization of the region. The organization contracts with SRS data provider. Figure 3 shows the providing system.

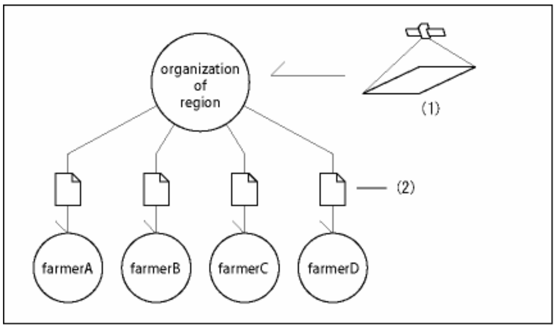

Fig. 3. Providing system for the planning support system
(1) SRS data of the region
(2) Providing values of the calculated data of each farmhouse field for the system on farmer's PC

3. Information Design Study on Visualizations for variables from SRS data

3.1. Visualizations

Values of the Variables are calculated from SRS data by functions constructed by SRS researcher (HONGO. 2004). Information designers visualize the variables. Purpose of the visualization is making legibility of the values for the farmers who deals with the values of crops, fertilizers, and his/her tasks on the fields.

Our study of the visualization has been based on SRS research for a couple of fields of potato that is grown by farmer YM in Tokachi as a case. Following visualizations are derived from the potato data.

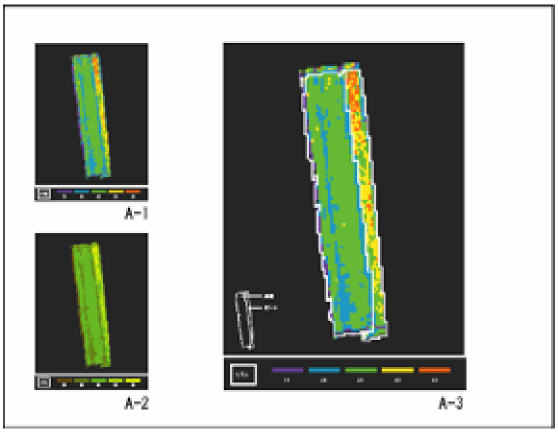

Fig. 4. Legible scatter-gram of Estimated yields of potato by SRS data
A-1. Scatter-gram of Estimated yields from SRS values
A-2. Scatter-gram of Estimated yields from SRS values (different color scale from A-1)
A-3. Overlapped visual expression depicting Preceding Crops

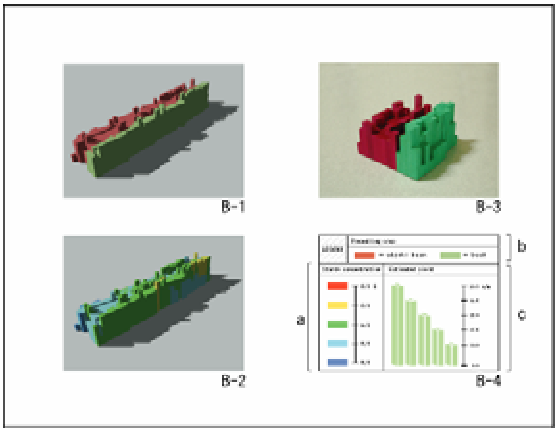

Fig.5. 3D Visual Expression depicting Yields, Starch-concentration and Preceding Crops
B-1. Visual Expression depicting Preceding Crops and Estimated yields (Height represents Estimated yield, Color is a kind of the crop)
B-2. Visual Expression depicting Estimated starch concentration and Estimated yields (Height represents Estimated yield, Color is Estimated starch concentration)
B-3. 3D Physical model of B-1
B-4. Legend;
a : Estimated starch concentration
b : Preceding Crops
c : Estimated yields

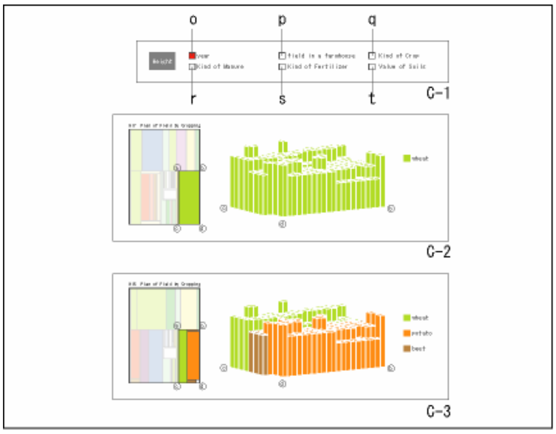

Fig. 6. 3D Visual Expression depicting Preceding Crops and Crops of this Year on specific Area of the fields
C-1. Check boxes of variables to visualize;
o : Year
p : Field in a farmhouse
q : Kind of crop, Yield, Sales of the crop, Value of harvest on the crop
r : Kind of manure, Quantity of the manure
s : Kind of fertilizer, Quantity of the fertilizer
t : Value of soil
C-2. Visualization of this year (Left), 3D Visual Expression (right)
C-3. Visualization of preceding year (Left), 3D Visual Expression (right)

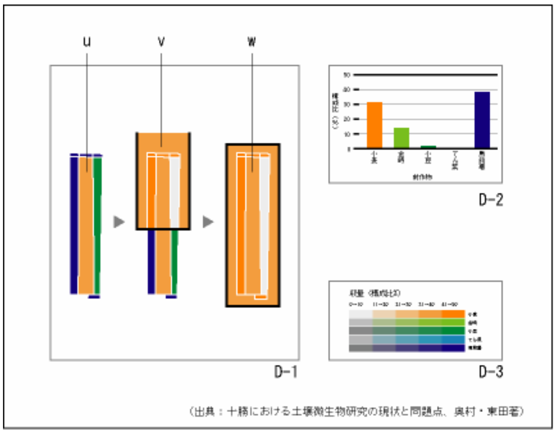

Fig. 7. Simulative Expression for the Influenced-by-the-preceding-crop Model
D-1.Simulative Expression for wheat with Influenced-by-the-preceding-crop
u : Preceding crop
v : Filter of “wheat” for preceding crop
w : Estimated yield of wheat
D-2. Graph of differentiations of Influenced-by-the-preceding-crop to crop of this year
D-3. Influenced-by-the-preceding-crop Model (OUMURA et al, 1991)

3.2. Evaluation for the visualizations

Evaluation for the visualizations has been received from farmer YK and other in a few times of meeting. Opinions from the hearing and discussion for some visualizations are presented as figure 8.

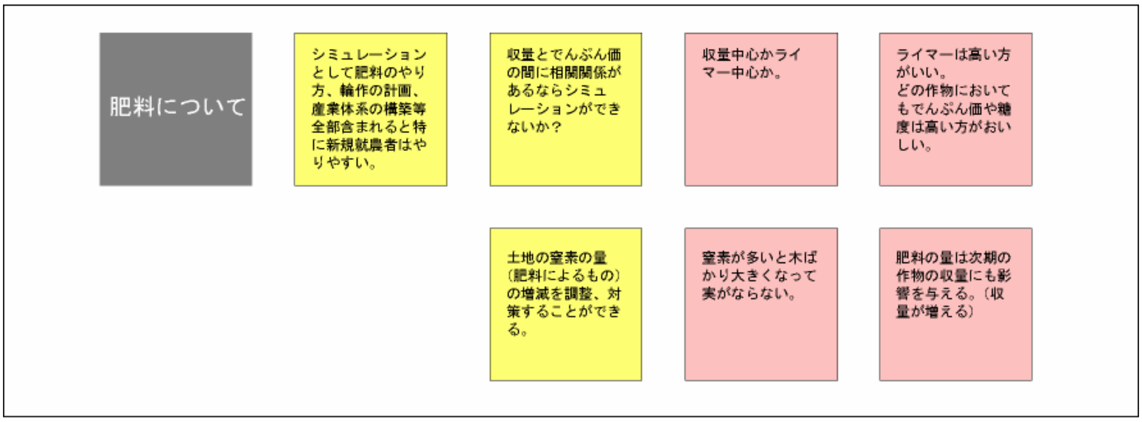

Fig. 8. Presentation of one discussion

Opinions of Farmers for the visualizations are followings.

(1) "The visualization is similar with farmer's image. And it demonstrates state of his field much more clear than usual image through his working. " This opinion is for the legible scatter-gram of estimated yields of potato by SRS data (Fig. 4.).
(2) "It may possible to simulate relationship between Estimated starch-concentration and Yield of potato on the field. " This opinion is for the 3D visual expression depicting yields, starch-concentration and preceding crops (Fig.5.).
(3) "It is useful that system represents estimations and facts of each field." This opinion is for the 3D visual expression depicting preceding crops and crops of this year on specific area of the fields (Fig. 6.).
(4) "The system allows new comers to learn their work and business on agriculture concerning to crops, fertilizers, distributions and so on." This opinion is for the simulative expression for the influenced-by-the-preceding-crop model (Fig. 7.).

4. Future work and Acknowledgements

Through the design development of the plant planning support system, it is figured out that SRS data allows a various understanding of relations between estimated values and harvested facts on their farming. Future work of our design studies is developing cyclic model of crops and soil. The cyclic model is able to describe as follows.

(i) Crops and fertilizers in preceding year have been comprised in values of soils.

(ii) The values of soils constraint plant planning of cropping and fertilizing in the next year.

(iii) Crops and fertilizers makes the yields of this year. And those are comprised in values of soils.

Finally, we thank partner farmers for their contribution to the design development.

Reference

(1) (Okumura et al, 1991) Masatoshi OKUMURA, Syuji HIGASHIDA, "Current Status and Problems of Research on Soil-Microorganisms in Tokachi district", Hokunou, vol.58, No.1, PP 6-15
(2) (Hongo, 2004) Chiharu HONGO, "The 10th CEReS International Symposium on Remote Sensing"

ANALYSIS OF SURFACE TEMPERATURE IN URBAN GREEN SPACES BY USING LANDSAT TM AND ETM+ DATA

Tsuyoshi HONJO[1] and Hiroshi UEDA[2] and Yui NAGATANI[3] and Eunmi LIM[4] and Kiyoshi UMEKI[5]
[1] Faculty of Horticulture, Chiba University [2,3,4,5] Chiba University Graduate School of Science and Technology
E-mail: honjo@faculty.chiba-u.jp

Abstract

In this study, we studied relations between surface temperature of urban green areas and factors of each green areas shown as Tab.1. We analyzed Landsat TM and ETM+ data (Path: 107;Row: 35) and the area which includes metropolitan Tokyo was chosen as analyzed area. Analysis of the relation of surface temperature and factors of green areas were done by regression analysis of each factors and combination of principle component analysis and multiple regressionss and neural network. As a result, surface temperature was obviously influenced by three major components deduced by principle component analysis. The first component represented the effect of factors related to the sizes and the shapes of green areas, the second component represented the effect of coverage of vegetation and the third component represented the water. The effect of factors related to the sizes and the shapes of green areas and thar related the water was significant for analyzing the decrease of surface temperature. We tried to compare the method estimating surface temperature by multiple regressionss with that by neural network. It is implied the mothod by neural network is more effective.

1. INTRODUCTION

It is well known that the surface temperature of urban green area is lower than surrounding urban area. The decrease of surface temperature of bigger green area is higher than smaller green area. But there have been few studies on the effect of many factors LANDSAT ETM+ data. In this study, we analyzed relations between surface temperature of urban green areas and factors related to the shape of green area. It was recongnized that the effect of shape factors of green area was important by the following analysis.

2. METHOD

2.1 Analyzed area

For the analysis, Landsat TM and ETM+ data of Kanto area in Japan (Path:107,Row:35) taken 24th July 1987 , 7th September 1997, and 4th June 2001 was used. Analyzed area was 1120 pixels x 1120 pixels including Tokyo metropolitan area. This area is proper for 33.6km^2 as shown in Fig.1.

2.2 Classification and analyzed green area

Classification of the surface cover was done by minimum distance classification method. The analyzed area was classified with five kinds of covers, i. e. water, tree, grass, bare, urban as shown in Fig.1. In this study, green area was defined as sum of the tree and grass covers. The green areas, which are more than 2 ha in Tokyo, were chosen for the analysis. The number of the green areas was 116 as shown in Fig.2.

2.3 Calculation and analysis of surface temperature

Surface Temperature, *T* was calculated based on following equation,

$$V_c = (9.299 \times 10^{-3} \times T - 3.2) \times T + 268.05,$$

where *Vc* is CCT value of Band 6.

For each 116 green areas, twelve factors shown in Tab.1 and surface temperature were calculated. Then, relation between the averaged surface temperature of each green area and averages of above twelve factors was analyzed by simple regression, combination of principle component analysis, multiple regressions analysis. It was also analyzed by neural network The result of neural network was compared to that of multiple regressions.The neural network with a back propagation algorithm was used as a method of nonlinear multiple regressions which has advantages over conventional linear regression. As shown in Fig.3, The network consists of 3 layers which have 12 units in the input layer, 1 unit in the output layer and 12 units in an intermediate layer. advantages over conventional linear regression. As shown in Fig.3, The network consists of 3 layers which have 12 units in the input layer, 1 unit in the output layer and 12 units in an intermediate layer.

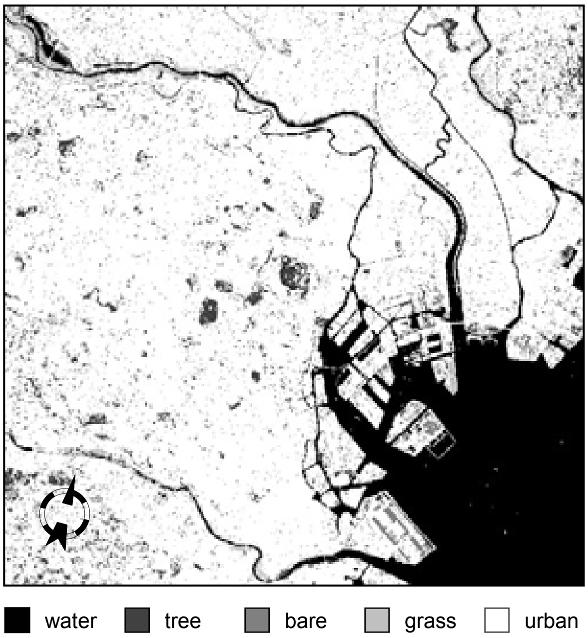

Fig.1 Result of classification.

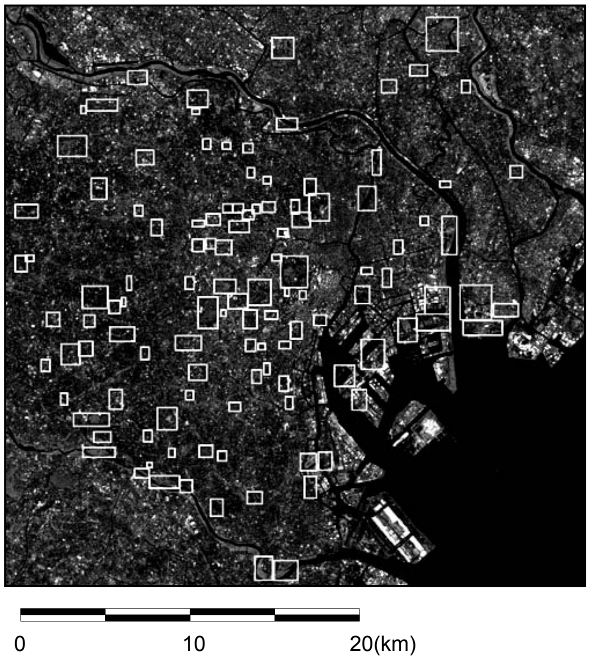

Fig.2 116 green spaces.

Tab.1 Various of green area.

NO.	Variables
①	Total area of greenspace(ha)
②	Tree area of greenspace(ha)
③	Grass area of greenspace(ha)
④	Ratio of perimeter to area(m^{-1})
⑤	Continuity Index(/8)
⑥	Minimum distance from center to water(km)
⑦	Minimum distance from center to coastline(km)
⑧	Ratio of tree within 1km range(%)
⑨	Ratio of grass within 1km range(%)
⑩	Ratio of water within 1km range(%)
⑪	Ratio of tree within 1km range except itself(%)
⑫	Ratio of grass within 1km range except itself(%)

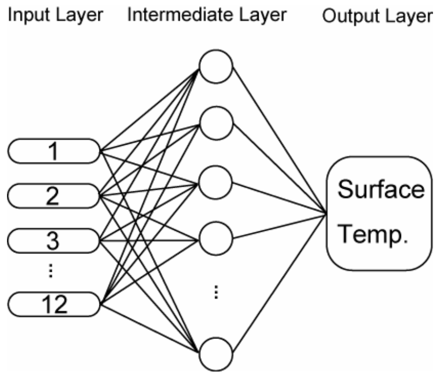

Fig.3 Neural network.

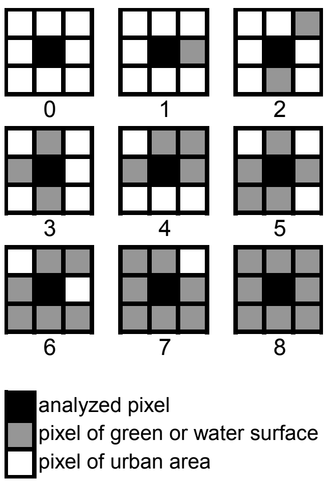

Fig.4 Definition of continuity index.

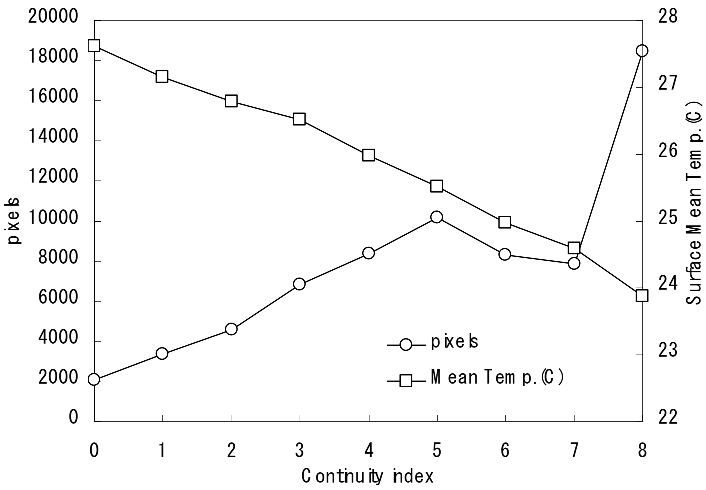

Fig.5 Result of the relation between surface temperature and the number of pixels in each index

Tab.2 Result of single regression analysis on the relation between surface temperature and each variable.

Dependent Variable: Surface Temp. (deg. C)

Valuables	2001			1997			1987		
	Reg. Coef.	Constant	Corr. Coef.	Reg. Coef.	Constant	Corr. Coef.	Reg. Coef.	Constant	Corr. Coef.
	a	b	r	a	b	r	a	b	r
①	-0.024	25.60	-0.36**	-0.013	24.82	-0.27**	-0.021	28.51	-0.49**
②	-0.026	25.54	-0.34**	-0.012	24.74	-0.21**	-0.021	28.42	-0.42**
③	-0.048	25.39	-0.22*	-0.039	24.80	-0.26**	-0.059	28.39	-0.39**
④	112.94	22.48	0.45**	63.326	23.05	0.32**	77.764	26.17	0.47**
⑤	-0.645	28.30	-0.49**	-0.385	26.42	-0.34**	-0.315	29.54	-0.41**
⑥	0.487	24.79	0.26**	0.358	24.16	0.35**	0.336	27.67	0.50**
⑦	0.115	24.18	0.42**	0.030	24.21	0.20*	0.084	27.41	0.45**
⑧	-0.061	25.60	-0.26**	-0.013	24.67	-0.08	-0.053	28.54	-0.36**
⑨	-0.084	25.36	-0.16	-0.057	24.75	-0.16	-0.108	28.39	-0.34**
⑩	-0.059	25.48	-0.39**	-0.064	24.88	-0.52**	-0.075	28.43	-0.63**
⑪	0.221	24.89	0.18	0.159	24.31	0.20*	-0.191	28.56	-0.29**
⑫	0.056	25.17	0.05	0.041	24.54	0.05	-0.095	28.23	-0.15

*P<0.05 **P<0.01

Tab.3 Result of Principle Component Analysis.

Variables / Principle Component	2001			1997			1987		
	1	2	3	1	2	3	1	2	3
①	0.439	-0.122	-0.142	0.445	0.128	0.021	0.445	0.153	0.016
②	0.394	-0.253	-0.195	0.407	0.242	-0.13	0.406	0.284	-0.023
③	0.329	0.312	0.081	0.291	-0.227	0.385	0.298	-0.345	0.13
④	-0.403	0.082	-0.026	-0.392	-0.088	0.133	-0.351	-0.177	-0.248
⑤	0.387	-0.053	0.042	0.379	0.076	-0.117	0.335	0.151	0.289
⑥	-0.118	-0.405	0.211	-0.158	-0.098	-0.376	-0.192	0.18	0.372
⑦	0.041	-0.206	0.536	0.022	-0.379	-0.325	-0.081	-0.103	0.558
⑧	0.345	-0.315	-0.107	0.362	0.179	-0.245	0.38	0.24	-0.151
⑨	0.294	0.424	0.309	0.276	-0.482	0.27	0.263	-0.512	0.161
⑩	0.049	0.438	-0.363	0.024	0.113	0.572	0.141	-0.161	-0.476
⑪	0.029	-0.137	0.393	0.076	-0.284	-0.31	0.14	-0.244	-0.3
⑫	0.09	0.344	0.455	0.122	-0.591	0.003	0.127	-0.524	0.151
Eigen value	4.322	2.082	1.896	4.176	2.107	2.056	4.047	2.364	1.998
Proportion (%)	38	17.2	15.8	34.8	17.6	17.1	33.7	19.7	16.7
Cumulative (%)	38	53.2	69	34.8	52.4	69.5	33.7	53.4	70.1

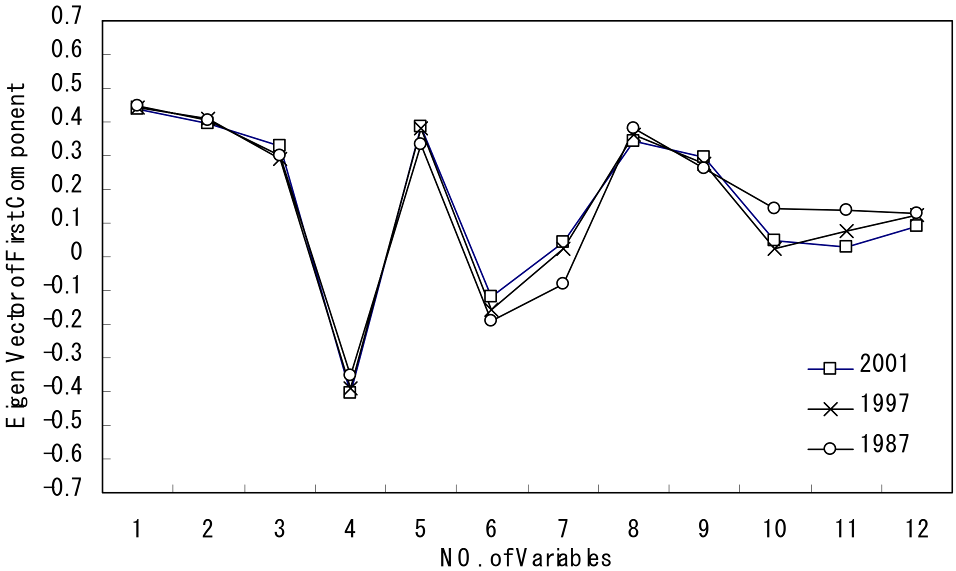

Fig.6 Eigen Vector of First Component with 3-year.

Tab.4 result of multiple regressions.

Dependent Variable: Surface Temp. (deg. C)									
Variables(Component	2001			1997			1987		
	1	2	3	1	2	3	1	2	3
Part Reg. Coef.	-0.31**	-0.16*	0.43**	-0.18**	-0.15*	-0.32**	-0.32**	0.07	0.25**
F value	33.64	4.52	29.81	16.12	5.54	25.87	112.22	3.56	34.86
Constant		25.21			24.59			28.16	
Coef. of Det		0.37**			0.30**			0.57**	

*P<0.05 **P<0.01

3. RESULTS AND DISCUSSION

3.1 Surface temperature and continuity index

Continuity index is Numbers of pixels of green area or water surface per 8 pixels, which surrounds a pixel of green area as shown in Fig.4. The continuity index has values from 0 to 8. The value of 8 means that all the surrounding pixels is green area. The value of 0 means that the pixel is sole green area. Relation between surface temperature and the number of pixels in each index is shown in Fig. 5. As the value of index is larger and lager, surface mean temperature becomes lower and lower. The total number of each index keeps rising until it gets the value of 5, and that of 6 and 7 gets lower. But that of 8 is the largest number.

3.2 Simple regression

The result of simple regression analysis was shown in Tab.2. Total area of green space, tree area of green space, grass area of green space, continuity index and ratio of water within 1km have minus correlation with surface temperature. On the contrary, ratio of perimeter to area, minimum distance from center to water, minimum distance from center to coastline has plus correlation with surface temperature.

3.3 Principle component analysis

The result of principle component analysis was shown in Tab.3. The meaning of each principle components was considered as follows. The first component represented the sizes and the shapes of green areas, the second component represented the effect of coverage of vegetation and the third component represented the water. Eigen vector of first component with 3-yaer is shown in Fig.6. Result of each year was shown a similar tendency. Result of second and third component was also shown same outcomes.

3.4 Multiple regressions and neural network

By using the three principle components as independent variable and surface temperature as dependent variable, multiple regressions analysis was taken and the result was shown in Tab.4. The 3-year coefficient of determination was 0.37, 0.30, and 0.57 respectively. The effect of factors related to the sizes and the shapes of green areas and that related the water was significant for analyzing the decrease of surface temperature. Result of multiple regressions and neural network in 2001 is shown in Fig.7. The scatter of the data of neural network was less than that of multiple regressions. The result of the other year was almost same difference.

4. Conclusion

From above analysis, in the first instance, the effect of continuity index was considered to be important for the decrease of surface temperature. Secondly, Eigen vector with 3-yaer was shown a similar tendency. Thirdly, The effect of factors related to the sizes and the shapes of green areas and thar related the water was significant for analyzing the decrease of surface temperature. Lastly, result of estimation by neural network was shown superiority to that multiple regressionss.

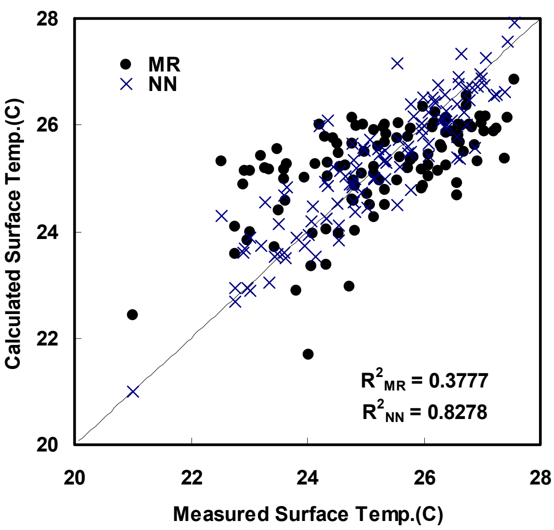

Fig.7 result of multiple regressions and neural network(2001).

Reference

Honjo, T. and Takakura T., 1986, Analysis of temperature distribution of urban green spaces using remote sensing data, Journal of Japanese institute of Landscape Architecture, 49, 299-304.

Sawada, D, Honjo, T, Maruta, Y and Kimura, K., 1986, Analysis of surface temperature in urban green spaces by using LANDSAT TM DATA, Journal of Environmental Information Science, 16, 393-398

Urban monitoring using former Japanese Army maps and remote sensing
- The 100 years of urban change of Jakarta city -

J. Tetuko S. S.[1], I. Indreswari S.[2], and R. Tateishi[1]

1 Center for Environmental Remote Sensing, Chiba University, 1-33, Yayoi, Inage, Chiba 263-8522 Japan, Tel +81(0)43 290 3840 Fax +81(0)43 290 3840, Email jtetukoss@faculty.chiba-u.jp

2 Department of Architecture, School of Graduate Study, Institute of Technology Bandung, Jalan Ganesha 10, Bandung 40132 Indonesia, Tel +62(0)22 250 1214 Fax +62(0)22-250 8059 Email innes@bdg.centrin.net.id

INTRODUCTION : A BRIEF HISTORY OF JAKARTA CITY

From prehistoric time to Muslim and Hindu-Javanese kingdoms, the Jakarta area (now the capital of Republic of Indonesia) was a small village called Sunda Kalapa in twelfth century (Simon 2003) which appears to have been a harbour for a Hindu-Javanese kingdom called Padjajaran, the capital of which was near the present mountain resort of Bogor, south of Jakarta. A port on the Ciliwung river (see Figure 1) emerged as an important part of Indonesian trade. The importance of Sunda Kalapa was similarly affected as the port of Malacca on the west coast of Malaya that was conquered by the Portuguese in 1511. The Sunda Kalapa was renamed to Jayakarta (Victorious and Prosperous) by the sultanate of Banten

Then this area was started to develop by building of Dutch East India Company (VOC) fort on west bank of the River Ciliwung in 1619 (Susan 1989). Then this area was familiar by calling 'Batavia' and about ten thousands people were living in this small city. Traders from India, China, England, Holland and other islands of the archipelago are recorded continuing to visit the port for spices trading.

Total population of Jakarta (inside the wall or fort Batavia) in 1673 was recorded 27,068 people. By the end of the eighteenth century, the VOC was bankrupt that affected the total population would be 35,000 peoples in 1730. This economic situation was worse; hence the population of city had dropped to 12,131, with 160,986 living in the environs, a large area extending south to the mountains (Bogor area or former Buitenzorg city). In 1815, although the power of VOC declined, the population increased slowly to be 47,000. The city was sprawling by the installing of modern public transport, therefore the population increased to be 70,000 in 1850, and 116,000 in 1900. The city was strung out over 10 to 12 km from north to south. By the 1930, the population of the city of Batavia had grown to 435,000 where the immigration caused it to expand. Most of the road network had been asphalted and public services (electricity and telephone) were established in 1940. In 1942, Japanese occupied the archipelago and divided it into regions, and changing the capital's name to Jakarta that was treated as the capital of one such region, Java. 1942 to 1949 periods is the struggle period of Indonesian for Independence of Indonesia from Dutch, and Jakarta assumed as the capital of an independent Indonesian nation-state in December 1949. Van des Plas reported the population was 844,000 in September 1945. After the independent and Jakarta was decided as the capital of Republic of Indonesia, the urbanization made increasing the population that recorded 1,050,000 in

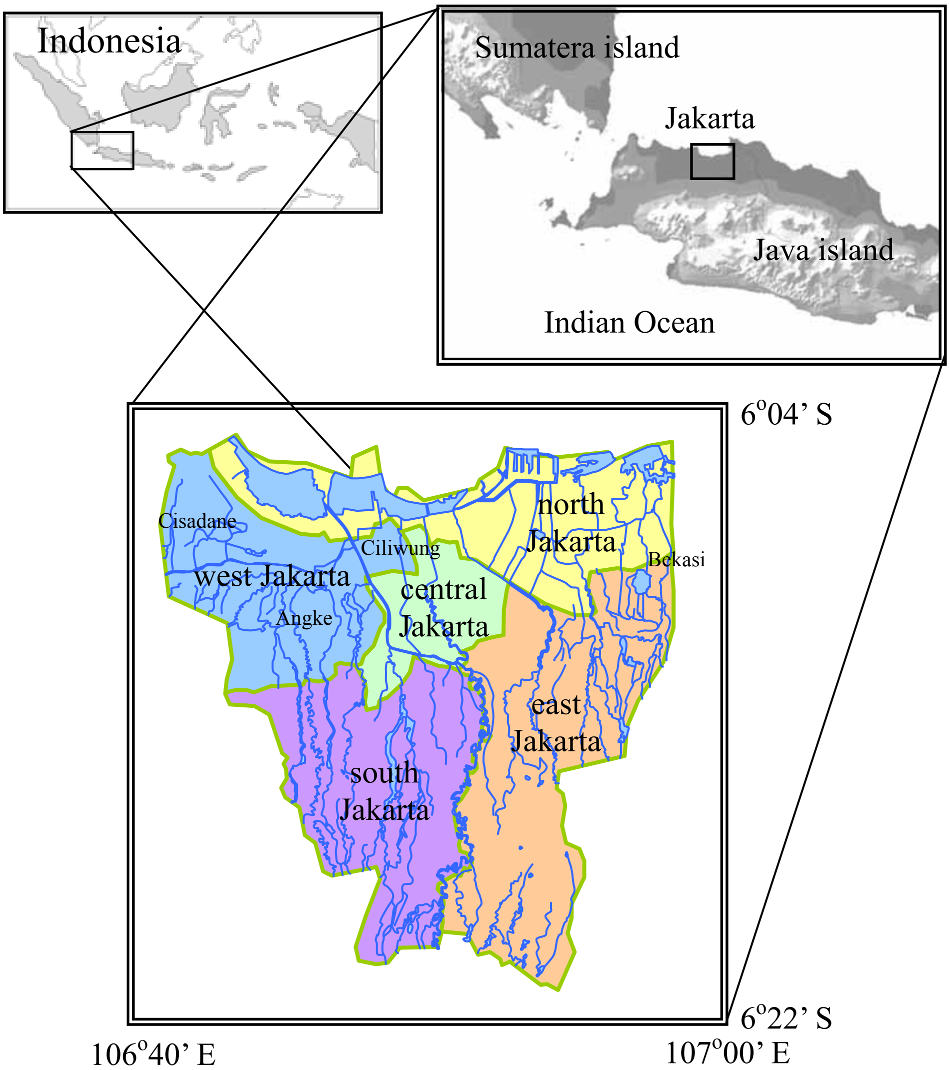

Figure 1. Study site : Jakarta city, Indonesia and its environment

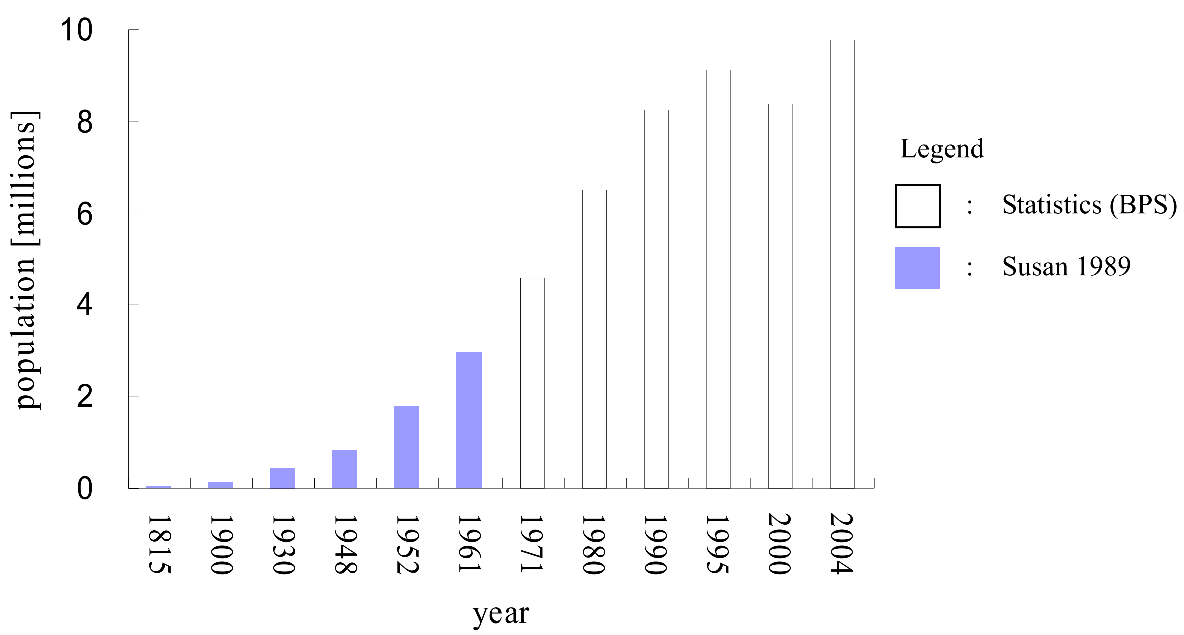

Table 1 Population of Jakarta city

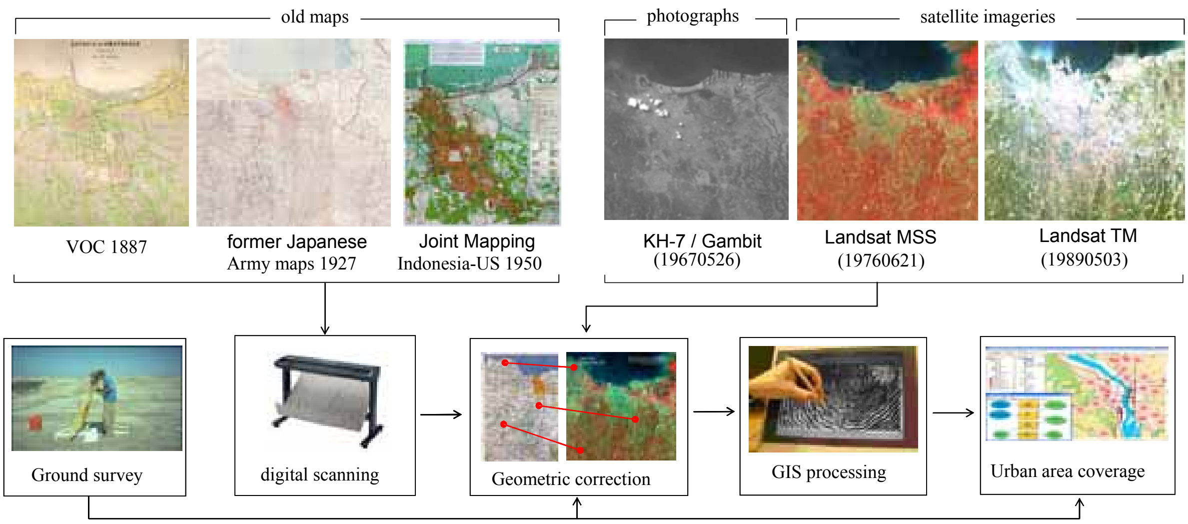

Figure 2 Flowchart of analysis

1948, almost double the figure for 1930. President Soekarno's visions had little relevance to the dominant fact of Jakartan life in the period, official figures show the the population was increasing drastically 1,782,000, 2,973,000 and 3,813,000 in 1952, 1961 and 1965, respectively. Base on the census report of Indonesian Govermental Statistics (BPS 2005), the population in 1971, 1980, 1990, 1995, 2000 and 2004 are 4,579,303; 6,503,449; 8,259,266; 9,112,652; 8,389,443; and 9,792,000, respectively. The population in 2000 decreased comparing to 1995, it is assumed the impact of Asian crisis in 1997. The population in 2004 was increasing again by the economy recovery for the crisis. The population trend of Jakarta city from 1815 to 2004 can be seen in Table 1.

The Statistics shows that the urban area coverage of Jakarta 93,7% in 1980, and 100% after 1990s (see Table 2), where total area is 661 km^2. The data shows the lack of information of urban area coverage before 1980. Therefore, in this research, old maps and satellite images were employed to obtain the urban area coverage. The detail analysis will be explained next.

STUDY SITE

Figure 1 shows the study site, Jakarta city (capital of Republic of Indonesia) that located in 106^{o}40'E - 107^{o}00'E, 6^{o}04'S - 6^{o}22' S and covering about 661 km^2. The area around the mouth of the Ciliwung river in west Java, the site of present-day Jakarta, has known human settlement from prehistoric times. Built up from the silt washed down from the volcanic mountain range to the south, an alluvial plain spreads out in a fan shape traversed by several rivers: Cisadane, Angle, Ciliwung, Bekasi and Citarum.

ANALYSIS

The urban area change of Jakarta city is investigated by using old maps and satellite images. The employed old maps are VOC (1887), former Japanese Army map (1927), and Joint Mapping Indonesia - US 1950 maps. Especially, the former Japanese Army map is composed or mosaicked by 11 maps (Gaihozu 1927) as shown in Figure 3. Jakarta city boundary in this Figure shows the present boundary of Jakarta. Then the satellite images are KH-7 / Gambit (26 may 1967), Landsat

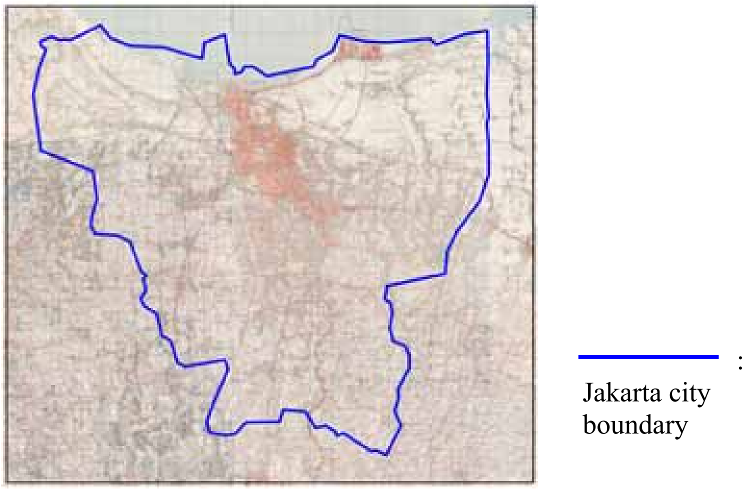

Figure 3 Mosaic maps of the former Japanese Army

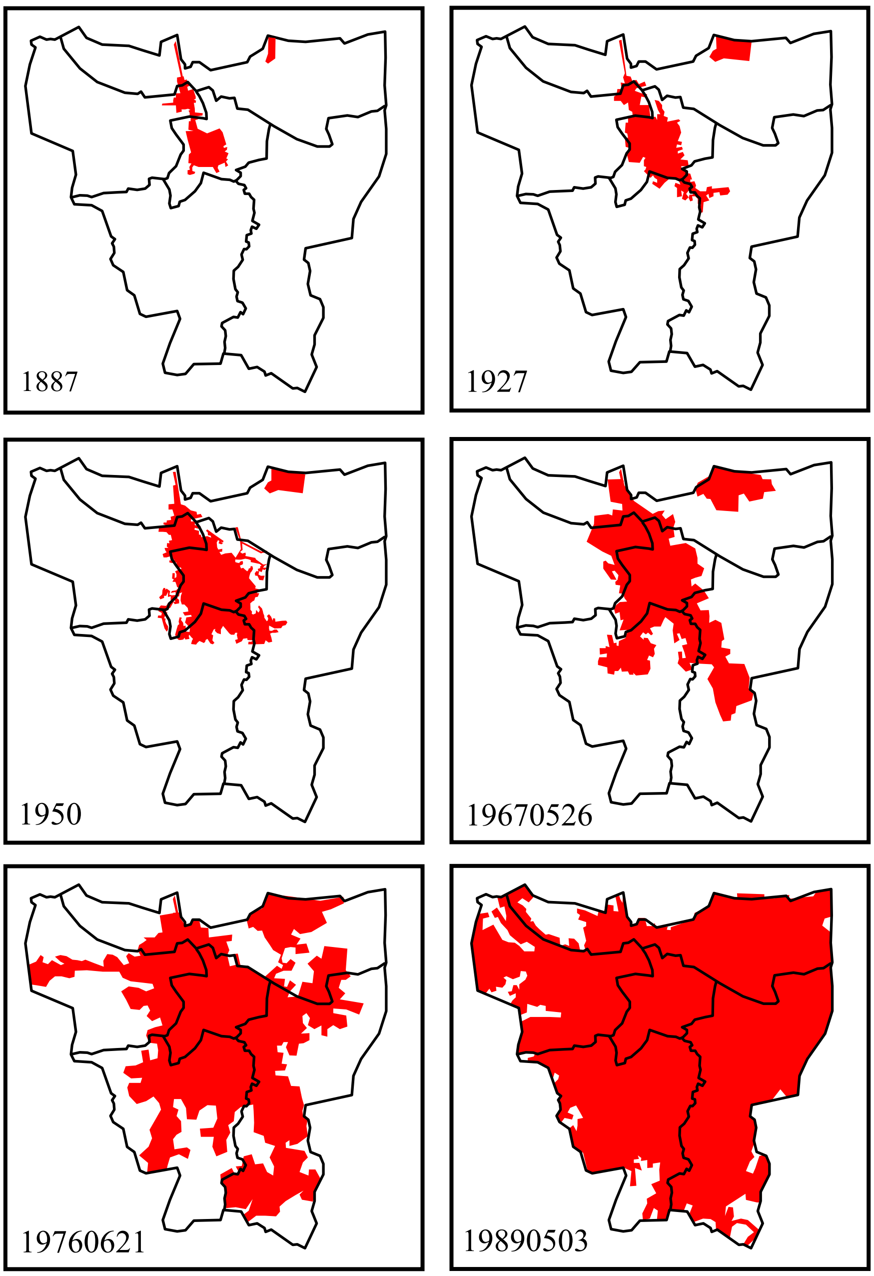

Figure 4. Urban area change of Jakarta city in time series

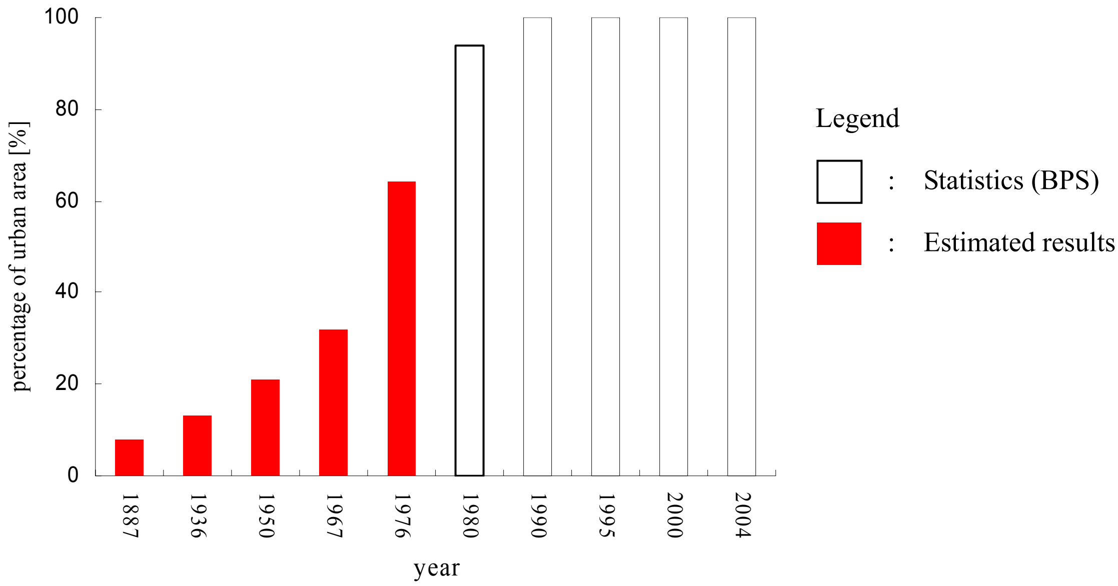

Table 2 Urban area of Jakarta in time series

MSS (21 June 1976) and Landsat TM (3 May 1989).

As shown in Figure 2, firstly the old maps are scanned. Secondly, the maps were geometric corrected before digitizing process (visually) to obtain the urban area class. The satellite images are also geometric corrected, then supervised classification process was employed to acquire the urban area class. The topographic maps (Bakosurtanal 2001) with 1:25,000 scale were used in the geometric correction.Then the urban area class only was delineated to obtain the urban area distribution more clearly. Base on the digitizing or delineation process, the coverage of urban city of Jakarta in each date could be acquired as shown in Figure 4. This Figure shows (visually) that the urban area was increasing drastically after 1945 or the independent year of Republic of Indonesia. Figure 4 shows that the urban area coverage is 8%, 13%, 21%, 32% and 64% in 1887, 1927, 1950, 1967 and 1976 respectively. Base on Landsat TM data (3 May 1989), the coverage in 1990s is almost 90% or matches well with the statistics data. Table 1 and Table 2, or the population and urban area change of Jakarta city respectively show the strong relationship. These tables mean the increased population caused the sprawling of urban area.

CONCLUSIONS

Like many big cities in developing countries, Jakarta city has almost 250 years history and suffers from major urbanization problems. The population has sharply risen after 1960s, and base on the old maps and satellite images extracting the urban area, this area covers whole of city (661 km2) in 40 years after the independent and the declaring of Jakarta as the capital of Republic of Indonesia. The result shows that the old maps (1887 - 1950) include former Japanese Army maps (Gaihozu), and satellite images (1967 - 1989) combination can be employed to monitor the city sprawling and its problems.

In the near future, the authors will employ these data and Geographical Information System (GIS) to retrieve the city spatial information and its change. The information of urban area, vegetation, digital elevation model (DEM), annotation, transportation network and hydrologic network will be retrieved from the former Japanese Army map to obtain the topographic information of 1900s. The high resolution of satellite images also will be employed to monitor the area around Jakarta city or known as buffer zone of Jakarta (Bekasi, Bogor, Tangerang, and Banten) called Jakarta Megapolitan area.

ACKNOWLEDGEMENT

Thank to the Museum of Natural History, Tohoku University to the Gaihozu; Pandhito Panji Foundation - Remote Sensing Research Center for old maps; and University of Maryland for Landsat datas.

REFERENCES

Bakosurtanal, 2001, Jakarta 1209-441, Tangerang 1209-432, Cakung 1209-442, Pasar Minggu 1209-423, Pondok Gede 1209-424, Teluk Naga 1209-434, Ancol 1209-443, Tanjung Priok 1209-444

BPS, 2005, Indonesian Statistics Report.

Gaihozu, 1927, Blad 36/XXXVIIA (oud No.17A) Maoek, 36/XXXVIIC (oud No.17C) Tangerang, 36/XXXVIIIA (oud No.18A) Paroeng Pandjang, 36/XXXVIIB (oud No.17B) Batavia, 36/XXXVIID (oud No.17D) Kebajoran, 36/XXXVIIIB (oud No.18B) Paroeng, 37/XXXVIIA (oud No.23A) Tandjoeng Priok, 37/XXXVIIC (oud No.23C) Meester Cornelis, 37/XXXVIIIA (oud No.24A) Depok, 37/XXXVIIB (oud No.23B) Moeara Bekasi, 37/XXXVIID (oud No.23D) Bekasi, 24B Tjibaroesa

Simon Winchester, 2003, Krakatoa - the day the world exploded: August 27, 1883, Sterling Lord Literistic

Susan Abeyasekere, 1989, Jakarta : A History, Revised edition. Oxford University Press.

APEX, a tool for the simulation, calibration and validation of Earth observation sensors

Jens Nieke[a,b], Yoshiaki Honda[b], Hiroshi Murakami[c], Daniel Schläpfer[a], Nobuo Takeuchi[b], Klaus I. Itten[a]
[a] Remote Sensing Laboratories (RSL), Winterthurerstr. 190, University Zurich, CH-8057 (CH)
[b] Center for Environmental Remote Sensing (CEReS), University of Chiba, 1-33 Yayoi, Chiba, 263-8522 (JP)
[c] Earth Observation Research and application Center (EORC), Japan Aerospace Exploration Agency (JAXA), 1-8-10, Harumi, Tokyo 104-6023 (JP)

Abstract:
In the next decades, JAXA plan to launch a series of GCOM satellites. Onboard the GCOM-C satellite the SGLI sensor will enable global observation of the environment and human activities. The successful calibration and validation of space sensors (such as SGLI) is crucially important and is depending on many factors, such as rigid ground-truth campaigns, the validation of the product algorithms. Also the transfer of ADEOS-2 GLI algorithms to the SGLI project needs a special validation effort. The airborne imaging spectrometer APEX is able to support these activities since it was especially designed for the calibration, validation (CalVal) and simulation of space sensors. In this paper the binning pattern are discussed to cover the spectral bands of the former GLI sensor in a way, it promises best results.

1. Introduction

The SGLI sensor series onboard the GCOM-C satellite will enable continuous observation of climate change and human interaction over 13 years from the year 2011. To cover the time range of 13 years, three series of satellites are planned to be launched every four years assuming a lifetime of each of the satellites of around five years and considering one year overlap for cross calibration between satellites. The APEX sensor is an airborne imaging spectrometer to be flown on various platforms, such as the DO-228, HALO. Within the APEX project a new exchange node of scientific ideas, methods and results, the APEX Science Center (ASC) is currently set-up, which allows the exchange of scientific knowledge in the science community using the open source code development. The APEX instrument has during operations two spectral modes, i.e., a spatial mode (about 300 spectral bands) and a spectral mode (about 500 spectral bands). While for the SWIR channel all 199 can be read-out simultaneously, the APEX VNIR channel has 312 spectral bands, where only 114 bands can be read out in spatial mode, i.e., 312 bands have to be binned in a way that is optimal for various applications, while offering appropriate Signal–to-Noise Ratio (SNR) performance. In this study, binning patterns for the various space sensors[1] simulation (up/down-scaling), such as GLI/SGLI, MODIS or MERIS, are proposed. For the cross-calibration also the edges of the Relative Spectral Response functions (RSR) of the space sensor bands have to be taken into considerations using weighted software binning methods.

2. Satellite Sensor SGLI

GCOM-C is a JAXA mission on environmental remote sensing, enabling global change monitoring over a long duration of 13 years. The SGLI sensor is the core sensor of this mission dedicated to environmental remote sensing in the spectral range from 0.38 to 12 micron with a spatial resolution of 250 m to 1 km[2,3]. In the following we assume similarity of SGLI and GLI[4] spectral bands.

3. APEX – the airborne simulator

APEX[5,6] is an dispersive pushbroom imaging spectrometer operating in the spectral range between 380 - 2500 nm. The spectral resolution will be better than 10 nm in the SWIR and < 5 nm in the VNIR range of the solar reflected range of the spectrum. The total FOV will be ± 14 deg, recording 1000 pixels across track with about 300 spectral bands simultaneously. A large variety of characterization measurements will be performed in the scope of the APEX project, e.g., on-board characterization, frequent laboratory characterization, and vicarious calibration. The retrieved calibration parameters will allow a data calibration in the APEX Processing and Archiving Facility (PAF). The data calibration includes the calculation of the required, time-dependent calibration coefficients from the calibration parameters and, subsequently, the radiometric, spectral and geometric calibration of the raw data.

4. Approach

To analyse the binning pattern for SGLI/GLI an approach was selected having the following steps:

1. For the calculation of all 312 peak-normalized APEX VNIR-channel RSR, the Spectral Sampling Interval (SSI),

the Center Wavelength (CW) and the ratio between SSI and the spectral band width (Dlambda) was used.
2. Calculation of APEX VNIR 312 RSR assuming Gaussian distribution using the above values.
3. All Gaussian RSR are plotted vs. the wavelength.
For the comparison with space sensor RSR, the following narrow bands (Dlambda ~10nm) were used: GLI (band 1 – 19), MERIS (band 1 – 15) and MODIS (band 8 – 19).
Note, for the simulation of broad-band RSR for sensors, such as ETM+ and SPOT, the 10-nm bands can be binned afterwards in the PAF.
3. Visualization of all APEX, MERIS and GLI RSR in 13 regions of interest.
4. Visual decision process selecting the appropriate APEX bands for each of the GLI, MERIS and MODIS bands. Note, this selection is still preliminary and has to be re-evaluated during future scaling and CalVal activities.
5. Calculation of the in-band irradiance values for all space sensor RSR using Thuillier-2003 data (E0)[7].
6. Calculation of the in-band irradiance values of binned APEX RSR representing 15 MERIS and 19 GLI bands.
7. Solar irradiance data and the in-band irradiance of 15 MERIS bands and 19 GLI bands are plotted in absolute scale and relatively as APEX (E0) / E0 (Meris, GLI) (see Figure 3).

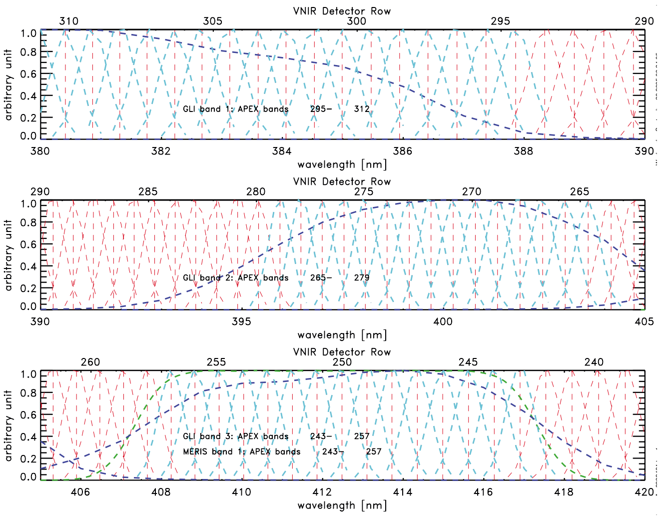

Figure 1: In the region of MERIS band 1 and GLI band 1,2,3 all APEX RSR are plotted vs wavelength.

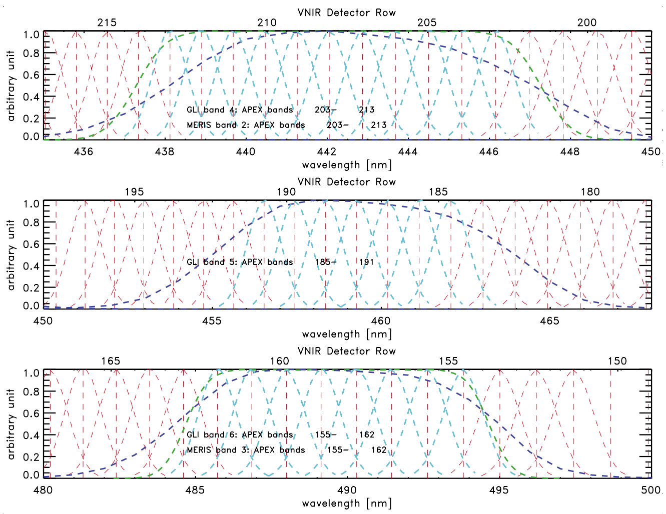

Figure 2: In the region of MERIS band 2,3 and GLI band 4,5,6, all APEX RSR are plotted vs wavelength.

5. Results

The results of the RSR calculations and the visualization of both, APEX bands and space sensor bands, and finally the evaluation of the binned pattern are outlined.
In Figure 3, the selection of the APEX binning pattern were evaluated. For the evaluation the in-band irradiance of

the 15 MERIS, 19 GLI bands and the corresponding APEX binned bands were calculated using the following equation:

$$in\_band\_irradiance = E_0^{Band} = \frac{\int_{\lambda_{min}}^{\lambda_{max}} E_{Thuillier2003}(\lambda) RSR_{band}(\lambda) d\lambda}{\int_{\lambda_{min}}^{\lambda_{max}} RSR_{band}(\lambda) d\lambda}$$

When plotting the ratio, E0(APEX)/E0(MERIS,GLI), ideally, the values should be around 1. All MERIS (and most of the GLI) in-band irradiance values are within the ±1% error bar. GLI bands 1,4,7 are underestimated by APEX binned bands and GLI band 14,15 are overestimated, however all bands are within the ±2% error range. The RSR of the outliner GLI band 1 (-7%) starts at 375 nm, thus the first APEX binning band is not able to cover the entire spectral range of this band (see Figure 1).

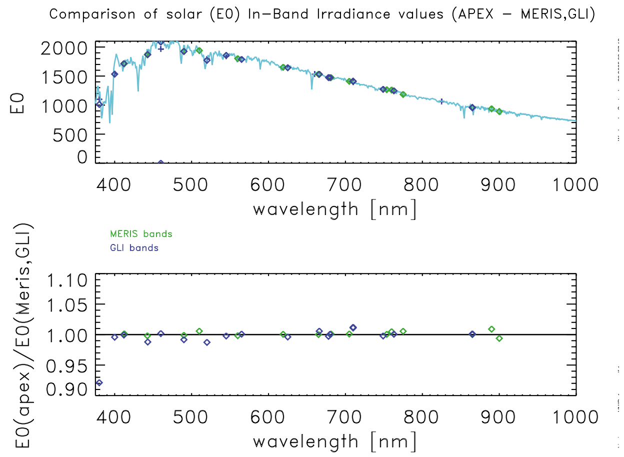

Figure 3: Solar irradiance data and the in-band irradiance of 15 MERIS bands and 19 GLI bands are plotted in absolute scale and relatively.

6. Conclusion

In this paper various binning patterns for APEX are proposed. This binning pattern will allow the simulation (up/down-scaling) of space sensors including the narrow spectral bands (~10nm) of GLI (and MODIS, MERIS). The results of the selection process are still preliminary, since these findings must be re-evaluated during future scaling and CalVal activities. The patterns are also validated for the retrieval algorithms of vegetation, water, soil-related parameter products.

Acknowledgement

Part of the work in this paper has been carried out under ESA/ESTEC contract no. 15440/01/NL/Sfe. The authors would like to express their appreciation to the JSPS, SNF and the Universities of Zurich and Chiba, enabling the visit of JN at CEReS.

References

[1] Nieke, Schwarzer, Neumann, Zimmermann; Imaging Spaceborne and Airborne Sensor Systems in the Beginning of the Next Century; SPIE Vol. 3221 (1997)

[2] Kimura, Tange, Tanaka, Itoh, Matsuyama, Okamura, Kasahara, Honda; Concept study of multispectral imager for next generation; SPIE, Vol. 5570 (2004)

[3] Honda, Y.; SGLI for global change monitoring; Geoscience and Remote Sensing Symposium, IEEE 2001 proceedings, Vol. 6 (2001)

[4] Nakajima T.Y., T. Nakajima, M. Nakajima, Fukushima, Kuji, Uchiyama, Kishino; Optimization of the Advanced Earth Observing Satellite II Global Imager channels by use of radiative transfer, calculations; Appl. Opt., 37, 3149-3163 (1998)

[5] Itten, Schaepman, De Vos, Hermans, Schlaepfer, Droz; APEX – Airborne PRISM Experiment: A new concept for an airborne imaging spectrometer, Proc. ERIM, Vol. 1 (1997)

[6] Nieke, Itten, Debruyn, et al., The imaging spectrometer APEX: from concept to realization, eproceedings EARSeL (2005)

[7] Thuillier et al., Solar Physics 214: 1–22 (2003)

A New Approach Using Various Remote Sensing Data For Vegetation Parameter Retrieval As Input To Ecosystem Models

Silvia Huber, Jürg T. Schopfer, Mathias Kneubühler,
Jens Nieke, and Klaus Itten
Remote Sensing Laboratories (RSL),
Dept. of Geography, University of Zurich,
Winterthurerstrasse 190, 8057 Zurich (Switzerland).
Email:shuber@geo.unizh.ch

Abstract

The objective of the following outline is to propose a method of combining various remote sensing data and to point out the potential of diverse remote sensing data as an input to local, regional or global ecosystem models. The combination of different data sources including several observation geometries and an ensured comparability of the retrieved data products demand for a uniform baseline of normalized ground reflectance data (geometrically, atmospherically, and BRDF corrected), which also provides the possibility of comparison between different sensors and observation geometries for calibration/validation purposes. Possible disadvantages of a spatial and spectral information loss have to be assessed, being a result of the necessary resampling and spectral convolution.

1. Introduction

Reflectance measurements are usually performed at a local scale and on a specific vegetation surface and therefore exhibit a limited significance for larger areas. During a field campaign of RSL in July 2004, a large dataset of spaceborne (MERIS, MODIS), airborne (HYMAP), and ground spectral information was acquired at the same time and of the same area. By combining this spectral information obtained by different sensors with different characteristics, the generation of a value added product is possible. The objective here is to propose an approach of how multi-source remote sensing data can be used as an input to local, regional or global ecosystem models. Therefore it is necessary to generate a uniform baseline of normalized ground reflectance. Various ground information is necessary either for correction or validation purposes. A BRDF correction is done by using spectro-directional field measurements, which were performed with the RSL field goniometer system FIGOS [1] or by using modeled HDRF data. Further reflectance information of different vegetation surfaces is gathered by an ASD field spectroradiometer. Validation of the retrieved model output parameters is assured by using various measured structural and biochemical vegetation parameters.

The Vordemwald study area (E 47°16' N 07° 53') is located in the canton of Aargau, Switzerland and covers an area of approximately 50 km^2 of mixed forest, cultivated fields and grassland. The field campaign was conducted by RSL in collaboration with the Swiss Federal Institute of Forest, Snow and Landscape Research (WSL).

2. Data

Field measurements were performed in the second half of July 2004 at six different sites in the forest of the Vordemwald study area. The forest consists of two main coniferous species (*Picea abies* and *Abies alba*) and five deciduous species (*Fagus sylvatica, Acer pseudoplatanus, Fraxinus excelsior, Quercus robur, and Quercus rubra*). At each plot the trees were georeferenced, diameter at breast height (DBH), tree height, crown base, and crown dimension were measured. Three top of canopy branches were excised by a tree climber from each sampled tree. The plant material from the treetop is important in order to compare remotely sensed data with ground truth information. A handful of leaf samples were packed from each tree, stored in a cool environment, and transported to the lab for a variety of analyses such as chlorophyll, specific leaf area (SLA), leaf water content (LWC), and C:N ratio.

Hemispherical photographs were taken to determine Leaf Area Index (LAI) and Gap fraction [Figure 1]. The photos were acquired with a digital camera and a hemispherical lens converter. Additionally, a gas exchange experiment was conducted in the field to measure the leaf net CO_2 uptake as well as the stomatal conductance.

The leaf optical properties (leaf reflectance and transmittance) of broadleaf plant types representative for the study site were measured. Spectral properties of single leaves are essential to understand the interaction of the incident radiation with the vegetation. The optical properties provide the critical link between remote sensing data on the canopy scale and the physiological energy and mass transfer processes on leaf level.

The acquisition of spectral measurements involved an ASD field spectroradiometer coupled to an integrating sphere and a custom made light source for improved illumination. Both adaxial and abaxial sides of the foliage elements were considered for reflectance and transmission measurements.

Fig. 1. Hemispherical photograph for the retrieval of canopy geometrical structure.

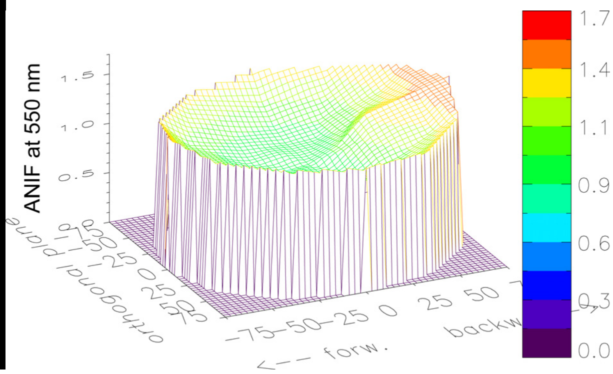

Fig. 2. Anisotropy factor of the observed meadow.

In order to validate and correct the acquired airborne and spaceborne at-sensor radiance with respect to the observation directions, spectro-directional measurements were performed with the RSL field goniometer system (FIGOS). FIGOS was therefore placed on a meadow at the intersection area of all three flight lines. The albedo normalized anisotropy factor ANIF of the observed meadow exhibits a slight bowl shape. The typical reflectance peak for vegetation in the backscattering region is less dominant than expected [Figure 2]. This effect might occur due to the specific constituents of the meadow, which included some white clover *(Trifolium repens)* leading to a higher reflectance at large observation zenith angles. Simultaneously, the direct and diffuse irradiance was measured with a MFR 7 sunphotometer in order to correct the measured hemispherical directional reflectances for the diffuse part of the incoming radiance [2].

HyMap airborne hyperspectral imagery was recorded on July 29, 2004 during excellent weather conditions. HyMap is an imaging spectrometer providing spectral coverage in the visible, near, shortwave and middle infrared in 125 bands with a bandwidth of 10–20 nm at 5 m spatial resolution. Three flight lines were acquired over the test site, two in direction NS and one in direction WE, in order to obtain spectro-directional information. Additionally to the imaging spectrometry data, MERIS (Full Resolution Level 1B) and MODIS (Level 1B) data were acquired. MERIS data was obtained one day before the HyMap and MODIS acquisition but under comparable weather conditions [Figure 3].

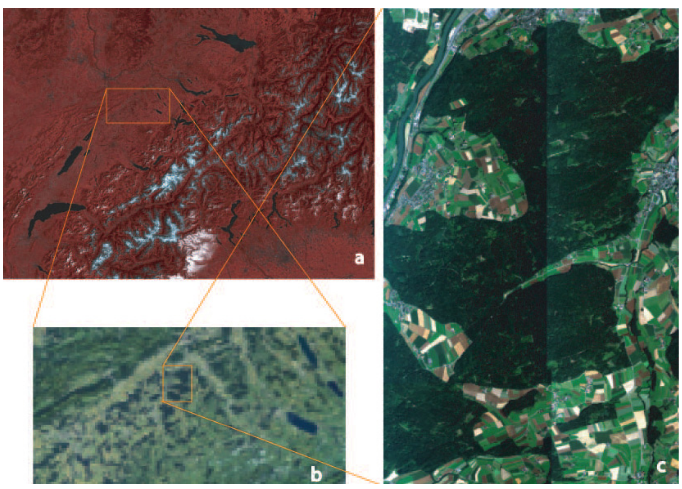

Fig. 3. a) MODIS 250 m spatial resolution, false color, b) MERIS 300 m spatial resolution RGB, and c) HyMap NS flight lines with 5 m spatial resolution.

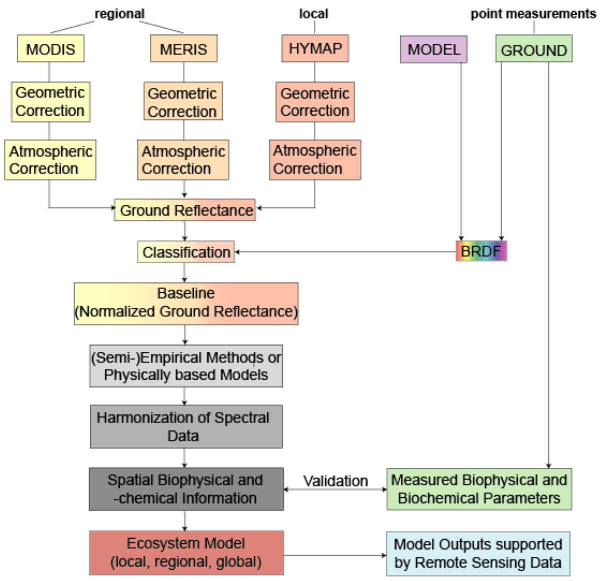

Fig. 4. Flowchart outlining the proposed approach for two the usage of various remote sensing data as input to local, regional or global ecosystem process models.

3. Methods

To obtain ground reflectance, the acquired reflectance data of every sensor has to be atmospherically and geometrically corrected. The airborne image data is orthorectified based on the parametric geocoding procedure PARGE [3]. The parametric geocoding methodology considers the terrain geometry and allows for the correction of altitude and flightpath-dependent distortions in airborne imagery. The approach relies on several auxiliary data such as Inertial Navigation System parameters, Ground Control Points (GCP), and a Digital Elevation Model (DEM) describing the terrain. Orthorectified imagery is a prerequisite for the subsequent radiometric correction. The radiometric correction of the geocoded and orthorectified imagery is performed using ATCOR4 [4], a software tool to invert the radiative transfer code MODTRAN4. ATCOR4 provides surface reflectance and temperatures performing a combined atmospheric/topographic correction where the effects of terrain of the observed surface are accounted for. The proposed approach for integrating various remote sensing data is given in Figure 4.

Classification: After preprocessing the data, main landcover classes have to be determined. Classification is a prerequisite for the subsequent landcover specific BRDF correction, which is performed using either measured or modeled HDRF data. Local spectro-directional observations are extrapolated across larger areas to retrieve corrected information.

Baseline: The atmospherically, geometrically and directionally corrected reflectance data are called baseline or normalized ground reflectance. This dataset serves as input to various semi-empirical and empirical techniques (e.g. vegetation indices, position of the inflection point of the red edge), physically based models (e.g. Prospect [5], Sail [6]), and analytical methods (e.g. Principal Component Analysis) for the acquisition of surface variables required by ecological models.

Harmonization: Since reflectance data of various sensors with different spectral and geometrical characteristics are combined, a convolution of the spectral data to the necessary bandwidth must be performed as well as a spatial upscaling to a common pixel size.

Validation: The retrieved spatial estimates of vegetation parameters are validated against ground truth data.

The verified spatial information can then be implemented into an ecosystem process model (e.g. Biome-BGC [7], PnET [8]). Ecosystem process models are important tools for applying the information provided by remote sensing products to quantify fluxes of carbon and other elements. Physiologically based process models, applied in a spatially distributed mode, can assimilate and effectively integrate a diverse assemblage of environmental data, including information on soils, climate, and vegetation [9].

4. Conclusion

The proposed approach shows the potential of combined remote sensing data in various model ouputs. Remote sensing data can be acquired with various instruments (sensors) and methods, leading to a large and heterogeneous dataset. In dependence of the research objective, the appropriate sensor or method is chosen in order to minimize disadvantages. But there lies also a great potential in the combination of multi-source remote sensing data both for correction purposes of sensor artefacts or directional effects and for the generation of an added value product.
The proposed approach reveals the following advantages:
- the generation of a remote sensing based input to regional and global models, which is spatially continuous and daily repeatable,
- retrieval of vegetation parameters over large areas, including spatial information on temporal dynamics
- validation/calibration of different sensors and observation geometries and
- datafusion in order to correct the image for bad pixels or clouds.

Possible disadvantages that strongly depend on the requested scale of the research objective are:
- a spatial and spectral information loss occurs due to the resampling and convolution process, which has to be performed,
- possible influence of a limited model performance (e.g. for modeled BRDF).

Acknowledgment

The authors would like to thank the Swiss Federal Institute for Forest, Snow and Landscape Research (WSL), DLR, and the Swiss National Science Foundation.

References

[1] Sandmeier S. and K.I. Itten, A Field Goniometer System (FIGOS) for Acquisition of Hyperspectral BRDF Data, *IEEE Transactions on Geoscience and Remote Sensing,* Vol. 37, 978–986, 1999.

[2] Schopfer, J.T. et al., Comparison of Field and Laboratory Spectrodirectional Measurements Using an Artificial Target, *Proceedings of 11th SPIE International Symposium on Remote Sensing*, Vol. 5570, 626–633, 2004.

[3] Schlaepfer, D. and R. Richter, Geo-atmospheric Processing of Airborne Imaging Spectrometry Data. Part 1: Parametric Orthorectification, *International Journal of Remote Sensing*, Vol. 23, 2609–2630, 2002.

[4] Richter, R. and D. Schlaepfer, Geo-atmospheric Processing of Airborne Imaging Spectrometry Data. Part 2: atmospheric/topographic correction, *International Journal of Remote Sensing*, Vol. 23, 2613–2649, 2002.

[5] Jacquemoud, S. and F. Baret, PROSPECT: a Model of Leaf Optical Properties Spectra, *Remote Sensing of Environment*, Vol. 34, 75–91, 1990.

[6] Verhoef, W., Light Scattering by Leaf Layers with Application to Canopy Reflectance Modeling: the SAIL Model, *Remote Sensing of Environment,* Vol. 16, 125–141, 1984.

[7] Running, S.W. and E.R. Hunt, Generalization of a Forest Ecosystem Process Model for other Biomes, Biome-BGC, and an Application for Global Scale Models. Scaling Processes between Leaf and Landscape Levels, *Scaling Physiological Processes: Leaf to Globe*, Academic Press, San Diego, 141–158, 1993.

[8] Aber, J.D. and C.A. Federer, A Generalized, Lumped-Parameter Model of Photosynthesis, Evapotranspiration and Net Primary Production in Temperate and Boreal Forest Ecosystems, *Oecologia*, Vol. 92, 463-474,1992.

[9] Turner, D.P. et al., Integrating Remote Sensing and Ecosystem Process Models for Landscape- to Regional-Scale Analysis of the Carbon Cycle, BioScience, Vol. 54, 573–584, 2004.

Application of Regression Tree Method for Estimating Percent Tree Cover of Asia with QuickBird images as training data

Rokhmatuloh[1*], H. Al-Bilbisi[1], K. Arihara[1], T. Kobayashi[1], D. Nitto[1], B. Erdene[1], K. Hirabayashi[1], T.A. Javzandulam[1], S.A Lee[1], E. Migita[1], N. Soliman[1], Y. Ouma[1], M. Aslam[2] and R. Tateishi[1]

[1]Center for Environmental Remote Sensing (CEReS), Chiba University, Japan
[2]Department of Post-Graduate Studies and Research in Geology,
Government College, Kerala, India
[*]Email: rahmat@graduate.chiba-u.jp

Abstract

Regression tree is more robust than linear regression method, primarily due to its capability of approximating complex non-linear relationships using a set of linear equations. The coarse resolution MODIS data were used as a predictor variable and as a training data, 22 scenes of very-high resolution QuickBird satellite were employed. Stepwise Linear Regression (SLR)-selected variables produced good result with prediction error of 5.70 percent and high correlation coefficient of 0.97. The zero percent tree covers wide areas in south-western parts of Asia, while 100 % tree distributed in south-eastern of Asia. This study also shows that regression tree method is more robust to overcome cloud problem existing in raw MODIS data, e.g. in the Equator areas.

Keyword: regression tree, predictor variable, training data, QuickBird, prediction erros

1. Introduction

Carbon dioxide (CO_2) in the atmosphere is a greenhouse gas that contributes significantly to global warming [1]. One possible strategy to reduce the green house gases with great potential is to use trees to sequester CO_2 [2]. The growing trees remove CO_2 from the atmosphere through the process of photosynthesis and store the carbon in plant structures [3]. Proportions of tree coverage are intended to be used within carbon models to improve our understanding of carbon dynamics at regional or global scales [4]. Different percent tree covers store different amounts of carbon and the changes in tree cover are used in the model to calculate annual changes of carbon [5][6]. Tree cover is the percentage of the ground surface area covered by a vertical projection of the outermost perimeter of the natural spread in the plants' folliage; small openings in the crown are included [7].

Previous studies to estimate tree cover percentage have utilized spectral mixture analysis (SMA) [8] and conventional linear regression techniques [9]. The SMA and linear regression techniques use linear model to approximate the relationship between spectral signal and canopy cover. However, such relationships are often very complex and highly variable, especially over large areas. A separate study of percent tree cover mapping was performed by the scientists from the University of Maryland (UM) using 500 m MODIS data [10]. This study applied regression tree method, which was subsequently modified by a stepwise procedure and bias adjustment. However, for training data, they used Landsat MSS (60 m) and TM (30 m) data where discrimination of tree and non-tree is relatively difficult. For each training data, each pixel was assigned one of four tree cover strata (0, 25, 50 or 80 %). Therefore, high resolution images, such as IKONOS or QuickBird, are required for better discrimination between tree, herbaceous, grass, urban and bare in the mix-land cover areas e.g. in [11][12].

This study describes an effort to develop a method to map percent tree cover of Asia with very-high resolution of QuickBird images as the training data or predicted variable. The explanatory or predictor variables were extracted from MODIS data. The percent tree cover information in annual basis is an important parameter in order to implement the Kyoto Protocol as committed by the United Nations Framework Convention on Climate Change (UNFCC) [9]. The percent tree cover estimation was accomplished using regression tree method. The regression-tree method estimates a case's target value in terms of its attribute values by constructing a model containing one or more rules, where each rule is a conjunction of conditions associated with a linear expression [13][14]. One advantage of the regression tree is the ability to effectively use proportion or continuous predictor data sets with different measurement scales [13].

2. Study Site and Data Acquisition

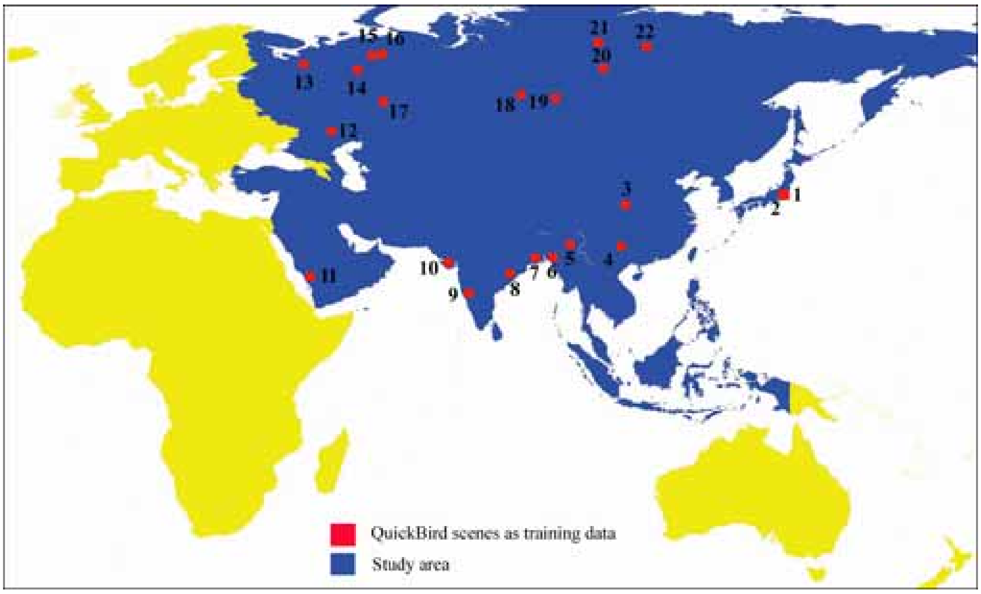

Fig. 1 Location of QuickBird scenes as training data

The study site is Asia, ranges from 70^0 U to 12^0 S and 25^0 E to 180^0 E and covering about 30 percent of the global land area (Fig. 1). To cover large area with daily acquisition, the coarse resolution of MODIS/TERRA nadir BRDF-adjusted reflectance 16 day L3 global 1 km SIN grid product (MOD43B4NBAR) data (MODIS) with seven bands (band 1 - 7) starting from January 1 to December 31, 2003 were used as input. The MODIS data were acquired from USGS in 10°x10° of Latitude/Longitude format. This data were then mosaicked and reprojected into Geographic Latitude/Longitude to have the same projection as QuickBird data. The 16-day MODIS bands data were composite to 32-day (monthly) data using maximum value (MVC) formula [15]. In addition to these monthly data, NDVI, Enhanced Vegetation Index (EVI) [16] and Normalized Difference Soil Index (NDSI) [17] were also extracted from MODIS data. Land Surface Temperature (LST) 8-day composite 1-km with same period as MODIS 16-day was also included in the explanatory or predictor variables for estimating percent tree cover [18]. The LST data are required to stratify geographically between dry woodland and moist forest in Asia [19]. This LST data contains two time observations: day and night data.

Table 1. QuickBird scenes employed in this study (22 scenes)

Scene	Acquisition Date (Y/M/D)	Center Coordinate (Lat/Long)	Off-Nadir Angle (degrees)	GLC2000`s Land Cover Classes
1	2003/06/05	35.17/139.86	27	Tree cover, needle-leaved, evergreen
2	2003/06/05	35.66/140.03	27	Artificial surfaces and associated areas
3	2003/06/14	33.93/107.28	14	Tree cover, broadleaved, deciduous, closed
4	2003/09/25	25.09/106.25	9	Shrub cover, closed-open, evergreen
5	2004/01/28	25.60/95.75	8	Tree cover, broadleaved, evergreen
6	2004/01/07	22.52/91.85	2	Shrub cover, closed-open, evergreen
7	2002/12/04	22.14/89.16	5	Tree cover, regularly flooded, saline water
8	2002/12/01	19.10/84.20	11	Tree cover, broadleaved, evergreen
9	2002/11/30	14.97/74.43	9	Tree cover, broadleaved, evergreen
10	2004/02/02	21.12/70.92	4	Tree cover, broadleaved, deciduous, open
11	2003/10/14	18.64/42.08	13	Sparse herbaceous or sparse shrub cover
12	2002/07/10	48.56/46.38	4	Sparse herbaceous or sparse shrub cover
13	2004/08/03	62.68/40.90	10	Tree cover, broadleaved, deciduous, closed
14	2004/06/27	64.54/55.67	7	Tree cover, needle-leaved, evergreen
15	2002/06/12	64.94/57.21	5	Tree cover, needle-leaved, evergreen
16	2003/09/10	61.76/52.30	5	Tree cover, needle-leaved, evergreen
17	2004/07/13	54.85/57.30	8	Tree cover, broadleaved, deciduous, closed
18	2002/07/19	56.57/85.71	10	Tree cover, broadleaved, deciduous, closed
19	2002/08/07	55.85/92.83	6	Tree cover, needle-leaved, evergreen
20	2004/06/27	62.02/102.65	5	Tree cover, needle-leaved, deciduous
21	2003/08/15	67.36/101.70	9	Bare areas
22	2002/08/29	66.33/111.60	8	Tree cover, needle-leaved, deciduous

For the training data, 22 scenes of QuickBird data were chosen to represent different land cover types according to Global Land Cover (GLC) 2000 map of Asia (Fig. 1 and Table 1) with each scene of QuickBird data covers an area of about 5 x 5 km in length and wide. QuickBird data is satellite imagery, which records high-resolution data in the visible and near-infrared range. The QuickBird data contains: multispectral data with 2.44 m resolution and panchromatic data with 0.60 m resolution. The multispectral bands are blue (450 – 520 nm), green (520 – 600 nm), red (630 – 690 nm), and near infrared (760 – 900 nm). For this study, the QuickBird pan sharpened 0.61 cm resolution data were used. The list of QuickBird scenes employed in this study is described in Table 1.

3. Methodology

Modeling an empirical relationship between percent tree cover as a predicted variable and MODIS 1 km data as a predictor or explanatory variables was accomplished using regression tree methods. The models were then applied to all pixels in a mapping area to produce a per-pixel estimation of a percent tree cover over Asia. This method quantifies the spatial distribution of tree cover as a continuous variable from 0 to 100%, and offers a repeatable technique to characterize percent tree cover for global area.

The main approach in this study consists of four steps:

1. Deriving percent tree data from very-high resolution QuickBird images using unsupervised clustering or supervised classification and visual interpretation,
2. Constructing predictor variables such as surface reflectance, NDVI, EVI, NDSI, and LST derived from MODIS data,
3. Selecting the potentially most useful predictor variables based on *Cp* statistics, and finally
4. Extrapolating spatially the developed models from Cubist to the entire 1-km MODIS data of Asia using National Land Cover Database (NLCD) mapping tool [20]. Fig. 2 illustrates the regression tree method applied in this study.

Percent tree covers, which then will be used as the ground truth data, from QuickBird scenes were obtained firstly, by clustering or supervised classification method. Then, this result will be refined by on-screen digitizing method in the areas where tree and non-tree were difficult to be separated each other. The predictor variables were extracted from monthly-composited MODIS data that consists of surface reflectances of band 1 to band 7, NDVI, EVI, NDSI and LST starting from January 1 to December 31, 2003. The selection of possible predictor variables is often a difficult process and expert knowledge is required. For this purpose, Stepwise Linear Regression (SLR) method [21] from S-PLUS [22], which is one of the classification and regression tree software, was accomplished and *Cp* statistic for each variable was examined. The SLR method selects the best subset of predictor variables to be employed in regression tree model using a stepwise procedure, which repeatedly altering the model at the previous step by adding or removing a predictor variables [21]. *Cp* statistic provides a convenient criterion for determining whether a model is improved by adding and dropping the predictor variables [22]. The *Cp* statistic specifies which predictor variables are significantly relevant to percent tree cover prediction. The *Cp* statistics is expressed in [21] as:

$$Cp = p + \frac{(n-p)(s_p^{\ 2} - \boldsymbol{\sigma}^2)}{\boldsymbol{\sigma}^2} \qquad (3)$$

where n is the number of observations (number of training data), p is the number of coefficients (number of predictor variables plus one), $s_p^{\ 2}$ is the mean square error (MSE) of the prediction model, and $\boldsymbol{\sigma}^2$ is the minimum MSE among the possible models which is the best estimate of the true error [21][22]. The best-selected predictor variables were then used for constructing model in Cubist by analyzing the relationships within the data and created an appropriate regression tree and rule set.

For evaluating the developed model, a total of 125 cells were separated from the total ground truth data (526 cells) in order to validate the model. The rules created from the developed model in Cubist were then extrapolated spatially to the entire 1-km MODIS data to produce a final percent tree cover map of Asia using NLCD mapping tool (see Fig. 2). The rules were applied according to the pixel values within the corresponding input imagery of predictor variables.

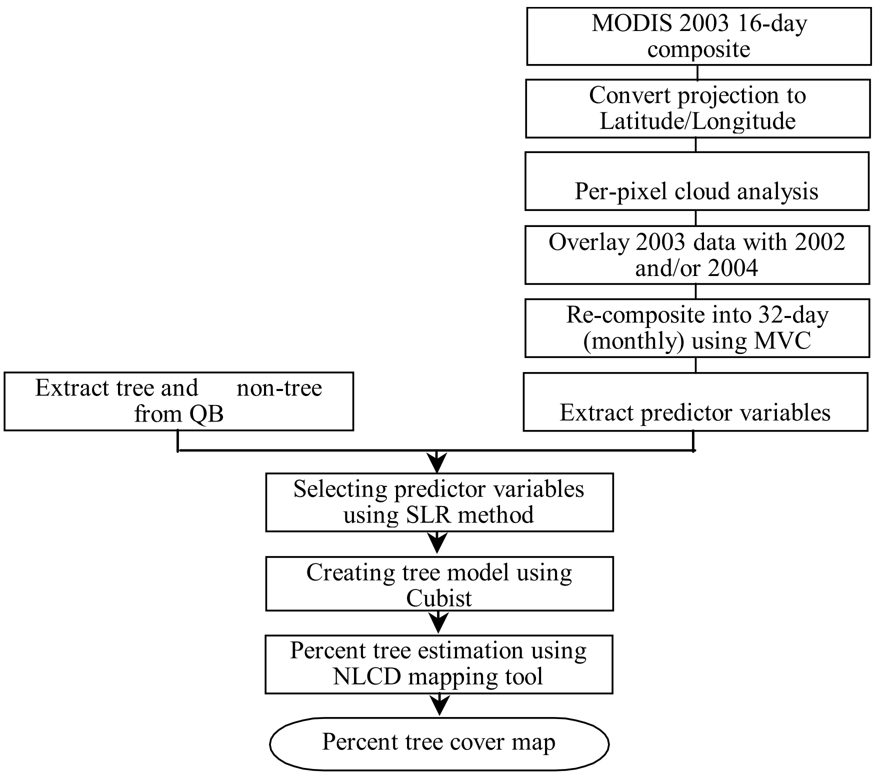

Fig. 2 Cloud contamination reduction and regression tree methods applied in this study.

4. Results and Analysis

The preliminary result of this study using only surface reflectances variables as predictor. With SLR-selected variables, the predictor variables were ordered in term of the months relevance to the percent tree cover estimation based on its *Cp* statistics. The higher *Cp* values compared to their initial *Cp* models means the more relevant variables for prediction (Table 2). The predictor variables with the *Cp* values greater than the *Cp* initial model were then included in developing model using Cubist. The *Cp* statistic for all significant variables are shown in Table 2 and it reveals that the *Cp* statistics varies depending on the variables selected for tree cover prediction.

Table 2. Selected predictor variables using SLR method for surface reflectances

Predictor Variable	Months
Surface reflectances	**Jan** (b3, b5, b7), **Feb** (b5, b6), **Mar** (b3, b5, b6, b7), **Apr** (b1, b2, b7), **May**(b1, b2, b4, b5, b6, b7), **Jun**(b5, b6), **Jul**(b2, b4, b7), **Aug**(b2, b4, b5, b6, b7), **Sep**(b1), **Oct**(b1, b3), **Nov**(b6, b7), **Dec** (b1, b3, b4, b5, b6, b7)

The percent tree cover map resulted from SLR-selected variables method is shown in Fig. 3. The values range from 0 to 100 %. The zero percent tree covers wide areas in south-western parts of Asia, while 100 % tree distributed in south-eastern of Asia. Low percentage of tree cover distributed also in the northern part of Asia and the central parts of Asia with the percentage ranges from 0 to 30 %. This figure shows also the percentage of tree covers in areas with frequently covered by cloud in raw MODIS data, e.g. in the

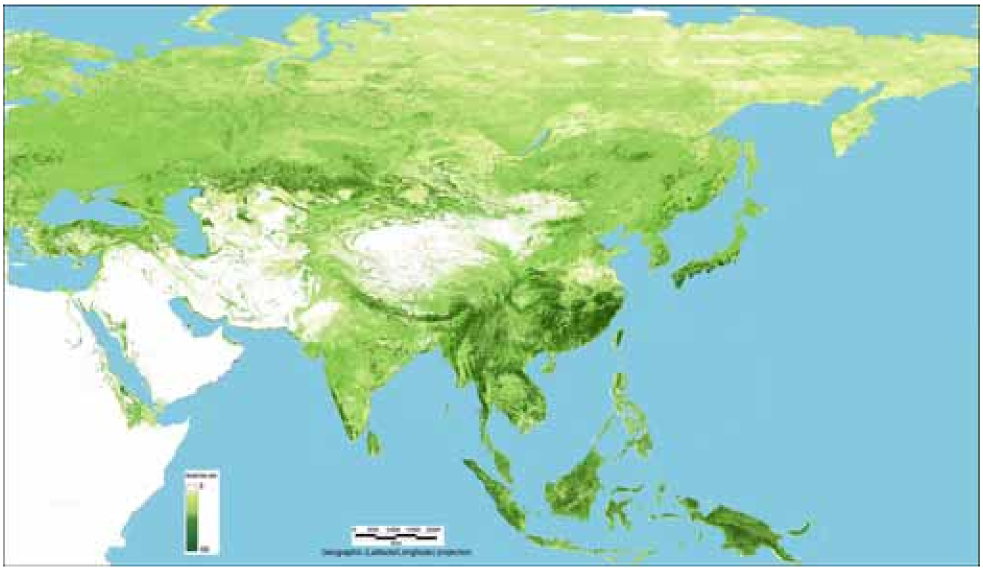

Fig. 3 Final percent tree cover map for Asia using SLR-selected variables.

Equator areas. With regression tree method such areas were resolved based on surface reflectance values from other cloud-free months. This advantage is important for frequent global forest/tree cover change study.

Validation of the regression tree result was made through validation cells (a total 125 cells) The validation cells were selected from the ground truth data based on a stratified random sampling method and also contain percent tree cover values ranging from 0 to 100 % (Table 3). The prediction model derived from SLR-selected variables produced a low prediction error (5.70%) and contributes significantly to depict percent tree cover mapping. Table 3 also demonstrates a high correlation coefficient for this result (0.97). The future of this study will use all predictor variables as described in the previous parts.

Table 3. Prediction error and correlation coefficient for SLR-selected variables

Predictor Variables	Prediction Errors (%)	Correlation Coefficients (R^2)
SLR-selected variables	5.70	0.97

5. Conclusions

The very-high resolution QuickBird data is an improvement for depicting a continuous percent tree cover of training data. From accuracy measurement demonstrated that SLR-selected variables produced good result with prediction error of 5.70 % and high correlation coefficient of 0.97. The zero percent tree covers wide areas in south-western parts of Asia, while 100 % tree distributed in south-eastern of Asia. Low percentage of tree cover distributed also in the northern part of Asia and the central parts of Asia with the percentage ranges from 0 to 30 %. The result shows also the percentage of tree covers in areas with frequently covered by cloud in raw MODIS data, e.g. in the Equator areas. The regression tree is an advance as well, in that it can handle the non-linear relationships in the training data.

Acknowledgments

The MODIS data used in this study were acquired as part of the NASA's Earth Science Enterprise. The data were processed by the MODIS Adaptive Processing System (MODAPS) and Goddard Distributed Active Archive Center (DAAC), and are archived and distributed by the Goddard DAAC. NLCD mapping tool software used courtesy of USGS. This study was carried out as a part of activities by Working Group 4 of Global Mapping project.

References

[1] IPCC, *Climate Change 1992: The Supplementary Report to the IPCC Scientific Assessment.* Cambridge University Press, Cambridge, 1992.

[2] World Bank, *World Development Report 1992: Development and the Environment*. Oxford University Press, New York, 1992

[3] R.K. Dixon, S. Brown, R.A. Houghton, A.M. Solomon, M.C. Trexler, and J. Wisniewski," Carbon pools and flux of global forest ecosystems," *Science*, no.263, pp. 185-190, 1994.

[4] C. Marsh, "Carbon dioxide offsets as potential funding for improved tropical forest management," *Oryx*, vol. 27, no. 1, pp. 2-3, Jan1993.

[5] R.A. Houghton and J.L. Hackler, " Changes in terrestrial carbon storage in the United States. I: The roles of agriculture and forestry, " *Glob. Ecol. Biogeo.,* vol. 9, pp. 125-144, Mar. 2000.

[6] R.B. Myneni. J.. Dong, C.J. Tucker, R.K. Kaufmann, P.E. Kauppi, J. Liski, L. Zhou, V. Alexeyev, and M.K. Hughes, "A large carbon sink in the woody biomass of Northern forests", *Proc. of the Nat. Acad. Sci.,* vol. 98, no. 26, pp. 14784-14789, Dec. 2001.

[7] FAO (Food and Agriculture Organization), *Forest resources assessment 2000: term and definition*. *FAO forestry paper 1*, FAO, Rome, 1998.

[8] L.R. Iverson, E.A. Cook, and R.L. Graham, "A technique for extrapolating and validating forest cover across large regions: calibrating AVHRR data with TM data," *Int. J. Remote Sens.,* vol. 10, no. 11, pp. 1805-1812, 1989.

[9] R. DeFries, M. Hansen, J.R.G. Townshend, A.C. Janetos, and T.R. Loveland, "A new global 1km data set of percent tree cover derived from remote sensing," *Glob. Change Bio.,* vol. 6, pp. 247-254, Feb. 2000.

[10] M.C. Hansen, R.S. DeFries, J.R.G. Townshend, M. Carroll, C. Dimiceli, and R.A. Sohlberg, "Global percent tree cover at a spatial resolution of 500 meters: first results of the MODIS vegetation continuous field algorithm," *Earth Inter.*, vol.7, no. 10, pp. 1-15, Dec. 2003.

[11] Y. Zhang, "Texture-integrated classification of urban treed areas in high-resolution color-infrared imagery," *Photogram. Enggineer. Remote Sen.,* vol. 67, no. 12, pp. 1359-1366, Dec. 2001.

[12] S. Myeong, D.J. Nowak, P.F. Hopkins and R.H. Brock, "Urban cover mapping using digital, high-spatial resolution aerial imagery," *Urban Eco.,* vol. 5, pp. 243-256, 2003.

[13] C. Huang and J.R.G. Townshend, "A stepwise regression tree for nonlinear approximation: applications to estimating sub-pixel land cover," *Int. J. Remote Sens.*, vol. 24, no.1, pp. 75-90, Jan. 2003.

[14] L. Breiman, J. Friedman, R. Olshen, and C. Stone, *Classification and RegressionTrees*. Chapman and Hall, New York, 1984, ch.2.

[15] A. Moody and A. H. Stahler, "Characteristics of composited AVHRR data and problem in their classification," *Int. J. Remote Sens*., vol. 15, no. 17, pp. 3473-3491, 1994.

[16] A.R. Heute, "Soil and atmospheric influences on the spectra of partial canopies," *Remote Sens. Environ*., vol. 25, no. 1, pp. 89-105, June 1988.

[17] W. Takeuchi and Y. Yasuoka, “Development of normalized vegetation, soil and water indices from satellite remote sensing data,” in *Proc. 25th ACRS*, Chiang Mai, Thailand, 2004, pp. 859-864.
[18] M. Hansen, R. Dubayah, and R. DeFries, ”Classification trees: an alternative to traditional land cover classifiers,” *Int. J. Remote Sens.*, vol. 17, no.5, pp. 1075-1081, Jan. 1996.
[19] Z. Zhu and E. Waller, “Global forest cover mapping for the United Nations Food and Agriculture Organization forest resources assessment 2000 program,” *For. Science*, vol. 49, no. 3, pp. 369-380, Jun. 2003.
[20] L. Yang, C. Huang, C.G. Homer, B.K. Wylie, and M.J. Coan, “An approach for mapping large-area impervious surface: synergistic use of Landsat 7 ETM+ and high spatial resolution imagery,” *Can. J. Remote Sens.*, vol. 29, no. 2, pp. 230-240, Apr. 2003.
[21] D.R. Helsel and R.M. Hirsch, *Statistical Methods in Water Resources*. Elsevier Science Publishers B.V, Amsterdam, The Netherland, 1992, ch.11.
[22] Insightful Corp., *S-PLUS 6.2. Guide to Statistics, Volume 2.* Seatle, Washington, 2001, ch.19.

Derivation of distributions of surface albedo over land areas in Japan from GMS-5/VISSR images

Koji Horiuchi,[1)] Hiroyuki Sakai,[1)] Mitsuo Minomura,[1,2)] Bannu,[1)]
Hiroaki Kuze,[1)] Nobuo Takeuchi,[1)]
[1)] Center for Environmental Remote Sensing, Chiba University,
1-33 Yayoi-cho, Inage-ku, Chiba 263-8522, Japan
[2)] Earth observation research and application center, Japan Aerospace Exploration Agency, 1-8-10 Harumi, Chuou-ku, Tokyo 104-6023, Japan

Abstract: Satellite remote-sensing data on the sea and land areas provide the information on both the surface albedo and aerosol optical thickness (AOT). In this study, the surface albedo distributions are derived from the satellite data on the monthly composite image with relatively clear atmosphere, and subsequently, the AOT at 550 nm is extracted for relatively turbid days. The temporal changes of the albedo and AOT distributions are derived from GMS-5/VISSR visible images with radiance components calculated by the MODTRAN4 code.
Keywords **:** GMS-5/VISSR, atmospheric correction, ground albedo, aerosol optical thickness, MODTRAN4

1. Introduction

Radiances measured by a satellite sensor include the effect of extinctions (i.e. the sum of scattering and absorption) due to air molecules and atmospheric aerosols. Although ground sensors provide local values of aerosol extinction, generally ground-based measurements over a wide range are not practical. If albedo distributions are available a priori, two-dimensional aerosol distributions can be readily obtained from satellite images. Recently, we have investigated the method of deriving the ground albedo and aerosol optical thickness (AOT) over the Chiba area from high-resolution, Landsat-5/TM data.[1)] In the present paper, we employ the GMS-5/VISSR data, which provide us with hourly data,[2)] in contrast with the data at fixed local time in the case of polar-orbiting satellites such as the Landsat satellite. From the GMS data, the atmospherically corrected albedo image (ρ_{clear} map) is derived over and around the main islands in Japan under relatively clear atmospheric conditions. This albedo information, in turn, is used to generate the two-dimensional distribution of AOT (τ map) every one hour during the daytime. We use the channel 1 (wavelength: 0.55-0.99 μm) data of GMS-5/VISSR on August and December 1998. Images are extracted by choosing 200 pixels×200 pixels around the main land area in Japan.

2. Method

2.1 Generation of the lookup table

The radiation-transfer code, MODTRAN4,[3)] is employed to calculate the total radiance L_{total} $(\rho, \bar{\rho}, \tau_{550})$ at the top of the atmosphere for the GMS-5/VISSR visible channel. Here, ρ stands for the diffuse albedo of the target (with the assumption of Lambertian reflectance), $\bar{\rho}$ is the average albedo around the target pixel, and τ_{550} the AOT at the wavelength of 550 nm. In the algorithm of the code, the wavelength dependence of the extinction (and absorption) is dictated by the aerosol model chosen in the calculation. Here we assume the maritime model throughout the present study. As explained below, the choice of the aerosol model does not influence the resulting albedo distribution in a significant way, though the choice is more influential in the AOT retrieval from relatively turbid images. For each pixel in the VISSR image, appropriate values of the solar and observation geometry are given to the code as well.

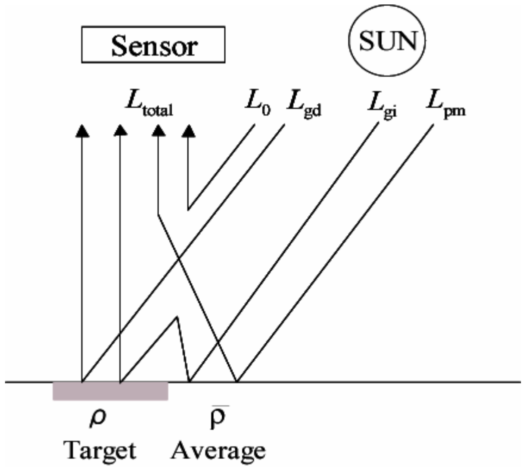

Fig.1 Radiance components at the top of the atmosphere. These values are calculated by the MODTRAN4 code.

Figure 1 illustrates the four radiance components required in the process of atmospheric correction.[4)] Among the four components, three components (direct reflection L_{gd}, indirect reflection L_{gi}, and path-radiance involving the surface scattering L_{pm}) are dependent on the surface albedo values, while the last component (L_0) stands for the path radiance that is dependent only on the atmospheric conditions. Using these four components, the total radiance (L_{total}) is given as

$$L_{total}\left(\rho, \bar{\rho}, \tau_{550}\right) = S_{gd}\left(\tau_{550}\right) \times \rho + S_{gi}\left(\tau_{550}\right) \times \rho \times \bar{\rho} + S_{pm}\left(\tau_{550}\right) \times \bar{\rho} + L_0\left(\tau_{550}\right) \qquad (1)$$

In the present analysis, we omit the consideration on the adjacency effect ($\rho = \bar{\rho}$).

2.2 Derivation of ground albedo

From the condition that the calculated value of the total radiance $L_{total}(\rho, \tau_{550})$ is equal to the observed radiance $L_{obs}(DN)$ (here DN stands for the digital number of a pixel in the satellite image), we can construct a lookup table (LUT) that shows the relationship among ρ, τ_{550} and DN. An example of this relationship is shown in Fig. 2. From Fig.2, it is evident that when the value of the AOT is small (clear atmosphere), the ρ-τ_{550} relation does not change significantly even when a different aerosol model is assumed for the calculation of the LUT. For clear atmosphere, in addition, the value of ρ varies only slightly for a small change of τ_{550}. Here the ρ_{clear} map is derived under these assumptions, and furthermore, the map is considered as representing the albedo distribution of the relevant region during the same season.

Unlike the case of TM images, it is rather difficult to find a completely "clear" day for the VISSR images around Japan. Therefore we deal with the images over a time span of one month, and synthesize a hypothetically clear image by

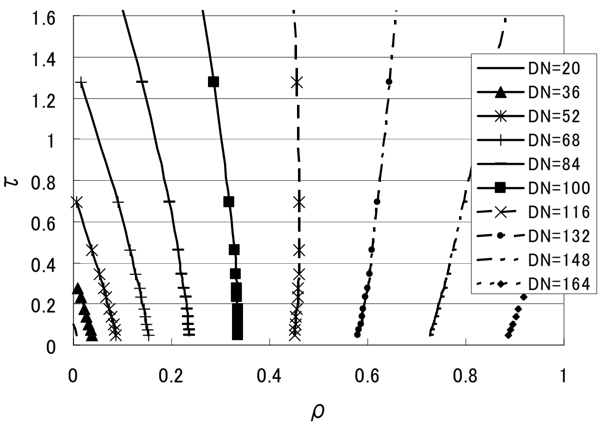

Fig.2 Relationship between albedo ρ and aerosol optical thickness τ=τ_{550}.

choosing pixels that exhibit the smallest (or second smallest) DN values. It is noted that sometimes, pixels with the second smallest DN must be chosen, since the rainfall on the day before, for example, might have caused irrelevantly small value of the surface albedo. We assume in this atmospheric correction procedure that the AOT can be given as τ_{550}=0.1. The error range associated with this assumption will be discussed in Sec. 3.3. Another important aspect about the present analysis is that the ρ_{clear} image needs to be prepared for each local time, since it is found that the albedo values exhibit non-negligible variations in accordance with the change of the solar position.

2.3 Derivation of aerosol optical thickness

In order to derive the distribution of AOT, we choose images that are mostly free from the effect of clouds, but considerably affected by aerosols. For each pixel, the determination of τ_{550} is straightforward, since the LUT calculated as mentioned above can be used to derive τ_{550} from each pixel using the corresponding *DN* (from the satellite data) and ρ (from the ρ_{clear} image) values.

3. Results and discussion

3.1 Albedo distribution

Examples of the ρ_{clear} maps are shown in Fig. 3. As a whole, as the local time (Japan Standard Time, JST) changes, the albedo values change as well. Since the viewing angle is kept constant in the case of the geo-stationary satellite, this change is traced back to the change in the solar zenith angle. In Fig. 3, some areas over the ocean show high albedo values. These correspond to the pixels with high DN values even in the case of the monthly composite image, indicating insufficient removal of the cloud effects.

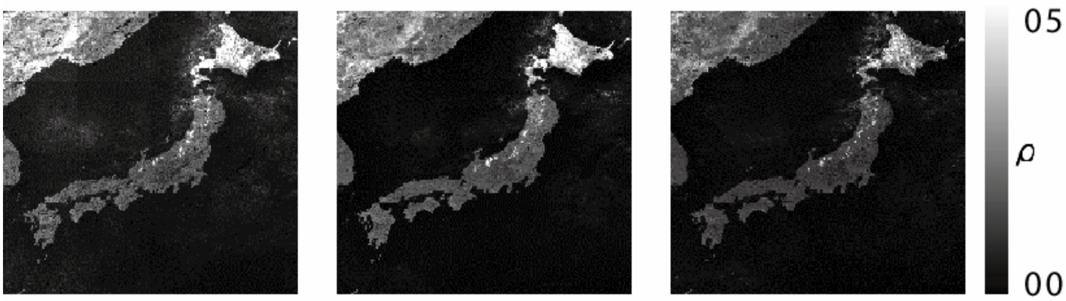

(a) (b) (c)

Fig.3 ρ_{clear} maps for (a) 9:00, (b) 11:00, (c) 13:00 JST in December 1998.

3.2 AOT distribution

Multi-temporal τ_{550} maps on a relatively turbid day (13 December 1998) are shown in Fig. 4, where the albedo image (monthly composite) used in the retrieval is the one at 10:00 JST. In this case, appropriate masks are applied for areas with outside the reasonable range in the ρ-τ_{550} relationship (e.g. τ_{550}>1) shown in Fig. 2. In Fig. 4, it is found that the temporal variation of AOT is large, and the resulting τ_{550} values are in general considered too high over the land regions. In Fig. 5, the temporal τ_{550} maps on the same day as in Fig. 4 are shown, but here they are based on the temporal ρ_{clear} maps, each corresponding to the same local time as the turbid image. In Fig. 5, the temporal change in τ_{550} is smoother, and reasonable values are obtained over both the ocean and land regions. This example indicates that in order to derive reasonable τ_{550} maps, it is required to employ the ρ_{clear} map that corresponds to the same local time.

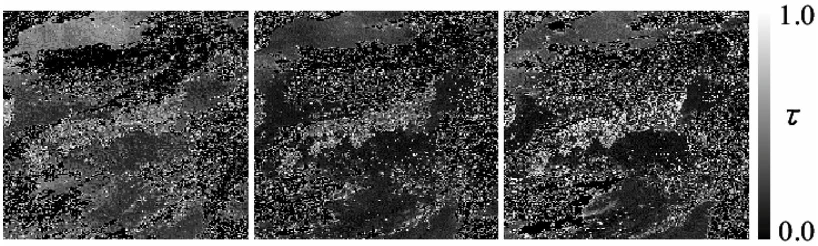

(a) (b) (c)

Fig.4 τ_{550} maps on a relatively turbid day (13 December 1998) calculated with a fixed ρ_{clear} map (10:00 JST, December 1998): (a) 9:00, (b) 11:00, and (c) 13:00 JST.

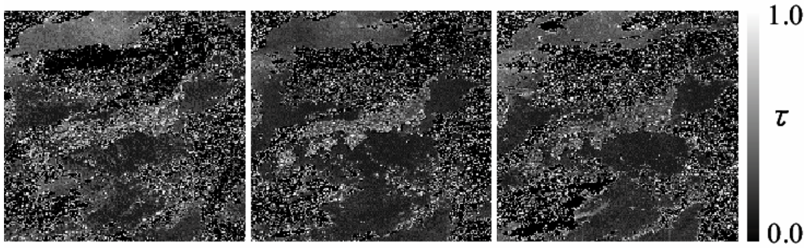

(a) (b) (c)

Fig.5 τ_{550} maps on a relatively turbid day (13 December 1998) calculated with the ρ_{clear} map for the same local time: (a) 9:00, (b) 11:00, and (c) 13:00 JST.

3.3 Accuracy of the albedo map

Comparison of ρ_{clear} images from the August and December observations is shown in Fig.6. In the latter (winter) case, high albedo values are observed in the Hokkaido (northern island) and northern areas along the Sea of Japan due to the ground snow. In the former (summer) case, low albedo values are observed over the land areas along the seashore. If no irregularities in the data are responsible for these low albedo values, the most plausible cause would be the local weather.

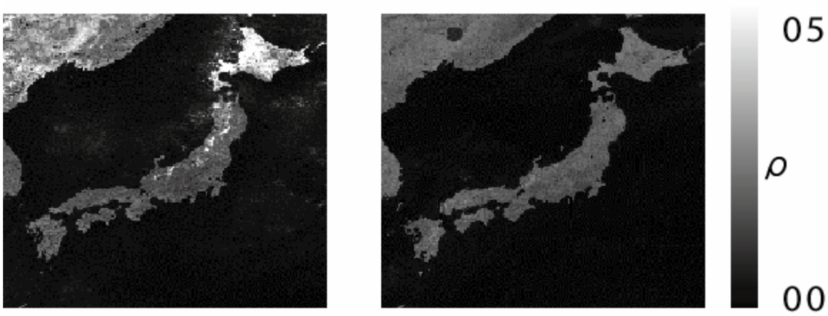

(a) (b)

Fig.6 ρ_{clear} map using the minimum *DN* image: (a) 10:00 JST, December 1998, (b) 10:00 JST, July 1999.

Figure 7 shows an example of the monthly variation of DN values for a pixel that has shown very small DN values. It is seen from Fig. 7 that such small values of DN are found just after the days with higher DN values, suggesting the occurrence of rainfall and subsequent enrichment in the soil moisture. In this context, the use of the lowest DN is often problematic. The ρ_{clear} map corresponding to the second lowest DN is shown in Fig. 8. Here, recovery of the seashore albedo values is seen, at the expense of somewhat insufficient removal of the cloud effects.

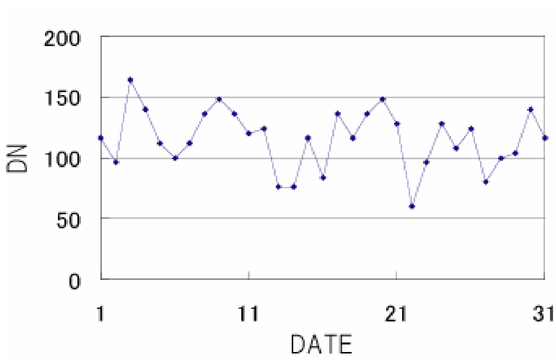

Fig.7 Monthly change of *DN* for a fixed pixel (December 1998, in land area).

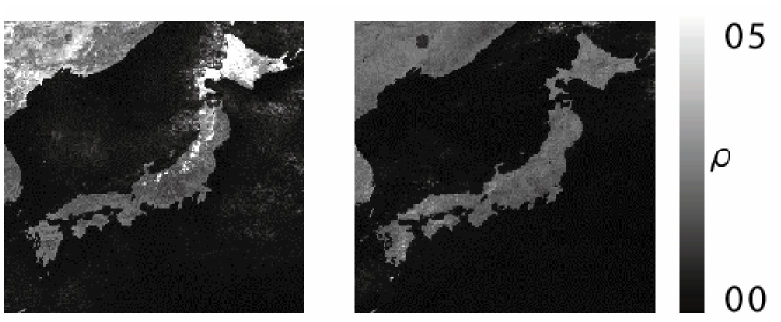

(a) (b)

Fig.8 ρ $_{\text{clear}}$ map using the second smallest *DN*.
(a) 10:00 JST, December 1998, (b) 10:00 JST, July 1999.

The effect of the AOT assumption (τ_{550}=0.1) in the derivation of the ρ_{clear} map is examined in the resulting ρ_{clear} maps. At two pixels over the land area each having *DN*=40 and 80 respectively, the values of ρ are studied for three values of AOT (τ_{550}=0.08, 0.10, and 0.12). The result is ρ=0.0397, 0.0391, and 0.0382 for *DN*=40 and ρ=0.2121, 0.2118, and 0.2114 for *DN*=80. Therefore the error is insignificant, on the order of 2%.

4. Conclusions

We have constructed time-dependent albedo maps form the monthly composite imagery of GMS-5/VISSR channel 1 (visible and near-infrared) data. These ρ_{clear} maps are used to derive the temporally changing AOT distribution maps (τ_{550} maps) for a relatively turbid day in the same season. By matching the local time between the albedo and AOT maps, we have obtained reasonable AOT distributions over both sea and land surfaces. In some regions, however, the separation between the sea and land areas is still evident: this can be treated more suitably by, for example, improving the aerosol model with consideration on the regional change of aerosol optical properties. More theoretical validation is needed to check the validity of the temporal changes found in the ρ_{clear} maps, since this apparent BRDF effect[6)] is significant in spite of the fact that the effect is brought about mainly by the change in the solar zenith angle.

It has also been turned out that the AOT value assumed for the derivation of the ρ_{clear} map does not affect the result in a significant way. However, care must be taken with respect to the appropriate choice of the dark pixels (low DN values). The long-term retrieval of accurate albedo and AOT maps will contribute greatly to the understanding of the atmospheric trends around the Japanese archipelago and East Asia. For that purpose, we will continue our effort on further improvement in the accuracy of the albedo and AOT maps.

References

1) Y. Todate. M. Minomura, K. Asakuma, H. Kuze, N. Takeuchi, Consideration on the derivation method of aerosol information over land areas from Landsat-5/TM data, Proceedings of 36th Scientific Meeting of Remote Sensing Soc. Jpn., pp.57-58 (2004) (in Japanese).

2) K. Horiuchi, M. Minoura, Y. Todate, H. Kuze, N. Takeuchi, Determination of albedo and AOT distributions around Japan using the visible data of GMS-5/VISSR, Proceedings of the 38th Scientific Meeting of Remote Sensing Soc. Jpn., pp.55-56 (2005) (in Japanese).

3) A. Berk, G.P. Anderson, P.K. Acharya, J.H. Chetwynd, M.L. Hoke, L.S. Berntein, E.P. Shettle, M.W. Matthew, and S.M. Adler-Gordon: MODTRAN4 Version2 USER'S MANUAL, Air Force Research Laboratory.

4) M. Minoura, H. Kuze, N. Takeuchi, Method for atmospheric correction and derivation of AOT distributions from Landsat-7 ETM+ imagery using the lookup table calculated with MODTRAN4 code, Proceedings of the 36th Scientific Meeting of Remote Sensing Soc. Jpn. pp.59-60 (2004) (in Japanese)

5) International Satellite Cloud Climatology Project (ISCCP) Web Site (http://isccp.giss.nasa.gov/)

6) P. North, Three-dimensional forest light interaction model using a Monte Carlo method, IEEE Transactions on Geoscience and Remote Sensing, 34, 946-956 (1996)

Cloud characterization in Chiba area from dual-site lidar observation and NOAA-AVHRR satellite

Gerry Bagtasa[1], Cheng Liu[1,2], Hiroaki Kuze[1], Nobuo Takeuchi[1],

Suekazu Naito[3], Akihiro Sone[4], Hirofumi Kan[4]

[1]*Center for Environmental Remote Sensing, Chiba University*

[2]*Science and Technology University of China*

[3]*Chiba Prefectural Environmental Research Center,*

[4]*Hamamatsu Photonics K.K.*

E-mail address: gerry@graduate.chiba-u.jp

Abstract

Cloud heights and cloud types are characterized from the lidar data observed by two continuously operated portable automated lidar (PAL) systems and images from the visible and thermal infrared channels of NOAA16-AVHRR. The PAL systems are located in Chiba and Ichihara city areas, separated by approximately 10 km from each other. Measurements from October 2003 to March 2004 reveal that similar cloud structures are observed especially when the wind is along the path connecting the two sites. Slight time lags are frequently observed in the cloud occurrence, and they can be explained from the wind velocity data in the region. Monthly average of cloud base height (CBH) and cloud cover ratio show good correlation between the two sites. Cloud-type classification using a threshold technique in split window data of NOAA16-AVHRR gives results that are found to be consistent with the PAL cloud observations.

1. Introduction

Cloud information such as the cloud type, structure and altitude is of importance for a variety of meteorological and climatological applications. By intercepting the solar radiation, clouds have a cooling effect on the earth's surface.[1)] Knowledge of cloud properties can give us the thermodynamic and hydrodynamic structure of the atmosphere. The height of an inversion layer can often be related to the cloud appearance.[2)] In this study, we compare the ground-based lidar observations with the satellite-derived cloud information over the Chiba area, continuously unaided operation of PAL allowed for long term cloud monitoring without sacrificing the high temporal and spatial resolution, also, this study validates the usefulness of the split-window technique in the cloud classification.

2. System

Lidar data are obtained from two identical portable automated lidar (PAL)[4)] systems. One of the PAL systems is located in Ichihara, at the Chiba Prefectural Environmental Research Center (CERC) (35.52N, 140.07E), while the CEReS PAL system is on the main campus of Chiba University (35.62 N, 140.12 E). These two sites are about 10 km apart from each other (Fig. 1). Both are Mie scattering lidar systems capable of measuring backscattered radiation of up to 15 km in altitude. Specifications of the two PAL systems are given in Table 2. Both systems are equipped with automatic realignment systems that adjust laser beam directions every 15 min to ensure proper lidar alignment.

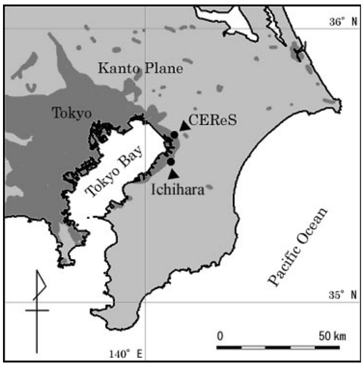

Fig. 1: Location of 2 PAL systems.

The images from thermal infrared channels (ch.4, 10.3-11.3 μm and ch.5, 11.5-12.5 μm) and visible channel (ch.1, 0.58-0.68 μm) of Advanced Very High Resolution Radiometer (AVHRR) on board the NOAA16 satellite are used for classifying cloud types. In the split-window technique, threshold values are assumed in the 2-D histogram whose axes are the brightness temperature of the ch.4 data and the brightness temperature difference (BTD) between the ch.4 and ch.5 data.[3)] Table 2 shows main characteristics of the NOAA16/AVHRR sensor

Table 1: Portable Automated Lidar System Specification

	Ichihara	**Chiba Univ.**
Configuration	Co-axial 38^0 slant path	Co-axial 90^0 Vertical
Laser	LD-pumped Q-switch Nd:YAG	
Wavelength	532nm	
Repetition rate	1.4 kHz	2.5 kHz
Laser energy	15mJ	
divergence	50μrad	
Receiver		
Diameter	20cm	
Type	Cassegrain	
Field of view	0.2 mrad	

Table 2: NOAA-16 Specification Orbital characteristics	
Orbit inclination	98.8 deg
Mean altitude (km)	851
Equator crossing time	Northbound 13:54A Southbound 1:54D
Period (min.)	102.1
AVHRR characteristics	
resolution	1.1 km
Swath width	3000 km
Spectral range / IFoV	
Channel 1 (visible)	0.50 - 0.68 μm / 1.39mrad
Channel 4 (infrared)	10.3-11.3 μm / 1.41 mrad

Figure 2 shows the two-dimensional diagram with threshold values used in the present analysis. The classes are cirrus (Ci), dense cirrus (with emissivity greater than about 0.8), cumulo-nimbus (Cb), and cumulus (Cu, including stratocumulus). The hatched area above Cu indicates non-classifiable region. Since the threshold values given in ref.3 are mainly for tropical clouds, here we have adopted slightly different values for the cloud retrieval over the Kanto plain area. This adjustment has been attained by inspecting visible, infrared, and BTD images. The result shows that (i) cirrus clouds show relatively larger values of BTD, (ii) cirrus clouds have low reflectivity and are relatively cold, (iii) cumulus clouds exhibit small BTD, and (iv) cumulus clouds have relatively high reflectivity in visible images and relatively warm in infrared images. By this method, very thin cirrus clouds can be detected, even if they cannot be seen clearly in visible images. Cumulus cloud cover is also retrieved reasonably well.

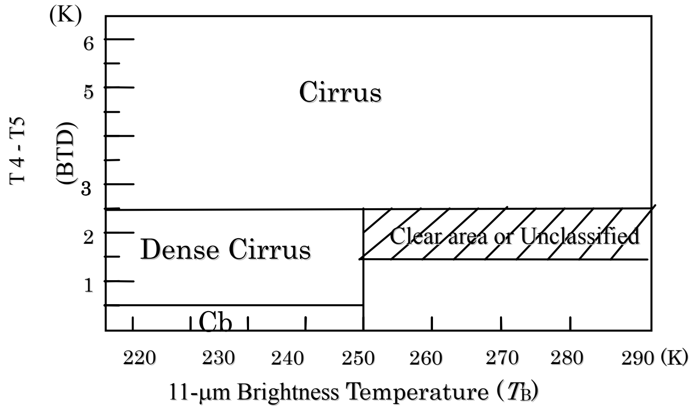

Fig. 2 Two-dimensional diagram for cloud-type classification used in this study

3. Results and discussion

The range-corrected back- scattered signal of the two PAL systems from 23:00 JST of 2 June to 4:00 of 3 June 2004 are shown in Fig. 4(a) and (b) for CEReS and Ichihara sites, respectively. Strong backscattering, shown with brighter shade, from clouds is found in the altitude range of about 5–7 km. Due to the orientation of the systems, both PAL systems are actually observing about the same cloud at this altitude range, thus we can observe similar cloud structure in Figs. 4(a) and (b). The observed clouds have downward streaks. This indicates the presence of falling cloud particles (heavy ice particles), the observed cloud is indicative of a cirrus type cloud. Figure 5 shows the cloud type classification map (1:00 JST on 3 June 2004). As indicated in the figure, cloud types of dense cirrus and cumulo-nimbus are seen, in addition to unclassified (or cloud free) area. This is consistent with the PAL observation.

Figure 6 shows the brightness temperature of the same scene as Fig. 3. The measured temperature in the area of the two PAL sites is about 253.5 K. Assuming that the cloud emissivity is around unity, we can estimate the cloud top height at approximately 6 km from the vertical temperature profile observed by a sonde at Tsukuba. Although Tsukuba is about 50 km away from Chiba, the high altitude of the clouds leads to the consistency among the results. However, for optically thin clouds, a previous study[5] using inversion of visible and infrared radiances from such clouds overestimates a typical cirrus cloud by about 15 K, which amounts to cloud top height underestimation of about 2 km. More results will be presented at the symposium.

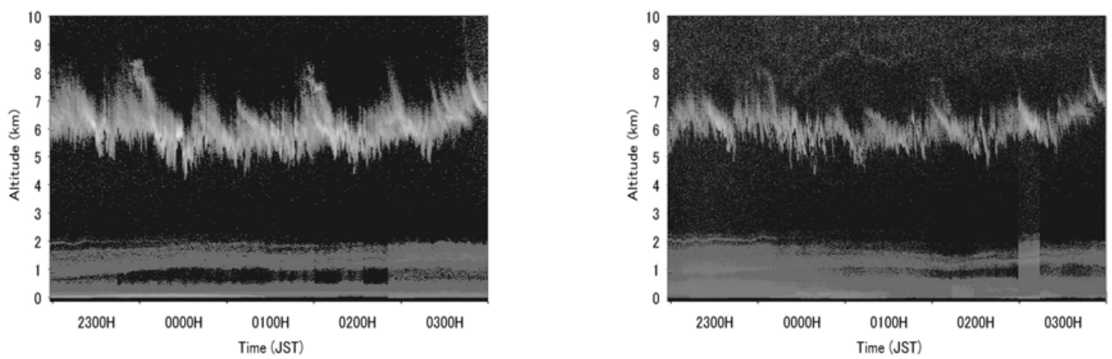

(a) (b)

Fig. 4 PAL data for 23:00 JST on 2 June 2004 to 4:00 JST on 3 June 2004: (a) CEReS PAL and (b) Ichihara PAL.

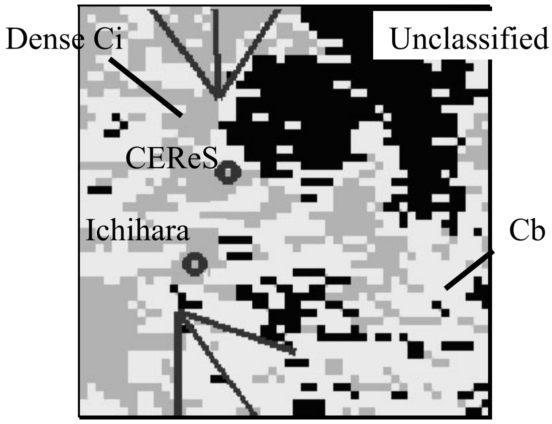

Fig. 5 Cloud classification map obtained from satellite data at 1:00 JST on 3 June 2004. The area of the image is approximately 80×60 km^2.

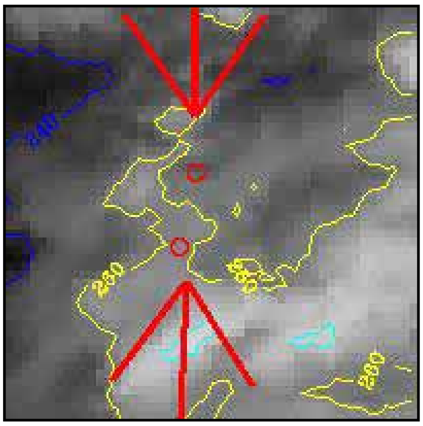

Fig.6 Brightness temperature map (channel 4) obtained from satellite data at 1:00 JST on 3 June 2004.

4. Conclusion

This study has shown that continuous cloud observation can be attained using the PAL system. The operation of two virtually identical lidar systems separated about 10 km has revealed that local cloud distribution is almost non-varying. We have applied the split-window technique to derive cloud-classification maps from NOAA-AVHRR images. The method is based on the brightness-temperature data in the infrared bands, mostly corresponding to the information at cloud top height. Lidar observations, on the other hand, can provide data that are mostly from the cloud base height. Nevertheless, consistent results in cloud type classification have been obtained between the cloud observations using the PAL systems and the result of cloud classification using the split-window data of NOAA16-AVHRR. Moreover, if clouds are not very thick, present results show that lidar data are useful for the validation of the cloud's physical structure as observed by satellite.

5. References

1. R.R. Rogers and M.K. Yau, 1989, A short course in cloud physics, Pergamon, 293pp.
2. Kokhanovsky, A.A. et al., 2004. The determination of a cloud altitude using SCIAMACHY on board ENVISAT. IEEE Trans. Geosci. Remo. Sen. Letter 1, 211-214
3. Inoue, T., 1987. A Cloud Type Classification With NOAA 7 Split-Window Measurements. JGR 92, 3991-4000
4. Lagrosas, N. et al., 2004. Observation of boundary layer aerosols using a continuously operated, portable lidar system. Atmospheric Environment 38, 3885-3892.
5. Minnis, P. et al., 1993. Inference of cirrus cloud properties using satellite-observed visible and infrared radiances. Part II: Verification of theoretical cirrus radiative properties. American Meteorological Society vol. 50 no. 9, 1305-1322

Growth analysis of potato using a satellite image and GIS

Chiharu Hongo[1] and Takuya Michiba[2]
E-mail:hongo@faculty.chiba-u.jp
[1] Center for Environmental Remote Sensing, Chiba University
[2] Farmer's Union, Memuro, Hokkaido

Abstract : Site-specific crop management requires the evaluation map of crop conditions, yields and crop quality. In Hokkaido, evaluation maps of rice and wheat were created and used effectively for precision farming. To continue with this trend of research, the current study focuses on producing potatoes. Then for developing the map of potato, the analysis of the growth was conducted in the Memuro town, Hokkaido. The equations to estimate root yields and starch concentration of potatoes were derived from Quick Bird satellite image acquired on July 18, 2004, and the spatial distribution maps were created through these equations. The result indicated that root yield and starch concentration were affected by species of preceding crop. The fields with the highest root yields were detected in the fields where the sugar beets were cultivated in the previous year, and the average yield was 37.4t/ha.
Keywords : precision farming, root yield, starch concentration

1. Introduction

It has succeeded in evaluating of wheat and sugar beet yields using satellite imagery in Hokkaido. For instance, these maps are used to decide the harvesting order. But the cost effectiveness is not approved to evaluate the crop yield because satellite data is expensive.

A rotation crop management is performed in Tokachi, so it is possible to extract some kinds of crop information. This is the effective method to resolve the cost effectiveness issue. In this study, the growth analysis was executed to potato crop to extract more crop information from a satellite image.

2. Methods

2.1 Study site

The study was conducted in Memuro town, Hokkaido, Japan(Fig.1). The size of test site for analysis is 8km in east and west, and 8km in north and south. A large-scale agricultural management is performed here. The cultivation area of Memuro town is 19,720ha, and the averaged cultivation area is 28ha per farmer. The major crops are sugar beets, potatoes, wheat, sweet corns and legumes at planting ratio of 20.9%, 19.8%, 36.0%, 5.6%, and 14.2% respectively(Fig.2). Rotation of crops are executed by combination of major crops and vegetables at three years or four years interval.

Potatoes were selected in order to analyze yields and quality. The usage of cultivated potatoes are for edible, for starch materials and for seeds at ratio of 47.2%, 30.0%, 16.1%, and 8.0% respectively. The mayqueen was selected as analysis crop with the highest planting ratio among nine cultivars of edible potatoes.

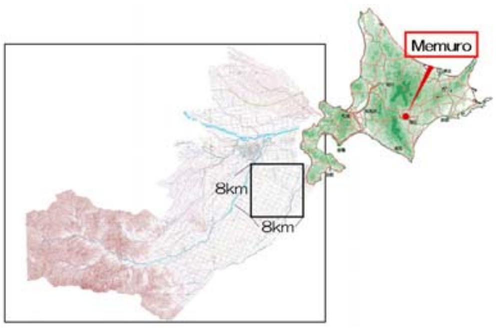

Fig.1 Study site

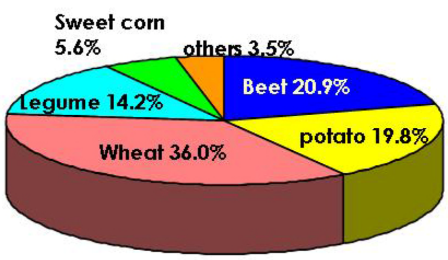

Fig.2 Planting ratio of major crops

2.1 Ground truth data

Farmer'sfields within the test site were used in this study. The investigation points were set in 33 places per five fields, which are two rows×2m width area. The field survey was performed on July 21 and 22, 2004. The plant height, hill number, leaf color were measured. Root yields(total amount of M,L,2L3Lsize) and starch concentration were measured on august 23 to 25.

2.3 satellite data and GIS deta

Quick Bird data was acquired on July 18,2004. The resolution is 2.4m. The GIS data of 2004 were selected from data base of JA Memuro data center to extract potato fields from satellite data. And the GIS data of 2003 was used to evaluate the yields of each kind of preceding crops.

2.4 Procedure

The procedure of image analysis is described in Figure 3. The satellite data and GIS data were rectified against 1:25000 digital topographic maps by nearest neighbor resampling algorithm using selected ground control points. The shape file of potato field was created from GIS data and overlaid to satellite data to extract potato fields. The position of investigation on satellite data was determined using ground based positioning data. The digital number(DN) values for investigation points were extracted and regression analysis was executed on yields and starch concentration, then the maps were developed. Finally the GIS data of 2003 was overlaid to these maps, and the relationships between root yields, starch concentration and preceding crops were evaluated.

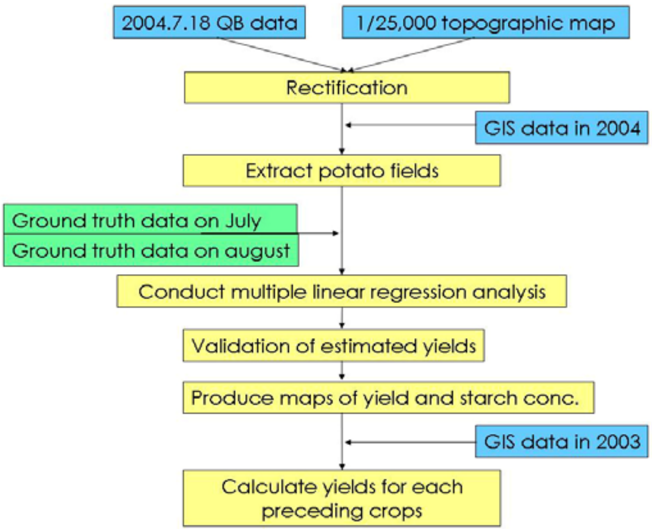

Fig.3 The procedure of image analysis

3 Result and discussion

Because harvest parts of the root vegetables like potatoes are hidden in the soil, information of root area is not contained on the satellite image. Therefore, the DN value extracted from the image is the only information on the potato with which soil face is covered stem and leaf. It is necessary to find the relation between the ground part and the underground part to estimate the amount of the yields from a image.

In general, growth rate of stem and leaf increases as the amount of nitrogen fertilizer application increases, also root weight increases. On the other hand starch concentration in root decreases. There was a positive relation between root yields and (SPAD x plant height)(Fig.4), on the other hand there was a negative relation between starch concentration in root and (SPAD x plant height)(Fig.5).

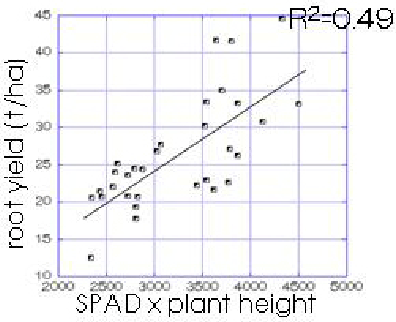

Fig.4 Relationships between root yield and vegetative parts

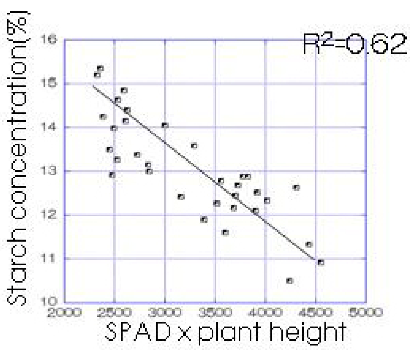

Fig.5 Relationships between starch concentration and vegetative parts

This relation indicates that root yields could be estimated from vegrtative parts. Regression analysis was executed on the root yield, starch concentration and DN value of satellite data. There was a positive relation between root yields and (B4-B2)/(B4+B2)(Fig.6). There was a negative relation between starch concentration in root and (B4-B2)/(B4+B2)(Fig.6).Then maps of yield and starch concentration were developed(Fig.7).The average of the percentage of relative error was 4.6% against root yields and 9.9% against starch concentration.

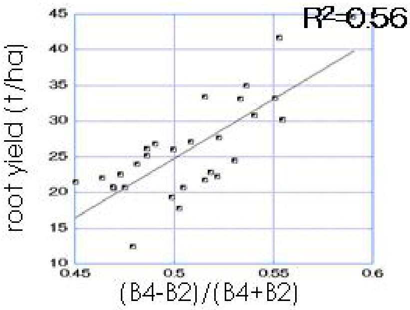

Fig.6 Relationships between root yield concentration and Band ratio

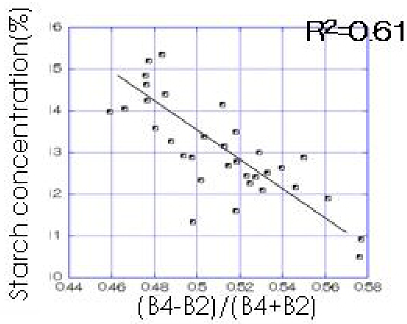

Fig.7 Relationships between starch and Band ratio

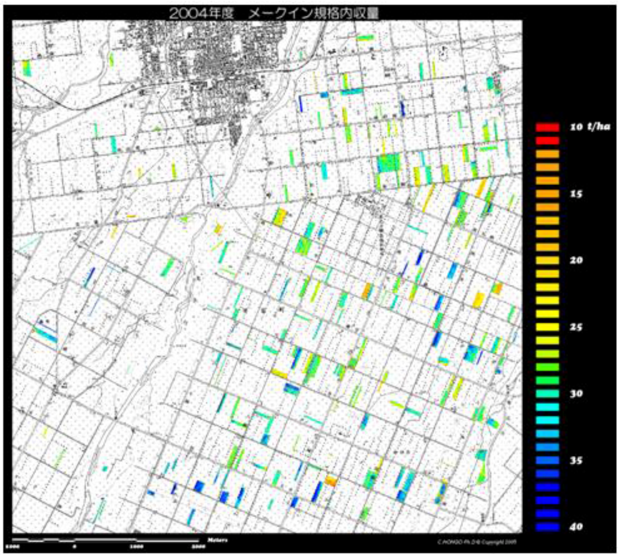

Fig.8 Sectional map of root yield

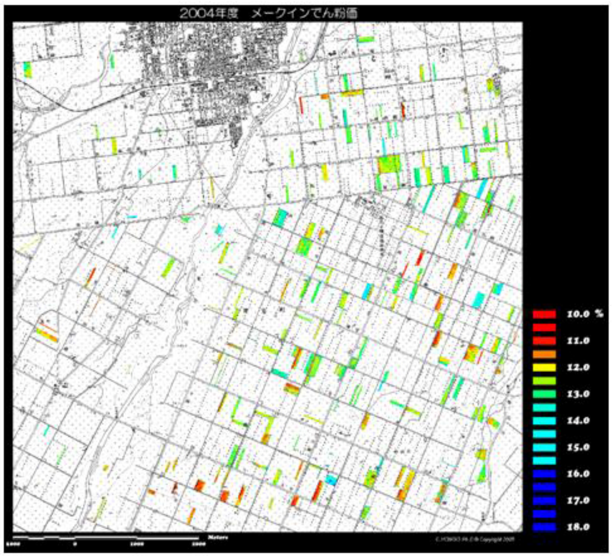

Fig.8 Sectional map of starch concentration

Comparing the yield data of each crop indicated that root yield and starch concentration were affected by species of preceding crop. The fields with the highest root weight were detected on the fields where the sugar beets were cultivated in the previous year, and the average yield was 37.4t/ha. The highest starch concentration value was found on the fields where the red beans were cultivated in the previous year.

It was possible to estimate the root yields and starch concentration of potato for large area using high resolution satellite data. The analysis of satellite data produced a better understanding of the relationship between preceding crops and yield. These results can be used for fertilizer application improvement, site specific planning for harvesting .

Preceding crop (2003)	Root yield (t/ha)	Starch concentration(%)
beet	37.4	12.3
Red beans	33.7	12.9
wheat	35.1	12.7
potato	35.1	12.8
Soy beens	36.4	12.6

Fig.10 Root yield and starch concentration on each crops

Monitoring ET with Remote Sensing and the Management of Water Resources on a Basin Scale

Jiemin WANG[1,2], Reiji KIMURA[1], Wim BASTIAANSSEN[3]

[1] Arid Land Research Center, Tottori University, Tottori, Japan

[2] Cold and Arid Regions Environmental and Engineering Research Institute, Chinese Academy of Sciences, Lanzhou, China

[3] WaterWatch, Wageningen, The Netherlands

Abstract

The shortage of water resources is serious in Hai River Basin. Managing water resources on the basis of evapotranspiration (ET), retrieved mainly from satellite remote sensing, is a new approach introduced in the GEF Hai Project. The most popular remote sensing algorithms in the retrieval of ET are reviewed, among them the SEBAL (Surface Energy Balance Algorithm for Land) is used for a preliminary analysis. Data from the MODerate resolution Imaging Spectroradiometer (MODIS) and Landsat TM/ ETM+ have been used to evaluate daily, seasonal and annual ET per county and per land use category. ET distributions and other related results for the Hai Basin, 2002 and 2003, are presented. Further studies will be continued in next five years, with an independent validation program to check and improve the ET retrieval algorithm. It is aimed to obtain a real saving of water resources through an ET reduction strategy, having more water resources remaining in the basin for production and environmental use, including that more freshwater discharge into the Bohai Sea.

1. Introduction – Water shortages in Hai River Basin

The shortage of water resources is serious in Hai River Basin, which is one of the seven largest river basins in China, with 10% of the country's population, including mega cities such as Beijing and Tianjin; Hai River Basin is also one of the most important agricultural and industrial regions in China. However, the water availability in the basin is only 305 m^3 per capita, which is 14% of national average and 4% of the world average. River channels and lakes on North China Plain are almost all dried up, because of the surface water over exploitation. Agricultural irrigation relies mainly on groundwater pumping; Net reduction of ground water is about 9 billion m^3 per year. The over exploitation of ground water causes water table declining continuously in last 30 years. Based on water balance analysis, in average, annual evapotranspiration (ET) of the basin exceeds about 4% of precipitation in recent decades. A quantitative description of the water balance components in Hai Basin for 1998, when the annual precipitation was about the multi-year average, is shown in Fig. 1. Water shortage also induces serious environment deterioration. In addition to the degradation of surface water quality, ecological environmental deterioration in the Bohai Sea, including mass mortalities of aquaculture species, is also striking because so less water discharged to the sea and heavy

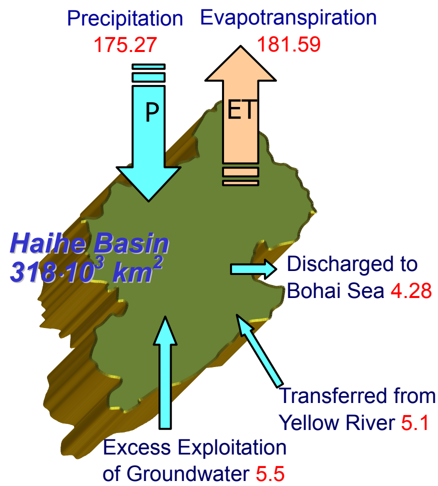

Fig. 1 Water balance components for an average year (1998, unit: 10^9 m^3)

land-based pollutants.

2. A new approach in basin-scale water management

As shown in Fig. 1, evapotranspiration (ET) and precipitation (P) are two major components for water balance in the Hai Basin. ET larger than P and supplemented by other water sources, mainly groundwater pumping, makes the severe non-sustainability. In a water-short area such as Hai Basin, it is important now to manage water resources in terms of the amount of water consumption, i.e. ET, which can be better monitored quantitatively as the rapid development of remote sensing in recent years. Actually, only the reduction of comprehensive ET, especially regional non-beneficial ET, can resolve gradually the shortage of water resources in the Hai River Basin. A GEF (Global Environment Facility) Hai River Basin Integrated Water and Environment Management Project is being carried out since 2004 (Olson, 2004). A new approach which uses the unit of evapotranspiration, monitored mainly by satellite remote sensing, is adopted in the water resources planning and managements. Remote sensing and ET management systems are to be built in the Basin. Better quantitative data on the spatial distribution and temporal variation of ET, for different land use and cropping periods in the entire Basin, will be supplied to water managers and consumers, and be used as the basis in the evaluation of water use efficiency and the formulation of water rights such as the allocation of irrigation (groundwater pumping) quota, etc. Reducing evapotranspiration that does not contribute to the plant growth could be achieved by, for example, reducing waterlogged areas, irrigation when evaporation being the lowest (such as at night), using moisture-retaining mulches, replacing open channels and ditches by pipes, fine-tuning deficient irrigation, and using water stress-resistant varieties, etc. A goal of real water saving and the recovery of water ecology in Hai River Basin should be reached finally.

3. Methods in the evaluation of regional evapotranspiration

Evapotranspiration has been observed for centuries; however, a better regional understanding is only possible by using satellite remote sensing. A simpler way is based on improved empirical or statistical models, such as the extended Priestley-Taylor method (Jiang & S.Ialam, 1999), the complementary relationship model, etc. A combined method have been used in the algorithm of MODIS evaporation product, MOD16, (Nishida et al., 2003) which calculates potential evaporation by Penman equation, calculates the 'wet surface' ET by Priestley-Taylor method (α=1.26), and calculate actual ET by Penman-Monteith method, then, using complementary relationship to calculate the 'evaporation fraction' for vegetated surface (EF_{veg}),

$$EF_{veg} = \frac{\lambda E_{veg}}{R_n - G_0} = \alpha \frac{\Delta}{\Delta + \gamma(1 + 0.5 r_s / r_a)} \tag{1}$$

Where R_n is net radiation, G_0 the soil heat flux at ground surface, λ the latent heat of evaporation, Δ is the slope of the saturation vapor pressure temperature relationship, γ is psychrometric constant, and r_s and r_a are the (bulk) surface and aerodynamic resistances. By using an estimation of vegetation coverage, also based on an evaluation of bare surface evaporation, evaporation fraction for a composite surface can be obtained accordingly.

Since the beginning of 1990's, the most popular remote sensing algorithms in the retrieval of ET are based on surface energy balance, such as the SEBAL (Surface Energy Balance Algorithm for Land) (Bastiaanssen et al. 1998) and SEBS (Surface Energy balance System) (Su, 2002), both developed in The Netherlands. Actual evaporation (E_a) is evaluated as the residual when net radiation, soil heat flux, and sensible heat flux (H) are retrieved with satellite data combined with some surface observations,

$$\lambda E_a = R_n - G_0 - H\ , \tag{2}$$

where λ is latent heat for evaporation. Both SEBAL and SEBS have better physical background. The major difference is that the latter tries to use meso-scale atmospheric model to predict meteorological fields near the surface. SEBAL has been used operationally in many countries since 1990's, and is now selected as the main algorithm in the GEF Hai Basin Project.

4. SEBAL procedures

SEBAL uses spectral radiances recorded by satellite-based sensors, mainly the MODIS (daily observation with surface resolution 250 m to 1 km) and Landsat TM/ETM+ (every 16 days, resolution 30 m). Combined with ordinary meteorological data, it retrieves at first the surface albedo, temperature, and vegetation index for each image pixel. Then, net radiation R_n is calculated by surface radiation balance,

$$R_n = (1 - r_0)R_{s\downarrow} + R_{L\downarrow} - R_{L\uparrow} + (1 - \varepsilon_0)R_{L\downarrow} \tag{3}$$

Where $R_{s\downarrow}$ is solar irradiance, $R_{L\downarrow}$ and $R_{L\uparrow}$ are long wave radiance emitted by atmosphere and land surface respectively, r_0 and ε_0 are surface albedo and emissivity respectively; all are calculated by standard algorithms and/or land surface parameterization schemes. Soil heat flux G_0 is evaluated by an empirical relation with net radiation and a few other surface parameters; it is a comparatively small component; however, the refinement in empirical formula is still a critical part in SEBAL application.

Sensible heat flux H is calculated, as the 'bulk' profile method in micrometeorology, by using the temperature difference between air and surface and the surface aerodynamic resistance to heat flow,

$$H = \rho C_p \frac{T_s - T_a}{r_a} \tag{4}$$

Where T_s is surface temperature retrieved by remote sensing. T_a is air temperature at specific height (such as 2 m above ground surface). ρ and C_p are air density and air specific heat at constant pressure respectively. r_a is the surface resistance to heat transfer; considered the effect of atmospheric stability, it is calculated by,

$$r_a = \frac{\ln(z/z_0) - \psi_h(z/L) + \psi_h(z_0/L)}{ku_*} \tag{5}$$

Where Ψ_h is the Monin-Obukhov stability function (L is Obukhov length). z_0 is surface roughness length, estimated by landuse status. The innovative point of SEBAL is the utilization of two "anchor" pixels, "hot" and "cold", in the image to fix boundary conditions for the air-surface temperature difference, and assumes a linear function between this difference and the radiometric surface temperature. An iterative way started from neutral stability assumption is used in the calculation of surface friction velocity (u_*), r_a, and then, the surface sensible heat flux H.

The instantaneous ET for each pixel is evaluated as the residual of the surface energy balance, then, daily (24 hr) evapotranspiration can be estimated based on the fact that 'evaporation fraction'

$$EF = \frac{\lambda E_a}{R_n - G_0} \tag{6}$$

is almost constant in daytime hours. Monthly ET are based on the results of a few days processing in the month, and using the index Kc = ET/ET_r to fill the gaps. Kc ('crop factor') is a more consistent ratio during daytime hours (Allen et al. 1998). ET_r, the reference ET, is computed from ground-based measurements of solar radiation, wind speed, air temperature, and humidity. For each land use category and each county of the whole Hai River Basin, daily, seasonal and annual ET are monitored accordingly.

5. Preliminary results

Preliminary analysis has been done for 2002 and 2003 for the whole Hai River Basin. By using of MODIS (1 km resolution, twice per month), DEM and land use/cover, and routine meteorological observations, the distribution of ET for year 2002 has been evaluated (Figure 2). 2002 was a very dry year, with a basin-wide annual precipitation 400 mm, 27% less than average; while the ET retrieved by SEBAL was much larger, about 714 mm. Spatial distribution showed that ET in some area, such as near the left bank of Yellow River, was higher (800-900 mm) because of higher water availability; while the ET in the downstream area of the Hai River, mainly south and southwest Tianjin, was much lower (400-500 mm) because of the dried up of surface water. Monthly variations of actual ET and biomass production have been compared with the local observation at Luancheng County and Yellow river embankment, which shows an acceptable agreement (Figure 3). A distribution map of the excess of annual actual evapotranspiration over precipitation for different counties in the Hai Basin also showed interesting results and could be a good reference for water management.

Year 2003 had much more precipitation about 582 mm (8.8% larger than average), while the ET retrieved was lower, about 556 mm. A distribution map of the basin-wide evapotranspiration of 2003 is shown in the left of Figure 4. Detailed analysis has been done for each land use categories in the Basin (Table 1), particularly, for the two major crops in the

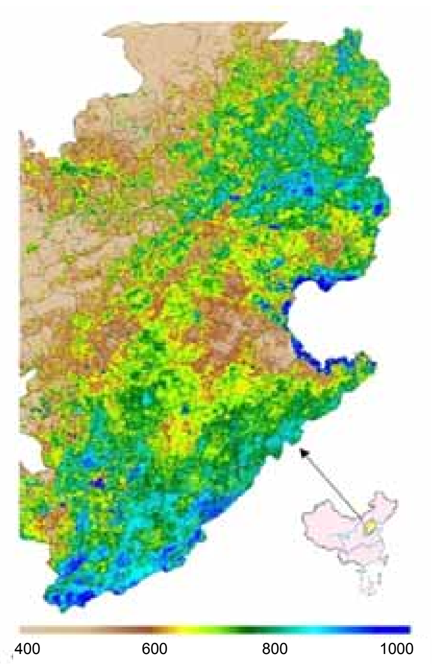

Fig. 2 Annual actual evapotranspiration for 2002 interpreted from MODIS measurements in the Hai Basin, with spatial resolution 1 km. The position of the river basin in China is also shown.

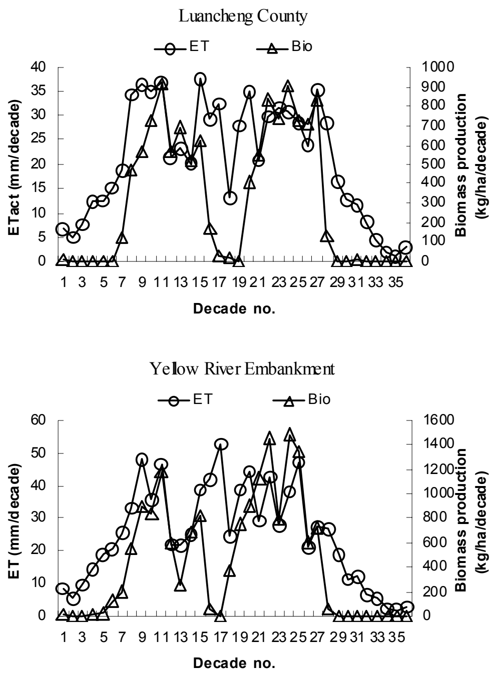

Fig. 3. Monthly variations of actual ET and biomass production of a 1 km * 1 km pixel in Luancheng County (upper) and the Yellow River embankment (lower) respectively.

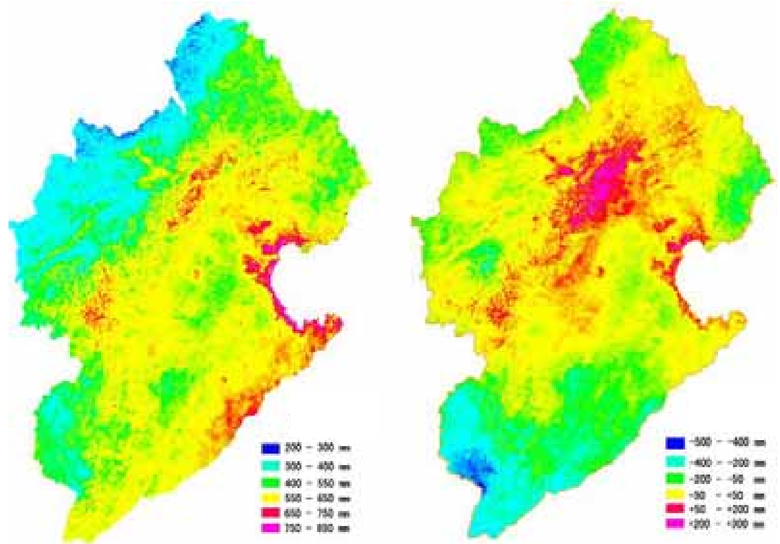

Fig. 4 Annual evapotranspiration (left) and the water depletion (precipitation minus ET) (right) of the Hai River Basin, 2003. Related values for each area (each county, each specific crop, etc.) can be tabulated accordingly.

river basin, winter wheat (winter to early summer) and maize (summer to autumn). Similar analysis can be also done for each prefecture, each county, and even smaller political area in the river basin. All of these results could be useful in the evaluation of water use efficiency and allocation of irrigation quota for different regions, so as to reduce the basin-wide ET, at same time, to maintain (if not increase) the agriculture production.

For 2004, an analysis has only been done for Beijing area so far, by using of Lansat TM data, which gave a much finer distribution. A comparison for a small area with field flux observations by eddy-correlation method showed very encouraged result (see Figure 5) (Mao, 2005).

6. Validation

It is always important to validate the remote sensing retrieved ET against local surface measurements, particularly in an operational use such as in Hai River Basin. This appeared not to be straight-forward due to discrepancies in scale. There have been no corresponding surface observations in the Hai Basin in 2002 and 2003 for proper validation. Nevertheless, some attempts have been done by referencing the results of a few agricultural stations in the basin and rather traditional results (see also Fig. 3). An independent validation program has been started in the GEF Hai Basin Project, with some specific stations built in southern and northern parts of the river basin, that have direct flux measurements with eddy-correlation method and the LAS (Large Aperture Scintillometer), in addition to standard observations of radiation components and automatic weather stations. These data have been used for the validation of the ET retrieved in 2004 for Beijing area (Fig. 5).

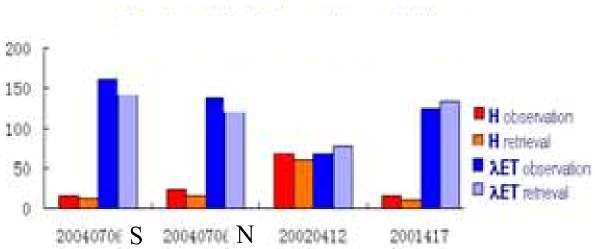

Fig. 5 Comparisons of sensible and latent heat fluxes retrieved from Landsat TM/ETM+ with observations by eddy-correlation method at Xiaotang Shan station near Beijing.

Table 1. Landuse categories of the Hai Basin, and the annual ET for each category in 2003.

Landuse name	Area (km2)	Area (%)	ET (mm)	ET (%)	ET(km2*mm)
plain irrigated field	142549	44.6929	569	47.601	81110381
mid-cover (20-25%) grassland	33573	10.526	500	9.8514	16786500
shrublands	28201	8.84177	539	8.9206	15200339
forest coverage >30%	23807	7.46413	524	7.3211	12474868
low-cover (5-20%) grassland	21468	6.73079	460	5.7955	9875280
forest coverage 10-30%	16788	5.26349	513	5.0542	8612244
hill non-irrigated field	16345	5.1246	428	4.1055	6995660
mountain non-irrigated field	9358	2.93398	475	2.6087	4445050
high-cover (50%) grassland	6635	2.08025	396	1.542	2627460
plain peddy	4311	1.35161	607	1.5357	2616777
reservoir & pond	3920	1.22903	701	1.6127	2747920
urban & town land	3716	1.16507	582	1.2692	2162712
other forest	2493	0.78162	579	0.8471	1443447
countryside residential area	1372	0.43016	593	0.4775	813596
bottom land	1094	0.343	545	0.3499	596230
saline-alkali land	954	0.2991	683	0.3824	651582
industrial & communication land	609	0.19094	623	0.2227	379407
river & channel	535	0.16774	603	0.1893	322605
marshes	437	0.13701	389	0.0998	169993
sandy land	369	0.11569	361	0.0782	133209
exposed rock	182	0.05706	455	0.0486	82810
tidal flat	117	0.03668	753	0.0517	88101
bare ground	49	0.01536	481	0.0138	23569
lake	30	0.00941	477	0.0084	14310
mountain paddy	20	0.00627	522	0.0061	10440
slope non-irrigated land	9	0.00282	525	0.0028	4725
other land	7	0.00219	688	0.0028	4816
hill paddy	4	0.00125	569	0.0013	2276

7. Concluding remarks

As shown in the preliminary works done in recent two years, it is feasible to have a better understanding of the basin-wide evapotranspiration by remote sensing schemes. Daily MODIS data, with resolution 1 km, are good in ET monitoring for a basin scale and long-term analysis, while the high resolution data such as Landsat TM and ASTER, with resolution 15-30 m, are good in detailed analysis in demonstration counties. Further studies will be continued for the Hai River Basin over next five years, including an independent validation sub-project which is essential in improving the ET monitoring reliability as well as improving the retrieving algorithm. The major task is the establishment of a real water saving program through an ET reduction strategy, with more water resources remaining in the basin for production and environmental use, including more freshwater discharges into the Bohai Sea. ET reduction is land use and crop type dependent. Other management factors also need to be included.

Acknowledgements

Many people participated in the tremendous works of the preliminary stage of the GEF Hai Basin Project. Various data collection particularly in situ flux observations done by Prof. Liu Shaomin and his group at Beijing Normal University are highly acknowledged.

References

Allen R G, Pereira L S, Raes D, smith M.,1998. Crop Evapotranspiration. FAO Irrigation and Drainage Paper 24, Rome.

Bastiaanssen, W.G.M., Menenti, M., Feddes R.A. and Holtslag, A.A.M., 1998. The Surface Energy Balance Algorithm for Land (SEBAL): Part 1 formulation. *J. of Hydr.* **212-213**: 198-212

Jiang L. & S.Ialam: A methodology for estimation of surface evapotranspiration over large areas using remote sensing observations [J]. Geophysical Research Letter 26(17), 1999, 2773-2776

Mao Defa, 2005. Evaluation of regional ET with high resolution satellite data. Master Thesis of Beijing Normal University (*In Chinese*)

Nishida,K, R.R.Nemani, S.W.Running, J.M.Glassy, 2003: An operational remote sensing algorithm of land surface evaporation. Journal of Geophysics Research, 108(D9), 4270, doi:10.1029/ 2002JD002062

Olson, D. C., 2004. Planning scarce water resources using ET quota: The GEF Hai Basin Integrated Water and Environment Project in China. 'Cases Database' *in* FAO-Netherlands International Conference on Water for Food and Ecosystems, The Hague, The Netherlands.

Su, Z., 2002. The Surface Energy Balance System (SEBS) for estimation of turbulent heat fluxes [J]. Hydrol. Earth Syst. Sci. 6(1), 2002, 85–99.

Comparison of monitoring applicability between Crop Production Index and conventional methods using satellites

Daijiro KANEKO[1],

[1]Department of Civil Engineering, Matsue National College of Technology, 14-4, Nishiikuma-chou, Matsue, 690-8518 Japan, Professor, Phone & Fax: +81-852-36-5266,E-mail: kand@ce.matsue-ct.ac.jp

ABSTRACT

This paper compares the applicability of the Crop Production Index CPI with conventional methods, taking into account the acquisition of the necessary data by remote sensing. The author has developed the CPI index as a remote sensing method for monitoring grain production in the early stages of crop growth in Japan and Asia. A photosynthesis based crop production index CPI takes into consideration the solar radiation, the effective air temperature, and NDVI as a factor representing vegetation biomass. The CPI index incorporates temperature influences such as the effect of temperature on photosynthesis by grain plant leaves, low-temperature effects of sterility, cool summer damage due to delayed growth, and high-temperature injury. These latter factors are significant at around the heading period of crops. The CPI index for rice was validated at ten monitoring sites in the central and northern half of Japan. This paper proves the ability of the CPI to predict poor crop production using rice yield statistics, contrasting it against conventional methods such as the cumulative Growing degree day GDD, integrated NDVI, and photosynthesis rate.
Keywords: monitoring, crop production, rice, photosynthesis, NDVI

1. INTRODUCTION

This research aims to monitor grain production by developing a photosynthesized type of crop production index, which displays functional dependence on solar radiation, temperature effects, stomatal opening, and vegetation biomass. It is important to oversee the quantity of grain in production in Japan and Asia at an early stage in the present era of increasing Asian population and water-resources restrictions. Continuous predictive monitoring of crop production in East Asia would allow orderly management of food security issues including Japan, which is one of the world's major grain importers. Conventional methods have generally been based on the cumulative value of the effective air temperature (growing degree day, GDD) by Idso [1)], Bollero et al. [2)]. or integrated NDVI proposed by Rasmussen[3)]. However, none of these methods correctly expresses the grain production by estimating the time-integrated photosynthesis rate. Many researchers have presented conventional papers on crop simulation, including Williams et al.[4)]. Priya et al.[5)] and Perez et al.[6)], and remote sensing data have been incorporated in the models by Maas [7)] and Wiegand [8)]. However, those models simulate the growth process of crops, making them highly complicated, as Monteith [9)], and Sinclair and Seligman [10)] have pointed out. Several methods use seasonal changes of the normalized difference vegetation index NDVI derived from satellite observation. The method in this paper takes the amount of growth and biomass as known, using remotely sensed data NDVI, and estimates the instantaneous photosynthesis velocity easily and accurately. The photosynthesis-based crop production index CPI proposed in this paper can predict the rice yield under conditions of low temperature sterility, sunshine shortage, and high temperature injury. This paper validates the CPI index at ten monitoring sites in Japan and verifies its particular ability to predict poor grain production, in contrast to conventional indices.

2. METHOD OF CROP PRODUCTION INDEX CPI

2.1 Conventional methods

Many conventional crop studies have correlated the grain quantity in production with the growth index of Growing Degree Day GDD, or with water stress indices such as stress degree day[1),2).]

$$GDD = \frac{T_{\max} + T_{\min}}{2} - T_b \tag{1}$$

where, T_{max} is the maximum daily air temperature, T_{min} is the minimum daily air temperature, and T_b is a threshold temperature for the crop, below which physical activity is inhibited and equal to 10 ℃.

In conventional research using remote sensing, the vegetation index NDVI [11),12),13),14)], concerning the vegetation biomass, is related to the crop production. Rasmussen[3)] defined the integrated NDVI (iNDVI) and related it to the grain yield.

$$Yield = a \cdot \int_{t1}^{t2} NDVI(t)dt + b \tag{2}$$

where, a and b are regression coefficients, and t1 and t2 are the day number of seeding and harvesting.

In grain production forecasting using the latest remote sensing, daily values of the photosynthetically active radiation PAR and the vegetation biomass (NDVI) are taken into the model. Frthermore, Rasmussen (1998) gave the net primary production NPP using satellite data according to the following formula:

$$NPP = \varepsilon \int_0^t (aNDVI + b) \cdot PAR \cdot dt \tag{3}$$

where ε is the efficiency coefficient,, t is the time, and PAR is the photosynthetically active radiation.

This NPP is a photosynthesis-type model. However, this formula does not allow for such important factors as temperature influences on photosynthesis, temperature sterility and stomatal opening of crops. The present research improves modeling based on the photosynthesis type of crop production index so as to incorporate the effects of global solar radiation, temperature, stomatal opening, and vegetation biomass. Although the areas of crop study and remote sensing have generated much research, especially on the production of wheat and corn, it is all restricted to consideration of the water stress or formulas based on vegetation indices. To give a more accurate value of the grain quantity in production, the crop production index should take the form of the photosynthesis velocity so as to express the growth of crop vegetation and filling of grain, both of which relate directly to the quantity produced.

2.2 Proposed method

Rasmussen [15)] proposed a net primary production (NPP) model by taking into account the daily photosynthetically active radiation PAR and the amount of vegetation biomass (NDVI), so as to estimate the NPP from satellite data. The equation of NPP is of photosynthetic type, but sterility due to low- and high-temperature injury and stomatal opening due to shortage of water resources or inadequate irrigation are not accounted for. It is reasonable to suppose that crop production can be estimated based on a daily photosynthesis rate. Generally, temperature has two effects on the quantity of grain production: its normal influence on the rate of photosynthesis, and the effect of extremes of temperature on sterility during the stages of heading, flowering, and filling. To model these two effects, three response functions, to photosynthesis, low-temperature sterility and high-temperature injury are employed in the period before and after heading.

This research expands the form of NPP by Rasmussen to consider air temperature and stomatal opening, as well as the solar radiation and the amount of vegetation biomass already considered. The photosynthesis velocity is defined by equation (1) as follows[16), 17), 18),19),20)]:

$$PSN = \frac{a \cdot APAR}{b + APAR} \cdot f_{Syn}(T_c) \cdot \beta_s \cdot eLAI \tag{4}$$

where *PSN* is the photosynthesis rate, *APAR* is the absorbed photosynthetically active radiation, β_s is the stomatal opening, *a* and *b* are Michaelis-Menten constants, T_c is the canopy temperature, *eLAI* is the effective leaf area index, and f_{ster} is the sterility response function for the air temperature.

The authors' former paper[16)] presents sensitivity analysis curves for the Michaelis-Menten-type response function versus solar radiation and the temperature response of the photosynthesis rate as well known as the Sigmoidal-Logistic type function :

$$f_{Syn}(T_c) = \left[\frac{1}{1 + \exp\{k_{syn}(T_c - T_{hv})\}} \right] \tag{5}$$

where T_{hv} is the temperature parameter at half of the maximum photosynthesis rate, and k_{syn} is the slope parameter. The temperature response functions for low-temperature sterility and high-temperature injury are defined by the following equation, referring to the curves obtained by Vong and Murata [21)]:

$$F_{Lster}(T_c) = 1 - \exp[k_{Lster}(T_{Lster} - T_c)], \tag{6a}$$

$$F_{Hster}(T_c) = 1 - \exp[k_{Hster}(T_c - T_{Hster})] \tag{6b}$$

where, k_{Lster} is the low temperature sterility constant, T_{Lster} is the low sterility limit temperature, k_{Hster} is the high temperature injury constant, T_{Hster} is the high injury limit temperature, and T_c is the plant leaf temperature.

Finally, the response function of the compounded temperature sterility effects due to both low and high temperatures in grain production is expressed by the following equation:

$$\begin{aligned} F_{Ster}(T_c) = & \{1 - \exp[k_{Lster}(T_{Lster} - T_c)]\} \\ & \cdot \{1 - \exp[k_{Hster}(T_c - T_{Hster})]\} \end{aligned} \tag{6c}$$

Next, integration of the photosynthesis rate over an interval from seeding t_s to the time t of crop plant stage defines the photosynthesis-based crop production index CPI for rice having the following forms:

During crop plant stage 1, of growth:

$$CPI_U = \int_{t_s}^{t} PSN_U \cdot dt \tag{7}$$

During crop plant stage 2, of booting, heading, flowering to ripening:

$$CPI_U = F_{Ster}(T_c) \cdot \int_{t_s}^{t} PSN_U \cdot dt \tag{7a}$$

$$F_{Ster} = \int_{t_f}^{t} f_{Ster}(T_c) \cdot dt \tag{7b}$$

At the crop plant stage 3 of harvesting:

$$CPI_U = F_{Ster}(T_c) \cdot \int_{t_s}^{t_r} PSN_U \cdot dt \tag{7c}$$

$$F_{Ster} = \int_{t_f}^{tr} f_{Ster}(T_c) \cdot dt \tag{7d}$$

It is necessary to normalize the NDVI so as to remove the effect of planting area (plant coverage ratio) on the photosynthesis rate at different paddy sites. Even if the crop yield in a year was the norm, the NDVI is liable to differ each year. The plant coverage ratio per data pixel of remote sensing is dependent on the individual sites. We therefore define the standardized NDVI, called the NDVI Unit, by dividing by the annual average yield as follows:

$$NDVI_{U,i} = \frac{NDVI_i}{iNDVI_{H100}} \tag{8}$$

The photosynthesis rate is similarly normalized to give the 'PSN Unit' upon dividing by the normal photosynthesis rate averaged annually, as follows:

$$PSN_U = \frac{\int_{t_s}^{t} PSN \cdot dt}{iPSN_{100}} \tag{9}$$

The EPIC (Erosion-Productivity Impact Calculator) uses the same idea to normalize the effect of accumulation of Growing Degree Day, by defining the Heat Unit Index.

The quantity of grain production in the growth stages of heading and filling is influenced by a crop physiological mechanism called low-temperature sterility, and by high temperature injury, in addition to cumulative photosynthesis up to heading. To transform the CPI index into the appropriate photosynthesis type of grain production index, the photosynthesis rate *PSN* of equation (1) must be multiplied by the temperature sterility function F_{str} of equation (3c) involving the heading term to be expressed via equation (5b and 6b), which is of time-integrated form to account for the effect of temperature on flowering, pollination, and ripening.

3. DATA USED IN THE MODELING

The present research uses domestic meteorological data to verify the CPI index. The ground air temperature data, which are supplied by the Japanese Meteorological Agency from the Automated Meteorological Data Acquisition System (AMeDAS) point at ten sites, distributed in the Japanese agricultural plains, have large acreages suitable for satellite monitoring of the paddy fields.

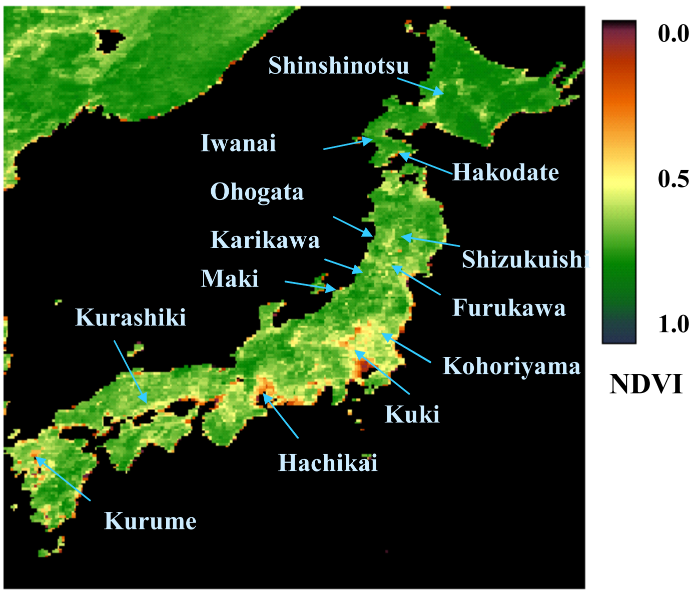

Figure 1: Distribution of NDVI and monitoringu sites in Japan for varidation of Crop Production Index CPI.

The Japanese Ministry of Agriculture, Forestry, and Fisheries provides grain statistical information, which includes crop situation index for the paddy rice at ten sites for monitoring and validation district. This crop situation index is the ratio of crop production in the year in question to the mean annual production for the ten most recent years. The Society of Agricultural Meteorology in Japan has published a special report, which summarizes the relation between the meteorological conditions and the poor harvest in 1993. The satellite NDVI data used in the CPI index is the 4-minute mesh set of vegetation index data derived from NOAA Advance Very High Resolution Radiometer (AVHRR) by Tateishi[22].

4. COMPARISON of the CPI and CONVENTIONAL METHODS

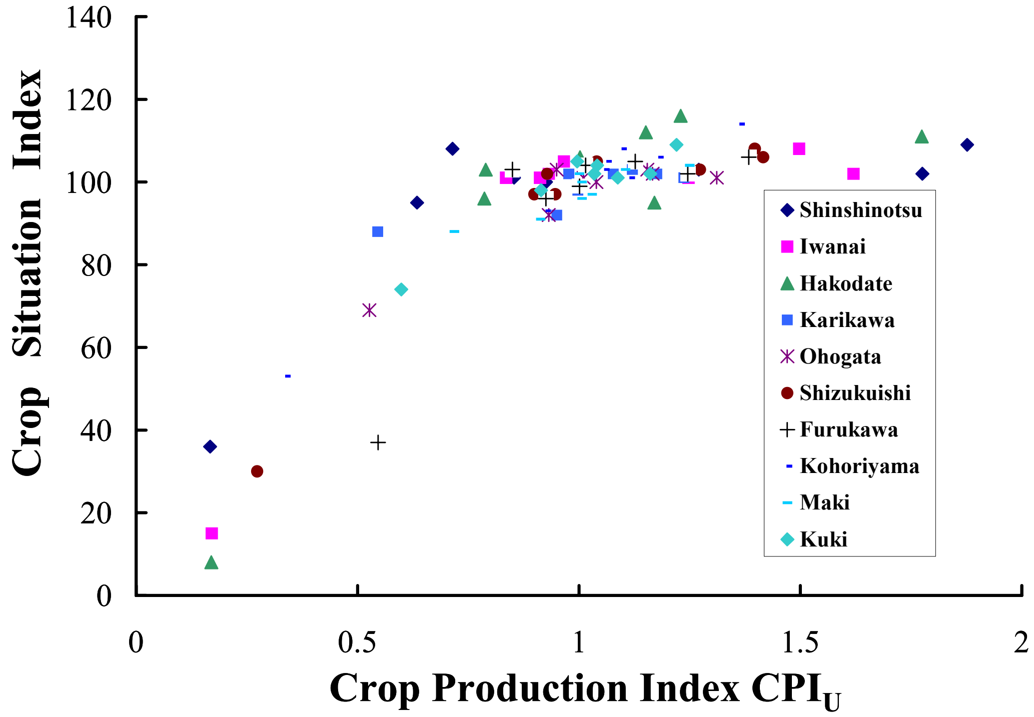

Figure 2: Relation between the crop production index CPI_U and Crop situation index at ten monitoring points.

Figure 2 shows the relation between crop situation index CSI and the CPI_U, to verify applicability to rice yields at 10 sites in Japan. The photosynthesis rate of the CPI_U index decreases as a result of the inadequate solar radiation or accumulation of air temperature. The CPI Unit becomes a little less than 1, implying poor production compared to the normal harvest averaged annually. The CPI_U can predict a trend of poor production, expressed by the crop situation index decreasing linearly to below 100. The many values of the CPI index close to 1 imply the usual behavior of the photosynthesis rate governing rice yields in most years. However, abnormal weather with low temperature and much cloud, which happens about every 10 years, causes low temperature sterility and late ripening of rice. The CPI_U then rapidly falls to zero, since the limiting problem is not photosynthesis but inadequate flowering and late ripening. The sterility function curve, which has a steep gradient for low air temperatures, is able to capture the very bad harvest in the worst case of the crop situation index below 50 in 1993. The third mechanism is high temperature injury, expressed by equation (6b). When the air temperature is excessive, the CSI decreases slightly with further increase in air temperature as

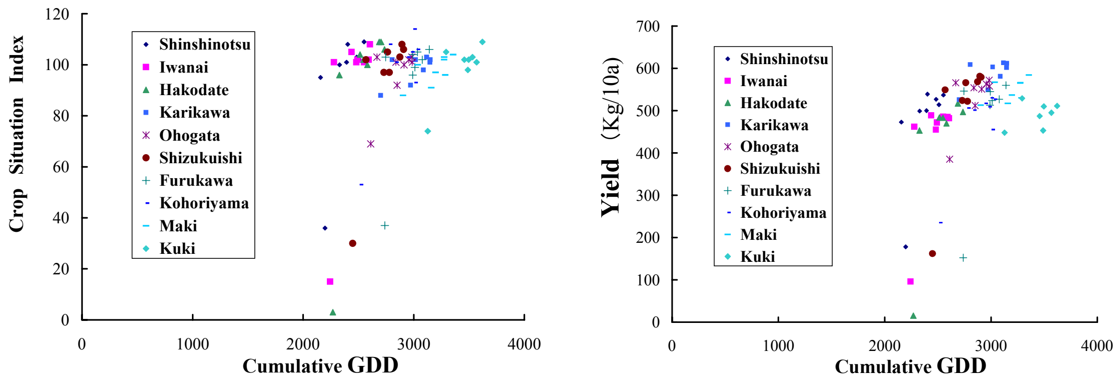

Figure 3: Comparison of monitoring applicability for Crop Production Index and conventional methods. The figures show relations between the cumulative growing degree day GDD and Crop Situation Index at ten monitoring points, and between yield and cumulative GDD.

seen on the right in Figure 2, though it is still greater than 100 in the right side range of x axis, that is greater than CPI_U=1 in the Figure2. According to the mechanisms included in the CPI_U index, CPI_U can predict rice production taking into account photosynthesis, low temperature sterility, and high temperature injury, depending on meteorological conditions.

Figure 3 shows relations between the crop situation index CSI and the cumulative growing degree day (GDD), and between the yield and cumulative GDD. The cumulative GDD has a linear relationship to the yield but shows no ability to distinguish bad production due to low temperature sterility from normal rice yields in other years. The air temperature has two effects, on growth and ripening by photosynthesis and on pollination from heading to flowering of the grain. This sterility effect on pollination is not linear in temperature, but cuts in rapidly below a threshold of about 18 degrees

Figure 4 shows relations between the crop situation index and the integrated NDVI (iNDVI), and between yield and the iNDVI. The integrated NDVI is not able to predict either the crop situation index or the yield, and in particular is unable to predict a bad harvest due to low temperature sterility. The iNDVI values depend strongly on regional characteristics such as soils, type of rice and mixcel effects, involving other plants (vegetables, trees, etc.).

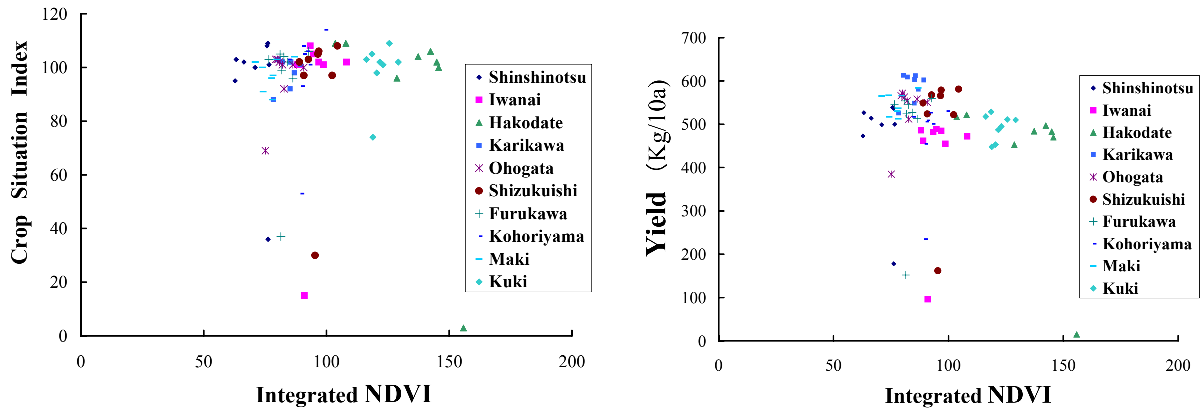

Figure4: Relations between the integrated NDVI and Crop Situation Index, and between yield and iNDVI.

Figure5: Applicability to crop production of integrated PSN based on remotely sensed data. The figures show relations between the Crop Situation Index and integrated PSN, and crop yield and iPSN.

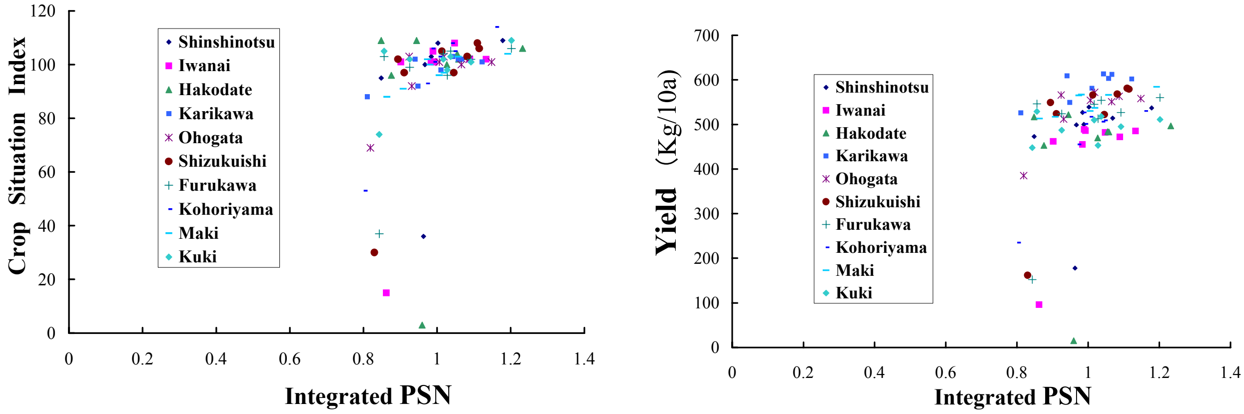

Figure5: Applicability to crop production of integrated PSN based on remotely sensed data. The figures show relations between the Crop Situation Index and integrated PSN, and crop yield and iPSN.

Figure 5 shows the performance of the integrated photosynthesis rate iPSN used as a crop yield index. The crop situation index decreases linearly with iPSN but shows no ability to predict low temperature sterility, because sterility is not dependent on photosynthesis but is related to flowering and pollination. The iPSN performs much better than the iGDD or iNDVI since it is linear with respect to crop yield; however, the iPSN values show considerable scatter arising from dependence on regional conditions.

Consequently, only CPI_u is able to predict a bad harvest due to sterility effects, by making the CPI_u values decrease sharply to zero based on the eigen-functional relationship between CPI_u and the crop situation index CSI, as well as the yield.

5. CONCLUSIONS

This paper compares the applicability of the Crop Production Index CPI and conventional indices, based on remotely sensed data. The aim is to develop a remote sensing method suitable for monitoring rice production from the early stages of crop growth right up to harvesting in Japan and Asia. The present paper proposed a photosynthesis-based crop production index CPI that takes into consideration the solar radiation, the effective air temperature, and NDVI as a factor representing vegetation biomass. The CPI index incorporates the mechanism of temperature influences such as the effect of temperature on photosynthesis by grain plant leaves, low-temperature effects of sterility, cool summer damage due to delayed growth, and high-temperature injury. These latter factors are significant at around the heading period of crops. The CPI index for rice was validated at ten monitoring sites in the central and northern half of Japan using the rice crop situation index. The validation exercise clearly proves the superior ability of the present index to predict poor production using rice yield statistics in comparison to conventional methods such as cumulated growing degree day GDD, integrated NDVI, and photosynthesis rate. The method is based on routine observation data, allowing automated monitoring of crop production at arbitrary sites without any special observations.

ACKNOWLEDGMENTS

This study was funded by Grants-in-Aid for Scientific Research. We wish to express thanks to the Japan Society for the Promotion of Science, which belongs to Ministry of Education, Culture, Sports, Science and Technology.

REFFERENCES

1. IDSO, S. B., PINTER, Jr. P.J., HATFIELD, J. L., "JACKSON, R. D., and REGINATO, R. J., A remote sensing model for the prediction of wheat yields prior to harvest", Journal of Theoretical Biology, **77**, 217-228, 1979.
2. BOLLERO, G. A., BULLOCK, D. G., and HOLLINGER, S. E., "Soil temperature and planting date effects on corn yield, leaf area, and plant development", Agronomy Journal, **88**, 385-390, 1996.
3. RASMUSSEN, M. S., "Assessment of millet yields and production in northern Burkina Faso using integrated NDVI from the AVHRR", International Journal of Remote Sensing, **13(18)**, 3431-3442, 1992.
4. WILLIAMS, J. R., JONES, C. A., KINIRY, J. R. and SPANEL, D. A., "The EPIC crop growth model", Transactions of the ASAE, **32(2**), 497-511, 1989.
5. PRIYA, S, SHIBASAKI, R., "National spatial crop yield simulation using GIS-based crop production model", Ecological Modeling, **135**, 113-129, 2001.
6. PEREZ, P., ARDLIE, N., KUNEEPONG, P., DIETRICH, C., and MERRITT, W. S.: CATCHCROP, "Modeling crop yield and water demand for integrated catchment assessment in northern Thailand", Environmental Modeling & Software, **17**, 251-259, 2002.
7. MAAS, S. J., "Using satellite data to improve model estimates of crop yield", Agronomy Journal, **80**, 655-662, 1988.
8. WIEGAND, C. L. RICHARDSON, A. J., JACKSON, R. D., PINTER, Jr. P. J., AASE J. K., SMIKA, D., LAUTENSCHLAGER, L. F., and McMURTREY, Ⅲ J.E., "Development of Agrometeorological crop model inputs from Remotely sensed information", IEEE Transactions on Geoscience and Remote Sensing, **GE-24 (1)**, 90-98, 1986.
9. MONTEITH, J. L., "The quest for balance in crop modeling", Agronomy Journal, **88**, 695-697, 1996.
10. SINCLAIR, T. R. and SELIGMAN N. G., "Crop modeling: from infancy to maturity", Agronomy Journal, **88**, 698-704, 1996.
11. AASE, J. K., and SIDDOWAY, F. H.,1981, Spring wheat yield estimates from spectral reflectance measurements, IEEE Transactions on Geoscience and Remote Sensing, **GE-19(2)**, 78-84.
12. GROTEN, S. M. E.,1992, NDVI-crop monitoring and early yield assessment of Burkina Faso, International Journal of Remote Sensing, **14(8)**, 1495-1515.
13. QUARMBY, N. A., MILNES, M., HINDLE, T. L., and SILLEOS, N., 1993, The use of multi- temporal NDVI measurements from AVHRR data for crop yield estimation and prediction, International Journal of Remote Sensing, **14(2)**, 199-210.
14. HAYES, M. J., and DECKER, W. L., 1996, Using NOAA AVHRR data to estimate maize production in the United States Corn Belt, International Journal of Remote Sensing, **17(16)**, 3189-3200.
15. RASMUSSEN, M. S., "Developing simple, operational, consistent NDVI-vegetation models by applying environmental and climatic information: Part II. Crop yield assessment", International Journal of Remote Sensing, **19(1)**, 119-137, 1998.

16. KANEKO, D., OHNISHI, M., and ISHIYAMA T., "Proposal of early monitoring method for crop production in China and India In the recent era of water resources restriction", Environmental Systems Research, Japan Society of Civil Engineering, **31**, 235-244, 2003 (In Japanese with English abstract).
17. KANEKO, D., OHNISHI, M., ISHIYAMA, T., and TATEISHI, R., "Modeling of a photosynthetic crop production index for early warning using NDVI and Meteorological data", Proceedings of SPIE, Remote Sensing for Agriculture, Ecosystems, and Hydrology Ⅵ, 11th SPIE International Symposium on Remote Sensing, 1-10, Gran Canaria, Spain, 2004.
18. KANEKO, D., OHNISHI, M., ISHIYAMA, T., and TATEISHI, R., " Proposal of a photosynthesis type of crop yield index for monitoring crop production in China and India in the era of water resource restriction", **4th** International Crop Science Congress, 4p, Brisbane, Australia.
19. KANEKO, D., ITOHARA, T., OHNISHI, M., ISHIYAMA, T. : Early warning method for rice production using remote sensing and meteorological data - Photosynthetic Crop Production Index -, Sustainable Development and Planning , Bologna, Italy, **2**, 815-824, 2005.
20. KANEKO, D., OHNISHI, M., and ISHIYAMA, T. : Photosynthetic rice production index for early warning using Remote Sensing and meteorological data, Proceedings of SPIE , Remote Sensing for Agriculture, Ecosystems, and HydrologyⅦ, 12th SPIE EUROPE International Symposium on Remote Sensing, 1-9, Bruges, Belgium, 2005.
21. VONG, N. Q., and MURATA, Y., "Studies on the physiological characteristics of C3 and C4 crop species. I. The effects of air temperature on the apparent photosynthesis, dark respiration and nutrient absorption of some crops", Japanese Journal of Crop Science, **46**, 45-52, 1997.
22. TATEISHI, R., "Twenty-year global 4-minute AVHRR NDVI dataset", CEReS, Chiba University, Chiba, 2001.

CEReS

Center for Environmental Remote Sensing,
Chiba University